

Chemical and biological studies on fungal secondary metabolites
from *Cortinarius* and *Sepedonium* species

DISSERTATION

zur Erlangung des Doktorgrades der Naturwissenschaften

(Dr. rer. nat.)

der

Naturwissenschaftlichen Fakultät II

Chemie, Physik und Mathematik

Der Martin-Luther-Universität

Halle-Wittenberg

vorgelegt von

Frau M.Sc. Yen Thi Hai Lam

geb. am 28.12.1990 in Hung Yen, Vietnam

This thesis has been developed under the supervision of Prof. Dr. Ludger Wessjohann and mentorship of Dr. Norbert Arnold at the Leibniz Institute of Plant Biochemistry (IPB) in cooperation with the Martin Luther University Halle-Wittenberg.

The results presented in this thesis include two chapters published as two peer-reviewed original research articles as well as one manuscript submitted as an original research article to a peer-reviewed journal.

1st Reviewer: Prof. Dr. Ludger Wessjohann

2nd Reviewer: Prof. Dr. Marc Stadler

Date of public defense: 21.12.2022

“We often think of peace as the absence of war, that if powerful countries would reduce their weapon arsenals, we could have peace. But if we look deeply into the weapons, we see our own minds –our own prejudices, fears and ignorance.

Even if we transport all the bombs to the moon, the roots of war and the roots of bombs are still there, in our hearts and minds, and sooner or later we will make new bombs.

To work for peace is to uproot war from ourselves and from the hearts of men and women. ”

—— Thich Nhat Hanh (1926-2022) ——

Acknowledgements

My long journey to PhD could not be achieved without the direct and indirect involvement of many extraordinary people.

I owe a great debt of gratitude to Prof. Dr. Ludger A. Wessjohann for giving me the opportunity to be his doctoral student at the Leibniz Institute of Plant Biochemistry (IPB) Halle, financially supporting me (and hence my family), and guiding me through my studies with valuable ideas and great foresight. He offers the independence but being always there for all of us – his students – for any questions or difficulties, gives many detailed comments for our oral presentations, posters, and manuscripts, and keeps reminding us to spend time for documentation to make sure that we are going on the right way. I have learned a lot from him.

I wish to express my special thanks to my mentor, Dr. Norbert Arnold, who took care not only of my academic life but also my family's private life. I am thankful to have him as a dedicated project group leader having highly critical thinking skills and brilliant ideas for my research, an excellent mushroom taxonomist, a very experienced natural product chemist, and a 'huge'-kind friend. I will remember our external trips for feeding experiments, hunting mushrooms and unstoppable lectures about mushrooms.

Many thanks to my cooperation partners inside and outside of IPB Halle: Dr. Andrea Porzel, Dr. Pauline Stark and Dr. Hidayat Hussain for NMR experiments and patience for discussion or any questions. Dr. Andrej Frolov, Alena Soboleva, and Annegret Laub for MS experiments and discussions. Dr. Wolfgang Brandt and Dr. Mehdi Davari for quantum chemical calculations. Dr. Robert Rennert and Martina Lerbs for cytotoxic assays. Dr. Katrin Franke, Dr. Haider Sultani, Martina Brode and Anker Dettmer for antimicrobial assays. Dr. Manuel Ricardo, Dr. Aldrin Vasco, Dr. Yanira Gomez and Prof. Bernhard Westermann for the synthesis work. Prof. Götz Palfner and Dr. Celia Lima, University of Concepción Chile for carrying out the phylogenetic study. Dr. Christoph Wagner and Prof. Kurt Merzweiler, Institute of Chemistry, Faculty of Natural Sciences II, Martin Luther University Halle-Wittenberg, for X-ray crystallography of my first PhD compound.

My sincere thanks to all members of IPB Halle, especially to all member of the Bioorganic Chemistry department (NWC) for the very friendly working atmosphere. To my dear friends, labmates, and colleagues: Ayu, Ismail, Dube, Nilufar, Alejandro, Lea, Jonas, Luisa, Ari, Dayma, Manuel, Carlos, Patricia, Ahyoung, Serge, Micjel, Matthias, Nicole, Tuvshin, Aldrin, Janoi, Leo, Mohamad, Ibrahim, many thanks for the nice memories and pleasant time together. To my co-supervised diplom students Jana Hoppe and Erik Henze, thanks for the good work. To Dr. Frank Broda, many thanks for providing quick support anytime I have problems with my computer. To all technicians, thank you for making my PhD life much easier. To Alejandro and Heena, thanks for helping me produce very nice microscope images for this thesis.

I also would like to express my sincere gratitude to my lecturers and colleagues in Faculty of Chemistry, Hanoi National University and Education, Vietnam, particularly to the members of

Organic Chemistry department. To my bachelor supervisor, Prof. Dien H. Pham, many thanks for developing my passion for natural products, encouraging and being a great role model for me. To my master supervisor, Prof. Quang N. Dang, many thanks for inspiring my scientific work, introducing me to Prof. Wessjohann, and contributing to one of the largest projects of my PhD. To the heads of the faculty and the department, many thanks for supporting my PhD time. To all members of the Organic Chemistry department, special thanks for taking my tasks so that I can focus on my study.

I also would like to thank the Vietnamese Ministry of Education and Training (MOET) for the scholarship, so that I can come to study in Germany.

To my external friends in Germany: Family Richwien, Mr. and Mrs. Christmann, my cousin (Tung) and his family, Tamil and Shindhu family, Minh and Santiago family, Thu Lin and Wand family, thank you all for offering my family the cozy family-like atmosphere.

Last but not least, I am indebted to my big family for bringing me to this life and giving me wholehearted support and unconditional love. Dear parents, I know you worked very hard to raise my siblings and me, but now you can be proud to see my name on a doctoral thesis. To my little angel, Quang An, thank you for coming to this world and motivating me to work at lab (not at home 😊). To my beloved husband, Quang, thanks for sacrificing everything to me and our son. Without your love, I could never ever get my PhD done.

Thank you for making my life so beautiful!

Halle, 22.02.2022

Yen Thi Hai Lam

Table of contents

Acknowledgements	V
List of abbreviations	VIII
Summary	XI
Zusammenfassung	XIII
Chapter 1. Introduction and objectives	1
Chapter 2. General introduction	8
Chapter 3. <i>Nor</i> -guanacastepene pigments from the Chilean mushroom <i>Cortinarius pyromyxa</i> ..	32
Chapter 4. Purpurascenines A-C, azepinoindole alkaloids from <i>Cortinarius purpurascens</i> Fr.: isolation, biosynthesis, and activity studies on 5-HT _{2A} receptor	50
Chapter 5. Rare glutamic acid methyl ester peptaibols from <i>Sepedonium ampullosporium</i> Damon KSH 534 exhibit promising antifungal and anticancer activity	78
Chapter 6. General discussion	106
Appendix	116
Declaration of the author contributions	163
Curriculum Vitae	165
Eidesstattliche Erklärung	169

List of abbreviations

[α]^T_D	Specific optical rotation	DEPT	Distortionless enhancement by polarization transfer
¹³C	Carbon 13	DFT	Density functional theory
1D/2D	One dimensional/two dimensional	DIPEA	Diisopropylethylamine
5-HT	5-Hydroxytryptamine (serotonin)	DMAPP	Dimethylallyl pyrophosphate
5-HT_{2A}	5-Hydroxytryptamine receptor subtype 2A	DMAT	Dimethylallyltryptophan
Ac₂O	Acetanhydride	DMF	Dimethylformamide
AChE	Acetylcholinesterase	DMSO	Dimethylsulfoxide
amu	atomic mass unit	DNA	Deoxyribonucleic acid
aq.	aqueous	EC₅₀	Concentration of a compound needed to give half of the response
BChE	Butyrylcholinesterase	eq.	equivalent(s)
Boc	<i>tert</i> -Butoxycarbonyl	ESI	Electrospray ionization
br	broad signal	EtOAc	Ethyl acetate
C₅H₅N	Pyridine	EtOH	Ethanol
calc.	calculated	FA	Formic acid
CD	Circular dichroism	Fmoc	Fluorenylmethoxycarbonyl
CH₂Cl₂	Dichloromethane	FPP	Farnesyl pyrophosphate
CH₃CN	Acetonitrile	FTMS	Fourier transform mass spectrometry
CHCl₃	Chloroform	GGPP	Geranylgeranyl pyrophosphate
CID	Collision induced dissociation	h	hour(s)
CoA	Coenzyme A	HATU	1-[bis(dimethylamino)methylene]-1H-1,2,3-triazolo[4,5-b]pyridinium 3-oxide hexafluorophosphate
coll.	collection		
COSY	Correlated spectroscopy		
d	doublet		
Da	Dalton		

HCD	Higher collision energy dissociation	MVA	Mevalonate
HMBC	Heteronuclear multiple bond correlation	NH₃	Ammonia
HPLC	High performance liquid chromatography	NMDA	<i>N</i> -methyl- <i>D</i> -aspartate
HR	High resolution	NMM	<i>N</i> -methylnorpholine
HSQC	Heteronuclear single quantum correlation	NMR	Nuclear magnetic resonance
IAA	Indole-3-acetic acid (auxin)	NOE	Nuclear Overhauser effect
IC₅₀	Concentration of a compound needed to inhibit the growth by half	NOESY	Nuclear Overhauser enhancement spectroscopy
IR	Infrared	NRP	Non-ribosomal peptides
ITS	Interal transcribed spacer	NRPS	Non-ribosomal peptide synthetase
<i>J</i>	Coupling constant	PK	Polyketides
KSH	Kultursammlung Halle	ppm	parts per million
LC-MS	Liquid chromatography - mass spectrometry	PyBOP	benzotriazol-1-yloxy- -tripyrrolidinophosphonium hexafluorophosphate
LSU	Large subunit	q	quartet
m	multiplet	r.t.	room temperature
<i>m/z</i>	mass-to-charge ratio	rDNA	Ribosomal deoxyribonucleic acid
MeOH	Methanol	R_f	Retention factor
MEP	Methylerythritol phosphate	RNA	Ribonucleic acid
MIC	Minimum inhibitory concentration	ROESY	Rotational frame Overhauser effect spectroscopy
min	minute(s)	s	singlet
MOE	Molecular Operating Environment	sp.	species
MPA	Malt peptone agar	SPE	Solid-phase extract
MS	Mass spectrometry	spp.	species (more than one)
		SPPS	Solid-phase peptide synthesis

t	triplet	TLC	Thin-layer chromatography
<i>t</i>-Bu	<i>tert</i> -Butyl	TMS	Tetramethylsilane
TFA	Trifluoroacetic acid	TOCSY	Total correlation spectroscopy
TFFH	tetramethylfluoroformamidinium hexafluorophosphate	TOF	Time of flight
TIPS	Triisopropylsilane	<i>t</i>_R	retention time
		UV/Vis	Ultraviolet/visible

Summary

The global fungal kingdom is remaining a huge and untapped source of natural products with only approximately 7% of over 1.5 million species occurring worldwide known to science. Fungal secondary metabolites are playing vital roles in the drug discovery and development process, as well as in agricultural application. Thus, the general objective of the present thesis was the isolation and identification of new natural products from fungal sources, focusing on the species of the two genera *Cortinarius* and *Sepedonium*, in order to find potential lead compounds for drug development and agricultural fungicides.

Cortinarius (Pers.) Gray (Agaricales, Basidiomycota) is one of the most species-rich, abundant and widespread ectomycorrhizal agaric genera, with more than 5600 epithets published to date. Herein, the pigment composition of basidiocarps from two *Cortinarius* species was studied under various aspects. Four new diterpenoids, named pyromyxones A-D (3.1-3.4), were isolated from fruiting bodies of *C. pyromyxa*, while three novel purpurascenines A-C (4.1-4.3) together with the new-to-nature 7-hydroxytryptophan (4.4) as well as adenosine (4.5) and riboflavin (4.6) were detected from fruiting bodies of *C. purpurascens*. The absolute configurations of the new pyromyxones A-D (3.1-3.4) and purpurascenines A-C (4.1-4.3) were established with the aid of quantum chemical CD calculation.

In addition, the biosynthesis of purpurascenine A (4.1) was investigated by *in vivo* feeding experiments using ^{13}C labeled sodium pyruvate, alanine, and sodium acetate applied on fruiting bodies of *C. purpurascens* in combination with the analysis of spectroscopic data. In the experiments with [3- ^{13}C]-pyruvate, the dramatic enrichment of ^{13}C was observed, compared to the abundance of ^{13}C in unlabeled control or from the other labeled samples, allowing to propose a biosynthetic route of purpurascenine A (4.1), and consequently also that of purpurascenine B and C (4.2-4.3), *via* a direct Pictet-Spengler reaction between the respective α -keto acid and 7-hydroxytryptophan (4.4).

Furthermore, pyromyxones A (3.1), B (3.2), and D (3.4) were evaluated for their inhibitory effects against gram-positive *Bacillus subtilis* and gram-negative *Aliivibrio fischeri* as well as the phytopathogenic fungi *Botrytis cinerea*, *Septoria tritici* and *Phytophthora infestans*, showing weak antimicrobial activity. Additionally, a new functional reporter gene assay was established indicating the ability of purpurascenine A (4.1) to antagonize the constitutive activity of the 5-HT_{2A} G protein-coupled receptor.

Beside the fruiting bodies, the semi-solid cultures of one *Sepedonium* species were also investigated for their chemical constituents. Two new peptaibols, named ampullosporin F (5.1) and G (5.2), together with two described peptaibols, ampullosporin A (5.3) and peptaibolin (5.4), as well as three known cyclopeptides, chrysosporide (5.5), c(Trp-Ser) (5.6) and c(Trp-Ala) (5.7), have been isolated from the culture of *Sepedonium ampullosporum* Damon KSH534. The total synthesis of 5.1 and 5.2 was carried out on solid-phase to confirm the absolute configuration of all chiral amino acids as L.

Ampullosporins (**5.1–5.3**) were examined for their biological activities. Ampullosporins (**5.1–5.3**) exhibited significant antifungal activity against *B. cinerea* and *P. infestans*, but were inactive against *S. tritici*. Likewise, the peptaibols (**5.1–5.3**) also showed potent anticancer activities against human prostate (PC-3) and colorectal (HT-29) cancer cells, whereby the antiproliferative IC₅₀ values were detected to be by twofold better for ampullosporin F (**5.1**) and G (**5.2**) than for ampullosporin A (**5.3**). Therefore, a molecular docking study was performed *in silico* demonstrating the better binding capacity of **5.1** and **5.2** than **5.3** to hydrophobic clefts of the *N*-methyl-*D*-aspartate receptor corresponding to the structure-activity correlation of the ampullosporins (**5.1–5.3**).

Zusammenfassung

Das Pilzreich ist nach wie vor eine riesige und wenig genutzte Quelle für Naturstoffe, wobei nur etwa 7 % der weltweit über 1,5 Millionen vorkommenden Pilz-Arten bisher überhaupt beschrieben sind. Sekundärmetaboliten aus Pilzen spielen nach wie vor eine wichtige Rolle bei der Entwicklung neuer Arzneimittel und Agrochemikalien. Die vorliegende Dissertationsschrift beinhaltet die Isolierung und Charakterisierung neuer (bioaktiver) Naturstoffe aus Pilzen der Gattungen *Cortinarius* und *Sepedonium*.

Die Gattung *Cortinarius* (Pers.) Gray (Agaricales, Basidiomycota) ist eine der artenreichsten und am weitesten verbreiteten Pilzgattungen. Bisher sind mehr als 5.600 Epitheta in der Literatur genannt. Im Rahmen dieser Arbeit wurden Fruchtkörper zweier *Cortinarius* Arten auf ihre (bioaktiven) Sekundärmetaboliten untersucht. Aus Fruchtkörpern der chilenischen Art *C. pyromyxa* wurden vier neue Diterpenoide, bezeichnet als Pyromyxone A-D (3.1-3.4) isoliert und in ihrer Struktur geklärt. Aus Fruchtkörpern von *C. purpurascens* wurden drei neuen Verbindungen, bezeichnet als Purpurascenine A-C (4.1-4.3), zusammen mit den bekannten Verbindungen Adenosin (4.5) und Riboflavin (4.6) isoliert und charakterisiert. Erstmals aus einer natürlichen Quelle konnte 7-Hydroxytryptophan (4.4) isoliert werden. Die absoluten Konfiguration der neuen Pyromyxone A-D (3.1-3.4) und Purpurascenine A-C (4.1-4.3) wurden mit Hilfe quantenchemischer CD-Berechnungen ermittelt.

Die Biosynthese von Purpurascenin A (4.1) wurde durch *in-vivo*-Verimpfungsexperimente an Fruchtkörpern von *C. purpurascens* mit ¹³C-markierten Biosynthesevorläufern wie Natriumpyruvat, Alanin und Natriumacetat in Kombination mit spektroskopischen Methoden untersucht. Bei den Verfütterungsversuchen mit [3-¹³C]-Pyruvat wurde eine drastische Anreicherung von ¹³C beobachtet. Dies ermöglichte es, einen Biosyntheseweg von Purpurascenin A (4.1) und damit auch für Purpurascenin B und C (4.2-4.3) über eine direkte Pictet-Spengler-Reaktion der korrespondierenden α -Ketosäure mit 7-Hydroxytryptophan (4.4) vorzuschlagen.

Darüber hinaus wurden die Pyromyxone A (3.1), B (3.2) und D (3.4) auf ihre bakterizide Wirkung gegen das gram-positive Bakterium *Bacillus subtilis* und das gram-negative Bakterium *Aliivibrio fischeri* sowie auf ihre fungizide Wirkung gegen die phytopathogenen Pilze *Botrytis cinerea*, *Septoria tritici* und *Phytophthora infestans* untersucht. Hier zeigten die Pyromyxone A (3.1), B (3.2) und D (3.4) nur geringe Aktivitäten. In einem Reporter-gen-Assay zeigte Purpurascenin A (4.1) eine antagonistische Wirkung gegen die konstitutive Aktivität des G-Protein-gekoppelten 5-HT_{2A}-Rezeptors.

Neben Pilzfruchtkörpern wurden auch Kulturen von *Sepedonium ampullosporum* auf ihre Sekundärmetaboliten untersucht. Zwei neue Peptaibole, benannt Ampullosporin F (5.1) und G (5.2) wurden zusammen mit zwei bekannten Peptaibolen, Ampullosporin A (5.3) und Peptaibolin (5.4) isoliert und charakterisiert. Zusätzlich konnten die drei bekannten Cyclopeptide Chrysosporid (5.5), c(Trp-Ser) (5.6) und c(Trp-Ala) (5.7) erstmals in *Sepedonium ampullosporum* nachgewiesen werden. Durch Totalsynthese von 5.1 und 5.2 konnte die absolute Konfiguration der chiralen Aminosäuren als L bestätigt werden.

Die Ampullosporine (**5.1-5.3**) wurden auf ihre biologischen Aktivitäten untersucht. Die Ampullosporine (**5.1-5.3**) zeigten eine signifikante fungizide Aktivität gegen die phytopathogenen Pilze *B. cinerea* und *P. infestans*, waren aber inaktiv gegen *S. tritici*. Weiterhin zeichnen sich die Peptaibole (**5.1-5.3**) durch hohe Aktivitäten gegen menschliche Prostata- (PC-3) und Darmkrebszellen (HT-29) aus, wobei die IC₅₀-Werte für Ampullosporin F (**5.1**) und G (**5.2**) um das doppelte höher lagen als für Ampullosporin A (**5.3**). Wie *in silico* Docking-Studie zeigten, binden **5.1** und **5.2** besser als **5.3** an hydrophobe Bereiche des *N*-Methyl-*D*-Aspartat Rezeptors.

Chapter 1

Introduction and objectives

The global fungal kingdom is remaining a huge and largely untapped source of natural products with only approximately 7% of over 1.5 million species occurring worldwide known to science (Bass and Richards, 2011; Cadelis et al., 2020; Hibbett et al., 2007). In human life, fungi e.g. *Ganoderma* spp. have been used for thousands of years in folk medicine. However, one of the first documented chemical studies on mushroom fruiting bodies, which resulted in the isolation of quinoid pigments, was published just around 1877 by Stahlschmidt and Thörner (Stadler and Hoffmeister, 2015). Since then, fungi have been exploited as the prolific source of secondary metabolites, especially during the recent decades, because of various technological advances (Cadelis et al., 2020).

Fungal secondary metabolites, which mostly possess unique chemical structures, are diverse, and can be classified as polyketides (PK), non-ribosomal peptides (NRP), ribosomal peptides, PK-NRP hybrids, indole alkaloids, and terpenoids, due to their biosynthetic pathway (Bhattarai et al., 2021; Stadler and Hoffmeister, 2015). In addition, fungal natural products also display a broad range of bioactivities e.g. antibiotic, cytotoxic, and antifungal activities (Bhattarai et al., 2021; Cadelis et al., 2020; Chen and Liu, 2017; Gill, 1994, 1996, 1999, 2003; Jiang et al., 2011; Liu, 2005, 2007; Zhou and Liu, 2010). Therefore, fungal natural products, together with their counterparts from plant and bacterial sources, are playing vital roles in the drug discovery and development process, as well as in agricultural application (Beutler, 2019; Bhattarai et al., 2021; Newman and Cragg, 2016, 2020).

One of the earliest prominent example is penicillin, which revolutionized the treatment of bacterial infections. In 2020, the global antibiotics market size was valued at USD 40.7 billion, of which penicillin contributed to the largest proportion of 23.9% and is expected to dominate the market in years afterwards. Penicillin drugs form the first line of choice in treating infections (2021).

Penicillin (i.e. penicillin G **1.1**), the antibiotic blockbuster, was first discovered from a green mold closely related to *Penicillium notatum* by Flemming in 1929 to have promising antibacterial properties, and then isolated by Chain et al. in 1940 (Chain et al., 1940). After that, production methods were improved, and penicillin could be manufactured in mass quantities by 1950 (Bardal et al., 2011). At the same time, since chemical structure of penicillin was established, semi-synthesis works were exploited to expand penicillin from a single drug to a range of semi-synthetic derivatives (e.g. methicillin **1.2** and ampicillin **1.3**). The antibiotic nature of penicillin is because of a β -lactam ring, hence most of the synthetic derivatives were modified on the side chain, leading to four generations of penicillin (Figure 1.1). The aim of modification is to either develop a steric hindrance and stabilize the β -lactam ring breakers or improve compound's permeability through bacterial cell wall, which ultimately contribute to a broad spectrum of activity. The natural and

semi-synthetic penicillin constituted a class of antibacterial drugs, the so-called beta-lactams, which comprise over 60% of antibiotics for human use (Bhattarai et al., 2021; Ribeiro da Cunha et al., 2019).

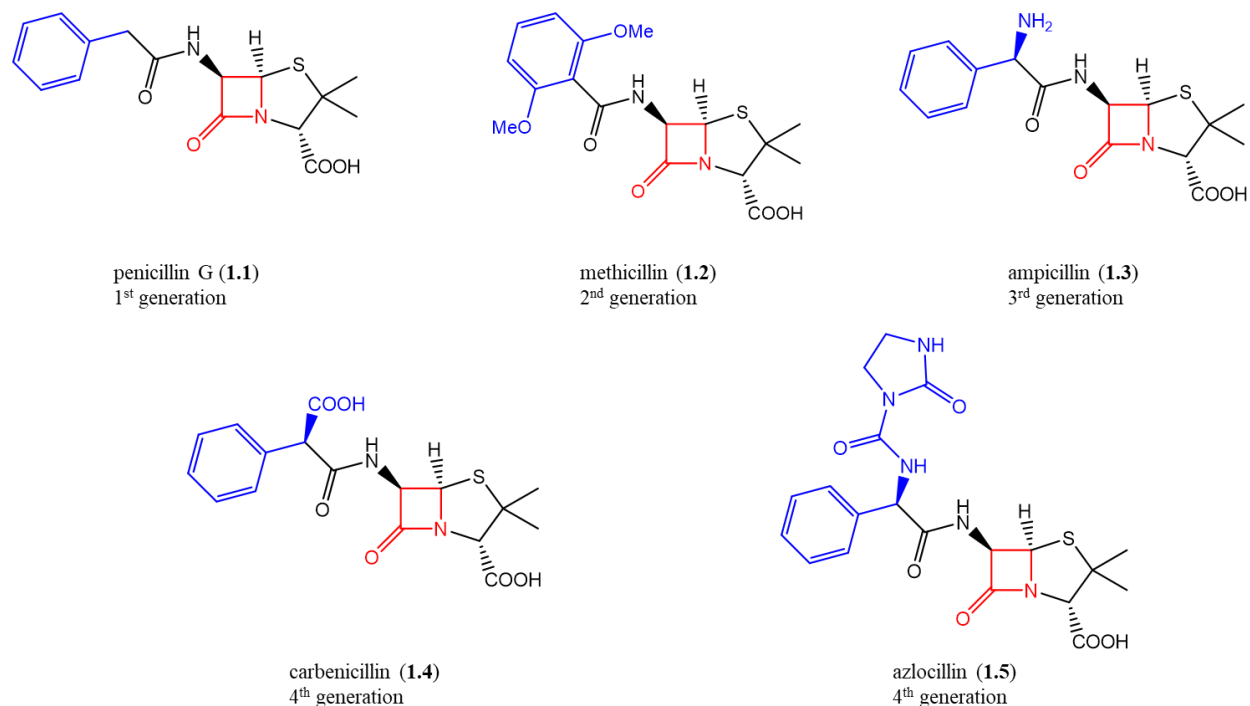
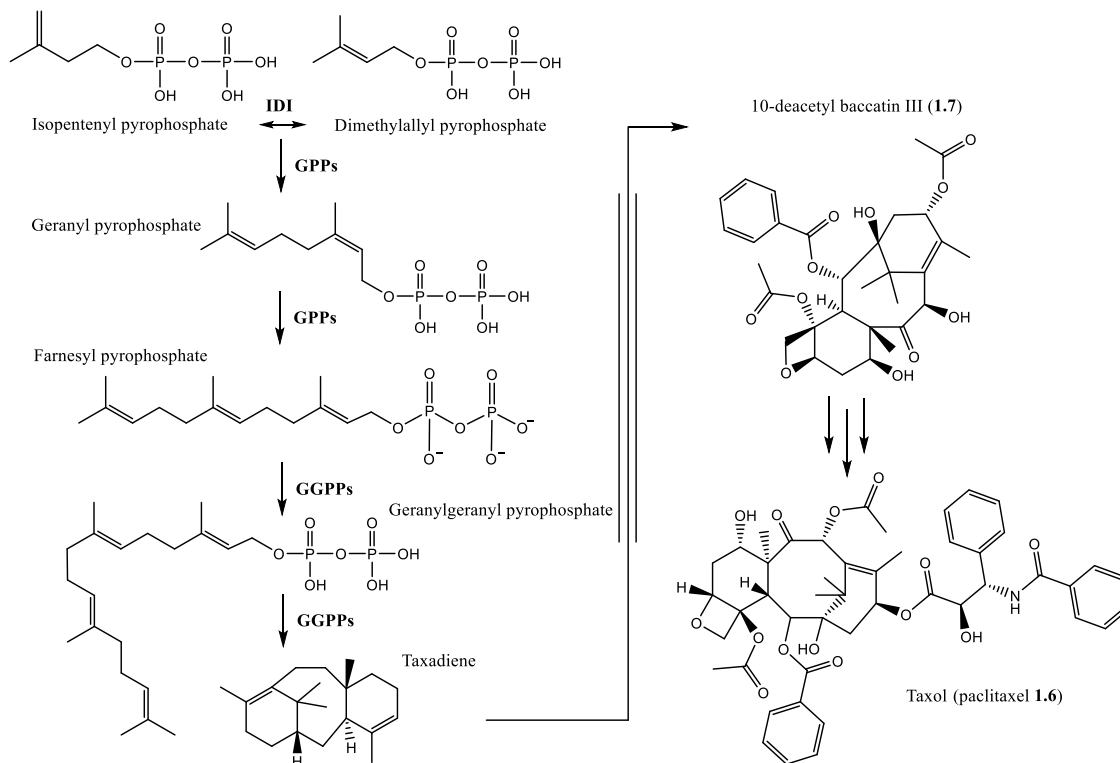


Figure 1.1. Structures of penicillin generations highlighting their featured β -lactam ring (red) and side chain (blue) adapted from Lobanovska and Pilla (2017).

The discovery and development of penicillin have paved the way for tremendous attention on metabolites from microbial origin to identify other antibiotics (Beutler, 2019; Bhattarai et al., 2021). Especially the period between 1940 and 1960 was referred to as the antibiotic golden age, in which most of the currently used antibiotic classes were identified (Ribeiro da Cunha et al., 2019). Thanks to this exploration of antibiotics, infectious diseases were optimistically believed to be a controlled health public issue (Ribeiro da Cunha et al., 2019). Unfortunately, antibiotic resistance has recently become a severe global health crisis as the consequence of multiple factors, ranging from high rates of antimicrobial prescriptions over antibiotic mismanagement (self-medication or interruption of therapy) to large-scale antibiotics which are used as growth promoters in livestock farming (Rather et al., 2017; Ribeiro da Cunha et al., 2019). Therefore, there is increasing need for continuous research to discover new antibiotics that hopefully can swing the war on infectious diseases back in our favor.

Beside penicillin, taxol also nicely illustrates the contribution of fungi as sources to enhance production of bioactive compounds to create drugs against cancer. Taxol global sales have been in the millions since it began to be marketed, reaching USD 1.5 billion in 2000. Over the years, taxol

and its alternative formulations (e.g. the nano-albumin-bound paclitaxel abraxane) have become one of the most-used agents for cancer treatment (Gallego-Jara et al., 2020).



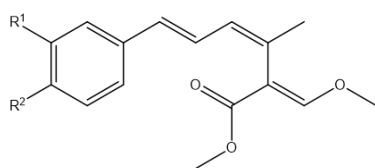
Scheme 1.1. Taxol biosynthetic pathway, adapted from Gallego-Jara et al. (2020). IDI: Isopentenyl diphosphate isomerase; GPPs: geranylpyrophosphate synthase; GGPPs: geranylgeranylpyrophosphate synthase.

Taxol (**1.6**), which has the generic name paclitaxel, was first isolated from stem bark of the Pacific yew tree *Taxus brevifolia* as a potent anticancer drug by Hartwell in the 1960s (Gallego-Jara et al., 2020). The presence of this active compound was also reported from several other *Taxus* species like *T. cuspidata* and *T. baccata*. However, the yield of taxol from natural extracts is very low that to treat a patient with 2g of taxol, four trees have to be felled (Gallego-Jara et al., 2020).

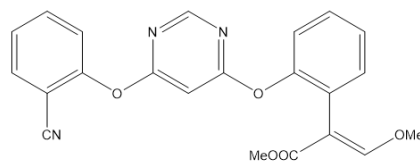
In 1971, the structure of taxol was established as a tricyclic diterpenoid with a complex chemical structure bearing a taxane ring by Wani et al. (Wani et al., 1971). This opened hopes for increasing the production of taxol by synthesis. Unfortunately, due to the complexity of the structure, the synthesis routes for taxol are normally very complex and expensive (Gallego-Jara et al., 2020; Wessjohann, 1998). Semi-synthesis was also considered. For instance, the semi-synthesis starting with taxol intermediates such as 10-deacetyl baccatin III (**1.7**), which could be isolated from the European yew *Taxus baccata* in a 10 times greater amount than taxol, was able to increase the yield of synthesis, but its production still relied on yew trees (Elsohly et al., 1994).

Alternatively, microbial fermentation is so far the most promising approach for cheaper and higher yield of taxol (Gallego-Jara et al., 2020). Particularly, isolation and identification of a taxol-producing endophytic fungus is a very prospective and feasible approach for the large-scale production of taxol (Kumar et al., 2019). To date there have been around 200 endophytic fungi reported as taxol producers (Gallego-Jara et al., 2020). For example, taxol production was identified from some *Aspergillus* sp.: *A. flavipes* (185 $\mu\text{g/L}$), *A. aculeatinus* (1.3 mg/L), *A. oryzae* (95 $\mu\text{g/L}$) (Gallego-Jara et al., 2020). And recently, the highest production of taxol (1.6 mg/L) was observed from *A. fumigatus*, an endophytic fungus isolated from Indian *Taxus* sp. by Kumar et al. in 2019 (Kumar et al., 2019). The main challenge of this approach is the loss of taxol productivity after multiple subcultures. This could be faced by optimizing the fermentation conditions (Gallego-Jara et al., 2020), while further research on endophytic fungi to identify the more productive source of taxol is obviously necessary.

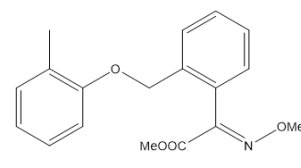
While the vital roles of fungal secondary metabolites in drug development is undeniable, their use as leading structures for agricultural fungicides should not be neglected. The excellent example for this is strobilurin, the mother compound of a new important class of agricultural fungicides. The discovery of strobilurin was inspired by a group of natural β -methoxyacrylates (Bartlett et al., 2002). The first and simplest natural substances of this class are strobilurin A (**1.8**) and B (**1.9**) isolated from the pinecones fungus *Strobilurus tenacellus* in 1977, which were found to be highly active against yeast and various filamentous fungi (Anke et al., 1977). Although these natural substances were not yet suitable as agricultural fungicides, their structures and properties had provided a useful starting point for many research programs from industrial companies and research institutes to develop strobilurins as fungicides (Bartlett et al., 2002; Sauter et al., 1999). Until 1999, well over 30,000 strobilurin analogues were synthesized (e.g. azoxystrobin **1.10**, kresoxim-methyl **1.11**) (Sauter et al., 1999), and the sales of strobilurin related fungicides reached approximately USD 620 million, representing over 10% of the global fungicide market in this year, only 4 years after the first sale (Bartlett et al., 2002). Especially the biggest contribution (USD 415 million) was from sales of azoxystrobin (**1.10**) itself, recording this compound as the world's biggest selling fungicide in the year 1999 (Bartlett et al., 2002). Nowadays, strobilurin fungicides are globally used to combat white mold, rot, early and late leaf spot, rusts and rice blast for cereals, turfgrass, grapevines, potatoes, and fruit, nut and vegetable crops (Bartlett et al., 2002; Feng et al., 2020).



strobilurin A (**1.8**) $R^1 = R^2 = \text{H}$
 strobilurin B (**1.9**) $R^1 = \text{OCH}_3, R^2 = \text{Cl}$



azoxystrobin (**1.10**)



kresoxim-methyl (**1.11**)

However, like the other fungicides, the intensive/large-scale application of strobilurin related fungicides in agricultural fields has increased both resistance and contamination of the surrounding

soil/water environments (Feng et al., 2020). To tackle the latter problem, the degradation of strobilurins was considered. Strobilurins can be degraded either through biotic or abiotic approaches, of which the microbial degradation using microorganisms like *Bacillus*, *Pseudomonas*, *Klebsiella*, *Stenotrophomonas*, *Arthrobacter*, *Rhodanobacter*, *Cupriavidus*, and *Aphanoascus* is emerging as an efficient and cost-effective bioremediation (Feng et al., 2020). However, strobilurins, as well as agricultural fungicides in general, should be used carefully and according to the manufacturer's recommendations. Also, there is still a need for better and/or environmentally friendlier fungicidal agents, which are highly likely inspired by natural sources such as fungi and plants.

Thus, the general objective of the present thesis was the isolation and identification of new natural products from fungal sources, focusing on the species of the two genera *Cortinarius* and *Sepedonium*, in order to find potential lead compounds for drug development and agricultural fungicides. Specifically, the main aim of this thesis is to deal with the following topics:

- Isolation and characterization of new compounds from fruiting bodies of two *Cortinarius* species as well as cultures of a *Sepedonium* species using chromatographic and spectroscopic methods
- Identification of absolute configuration of isolated compounds by means of CD and quantum chemical calculation and/or synthesis
- Study on the biosynthetic pathways of some selected compounds by feeding labelled precursors to the fungi
- Evaluation of selected biological activities of isolated compounds, concentrating on antibacterial, anticancer and antifungal activities, as well as activities suggested by literature to be relevant to related structures.

References

- Anke, T., Oberwinkler, F., Steglich, W., Schramm, G., 1977. The strobilurins-new antifungal antibiotics from the Basidiomycete *Strobilurus tenacellus*. *J Antibiot* 30, 806-810.
- Bardal, S. K., Waechter, J. E., Martin, D. S., 2011. Chapter 9: Drug discovery and evaluation. In: Applied pharmacology. Elsevier/Saunders, St. Louis, pp. 1-470.
- Bartlett, D. W., Clough, J. M., Godwin, J. R., Hall, A. A., Hamer, M., Parr-Dobrzanski, B., 2002. The strobilurin fungicides. *Pest Manag Sci* 58, 649-662.
- Bass, D., Richards, T. A., 2011. Three reasons to re-evaluate fungal diversity 'on Earth and in the ocean'. *Fungal Biol Rev* 25, 159-164.
- Beutler, J. A., 2019. Natural products as a foundation for drug discovery. *Curr Protoc Pharmacol* 86, 1-28.
- Bhattacharai, K., Bhattacharai, K., Kabir, M. E., Bastola, R., Baral, B., 2021. Fungal natural products galaxy: Biochemistry and molecular genetics toward blockbuster drugs discovery. *Adv Genet* 107, 193-284.

- Cadelis, M. M., Copp, B. R., Wiles, S., 2020a. A review of fungal protoilludane sesquiterpenoid natural products. *Antibiotics* (Basel) 9, 928.
- Chain, E., Florey, H. W., Gardner, A. D., Heatley, N. G., Jennings, M. A., Orr-Ewing, J., Sanders, A. G., 1940. Penicillin as a chemotherapeutic agent. *Lancet* 236, 226-228.
- Chen, H. P., Liu, J. K., 2017. Secondary metabolites from higher fungi. In: Progress in the chemistry of organic natural products 106, Springer International Publishing AG, Cham, pp. 1-201.
- Elsohly, H. N., Croom, E. M., el-Kashoury, E. S., elSohly, M. A., McChesney, J. D., 1994. Taxol content of stored fresh and dried *Taxus* clippings. *J Nat Prod* 57, 1025-1028.
- Feng, Y., Huang, Y., Zhan, H., Bhatt, P., Chen, S., 2020. An overview of strobilurin fungicide degradation: current status and future perspective. *Front Microbiol* 11, 389.
- Gallego-Jara, J., Lozano-Terol, G., Sola-Martinez, R. A., Canovas-Diaz, M., de Diego Puente, T., 2020. A compressive review about taxol: history and future challenges. *Molecules* 25, 5986.
- Gill, M., 1994. Pigments of fungi (Macromycetes). *Nat Prod Rep* 11, 67-90.
- Gill, M., 1996. Pigments of fungi (Macromycetes). *Nat Prod Rep* 13, 513-528.
- Gill, M., 1999. Pigments of fungi (Macromycetes). *Nat Prod Rep* 16, 301-317.
- Gill, M., 2003. Pigments of fungi (Macromycetes). *Nat Prod Rep* 20, 615-639.
- Hibbett, D. S., Binder, M., Bischoff, J. F., Blackwell, M., Cannon, P. F., Eriksson, O. E., Huhndorf, S., James, T., Kirk, P. M., Lucking, R., Thorsten Lumbsch, H., Lutzoni, F., Matheny, P. B., McLaughlin, D. J., Powell, M. J., Redhead, S., Schoch, C. L., Spatafora, J. W., Stalpers, J. A., Vilgalys, R., Aime, M. C., Aptroot, A., Bauer, R., Begerow, D., Benny, G. L., Castlebury, L. A., Crous, P. W., Dai, Y. C., Gams, W., Geiser, D. M., Griffith, G. W., Gueidan, C., Hawksworth, D. L., Hestmark, G., Hosaka, K., Humber, R. A., Hyde, K. D., Ironside, J. E., Koljalg, U., Kurtzman, C. P., Larsson, K. H., Lichtwardt, R., Longcore, J., Miadlikowska, J., Miller, A., Moncalvo, J. M., Mozley-Standridge, S., Oberwinkler, F., Parmasto, E., Reeb, V., Rogers, J. D., Roux, C., Ryvarden, L., Sampaio, J. P., Schussler, A., Sugiyama, J., Thorn, R. G., Tibell, L., Untereiner, W. A., Walker, C., Wang, Z., Weir, A., Weiss, M., White, M. M., Winka, K., Yao, Y. J., Zhang, N., 2007. A higher-level phylogenetic classification of the Fungi. *Mycol Res* 111, 509-547.
- Jiang, M. Y., Feng, T., Liu, J. K., 2011. N-containing compounds of Macromycetes. *Nat Prod Rep* 28, 783-808.
- Kumar, P., Singh, B., Thakur, V., Thakur, A., Thakur, N., Pandey, D., Chand, D., 2019a. Hyper-production of taxol from *Aspergillus fumigatus*, an endophytic fungus isolated from *Taxus* sp. of the Northern Himalayan region. *Biotechnol Rep* (Amst) 24, 00395.
- Liu, J. K., 2005. N-containing compounds of Macromycetes. *Chem Rev* 105, 2723-2744.
- Liu, J. K., 2007. Secondary metabolites from higher fungi in China and their biological activity. *Drug Discov Ther* 1, 94-103.
- Lobanovska, M., Pilla, G., 2017. Penicillin's discovery and antibiotic resistance: lessons for the future? *Yale J Biol Med* 90, 135-145.
- Newman, D. J., Cragg, G. M., 2016. Natural products as sources of new drugs from 1981 to 2014. *J Nat Prod* 79, 629-661.
- Newman, D. J., Cragg, G. M., 2020. Natural products as sources of new drugs over the nearly four decades from 01/1981 to 09/2019. *J Nat Prod* 83, 770-803.

- Rather, I. A., Kim, B. C., Bajpai, V. K., Park, Y. H., 2017. Self-medication and antibiotic resistance: Crisis, current challenges, and prevention. *Saudi J Biol Sci* 24, 808-812.
- Grand view research, 2021. Antibiotics market size, share & trends analysis report by drug class (cephalosporin, penicillin, fluoroquinolone, macrolide, carbapenem, aminoglycoside, sulfonamide, 7-ACA), by action mechanism, and segment forecasts, 2021 - 2028. *Grand view research*, 1-120; <https://www.grandviewresearch.com/industry-analysis/antibiotic-market>, last access 11.04.2022.
- Ribeiro da Cunha, B., Fonseca, L. P., Calado, C. R. C., 2019. Antibiotic discovery: where have we come from, where do we go? *Antibiotics* (Basel) 8, 45.
- Sauter, H., Steglich, W., Anke, T., 1999. Strobilurins: evolution of a new class of active substances. *Angew Chem Int Ed* 38, 1328-1349.
- Stadler, M., Hoffmeister, D., 2015. Fungal natural products-the mushroom perspective. *Front Microbiol* 6, 127.
- Wani, M. C., Taylor, H. L., Wall, M. E., Coggon, P., McPhail, A. T., 1971. Plant antitumor agents. VI. The isolation and structure of taxol, a novel antileukemic and antitumor agent from *Taxus brevifolia*. *J Am Chem Soc* 93, 2325-2327.
- Wessjohann, L. A., 1998. The first total syntheses of taxol. In: Organic synthesis highlights III. Wiley-VCH Verlag GmbH. Weinheim, Germany, pp. 295-305.
- Zhou, Z. Y., Liu, J. K., 2010. Pigments of fungi (Macromycetes). *Nat Prod Rep* 27, 1531-1570.

Chapter 2

General introduction

2.1 Genus *Cortinarius* (Pers.) Gray

2.1.1 Taxonomy

Cortinarius (Pers.) Gray (Agaricales, Basidiomycota) is one of the most species-rich, abundant and widespread ectomycorrhizal agaricaceous genera. It is characterized by the fugacious veil forming a fine cob-web (“cortina”) between the stipe and pileus margin, as well as by the production of ornamented, cinnamon brown to fulvous basidiospores (Kirk et al., 2008). Another feature of *Cortinarius* spp. is the ectomycorrhizal association with a large diversity of trees and shrubs belonging to families like Betulaceae, Caesalpiniaceae, Cistaceae, Dipterocarpaceae, Fagaceae, Myrtaceae, Pinaceae, Rhamnaceae, Rosaceae Salicaceae and Nothofagaceae, as well as some herbaceous plants in the families Cyperaceae and Polygonaceae (Bidaud et al., 2021; Frøslev et al., 2006; Niskanen, 2008; Xie et al., 2021). For the genus *Cortinarius*, there are more than 5,600 epithets named to date (<http://www.indexfungorum.org>). Most of these species were described from Europe (over 1900 species), followed by North America (more than 500 species) and South America (around 270 species) (Bidaud et al., 2021; Garnica et al., 2002; Liimatainen et al., 2020; Salgado Salomon et al., 2021; San-Fabian et al., 2018; Soop, 2021; Soop et al., 2019). Besides, *Cortinarius* spp. were also known from Central America, Australasia, and Asia (e.g. Horak, 1983; Horak and Wood, 1990; Kuhdorf et al., 2016; Miyauchi, 2001; Naseer et al., 2020; Peintner et al., 2003; Soop, 2017; Xie et al., 2021; Xie et al., 2020).



Figure 2.1. Selected *Cortinarius* species. (A) *C. balteatocumatilis*; (B) *C. diemii*; (C) *C. sulfureomyceilatus*. (Photos: Dr. Norbert Arnold)

The taxonomy of genus *Cortinarius* is very challenging and remaining controversially discussed. According to macro-morphological and ecological data, different infrageneric classification systems have been proposed for *Cortinarius*. Moser in Singer (1986) classified *Cortinarius* into eight subgenera (*Cortinarius*, *Phlegmacium*, *Myxacium*, *Telamonia*, *Leprocycbe*, *Sericeocybe*, *Cystogenes*, and *Paramyxacium*; Figure 2.2) and regarded *Dermocybe* as a separate genus (Singer, 1986). However, there is underestimated or misinterpreted phenotypic plasticity and morphological convergence across the genus, resulting in the publication of many synonymous

names and misidentifications, and consequently leading to the acceptance of many unnatural higher taxa (e.g. Frøslev et al., 2006; Garnica et al., 2003a; Garnica et al., 2003b; Liimatainen et al., 2014; Niskanen et al., 2011; Peintner et al., 2004).

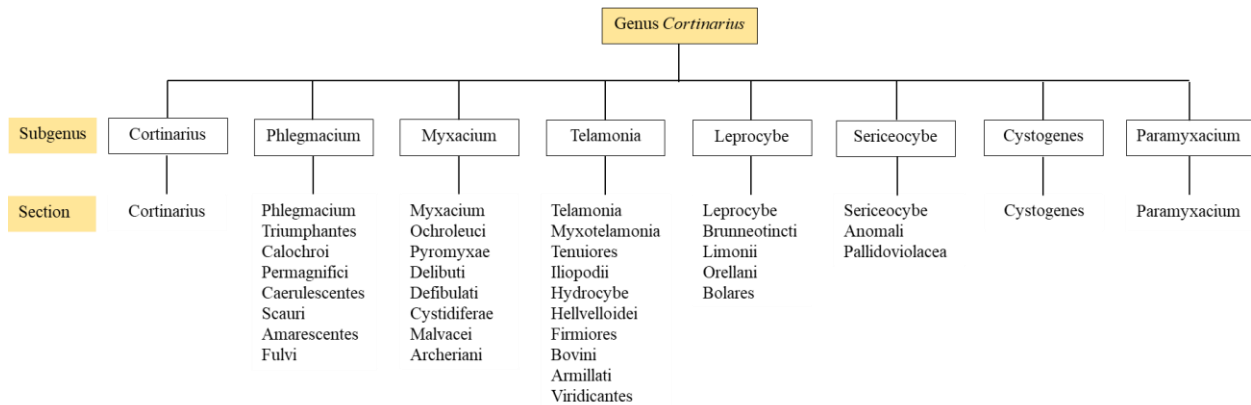


Figure 2.2. Classification of the genus *Cortinarius* according to Singer (1986).

Starting with the discovery of polymerase chain reaction, molecular phylogenetics primarily based on two rDNA loci (i.e. ITS and LSU) and two protein-coding genes (i.e. RNA polymerase II largest subunit RPB1 and DNA replication licensing factor MCM7) have been used to study the taxonomy of fungi (e.g. Asemaninejad et al., 2016; Garnica et al., 2016; Liimatainen et al., 2020; Soop et al., 2019; Stefani et al., 2014). The phylogenetic studies using molecular markers has been proven highly effective for species identification in the genus *Cortinarius*, and showed that many traditional infrageneric groups of this genus (e.g. *Phlegmacium* and *Myxadium*) are not monophyletic (e.g. Frøslev et al., 2006; Froslev et al., 2007; Garnica et al., 2016; Garnica et al., 2003b; Liimatainen et al., 2014; Peintner, 2008; Peintner et al., 2004; Soop et al., 2019). Nevertheless, even for ITS, the most widely used gene region for studies at species rank, no consensus of the limits between the intra- and inter-specific variation exists to date, meaning that taxa can be overlooked or simply underestimated at low cut-off thresholds used for delimiting species (Garnica et al., 2016; Niskanen et al., 2011). Also, ITS sequences did not always differentiate the morphologically accepted species. For instance, *C. atrovirens* and *C. ionocholorus*, or *C. xanthophyllus* and *C. claroflavus* have distinguishable morphological characters but exhibited identical ITS regions, respectively (Froslev et al., 2007; Garnica et al., 2005). Therefore, neither phylogenetic nor morphological/ecological data alone is sufficient for recognizing natural units in the genus *Cortinarius*.

In addition, very recently Liimatainen and coworkers have revised the classification of the genus *Cortinarius* using a genomic approach (Liimatainen et al., 2022). *Cortinarius*, the only genus of Cortinariaceae family, is now divided into ten different genera – *Cortinarius*, *Phlegmacium*, *Thaxterogaster*, *Calonarius*, *Aureonarius*, *Cystinarius*, *Volvanarius*, *Hygronarius*, *Mystinarius*, and *Austrocortinarius*. However, there is time needed to know whether this revised classification is appropriate for this huge genus including its undescribed taxa.

Nevertheless, there is hope that a more accurate classification of the genus can probably be achieved by conducting integrated morphological/ecological, molecular and so far neglected

chemical studies on secondary metabolites covering the whole systematic spectrum of *Cortinarius* species.

2.1.2 Secondary metabolites and their biological activities

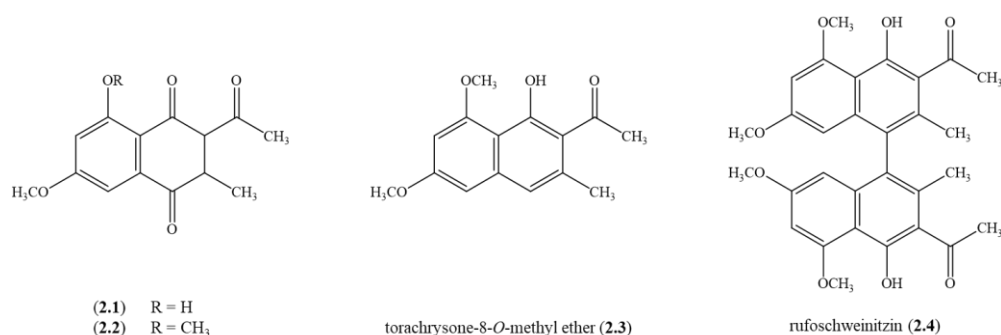
Given the huge number of species, the genus *Cortinarius* chemically remains poorly investigated. For European taxa, the chemical structures, properties, and biosynthetic pathways were mainly studied by the Steglich group based on well-defined species (Gill and Steglich, 1987). For Australasian *Cortinarius* species, the chemical components and their bioactivities were mainly reported by Gill and coworkers (Beattie et al., 2010; Gill, 1994, 1996, 1999, 2003; Keller et al., 2002; Nicholas et al., 2001). However, little is known from the rest of this worldwide distributed genera (i.e. South American and Asian *Cortinarius* species).

The secondary metabolites from *Cortinarius* species are very diverse. The majority of them belongs to the class of polyketides, including naphthoquinones, monomeric and dimeric pre-anthraquinones and anthraquinones, as well as xanthone chromophores. The second biggest group of *Cortinarius* secondary metabolites are nitrogen heterocycles, comprising β -carboline, *N*-glucosyl-indole derivatives, bipyridine *N*-dioxides, dithiopyridine *N*-oxide metabolites, polyenes, quinolones, isoquinolines, sphingolipids, and pigments with 3,6,9-trimethylazuleno[4,5-*b*]furan-2,7-dione moiety. Other constituents include a nitroaromatic compound, an aromatic aminoaldehyde, styrylpyrones, terpenoids, and iron (III) complexes (Chen and Liu, 2017; Gill, 1994, 1996, 1999, 2001, 2003; Gill and Steglich, 1987; Jiang et al., 2011; Liu, 2005). Nevertheless, only a minor fraction of these compounds were known for their biological activities. Besides the major group polyketides, the chemical structure and biological activity as well as the biosynthesis (where possible) of selected nitrogen heterocycles and terpenoids will be discussed in this chapter due to their role as chemical markers of the genus or their relationship with compounds described in this thesis.

2.1.2.1 Polyketides

The genus *Cortinarius* is a great source of polyketide pigments, mostly consisting of heptaketides, octaketides, and nonaketides, which biosynthetically arise from the acetate-malonate pathway.

In *Cortinarius* species, heptaketides are quite rare. So far, only two naphthoquinones (**2.1**) and (**2.2**), together with the ketone torachryson-8-*O*-methyl ether (**2.3**) and its dimer rufoschweinitzin (**2.4**) were isolated from the mature fruit bodies of *C. rufo-olivaceus* (Gill and Steglich, 1987; Thiele et al., 2020). Compound (**2.3**) is also present in cultures of *C. orichalceus* (Gill and Steglich, 1987).



In contrast, octaketide (pre-)anthraquinone pigments, found in great variety in toadstools of *Cortinarius* species, form the largest and most important compound class providing valuable aid to the taxonomy of this genus. A plausible biosynthetic relationship between various pre-anthraquinones and anthraquinones was proposed, and confirmed by works of Steglich and Gill groups (Figure 2.3) (Gill, 2001; Gill and Steglich, 1987).

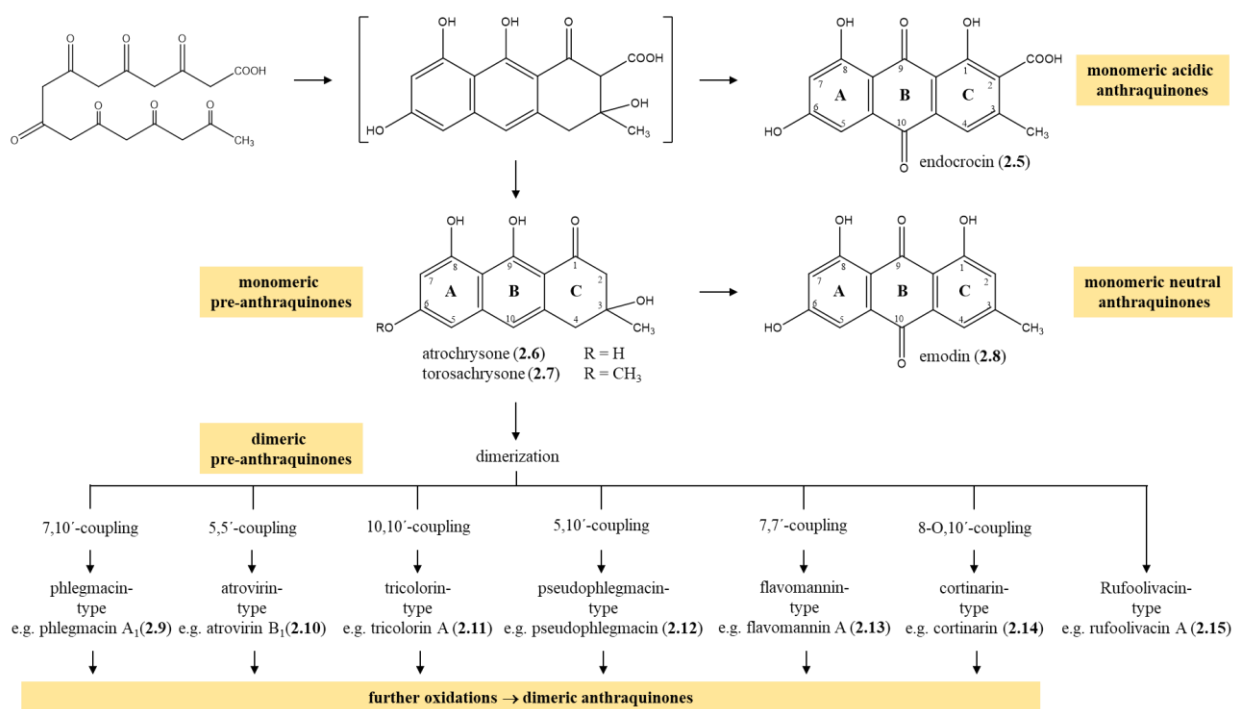
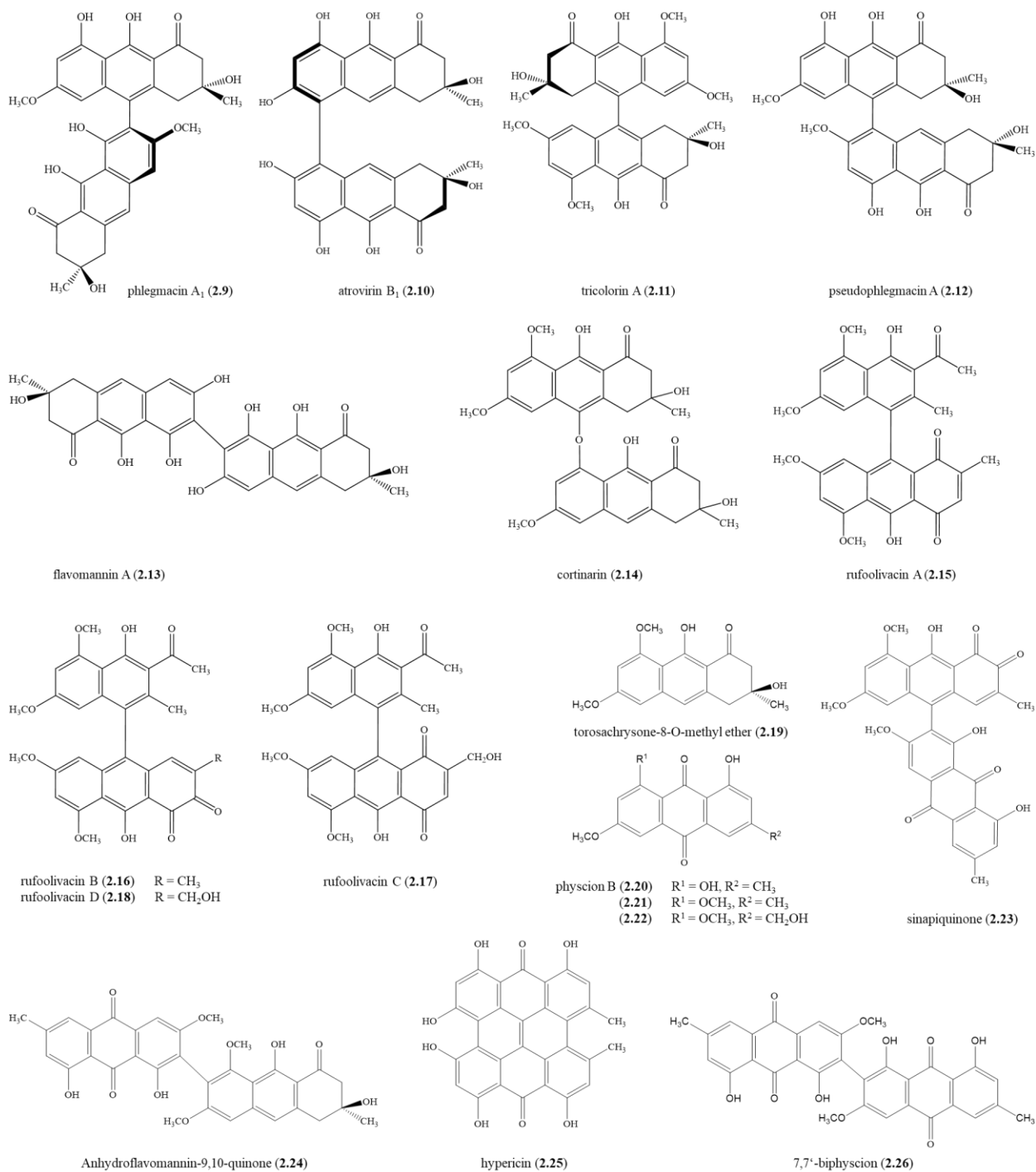


Figure 2.3. Biosynthesis of octaketide derivatives from *Cortinarius* species according to Gill and Steglich (1987).

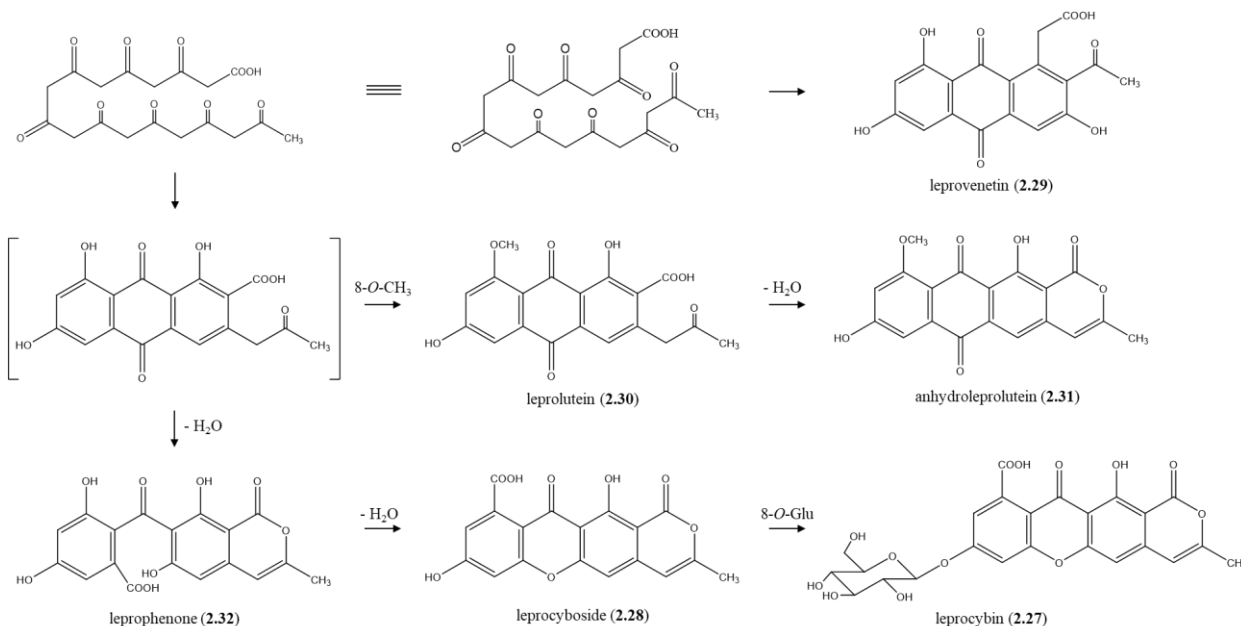
Among the dimeric pre-anthraquinones, rufoolivacin-type compounds (e.g. rufoolivacins A (2.15) – D (2.18)) are unique and seems to be characteristic for the mushroom *C. rufo-olivaceus* (Gao et al., 2010; Gill and Steglich, 1987; Zhang et al., 2009). Instead of two pre-anthraquinone units, their structures are composed of a ketone torachryson-8-*O*-methyl ether (2.3), which was also isolated from this species, and a 1,2- or 1,4-anthracenequinone. Besides, other octaketides including torosachryson-8-*O*-methyl ether (2.19), phycion (2.20), 6,8-dimethoxy-3-methylanthraquinone (2.21) and citreosein-6,8-dimethyl ether (2.22), sinapiquinone (2.23), and

anhydroflavomannin-9,10-quinone (**2.24**) were also present from a species named *C. rufolivaceus* (Gao et al., 2010).



However, nonaketides, similar to heptaketides, were mainly observed from some European and North American *Cortinarius* species belonging to subgenus *Leprocybe* (e.g. *C. cotoneus*, *C. melanotus*, and *C. venetus*). The xanthone chromophores leprocybin (**2.27**) and its aglycone, leprocyboside (**2.28**), are responsible for the fluorescence of different fungi in subgenus *Leprocybe* under UV light. Together with the isolation of other leprocybin-related constituents (i.e.

leprovenetin (**2.29**), leprolutein (**2.30**), anhydroleprolutein (**2.31**), and leprophenone (**2.32**) from this subgenus, a biosynthesis inter-relationship of these *Leprocyebe* pigments was confidently assumed (Figure 2.2) (Gill and Steglich, 1987).



Polyketides with anthraquinone core structure are not only abundant in species of genus *Cortinarius* but also in other fungal genera and other natural sources such as plants, lichens, and marine sources, leading to various biological activities documented (Malik et al., 2021). For example, the monomeric anthraquinones emodin (**2.8**) and physcion (**2.20**) strongly inhibit the growth of the Gram-positive bacterium *Staphylococcus aureus* (IC₅₀ 0.7 and 23 µg/mL, respectively) and exhibited potency against the Gram-negative bacterium *Pseudomonas aeruginosa* (IC₅₀ 1.5 and 2.0 µg/mL, respectively) (Beattie et al., 2010). Furthermore, emodin (**2.8**) also displays a broad range of activities such as anticancer, cytotoxic, DNA and RNA precursor incorporation inhibitory, protein tyrosine kinase inhibitory, phytotoxic, mutagenicity inhibitory, anti-trichomonal, and antifungal activity (Ogwuru and Adamczeski, 2000). Likewise, the dimeric anthraquinone hypericin (**2.25**), a multifunctional agent in drug and medicinal applications, exhibit antidepressive, antineoplastic, antitumor and antiviral activity (Kubin et al., 2005). In addition, hypericin (**2.25**) and 7,7'-biphyscion (**2.26**) were recently shown to be promising novel therapeutic and diagnostic agent in treatment and detection of cancer due to their photodynamic activation of free radical production (Hammerle et al., 2021a; Hammerle et al., 2021b; Kubin et al., 2005).

2.1.2.2 Nitrogen heterocycles

Nitrogen heterocycles represent the second biggest group, of secondary metabolites from *Cortinarius* species, but to a far lesser extent than polyketides. They can be classified as β-carbolines, *N*-glucosyl-indole derivatives, nephrotoxic bipyridine *N*-dioxides, dithiopyridine *N*-oxide metabolites, polyenes, quinolones, isoquinolines, sphingolipids, and pigments with 3,6,9-

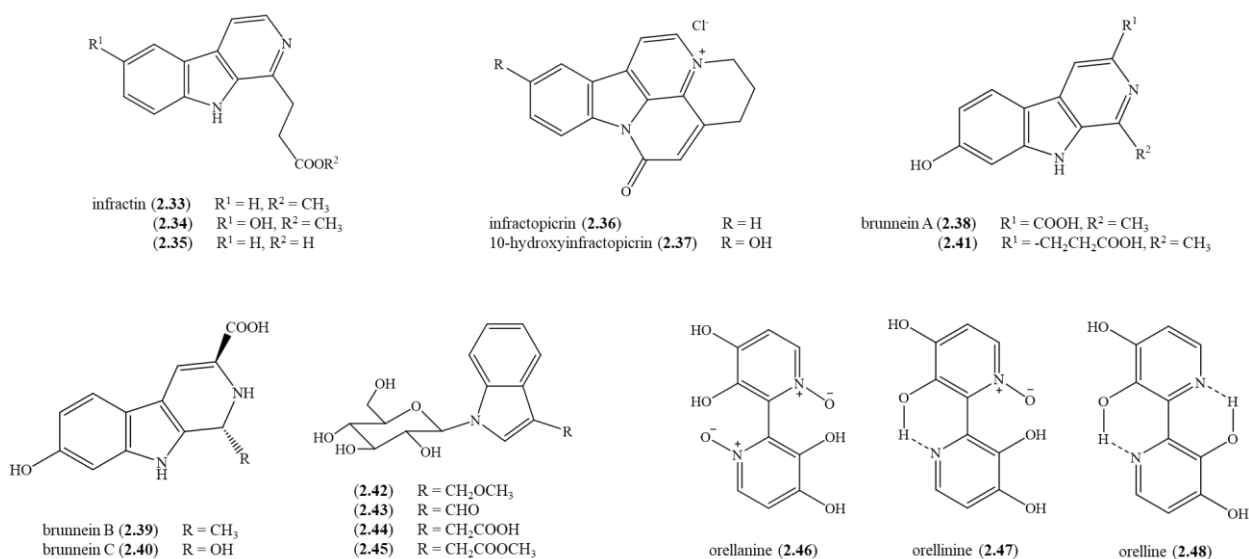
trimethylazuleno[4,5-b]furan-2,7-dione structure. Among them, the first five compound classes and their biological behaviors are discussed here.

Five β -carboline alkaloids, including three fluorescent compounds infractin (**2.33**), 6-hydroxyinfractin (**2.34**), and β -carboline-1-propionic acid (**2.35**) together with the bitter principle infractopicrin (**2.36**) and its derivative 10-hydroxyinfractopicrin (**2.37**), are responsible for the fluorescence and bitter taste of the flesh of the toadstool *C. infractus* (Geissler et al., 2010; Gill and Steglich, 1987; Steglich, 1994). Both compounds **2.36** and **2.37** exhibit acetylcholinesterase (AChE)-inhibitory effect (IC_{50} 9.7 and 12.7 μ M, respectively) in the similar capacity as the approved drug against Alzheimer's disease, galanthamine (IC_{50} 8.7 μ M). Interestingly, for butyrylcholinesterase (BChE) no inhibition of infractopicrin (**2.36**) and 10-hydroxyinfractopicrin (**2.37**) could be detected up to the concentration of 100 μ M, indicating their higher selectivity than galanthamine (IC_{50} 24.4 μ M against BChE), and hence, their potential for drugs against Alzheimer's disease (Geissler et al., 2010).

A fluorescence-guided isolation of the methanol extract of *C. brunneus* had led to the purification of further four β -carbolines, named brunnein A (**2.38**) – C (**2.40**) and 3-(7-hydroxy-9H- β -carboline-1-yl)propanoic acid (**2.41**). Brunnein A (**2.38**) shows very low inhibition against both AChE and BChE (IC_{50} >100 μ M) and no cytotoxicity against human prostate (PC-3) cancer cells (Teichert et al., 2007).

Besides, four *N*-glucosyl-indole alkaloids (i.e. *N*-1- β -glucopyranosyl-3-methoxymethyl-1*H*-indole (**2.42**), *N*-1- β -glucopyranosyl-1*H*-indole-3-carbaldehyde (**2.43**), *N*-1- β -glucopyranosyl-1*H*-indole-3-acetic acid (**2.44**), and methyl *N*-1- β -glucopyranosyl-1*H*-indole-3-acetate (**2.45**)) were also isolated in the methanol extract of *C. brunneus*. Due to its structural similarity to 1*H*-indole-3-acetic acid (IAA; auxin), a plant-growth regulator, compound **2.44** was tested in a modified *Arabidopsis thaliana* tap root elongation assay, but shows no auxin-like activity. This suggests that compound **2.44** may either act as an inactive transport or storage form of IAA in the fungus *C. brunneus*, or it is merely a detoxification product when IAA is no longer needed (Teichert et al., 2008).

The mushroom genus *Cortinarius* (e.g. *C. orellanus* and *C. speciosissimus*) is also well-known and well-documented for the toxicity. Toxins causing the toxicity of these species were assigned as the mono- and bis-*N*-oxides named orellanine (**2.46**) and orellinine (**2.47**) (Antkowiak and Gessner, 1979). The former nephrotoxic substance orellanine (**2.46**) eliminated oxygen by slow heating at 150 °C or sunlight to form orellinine (**2.47**), and finally the nontoxic bipyridyl orelline (**2.48**), which exists as a minor constituent of the mushrooms *C. orellanus* and *C. speciosissimus* (Antkowiak and Gessner, 1985). Orellanine (**2.46**) was also detected in other *Cortinarius* species like *C. orellanoides* and *C. rainierensis* (Gill and Steglich, 1987).



In 2003, based on the presence of 3,4-dihydroxypyridine-2-carboxylic acid (**2.49**) and 3-hydroxy-1*H*-pyridine-4-one (**2.50**) in the acidified methanolic extract of *C. orellanus* as well as the isolation of orellanine-4,4'-di- β -D-glucopyranoside (**2.51**) after feeding *C. speciosissimus* with [U - ^{13}C]glucose, the biosynthesis of orellanine (**2.46**) starting from anthranillic acid could be unambiguously proposed by Spiteller and coworkers (Figure 2.5) (Spiteller et al., 2003).

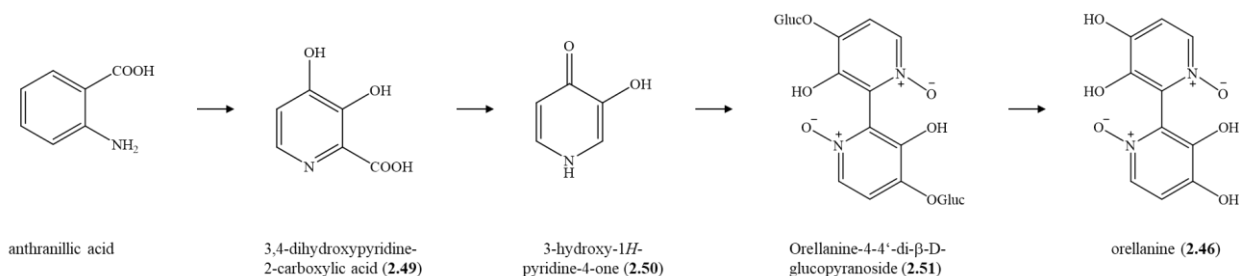


Figure 2.5. Biosynthesis of orellanine (**44**) according to Spiteller et al. (2003).

2.1.2.3 Terpenoids

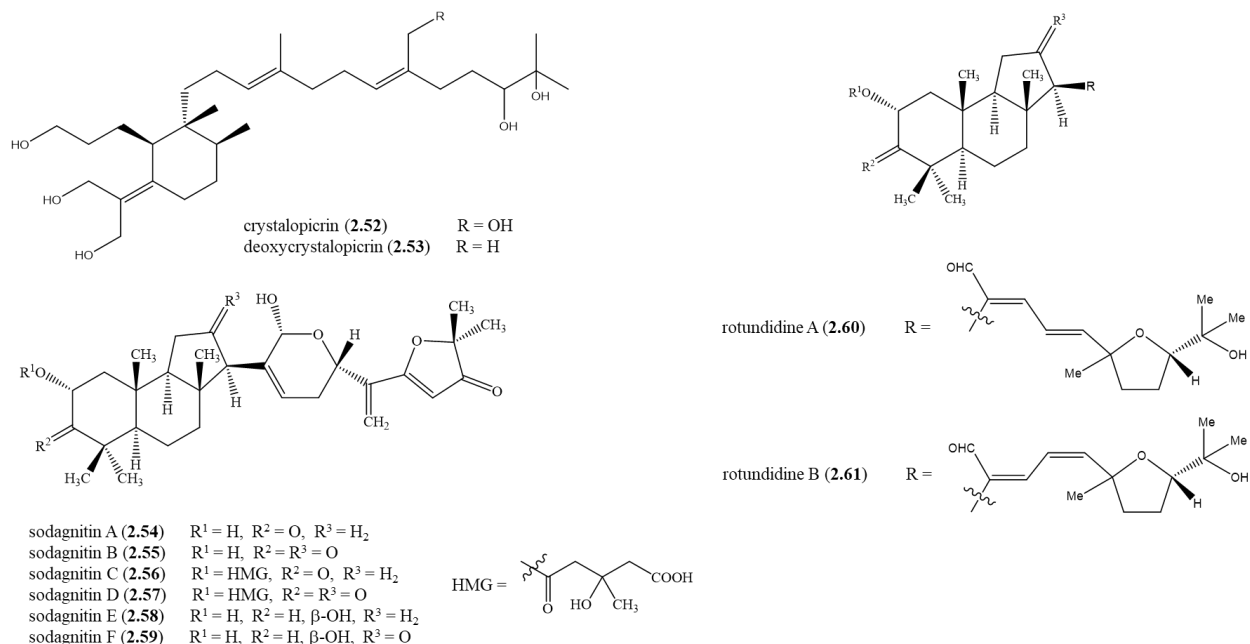
Terpenoids is the most diverse compound class in higher fungi (e.g. *Russula* and *Garnoderma*) not only because of their overall number but also the range of structural scaffolds (Chen and Liu, 2017). Nonetheless, this type of compounds is seldom found from the genus *Cortinarius*, with only three reports so far (Gill, 1999; Nicholas, 1998; Sontag et al., 1999; Steglich et al., 1990).

Firstly, the extremely bitter triterpenoid crystallopicrin (**2.52**) and its deoxy derivative (**2.53**) were isolated from the viscid caps of *C. crystallinus*, *C. croceo-coeruleus*, and *C. vibratilis*. This bitter principle (**2.52**) may act as the protector of these fungi from insects and other fungivores (Steglich et al., 1990).

Secondly, six sesquiterpene chromogens, named sodagnitins A (**2.54**) – F (**2.59**), were detected to be responsible for the remarkable ink-red color reaction of the toadstools *C. sodagnitus*,

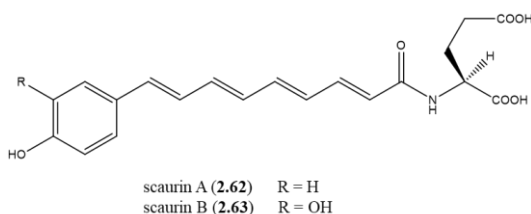
C. fulvoincarnatus, and *C. acuatorum* when treated with aqueous base (Sontag et al., 1999). Sodagnitin A and C exhibit antimicrobial activity against *Bacillus subtilis*, *Bacillus brevis* and *Nematospora coryli* at concentration from 5 µg/disc, as well as cytotoxicity against L 1210 tumor cells at concentration higher than 1 and 5 µg/mL, respectively (Sontag et al., 1999).

Finally, two other sesquiterpenoids, rotundidines A (2.60) and B (2.61), were isolated from the cytotoxic extract of *C. rotundisporus*. Both compounds showed moderate cytotoxicity against the P388 cell line (IC₅₀ 150 and 120 ng/mL, respectively) and against the host cells of the antiviral, with a visual description of type 12 (large scuffy cells) (Nicholas, 1998).



2.1.2.4 Polyenes

Until now, polyene pigments documented in *Cortinarius* are only scaurins A (2.62) and B (2.63) from the fruiting bodies of *C. scaurus*, a fungus that grows abundantly in *Sphagnum* bogs in the European Alps (Gill, 2003).



2.1.3 *Cortinarius pyromyxa* M. M. Moser and E. Horak

Cortinarius pyromyxa M. M. Moser & E. Horak (Cortinariaceae) was described first in two collections from Argentinian Patagonia (Moser and Horak, 1975), and then in one collection from Chile (Garrido, 1988). In all reported collections, fruiting bodies of *C. pyromyxa* grow under *Nothofagus dombeyi* (Figure 2.6A). The gelatinous cap is 7 – 33 mm in diameter, and ochre-brown

in the center reducing to ochre towards the margin. The sticky cylindrical stem is 40 – 73 mm long, 3 – 10 mm thick, and ochre but orange fronting the base. The yellow lamellae is mixed, crowded, and is bent back and forth towards the margin. By treating with KOH, the cap, stem and flesh turn to dark red-brown (Figure 2.6B). The reddish brown and elliptic to almond-shaped spores are 9-10 μm long and 5-6 μm wide, while the basidia are 30-47 μm long and 6-7 μm wide.



Figure 2.6. *Cortinarius pyromyxa* M. M. Moser & E. Horak. (A) Basidiocarps (Araucania, Chile); (B) the cap, stem and flesh turn dark red-brown after treatment with KOH.

Due to its macro- and microscopic characters, *C. pyromyxa* was considered typical for section *Pyromyxa* within subgenus *Myxacium*, which also includes the Australian species *C. erythraeus* and *C. sinapicolor* (Moser and Horak, 1975). On the one hand, later studies showed that *C. erythraeus*, which exclusively enters ectomycorrhiza with *Eucalyptus* instead of *Nothofagus*, actually does not belong to the section *Pyromyxa* (Horak and Wood, 1990). Recently, investigated ITS sequences indicated that the Australian species *C. erythraeus* should be inserted into section *Delibuti* within the subgenus *Myxacium* (Garnica et al., 2016). On the other hand, ITS sequence data of *C. sinapicolor* fairly resemble that of some species of subgenus *Phlegmacium* (e.g. *C. ponderosus* and *C. effundens*) (Garnica et al., 2016). Interestingly, the occurrence of dimeric dihydroanthracenone pigments in fruiting bodies of *C. sinapicolor* also suggests a relation between this mushroom and species of the subgenus *Phlegmacium* (Elsworth et al., 1999). Therefore, *C. pyromyxa* seems to be monotypic in section *Pyromyxa* within subgenus *Myxacium*.

2.1.4 *Cortinarius purpurascens* Fr.

Fruiting bodies of *C. purpurascens* Fr. usually grow in coniferous forest (*Abies*, *Cedrus*, *Picea*, *Pinus*) on limestone, but also in deciduous forest (*Castanea*, *Fagus*, *Quercus*) and under *Cistus*, on non-calcareous soils, in southern and central Europe as well as in Scandinavia (Figure 2.7A) (Saar et al., 2014). The slimy cap can be up to 10 cm in diameter and gray-blue, purple-blue, purple-brown or olive-brown in color. The blue-purple and white-flecked bulbous stipe is up to 9 cm long and 2.2 cm thick, with a purple to violet velum on tuber margin towards the base often found for young fruit bodies. By pressing or cutting, the stipe turns purple (Figure 2.7A). The crowded lamellae are violet-blue to violet-gray when young, turning violet on pressure. The mushroom has a mild taste and honey-like to mushroom-like odor. Treating the flesh with KOH causes no color

reaction or, sometimes, change to yellow-brownish, whereas the cap turns brown or even red tones. Adding Lugol causes wine reddish to purplish color on the cap and flesh (Figure 2.7B). The flesh showed blue-green fluorescence under UV light ($\lambda = 366 \text{ nm}$) (Figure 2.7C-D). The elliptical or almond-shaped spores are $7.2\text{--}8.8 \mu\text{m}$ long, $4.5\text{--}5.3 \mu\text{m}$ wide, and strong to coarse black (Saar et al., 2014).



Figure 2.7. *Cortinarius purpurascens* Fr. (A) basidiocarps in Bavaria, Germany, the stem turns violet by pressing (middle basidiocarp) or cutting (right basidiocarp); (B) the flesh (right basidiocarp) turns violet after treatment with Lugol; (C) the flesh under white light; (D) the flesh under UV light ($\lambda = 366 \text{ nm}$).

C. purpurascens Fr. was inserted in “Sektion Laeticolores” as “Kreis Purpurascens” within the subsection Purpurascentes, which also contains the “Kreis Scaurum” (Moser, 1960). However, molecular genetic analyses have shown that these “Kreises” are two well-defined monophyletic groups within the genus *Cortinarius* (Garnica et al., 2005). Therefore, *C. purpurascens* is totally different from the considered sister species, *C. scaurus*. In 1990s, *C. scaurus* was inserted in the newly established section Scauri, while *C. purpurascens* was transferred to the section Subpurpurascentes within the subgenus Phlegmacium in 2009 (Bidaud et al., 2009; Brandrud et al., 1990-1998). However, in 2014 *C. purpurascens* was assigned to section Purpurascentes (within subgenus Phlegmacium) together with other four species from Europe, three species from New Zealand, and seven from Australia (Saar et al., 2014).

Very recently, in the revised classification of genus *Cortinarius*, was *C. purpurascens* renamed as *Thaxterogaster purpurascens* and inserted into genus *Thaxterogaster*, subgenus Scauri, which comprises the previous Scauri and Purpurascentes sections (Liimatainen et al., 2022).

2.2 Genus *Sepedonium* Link

2.2.1 Taxonomy

The anamorphic genus *Sepedonium* (teleomorph Hypocrea, Ascomycota) was established by H.F. Link in 1809 and restricted to mold-like fungal parasites. Nowadays, species of this anamorphic genus is limited to mycophylic fungi with two synanamorphs including aleurioconidia (for persistence) and phialoconidia (for fast propagation) (Sahr, 1999). *Sepedonium* species distributed worldwide (e.g. Europe, America, Australasia and Asia) (Rogerson and Samuels, 1989; Sahr, 1999). The preferred hosts of *Sepedonium* species are genera within Boletales, (e.g. *Boletus*, *Xerocomus*, and *Paxillus*), where infections can cause up to total necrosis and usually form large quantities of yellow aleurioconidia (Neuhof et al., 2007). Interestingly, once infected by *Sepedonium* species, host fruiting bodies are rarely colonized by other parasitic microorganisms, not even by those known to be also associated to Boletales, suggesting the role of secondary metabolites produced by the mycoparasite as chemical defense (Yurkov et al., 2012).



Figure 2.8. *Sepedonium* infection of (A) *Xerocomus chrysenteron*, (B) *Paxillus involutus*, and (C) *Boletus loyita* in nature. (Photos Dr. Norbert Arnold)

Traditionally, *Sepedonium* species are classified according to morphological features like the shape, size and ornamentation of conidia and aleurioconidia, respectively, the architecture of conidiophores as well as *in vitro* culture characteristics. For instance, the type species *S. chrysospermum* (Bull.) Fr. is characterized by two types of spores: ellipsoidal to cylindrical, colorless, smooth-walled phialoconidia and globose, bright yellow, 14-21 μm in diameter aleurioconidia with a coarsely verrucose spore wall, both formed on verticillate conidiophores (Helfer, 1991; Mitova et al., 2006; Sahr, 1999). However, these observed morphological features are not always distinctive and mostly require the examination of live cultures (Damon, 1952; Helfer, 1991; Sahr, 1999). In recent years, as a complement to classical taxonomy, DNA-sequence-based molecular phylogeny has been evaluated and proven a valuable tool to investigate the taxonomic position of *Sepedonium* species, whereby new species like *S. laevigatum* and *S. loyorum*

were detected (Binimelis-Salazar et al., 2021; Otto et al., 2016b; Sahr, 1999). So far, 58 epithets were named for genus *Sepedonium* in Index Fungorum (<http://www.indexfungorum.org>).

2.2.2 Secondary metabolites and their biological activities

In natural habitats, it was observed that *Boletales* fruiting bodies primarily infected by *Sepedonium* spp. are hardly ever colonized by other secondary fungal parasites competing with *Sepedonium* for host nutrients (Otto et al., 2016a). This intriguing monopoly of *Sepedonium* species is probably due to their secondary metabolites, which may act as chemical defenders against other microorganisms. Therefore, the secondary metabolites from genus *Sepedonium* are of interest to not only chemists but also pharmacists. Nevertheless, there are only few reports on chemical constituents of this genus to date, leading, however, to the identification of various compound classes such as peptaibols (Dornberger et al., 1995; Hulsman et al., 1998; Kronen et al., 2001; Mitova et al., 2008; Neuhof et al., 2007; Otto et al., 2016a; Otto et al., 2016b; Ritzau et al., 1997; Stadler, 2001), cyclic peptides (Mitova et al., 2006), tropolones (Divekar et al., 1965; Divekar and Vining, 1964), anthraquinones (mono-, dimeric) (Shibata et al., 1957), isoquinoline alkaloids (Quang et al., 2010), and azaphilones (Closse and Hauser, 1973). Because peptaibols and cyclic peptides are related to compounds described in this thesis, the next part of this chapter is dedicated to them.

2.2.2.1 Peptaibols

As stated by Degenkolb and co-workers, pept''Aib''ols are linear peptides, which *i*) have a molecular weight between 500 and 2,200 Da, with 5–20 amino acid residues; *ii*) possess a high content of the marker α -aminoisobutyric acid (Aib); *iii*) are featured by the presence of non-proteinogenic amino acids (e.g. isovaline (Iva) and *trans*-4-hydroxy-L-proline (Hyp)) (Figure 2.9); *iv*) carry an acylated *N*-terminus, while the *C*-terminus is reduced to a 2-amino alcohol (e.g. leucinol (Leuol) and tryptophanol (Trpol)) (Degenkolb et al., 2003; Degenkolb and Brückner, 2008).

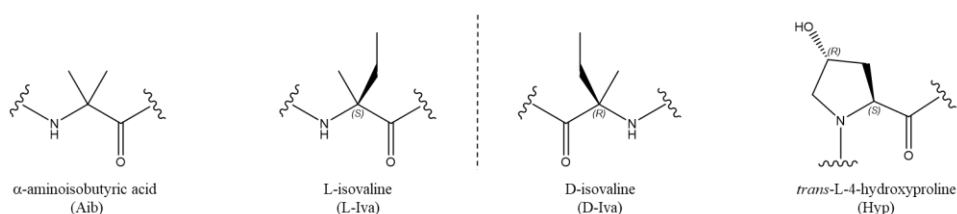


Figure 2.9. Selected non-proteinogenic amino acids occurring in peptaibols.

So far, approximately 1,000 peptaibols were solely isolated from filamentous fungi (Iijima et al., 2017; Jiao et al., 2018; Kai et al., 2018; Katoch et al., 2019; Kim et al., 2021; Marik et al., 2018; Momose et al., 2019; Neumann et al., 2015; Rawa et al., 2021a; Rawa et al., 2021b; Rivera-Chavez et al., 2017; Sica et al., 2017; Touati et al., 2018; van Bohemen et al., 2021; Wu et al., 2021; Zhang et al., 2021). The majority (over 80%) of peptaibols was described for *Trichoderma* species (Speckbacher and Zeilinger, 2018), while the rest of this compound class was found from other

genera like *Sepedonium*, *Gliocladium*, *Acremonium*, *Paecilomyces*, *Emericellopsis*, *Clonostachys*, *Tolyposcladium*, and *Stilbella* (Neuhof et al., 2007). According to their main chain length, peptaibols can be classified into three categories: short-chain (5–10 residues), medium-chain (11–16 residues), and long-chain (17–20 residues) sequences (Degenkolb and Brückner, 2008).

Although only several reports on chemical constituents of *Sepedonium* species were published, 32 peptaibols were isolated and divided into three categories mentioned above (for peptaibol sequences, see Table A1, appendix).

Peptaibolin (**2.64**), the shortest peptaibol so far with only 5 residues, was found in cultures of *Sepedonium* sp. HKI-0117 and *S. ampullosporum* HKI-0053, which showed moderate antimicrobial activity against Gram-positive bacterium *Bacillus subtilis* (MIC 100 µg/ml) and yeast *Candida albicans* (MIC 100 µg/ml) (Hulsmann et al., 1998).

The medium-chain sequences were detected from fungal cultures of *S. ampullosporum*, *S. chalcipori*, and *S. chrysospermum*. Firstly, eight characteristic 15-residue peptaibols, named ampullosporins A (**2.65**) – D (**2.68**) and E₁ (**2.69**) – E₄ (**2.72**), besides peptaibolin (**2.64**), were isolated from cultures of *S. ampullosporum* HKI-0053 (Kronen et al., 2001; Ritzau et al., 1997). Among them, ampullosporin A (**2.65**) – D (**2.68**) displayed neuroleptic-like activity in mice and acted as inducers of pigment formation by the fungal strain of *Phoma destructiva* in the same manner as described for the immunosuppressant drug cyclosporin A (Kronen et al., 2001; Ritzau et al., 1997). Secondly, six 15-member sequences, including chalciporins A (**2.73**) and B (**2.74**), tylopeptins A (**2.75**) and B (**2.76**), together with chilenopeptins A (**2.77**) and B (**2.78**), were detected from solid-state cultures of different strains of *S. chalcipori* and closely related taxa (Neuhof et al., 2007; Otto et al., 2016b). It is noteworthy that tylopeptins A (**2.75**) and B (**2.76**) were first described for the Boletales basidiomycete *Tylopilus neofelleus* (Lee et al., 1999), but turned out to be produced by the ascomycete *S. chalcipori* parasitizing on Boletales hosts (Neuhof et al., 2007). Compounds **2.75** – **2.78** showed strong antifungal activity against *Botrytis cinerea* and *Phytophthora infestans* (IC₅₀ 5.3 – 17.8 µM) (Otto et al., 2016b). In addition, tylopeptins A (**2.75**) and B (**2.76**) also exhibited inhibitory effects against different Gram-positive bacteria like *Bacillus subtilis*, *Staphylococcus aureus*, and *Corynebacterium lilium* (Lee et al., 1999). Finally, the bioactivity-guided isolation on the cytotoxic crude extract of *S. chrysospermum* CANU E609 yielded a medium-chain peptaibol, named chrysaibol (**2.79**), which displayed cytotoxic effect against the P388 murine leukemia cell line (IC₅₀ 6.6 µM) and potent antibacterial activity against *Bacillus subtilis* (IC₅₀ 1.5 µM) (Mitova et al., 2008).

Furthermore, the long-chain peptaibols were derived from *S. chrysospermum*, *S. microspermum* and *S. tulasneanum*. Firstly, four 19-residue chrysospermins A (**2.80**) – D (**2.83**) were found from *S. chrysospermum* (teleomorph *Apiocrea chrysosperma*), showing antimicrobial activity against bacteria like *Bacillus subtilis*, *Staphylococcus aureus*, and *Klebsiella pneumoniae*, as well as fungi *Sporobolomyces salmonicolor* (Dornberger et al., 1995). Secondly, the bioassay-guided isolation on fungal cultures of had led to the identification of a series 19-member peptaibols named microspermins A (**2.84**) – H (**2.91**), which strongly inhibited herpes simplex virus type 1 (HSV1) (IC₅₀ 0.5 – 2.0 µM) (Stadler, 2001). Finally, Otto et al. (2016) isolated tulasporins A (**2.92**) – D

(**2.95**) with 19 amino acid residues from semi-solid cultures of *S. tulasneanum*. Compounds **2.92** – **2.95** exhibited potent fungal inhibitory effects against *Botrytis cinerea* and *Phytophthora infestans* (IC₅₀ 3.7 – 22.6 μM).

Similar to other microbial peptides, peptaibols are biosynthesized by non-ribosomal peptide synthetases (NRPS), enzymes that are characterized by the core domains for adenylation, thiolation and condensation, producing the peptide in one by one steps (Figure 2.10) (Llewellyn and Spencer, 2007; Speckbacher and Zeilinger, 2018). After their synthesis outside of the ribosome, peptaibols frequently pass extensive secondary modifications. Especially, unlike most peptide synthetases with a thioesterase domain at the C-terminus, peptaibol synthetases possess a dehydrogenase domain. This dehydrogenase leads to the formation of the amino alcohol, which presents at the C-terminus as a defining characteristic of peptaibols (Fuente-Núñez et al., 2013).

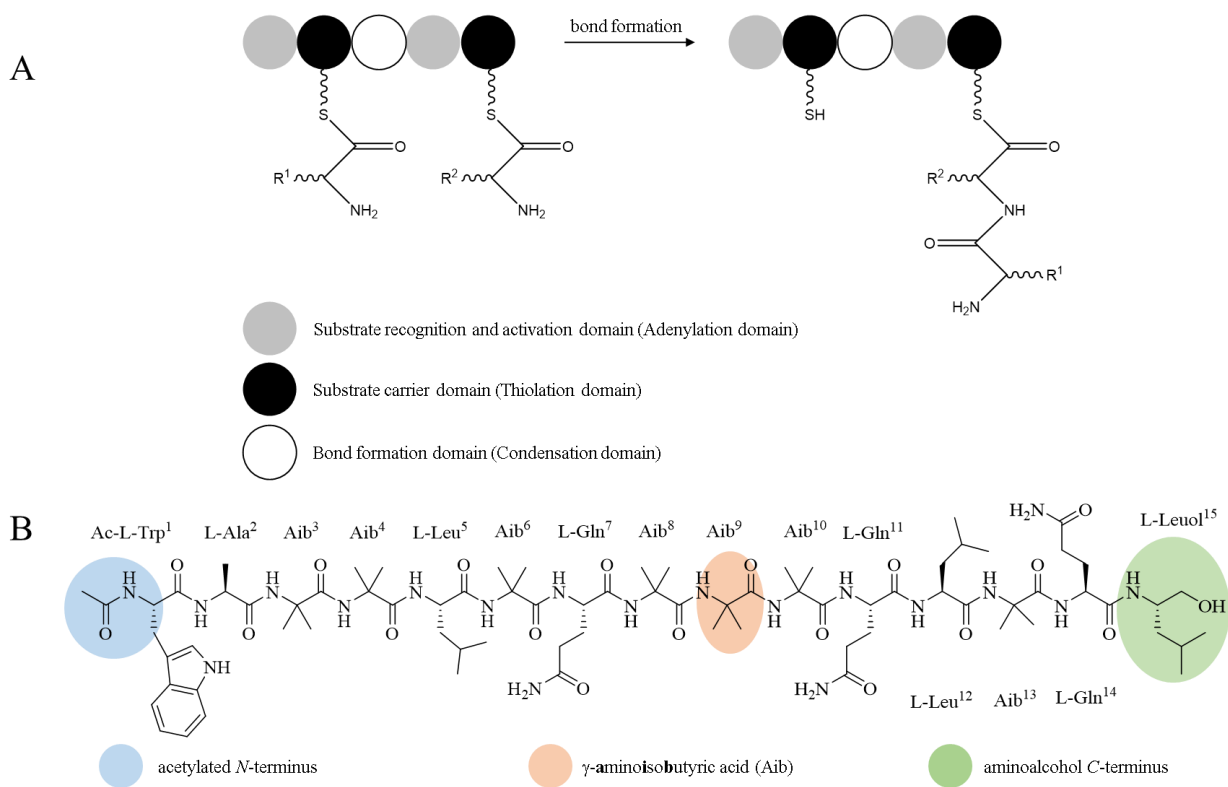
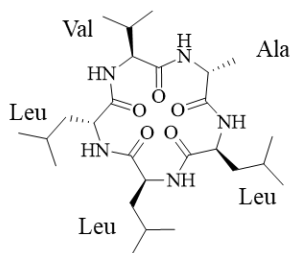


Figure 2.10. (A) *in vivo* posttranslational synthesis of peptaibols by nonribosomal peptide synthetases (NRPS) according to Llewellyn and Spencer (2007) as well as Fuente-Núñez et al., (2013); (B) the structure of ampullosporin A (**2.65**) highlighting typical features of a peptaibol.

2.2.2.2 Cyclic peptides

Until now, the occurrence of cyclic peptides in *Sepedonium* was only found for the cyclic pentapeptide chrysosporide (**2.96**) from the cultures of *S. chrysopermum* CANU E609, a fungus isolated from a degraded basidiomycete sporophore collected in New Zealand (Mitova et al., 2006). Compound **2.96** displayed moderate cytotoxic activity against the murine leukemia cell line (IC₅₀ 33.4 μM) (Mitova et al., 2006).



chrysosporide (2.96)

2.2.3 Solid-phase synthesis of peptaibols

Under *in vitro* conditions, peptaibols could be synthesized via classical peptide synthetic strategies, which can be carried out either entirely in solution or in solid phase. The solid-phase peptide synthesis (SPPS), implemented by Merrifield in 1963, has become the preferred method due to its possibility to use robotic peptide synthesizer (Hjørringgaard et al., 2009). The first requirement of this automatic technique is to find a suitable resin – a solid polymer that is insoluble in all of the solvents used during synthetic process – which is not only able to carry the growing peptide chain but also convenient to be filtered and washed free of reagents and by-products (Merrifield, 1963). Furthermore, the resin also needs to bear a functional group to which the first protected amino acid could be firmly linked by a covalent bond. The most suitable resin is a chloromethylated copolymer of styrene and divinylbenzene (Merrifield, 1963). In addition, Boc- and Fmoc- are commonly used as the *N*- α -protecting groups of amino acids, of which Fmoc-approach is devoid of hazardous hydrofluoric acid usage and, thus, becoming popular nowadays (Hjørringgaard et al., 2009).

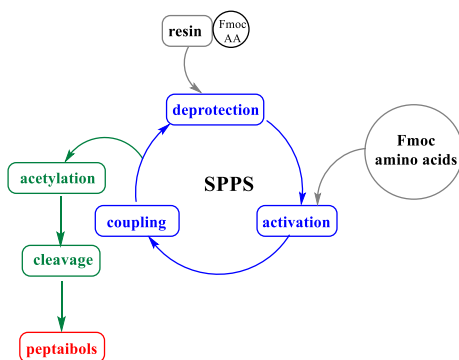


Figure 2.11. The solid-phase based synthetic route of peptaibols, adapted from Kitson (2014).

As illustrated in Figure 2.11, the synthetic protocol of peptaibols starts with the attachment of the *C*-terminus amino acid to the resin. In this step, amino alcohol is used to achieve the *C*-terminus amino alcohol characterizing peptaibol sequences. After that, the route continues with the SPPS cycle, which can be divided into three steps: (a) the Fmoc-protected amino group is deprotected (**deprotection**); (b) the next amino-protected amino acid is treated with TFFH to form an activated acyl fluoride from the carboxylic acid (**activation**); (c) the activated amino acid is coupled to the amino group of the resin-bound amino acid (**coupling**). This cycle is repeated until

the desired peptide length is achieved. Later on, the *N*-terminus is acetylated using acetic anhydride (**acetylation**) followed by final deprotection and **cleavage** from the resin.

2.2.4 Membrane activity of peptaibols

Many peptaibols (e.g. compounds **2.64** – **2.68**, **2.75** – **2.83**) were known for their antimicrobial activity, which seems to lie in their ability to permeabilize lipid bilayers. Peptaibols can not only form transmembrane pores and carriers, but also modify the membrane surface in a surfactant-like mode. When pores are formed in membranes, they generally take the form of voltage-gated ion channels, which might be formed by several peptaibol molecules (from 6 to 12 units) creating a bundle (Duclouhier et al., 2004). This bundle is then inserted into the membrane, creating a hydrophilic channel through its center (Figure 2.12A) (Fuente-Núñez et al., 2013).

The basis for the antimicrobial activity of peptaibols can be explained by the leakage of cytoplasmic material through the peptaibol-induced channels. For example, alamethicin (**2.97**), one of the most extensively studied peptaibols isolated from cultures of *Trichoderma viride*, follows the so-called “barrel-stave model” to form amphipathic α -helical structure in biological membranes (Figure 2.12B) (Brogden, 2005; Leitgeb et al., 2007). The alamethicin (**2.97**) molecules attach to, aggregate and insert into oriented bilayers. While the hydrophobic regions of the peptides contact with the core of bilayer lipid, the hydrophilic regions create the inner region of the pore.

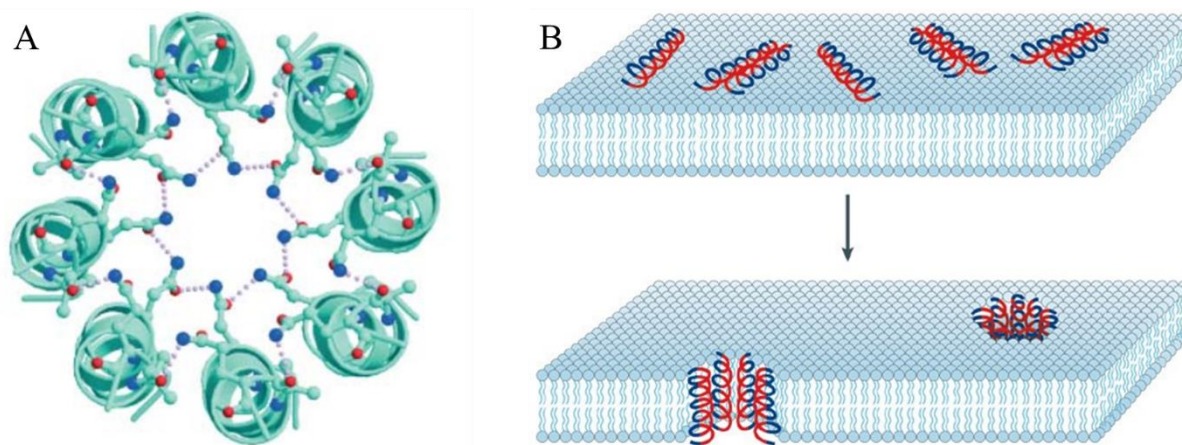


Figure 2.12. (A) View from *C*-terminus of the octameric bundle pore structure of trichotoxin A50E (**93**) (from Duclouhier et al. 2004). (B) The barrel-stave model of antimicrobial-peptide-induced killing (for peptides, hydrophilic regions in red, hydrophobic regions in blue) (from Brogden 2005).

2.2.5 *Sepedonium ampullosporum* Damon

Sepedonium ampullosporum Damon is characterized by bottle-shaped ampulloconidia with a truncate basis and a knob at the tip (Damon, 1952). The investigated strain KSH 534 was isolated from *Boletus calopus*. The fast growing culture of strain KSH 534 is white at first and produces after roughly one week golden-yellow, globose to subglobose, rough-tuberculate aleuriospores, leading to the golden color that appears in the center and gradually spreads over the colony. The aleurioconidia in *S. ampullosporum* was found to be shorter than in *S. chrysospermum* (Sahr, 1999).

The DNA-sequence analysis supported this close relationship between *S. ampullosporum* and *S. chrysospermum*, both forming a monophyletic group together with *S. microspermum* (Sahr, 1999).

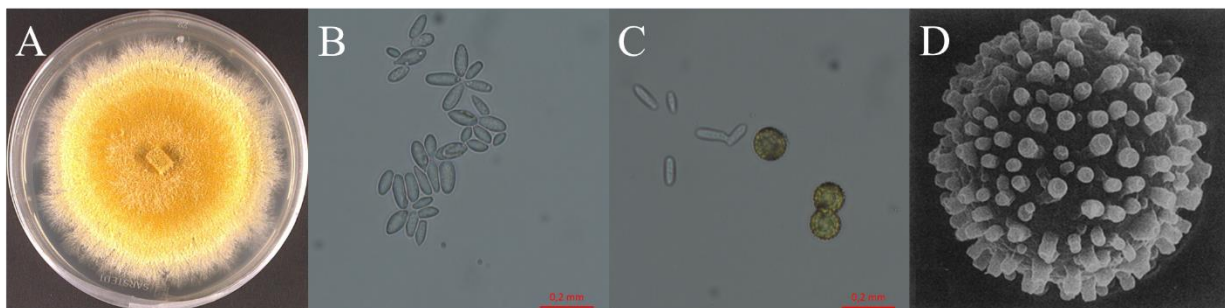


Figure 2.13. Morphological analyses of *Sepedonium ampullosporum* strain KSH 534. (A) Eight-day-old culture grown on malt peptone agar; (B) bottle-shaped ampulloconidia; (C) golden-yellow globose aleurioconidia; (D) scanning electron micrograph of aleurioconidia (3500x, photo from Sahr et al., 1999).

2.3 References

- Antkowiak, W. Z., Gessner, W. P., 1979. The structures of orellanine and orelline. *Tetrahedron Lett* 20, 1931-1934.
- Antkowiak, W. Z., Gessner, W. P., 1985. Photodecomposition of orellanine and orellinine, the fungal toxins of *Cortinarius orellanus* Fries and *Cortinarius speciosissimus*. *Experientia* 41, 769-771.
- Asemaninejad, A., Weerasuriya, N., Gloor, G. B., Lindo, Z., Thorn, R. G., 2016. New primers for discovering fungal diversity using nuclear large ribosomal DNA. *PLoS ONE* 11, e0159043.
- Beattie, K. D., Rouf, R., Gander, L., May, T. W., Ratkowsky, D., Donner, C. D., Gill, M., Grice, I. D., Tiralongo, E., 2010. Antibacterial metabolites from Australian macrofungi from the genus *Cortinarius*. *Phytochemistry* 71, 948-955.
- Besl, H., Hagn, A., Jobst, A., Lange, U., 1998. Der Goldschimmel der Rohrlinge und seine Verwandten. *Z Mykol* 64, 45-52.
- Bidaud, A., Carteret, X., Moenne-Loccoz, P., Reumaux, P., 2009. Atlas des Cortinaires XVIII. S.A.R.L. Editions fédérations mycologique Dauphiné-Savoie. Marlioz.
- Bidaud, A., Loizides, M., Armada, F., de Dios Reyes, J., Carteret, X., Corriol, G., Consiglio, G., Reumaux, P., Bellanger, J. M., 2021. *Cortinarius* subgenus Leprocyebe in Europe: expanded Sanger and next generation sequencing unveil unexpected diversity in the Mediterranean. *Persoonia* 46, 188-215.
- Binimelis-Salazar, J., Casanova-Katny, A., Arnold, N., Lima, C. A., Norambuena, H. V., González-Rocha, G., Palfner, G., 2021. Diversity and host relationships of the mycoparasite *Sepedonium* (Hypocreales, Ascomycota) in temperate central Chile. *Microorganisms* 9, 2261.
- Brandrud, T. E., Linström, H., Marklund, H., Melot, J., Muskos, S., 1990-1998. *Cortinarius* flora photographica. Deutsche Ausgabe. Color-Tryck. S-Härnösand.
- Brogden, K. A., 2005. Antimicrobial peptides: pore formers or metabolic inhibitors in bacteria? *Nat Rev Microbiol* 3, 238-250.
- Chen, H. P., Liu, J. K., 2017. Secondary metabolites from higher fungi. In: Progress in the chemistry of organic natural products 106, Springer International Publishing AG, Cham, pp. 1-201.

- Closse, A., Hauser, D., 1973. Isolierung und Konstitutionsermittlung von Chrysodin. *Helv Chim Acta* 56, 2694-2698.
- Damon, S. C., 1952. Two noteworthy species of *Sepedonium*. *Mycologia* 44, 86-96.
- Degenkolb, T., Berg, A., Gams, W., Schlegel, B., Grafe, U., 2003. The occurrence of peptaibols and structurally related peptaibiotics in fungi and their mass spectrometric identification via diagnostic fragment ions. *J Pept Sci* 9, 666-678.
- Degenkolb, T., Brückner, H., 2008. Peptaibiotics: towards a myriad of bioactive peptides containing C-dialkylamino acids? *Chem Biodivers* 5, 1817-1843.
- Divekar, P. V., Raistrick, H., Dobson, T. A., Vining, L. C., 1965. Studies in the biochemistry of microorganisms part 117. Sepedonin, a tropolone metabolite of *Sepedonium chrysospermum* Fries. *Can J Chem* 43, 1835-1848.
- Divekar, P. V., Vining, L. C., 1964. Reaction of anhydrosepedonin with alkali synthesis of a degradation product and some related dimethylhydroxybenzoic acids. *Can J Chem* 42, 63-68.
- Dornberger, K., Ihn, W., Ritzau, M., Grafe, U., Schlegel, B., Fleck, W. F., Metzger, J. W., 1995. Chrysospermins, new peptaibol antibiotics from *Apiocrea chrysosperma* Ap101. *J Antibiot* (Tokyo) 48, 977-989.
- Duclohier, H., Alder, G. M., Bashford, C. L., Brückner, H., Chugh, J. K., Wallace, B. A., 2004. Conductance studies on trichotoxin_A50E and implications for channel structure. *Biophys J* 87, 1705-1710.
- Elsworth, C., Gill, M., Giménez, A., M. Milanovic, N., Raudies, E., 1999. Pigments of fungi. Part 50.1 Structure, biosynthesis and stereochemistry of new dimeric dihydroanthracenones of the phlegmacin type from *Cortinarius sinapicolor* Cleland. *J Chem Soc Perkin Trans I*, 119-126.
- Frøslev, T. G., Brandrud, T. E., Jeppesen, T. S., 2006. New species and combinations in *Cortinarius* subgenus Phlegmacium section Calochroi. *Mycotaxon* 97, 367-377.
- Froslev, T. G., Jeppesen, T. S., Laessoe, T., Kjoller, R., 2007. Molecular phylogenetics and delimitation of species in *Cortinarius* section Calochroi (Basidiomycota, Agaricales) in Europe. *Mol Phylogenet Evol* 44, 217-227.
- Fuente-Núñez, C. d. I., Whitmore, L., Wallace, B. A., 2013. Chapter 22 - Peptaibols. In: Kastin, A. J. (Ed.), Handbook of biologically active peptides (second edition). Academic Press, Boston, 150-156.
- Gao, J. M., Qin, J. C., Pescitelli, G., Di Pietro, S., Ma, Y. T., Zhang, A. L., 2010. Structure and absolute configuration of toxic polyketide pigments from the fruiting bodies of the fungus *Cortinarius rufolivaceus*. *Org Biomol Chem* 8, 3543-3551.
- Garnica, S., Schon, M. E., Abarenkov, K., Riess, K., Liimatainen, K., Niskanen, T., Dima, B., Soop, K., Froslev, T. G., Jeppesen, T. S., Peintner, U., Kuhnert-Finkernagel, R., Brandrud, T. E., Saar, G., Oertel, B., Ammirati, J. F., 2016. Determining threshold values for barcoding fungi: lessons from *Cortinarius* (Basidiomycota), a highly diverse and widespread ectomycorrhizal genus. *FEMS Microbiol Ecol* 92, fiw045.
- Garnica, S., Weiss, M., Oberwinkler, F., 2002. New *Cortinarius* species from *Nothofagus* forests in South Chile. *Mycologia* 94, 136-145.
- Garnica, S., Weiss, M., Oberwinkler, F., 2003a. Morphological and molecular phylogenetic studies in South American *Cortinarius* species. *Mycol Res* 107, 1143-1156.
- Garnica, S., Weiß, M., Oertel, B., Oberwinkler, F., 2005. A framework for a phylogenetic classification in the genus *Cortinarius* (Basidiomycota, Agaricales) derived from morphological and molecular data. *Can J Bot* 83, 1457-1477.

- Garnica, S., Weiss, M., Oertel, B., Oberwinkler, F., 2003b. Phylogenetic relationships of European Phlegmacium species (*Cortinarius*, Agaricales). *Mycologia* 95, 1155-1170.
- Garrido, N., 1988. Agaricales s.l. und ihre Mykorrhizen in den Nothofagus-Wäldern Mittelchiles. J. Cramer, Berlin, Stuttgart, Germany, pp. 1-520.
- Geissler, T., Brandt, W., Porzel, A., Schlenzig, D., Kehlen, A., Wessjohann, L., Arnold, N., 2010. Acetylcholinesterase inhibitors from the toadstool *Cortinarius infractus*. *Bioorg Med Chem* 18, 2173-2177.
- Gill, M., 1994. Pigments of fungi (Macromycetes). *Nat Prod Rep* 11, 67-90.
- Gill, M., 1996. Pigments of fungi (Macromycetes). *Nat Prod Rep* 13, 513-528.
- Gill, M., 1999. Pigments of fungi (Macromycetes). *Nat Prod Rep* 16, 301-317.
- Gill, M., 2001. The Biosynthesis of Pigments in Basidiomycetes. *Aust J Chem* 54, 721-734.
- Gill, M., 2003. Pigments of fungi (Macromycetes). *Nat Prod Rep* 20, 615-639.
- Gill, M., Steglich, W., 1987. Pigments of fungi (Macromycetes). In: Herz, W., Grisebach, H., Kirby, G. W., Tamm, C. (Eds.), Progress in the chemistry of organic natural products 51. Springer-Verlag, Wien, New York, pp. 1-317.
- Hammerle, F., Bingger, I., Pannwitz, A., Magnutzki, A., Gstir, R., Rutz, A., Wolfender, J.-L., Peintner, U., Siewert, B., 2021a. Targeted isolation of photoactive pigments from mushrooms yielded a highly potent new photosensitizer: 7,7'-Biphyscion. *ChemRxiv*. Cambridge: Cambridge Open Engage preprint.
- Hammerle, F., Quiros-Guerrero, L., Rutz, A., Wolfender, J. L., Schobel, H., Peintner, U., Siewert, B., 2021b. Feature-based molecular networking-an exciting tool to spot species of the genus *Cortinarius* with hidden photosensitizers. *Metabolites* 11, 791.
- Helfer, W., 1991. Pilze auf Pilzfruchtkörpern: Untersuchungen zur Ökologie, Systematik und Chemie. IHW-Verlag, Eching, Germany, pp. 1-157.
- Hjørringgaard, C. U., Pedersen, J. M., Vosegaard, T., Nielsen, N. C., Skrydstrup, T., 2009. An automatic solid-phase synthesis of peptaibols. *J Org Chem* 74, 1329-1332.
- Horak, E., 1983. Mycogeography in the South Pacific Region: Agaricales, Boletales. *Aust J Bot* 13, 1-42.
- Horak, E., Wood, A. E., 1990. *Cortinarius* Fr. (Agaricales) in Australasia. 1. Subgen. *Myxacium* and subgen. *Paramyxacium*. *Sydowia* 42, 88-168.
- Hulsmann, H., Heinze, S., Ritzau, M., Schlegel, B., Grafe, U., 1998. Isolation and structure of peptaibolin, a new peptaibol from *Sepedonium* strains. *J Antibiot (Tokyo)* 51, 1055-1058.
- Iijima, M., Amemiya, M., Sawa, R., Kubota, Y., Kunisada, T., Momose, I., Kawada, M., Shibasaki, M., 2017. Acremopeptin, a new peptaibol from *Acremonium* sp. PF1450. *J Antibiot (Tokyo)* 70, 791-794.
- Jiang, M. Y., Feng, T., Liu, J. K., 2011. N-containing compounds of Macromycetes. *Nat Prod Rep* 28, 783-808.
- Jiao, W. H., Khalil, Z., Dewapriya, P., Salim, A. A., Lin, H. W., Capon, R. J., 2018. Trichodermides A-E: new peptaibols isolated from the Australian termite nest-derived fungus *Trichoderma virens* CMB-TN16. *J Nat Prod* 81, 976-984.
- Kai, K., Mine, K., Akiyama, K., Ohki, S., Hayashi, H., 2018. Anti-plant viral activity of peptaibols, trichorzins HA II, HA V, and HA VI, isolated from *Trichoderma harzianum* HK-61. *J Pestic Sci* 43, 283-286.
- Katoch, M., Singh, D., Kapoor, K. K., Vishwakarma, R. A., 2019. *Trichoderma lixii* (IIIM-B4), an endophyte of *Bacopa monnieri* L. producing peptaibols. *BMC Microbiol* 19.

- Keller, C., Maillard, M., Keller, J., Hostettmann, K., 2002. Screening of European fungi for antibacterial, antifungal, larvicidal, molluscicidal, antioxidant and free-radical scavenging activities and subsequent isolation of bioactive compounds. *Pharm Biol* 40, 518-525.
- Kim, C. K., Krumpal, L. R. H., Smith, E., Henrich, C. J., Brownell, I., Wendt, K. L., Cichewicz, R. H., O'Keefe, B. R., Gustafson, K. R., 2021. Roseabolin A, a new peptaibol from the fungus *Clonostachys rosea*. *Molecules* 26, 3594.
- Kirk, P. M., Cannon, P. F., Minter, D. W., Stalpers, J. A., 2008. Dictionary of the Fungi. CABI Wallingford, UK, pp. 1-784.
- Kitson, S., 2014. Carbon-14 labelled ADCs and peptides. <https://www.slideshare.net/seankitson/s-kitson-carbon14-labelled-adcs-and-peptides-26feb2014>, last access 11.04.2022.
- Kronen, M., Kleinwachter, P., Schlegel, B., Hartl, A., Grafe, U., 2001. Ampullosporines B, C, D, E1, E2, E3 and E4 from *Sepedonium ampullosporum* HKI-0053: structures and biological activities. *J Antibiot* (Tokyo) 54, 175-178.
- Kubin, A., Wierrani, F., Burner, U., Alth, G., Grunberger, W., 2005. Hypericin - the facts about a controversial agent. *Curr Pharm Des* 11, 233-253.
- Kuhdorf, K., Munzenberger, B., Begerow, D., Gomez-Laurito, J., Huttel, R. F., 2016. Arbutoid mycorrhizas of the genus *Cortinarius* from Costa Rica. *Mycorrhiza* 26, 497-513.
- Lee, S. J., Yun, B. S., Cho, D. H., Yoo, I. D., 1999. Tylopeptins A and B, new antibiotic peptides from *Tylophilus neofelleus*. *J Antibiot* (Tokyo) 52, 998-1006.
- Leitgeb, B., Szekeres, A., Manczinger, L., Vágvolgyi, C., Kredics, L., 2007. The history of alamethicin: a review of the most extensively studied peptaibol. *Chem Biodivers* 4, 1027-1051.
- Liimatainen, K., Kim, J. T., Pokorny, L., Kirk, P. M., Dentinger, B. T., Niskanen, T., 2022. Taming the beast: a revised classification of Cortinariaceae based on genomic data. *Fungal Divers* 112, 89-170.
- Liimatainen, K., Niskanen, T., Dima, B., Kytovuori, I., Ammirati, J. F., Froslev, T. G., 2014. The largest type study of Agaricales species to date: bringing identification and nomenclature of Phlegmacium (*Cortinarius*) into the DNA era. *Persoonia* 33, 98-140.
- Liimatainen, K., Niskanen, T., San-Fabian, B., Mujic, A. B., Peintner, U., Dresch, P., Furci, G., Nouhra, E., Matheny, P. B., Smith, M. E., 2020. *Cortinarius* section Thaumasti in South American Nothofagaceae forests. *Mycologia* 112, 329-341.
- Liu, J. K., 2005. N-containing compounds of Macromycetes. *Chem Rev* 105, 2723-2744.
- Llewellyn, N. M., Spencer, J. B., 2007. Enzymes line up for assembly. *Nature* 448, 755-756.
- Malik, M. S., Alsantali, R. I., Jassas, R. S., Alsimaree, A. A., Syed, R., Alsharif, M. A., Kalpana, K., Morad, M., Althagafi, I. I., Ahmed, S. A., 2021. Journey of anthraquinones as anticancer agents – a systematic review of recent literature. *RSC Advances* 11, 35806-35827.
- Marik, T., Tyagi, C., Racic, G., Rakk, D., Szekeres, A., Vagvolgyi, C., Kredics, L., 2018. New 19-residue peptaibols from *Trichoderma* clade Viride. *Microorganisms* 6, 85.
- Merrifield, R. B., 1963. Solid phase peptide synthesis. I. The synthesis of a tetrapeptide. *J Am Chem Soc* 85, 2149-2154.
- Mitova, M. I., Murphy, A. C., Lang, G., Blunt, J. W., Cole, A. L., Ellis, G., Munro, M. H., 2008. Evolving trends in the dereplication of natural product extracts. 2. The isolation of chrysaibolin, an antibiotic peptaibol from a New Zealand sample of the mycoparasitic fungus *Sepedonium chryso-spermum*. *J Nat Prod* 71, 1600-1603.

- Mitova, M. I., Stuart, B. G., Cao, G. H., Blunt, J. W., Cole, A. L., Munro, M. H., 2006. Chrysosporide, a cyclic pentapeptide from a New Zealand sample of the fungus *Sepedonium chrysospermum*. *J Nat Prod* 69, 1481-1484.
- Miyauchi, S., 2001. A new species of *Cortinarius* section Hydrocybe from Japan. *Mycoscience* 42, 223-225.
- Momose, I., Onodera, T., Doi, H., Adachi, H., Iijima, M., Yamazaki, Y., Sawa, R., Kubota, Y., Igarashi, M., Kawada, M., 2019. Leucinostatin Y: a peptaibiotic produced by the entomoparasitic fungus *Purpureocillium lilacinum* 40-H-28. *J Nat Prod* 82, 1120-1127.
- Moser, M., 1960. Die Gattung *Phlegmacium* (Schleimköpfe). In: Die Pilze Mitteleuropas IV. Verlag Julius Klinkhardt. Bad Heilbrunn, Germany, pp. 1-440.
- Moser, M., Horak, E., 1975. *Cortinarius* Fr. und nahe verwandte Gattungen in Sudamerika. *Beih. Nov. Hed.* 52, pp. 1-628.
- Naseer, A., Garrido-Benavent, I., Khan, J., Ballara, J., Mahiques, R., Khalid, A. N., Sher, H., 2020. *Cortinarius pakistanicus* and *C. pseudotorvus*: two new species in oak forests in the Pakistan Himalayas. *MycKeys* 74, 91-108.
- Neuhof, T., Berg, A., Besl, H., Schwecke, T., Dieckmann, R., von Dohren, H., 2007. Peptaibol production by *Sepedonium* strains parasitizing Boletales. *Chem Biodivers* 4, 1103-1115.
- Neumann, N. K., Stoppacher, N., Zeilinger, S., Degenkolb, T., Bruckner, H., Schuhmacher, R., 2015. The peptaibiotics database--a comprehensive online resource. *Chem Biodivers* 12, 743-751.
- Nicholas, G. M., 1998. Australian fungi: a natural product study. Chemistry Department, PhD thesis. University of Canterbury, 1-184.
- Nicholas, G. M., Blunt, J. W., Munro, M. H., 2001. Cortamidine oxide, a novel disulfide metabolite from the New Zealand basidiomycete (mushroom) *Cortinarius* species. *J Nat Prod* 64, 341-344.
- Niskanen, T., 2008. *Cortinarius* subgenus *Telamonia* p.p. in North Europe. Department of Biological and Environmental Sciences, PhD thesis. University of Helsinki, Finland, 1-33.
- Niskanen, T., Kytovuori, I., Liimatainen, K., 2011. *Cortinarius* sect. *Armillati* in northern Europe. *Mycologia* 103, 1080-1101.
- Ogwuru, N., Adamczeski, M., 2000. Bioactive natural products derived from polygonum species of plants: their structures and mechanisms of action. In: Atta-ur, R. (Ed.), *Studies in Natural Products Chemistry*. Elsevier 22, pp. 607-642.
- Otto, A., Laub, A., Haid, M., Porzel, A., Schmidt, J., Wessjohann, L., Arnold, N., 2016a. Tulasporins A-D, 19-residue peptaibols from the mycoparasitic fungus *Sepedonium tulasneanum*. *Nat Prod Commun* 11, 1821-1824.
- Otto, A., Laub, A., Wendt, L., Porzel, A., Schmidt, J., Palfner, G., Becerra, J., Kruger, D., Stadler, M., Wessjohann, L., Westermann, B., Arnold, N., 2016b. Chilenopeptins A and B, peptaibols from the Chilean *Sepedonium* aff. *chalcipori* KSH 883. *J Nat Prod* 79, 929-938.
- Peintner, U., 2008. *Cortinarius alpinus* as an example for morphological and phylogenetic species concepts in ectomycorrhizal fungi. *Sommerfeltia* 31, 161 - 177.
- Peintner, U., Moncalvo, J. M., Vilgalys, R., 2004. Toward a better understanding of the infrageneric relationships in *Cortinarius* (Agaricales, Basidiomycota). *Mycologia* 96, 1042-1058.
- Peintner, U., Moser, M. M., Thomas, K. A., Manimohan, P., 2003. First records of ectomycorrhizal *Cortinarius* species (Agaricales, Basidiomycetes) from tropical India and their phylogenetic position based on rDNA ITS sequences. *Mycol Res* 107, 485-494.

- Quang, D. N., Schmidt, J., Porzel, A., Wessjohann, L., Haid, M., Arnold, N., 2010. Ampullosine, a new isoquinoline alkaloid from *Sepedonium ampullosporum* (Ascomycetes). *Nat Prod Commun* 5, 869-872.
- Rawa, M. S. A., Nogawa, T., Okano, A., Futamura, Y., Nakamura, T., Wahab, H. A., Osada, H., 2021a. A new peptaibol, RK-026A, from the soil fungus *Trichoderma* sp. RK10-F026 by culture condition-dependent screening. *Biosci Biotechnol Biochem* 85, 69-76.
- Rawa, M. S. A., Nogawa, T., Okano, A., Futamura, Y., Wahab, H. A., Osada, H., 2021b. Zealpeptaibolin, an 11-mer cytotoxic peptaibol group with 3 Aib-Pro motifs isolated from *Trichoderma* sp. RK10-F026. *J Antibiot* (Tokyo) 74, 485-495.
- Ritzau, M., Heinze, S., Dornberger, K., Berg, A., Fleck, W., Schlegel, B., Hartl, A., Grafe, U., 1997. Ampullosporin, a new peptaibol-type antibiotic from *Sepedonium ampullosporum* HKI-0053 with neuroleptic activity in mice. *J Antibiot* (Tokyo) 50, 722-728.
- Rivera-Chavez, J., Raja, H. A., Graf, T. N., Gallagher, J. M., Metri, P., Xue, D., Pearce, C. J., Oberlies, N. H., 2017. Prelamethicin F50 and related peptaibols from *Trichoderma arundinaceum*: Validation of their authenticity via in situ chemical analysis. *RSC Adv* 7, 45733-45751.
- Rogerson, C. T., Samuels, G. J., 1989. Boleticolous Species of *Hypomyces*. *Mycologia* 81, 413-432.
- Saar, G., Dima, B., Schmidt-Stohn, G., Brandrud, T. E., Bellù, F., Frøslev, T. G., Oertel, B., Soop, K., 2014. *Cortinarius* Untergattung Phlegmacium Sektion Purpurascens in Europa. *J JEC* 14, 140 – 161.
- Sahr, T. A., H.; Besl, H.; Fischer, M., 1999. AmericaInfrageneric classification of the boleticolous genus *Sepedonium*: species delimitation and phylogenetic relationships. *Mycologia* 91, 935-943.
- Salgado Salomon, M. E., Barroetavena, C., Niskanen, T., Liimatainen, K., Smith, M. E., Peintner, U., 2021. Loose ends in the *Cortinarius* phylogeny: five new myxotelamonoid species indicate a high diversity of these ectomycorrhizal fungi with South American Nothofagaceae. *Life* (Basel) 11, 420.
- San-Fabian, B., Niskanen, T., Liimatainen, K., Kooij, P. W., Mujic, A. B., Truong, C., Peintner, U., Dresch, P., Nouhra, E., Matheny, P. B., Smith, M. E., 2018. New species of *Cortinarius* sect. *Austroamerici*, sect. nov., from South American Nothofagaceae forests. *Mycologia* 110, 1127-1144.
- Shibata, S., Shoji, J., Ohta, A., Watanabe, M., 1957. Metabolic products of fungi. XI. Some observation on the occurrence of skyrin and rugulosin in mold metabolites, with a reference to structural relationship between penicillipsin and skyrin. *Pharma Bullet* 5, 380-382.
- Sica, V. P., Rees, E. R., Raja, H. A., Rivera-Chavez, J., Burdette, J. E., Pearce, C. J., Oberlies, N. H., 2017. In situ mass spectrometry monitoring of fungal cultures led to the identification of four peptaibols with a rare threonine residue. *Phytochemistry* 143, 45-53.
- Singer, R., 1986. The Agaricales in modern taxonomy. Koeltz Scientific Books, Koenigstein, Germany, pp. 1-981.
- Sontag, B., Fröde, R., Bross, M., Steglich, W., 1999. Chromogenic triterpenoids from *Cortinarius fulvoincarnatus*, *C. sodagnitus* and related toadstools (Agaricales). *Eur J Org Chem* 1999, 255-260.
- Soop, K., 2017. *Cortinarioid* fungi of New Zealand: an iconography and key. Karl Soop, Mora, Sweden, pp. 1-57.
- Soop, K., 2021. *Cortinarius* in Sweden. Karl Soop, Mora, Sweden, pp. 1-184.
- Soop, K., Dima, B., Cooper, J. A., Park, D., Oertel, B., 2019. A phylogenetic approach to a global supraspecific taxonomy of *Cortinarius* (Agaricales) with an emphasis on the southern mycota. *Persoonia* 42, 261-290.
- Speckbacher, V., Zeilinger, S., 2018. Chapter 3: Secondary metabolites of mycoparasitic fungi. In: Vijayakumar, R., Raja, S. (Eds.), *Secondary metabolites-sources and applications*. Intechopen, London, UK, pp. 37-55.

- Spiteller, P., Spiteller, M., Steglich, W., 2003. Occurrence of the fungal toxin orellanine as a diglucoside and investigation of its biosynthesis. *Angew Chem Int Ed* 42, 2864-2867.
- Stadler, M. S., S.; Müller, H.; Henkel, T.; Lagojda, A.; Kleymann, G., 2001. New antiviral peptaibols from the mycoparasitic fungus *Sepedonium microspermum*. Irseer Naturstofftage der DECHEMA, Germany.
- Stefani, F. O. P., Jones, R. H., May, T. W., 2014. Concordance of seven gene genealogies compared to phenotypic data reveals multiple cryptic species in Australian dermocyboid *Cortinarius* (Agaricales). *Mol Phylogenet Evol* 71, 249-260.
- Steglich, W., 1994. Mushrooms - seen through the eyes of an organic chemist. Ernst Schering Research Foundation, Berlin, Germany, pp. 1-23.
- Steglich, W., Steffan, B., Eizenhofer, T., Fugmann, B., Hermann, R., Klamann, J. D., 1990. Some problems in the structural elucidation of fungal metabolites. Ciba Foundation Symposium 154 -Bioactive Compounds from Plants John Wiley & Sons Ltd., Chichester, England, Bangkok, Thailand, pp. 56-65.
- Teichert, A., Schmidt, J., Porzel, A., Arnold, N., Wessjohann, L., 2007. Brunneins A-C, beta-carboline alkaloids from *Cortinarius brunneus*. *J Nat Prod* 70, 1529-1531.
- Teichert, A., Schmidt, J., Porzel, A., Arnold, N., Wessjohann, L., 2008. *N*-glucosyl-1*H*-indole derivatives from *Cortinarius brunneus* (Basidiomycetes). *Chem Biodivers* 5, 664-669.
- Thiele, W., Froede, R., Steglich, W., Müller, M., 2020. Enzymatic formation of rufoschweinitzin, a binaphthalene from the Basidiomycete *Cortinarius rufolivaceus*. *ChemBioChem* 21, 1423-1427.
- Touati, I., Ruiz, N., Thomas, O., Druzhinina, I. S., Atanasova, L., Tabbene, O., Elkahoui, S., Benzekri, R., Bouzlama, L., Pouchus, Y. F., Limam, F., 2018. Hyporientalin A, an anti-Candida peptaibol from a marine *Trichoderma orientale*. *World J Microbiol Biotechnol* 34, 98.
- van Bohemen, A. I., Ruiz, N., Zalouk-Vergnoux, A., Michaud, A., Robiou du Pont, T., Druzhinina, I., Atanasova, L., Prado, S., Bodo, B., Meslet-Cladiere, L., Cochereau, B., Bastide, F., Maslard, C., Marchi, M., Guillemette, T., Pouchus, Y. F., 2021. Pentadecaibins I-V: 15-residue peptaibols produced by a marine-derived *Trichoderma* sp. of the *Harzianum* clade. *J Nat Prod* 84, 1271-1282.
- Wu, G., Dentinger, B. T. M., Nielson, J. R., Peterson, R. T., Winter, J. M., 2021. Emerimicins V-X, 15-residue peptaibols discovered from an *Acremonium* sp. through integrated genomic and chemical approaches. *J Nat Prod* 84, 1113-1126.
- Xie, M. L., Chen, J. L., Phukhamsakda, C., Dima, B., Fu, Y. P., Ji, R. Q., Wang, K., Wei, T. Z., Li, Y., 2021. *Cortinarius subsalor* and *C. tibeticisalor* spp. nov., two new species from the section Delibuti from China. *Peer J* 9, e11982.
- Xie, M. L., Wei, T. Z., Fu, Y. P., Li, D., Qi, L. L., Xing, P. J., Cheng, G. H., Ji, R. Q., Li, Y., 2020. Three new species of *Cortinarius* subgenus *Telamonia* (Cortinariaceae, Agaricales) from China. *MycoKeys* 69, 91-109.
- Yurkov, A., Krüger, D., Begerow, D., Arnold, N., Tarkka, M. T., 2012. Basidiomycetous yeasts from Boletales fruiting bodies and their interactions with the mycoparasite *Sepedonium chrysospermum* and the host fungus *Paxillus*. *Microb Ecol* 63, 295-303.
- Zhang, A. L., Qin, J. C., Bai, M.-S., Gao, J. M., Zhang, Y. M., Yang, S. X., Laatsch, H., 2009. Rufolivacin B, a novel polyketide pigment from the fruiting bodies of the fungus *Cortinarius rufo-olivaceus* (basidiomycetes). *Chin Chem Lett* 20, 1324-1326.
- Zhang, S. H., Yang, J., Ma, H., Yang, Y., Zhou, G. F., Zhao, X., Xu, R., Nie, D., Zhang, G. G., Shan, J. J., Cui, C. B., Li, C. W., 2021. Longibramides A-E, peptaibols isolated from a mushroom derived fungus *Trichoderma longibrachiatum* Rifai DMG-3-1-1. *Chem Biodivers* 18, e2100128.

Chapter 3

Nor-guanacastepene pigments from the Chilean mushroom *Cortinarius pyromyxa*

This Chapter has been published as:

Yen T. H. Lam, Götz Palfner, Celia Lima, Andrea Porzel, Wolfgang Brandt, Andrej Frolov, Haider Sultani, Katrin Franke, Christoph Wagner, Kurt Merzweiler, Ludger A. Wessjohann, and Norbert Arnold. *Phytochemistry* **2019**, 165, 112048, DOI: 10.1016/j.phytochem.2019.05.021*

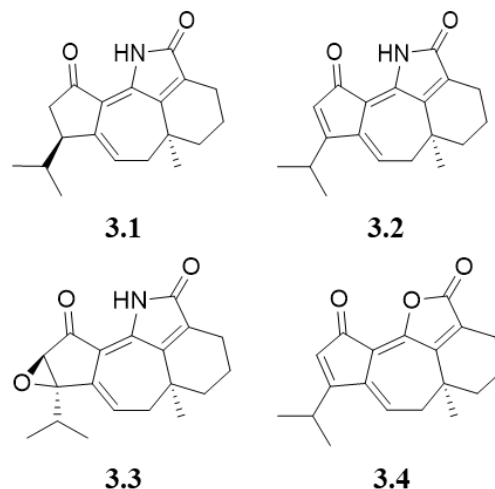
*Reprinted (adapted) with permission from Elsevier. Copyright © 2019

Graphical abstract

Pyromyxones are responsible for the bright orange stipe color



Cortinarius pyromyxa



Highlights

- Four undescribed diterpenoids were isolated from *Cortinarius pyromyxa*.
- The isolated diterpenoids possess the undescribed *nor-guanacastane* skeleton.
- Pyromyxones A, B, and D exhibit weak antibacterial and antifungal activity.
- Chemical and morphological studies support the monotypic position of *C. pyromyxa*.

Abstract

For the first time, the pigment composition of basidiocarps from the Chilean mushroom *Cortinarius pyromyxa* was studied under various aspects like phylogeny, chemistry and antibiotic activity. A molecular biological study supports the monotypic position of *C. pyromyxa* in subgenus *Myxacium*, genus *Cortinarius*. Four undescribed diterpenoids, named pyromyxones A-D (**3.1-3.4**), were isolated from fruiting bodies of *C. pyromyxa*. Their chemical structures were elucidated based on comprehensive one- and two-dimensional NMR spectroscopic analysis, ESI-HRMS measurements, as well as X-ray crystallography. In addition, the absolute configurations of pyromyxones A-D (**3.1-3.4**) were established with the aid of $J_{H,H}$, NOESY spectra and quantum chemical CD calculation. The pyromyxones A-D (**3.1-3.4**) possess the undescribed *nor-guanacastane* skeleton. Tested pyromyxones A (**3.1**), B (**3.2**), and D (**3.4**) exhibit only weak activity against gram-positive *Bacillus subtilis* and gram-negative *Aliivibrio fischeri* as well as the phytopathogenic fungi *Botrytis cinerea*, *Septoria tritici* and *Phytophthora infestans*.

Keywords: *Cortinarius pyromyxa* M. M. Moser & E. Horak; Cortinariaceae; diterpenoids; phylogeny; *nor-guanacastepenes*; pyromyxones.

3.1 Introduction

Cortinarius Fr. (Fungi, Basidiomycota) is under current knowledge the most species-rich of fungal genera forming gilled mushrooms (Kirk et al., 2008). It is characterized by obligate ectomycorrhizal associations with diverse groups of woody seed plants, mainly across boreal and temperate forest ecosystems around the globe (Peintner et al., 2004). Also, *Cortinarius* dominates the ectomycorrhizal mycobiota in South American *Nothofagus* forests, with more than 260 species described so far (Garnica et al., 2002; Garrido, 1988; Harrower et al., 2015; Moser and Horak, 1975). Its outstanding richness of species and supraspecific lineages is reflected by a high diversity of secondary metabolites, although to date, only a minor fraction of *Cortinarii* has been analyzed on the chemical level. The earlier studies on the chemical constituents of *Cortinarius* species have led to the isolation of different compound classes, including monomeric and dimeric dihydroanthracenones and anthraquinones (Gill, 1994, 1996, 1999, 2001; Gill and Steglich, 1987; Zhou and Liu, 2010), pyronaphthoquinones (Gill, 1999, 2001, 2003; Zhou and Liu, 2010), pigments containing a xanthone chromophore (Gill, 1999; Gill and Steglich, 1987), styrylpyrones (Gill, 1994, 2003; Moser, 1985), sesquiterpenes (Gill, 1999, 2003), polyenes (Gill, 1999, 2003), quinolines and isoquinolines (Jiang et al., 2011; Zhou and Liu, 2010), *N*-glucosyl-indole derivatives (Jiang et al., 2011; Zhou and Liu, 2010), nephrotoxic bipyridine *N*-dioxides (Chen and Liu, 2017; Gill, 1994, 2003; Gill and Steglich, 1987), β -carbolines (Chen and Liu, 2017; Gill, 1996; Gill and Steglich, 1987; Jiang et al., 2011; Zhou and Liu, 2010), nitro-aromatic pigments (Gill, 1994, 2001; Gill and Steglich, 1987), dithiopyridine *N*-oxide metabolites (Gill, 1999, 2003), sphingolipids (Jiang et al., 2011), and compounds based on a charge transfer complex between a phenol and a transition metal (Gill, 1999, 2003), and pigments with 3,6,9-trimethylazuleno[4,5-b]furan-2,7-dione structure (Gill, 2003).

Traditionally the genus *Cortinarius* has been divided into several subgenera like *Myxacium*, *Phlegmacium* etc., based on microscopical and morphological characters. *Cortinarius pyromyxa* M.M. Moser & E. Horak (Cortinariaceae) was first described from Argentinian Patagonia based on two collections (Moser and Horak, 1975). Beside the Argentinian type locality, in Chile this rare species is so far only reported in one collection (Garrido, 1988). It belongs to subgenus *Myxacium* within genus *Cortinarius*, comprising species featuring a gelatinous layer on pileus and stipe. *C. pyromyxa* is especially characterized by a bright orange stem cortex and yellow flesh towards the base. According to macro- and microscopic characters, the species is monotypic for section *Pyromyxa* within subgenus *Myxacium* (Horak and Wood, 1990). Suggested relationship between *C. pyromyxa* and the Australian species *C. erythraeus* and *C. sinapicolor* became doubtful since *C. erythraeus* was inserted in Sect. *Delibuti* within subgenus *Myxacium* according to investigated ITS sequences, whereas the systematic position of *C. sinapicolor* becomes uncertain (Garnica et al., 2016). Chemical investigations into pigments of *C. sinapicolor* demonstrate the occurrence of dimeric dihydroanthracenone pigments which suggest a relation to species of the subgenus *Phlegmacium* (Elsworth et al., 1999).

To the best of our knowledge, no chemical investigation into pigments of basidiocarps from *Cortinarius* subgenus *Myxacium* has been carried out so far. There is only two reports about the isolation and structural elucidation of secondary metabolites. The bitter triterpenoid crystallopicrin was isolated from *C. crystallinus*, *C. croceocoeruleus* and *C. vibratilis*, which is accompanied in the latter species by deoxyderivative (Steglich, 1994; Steglich et al., 1990). Structurally, both compounds are closely related to iridals from *Iris* spp. (Jaenicke and Marner, 1986). Vibratilicin, a representative of the rare group of natural products containing hydroxamic acid moieties, was also recognized from *C. vibratilis* (Wang et al., 2004).

In the present paper, we describe for the first time the isolation and structural elucidation of diterpenoid pigments from fruiting bodies of *C. pyromyxa* with an undescribed *nor*-guanacastane core structure, named pyromyxones A-D (**3.1-3.4**). Compounds **3.1**, **3.2**, and **3.4** were tested against (+)-gram *Bacillus subtilis* and (-)-gram *Aliivibrio fischeri* as well as the phytopathogenic organisms *Botrytis cinerea*, *Septoria tritici* and *Phytophthora infestans*. Our preliminary molecular phylogenetic data support the monotypic status of *C. pyromyxa*.

3.2 Results and discussion

3.2.1 Isolation and structural elucidation of compounds 3.1-3.4

Repeated column chromatography of the *C. pyromyxa* crude extract on Diaion HP20, silica gel, and sephadex LH20 in combination with semipreparative HPLC yielded four yellow compounds **3.1-3.4** (Figure 3.1).

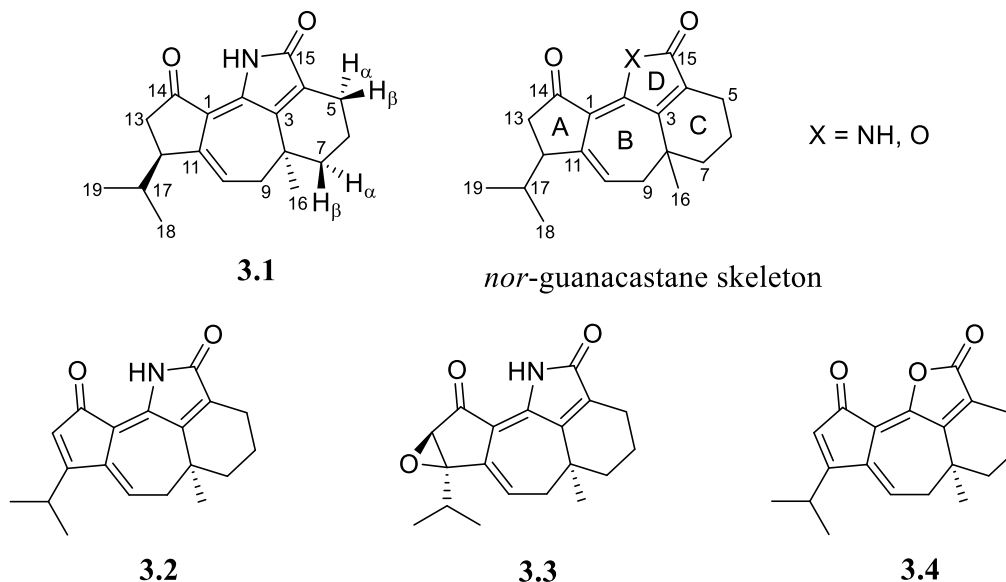


Figure 3.1. Structure of pyromyxones A-D (**3.1-3.4**) and their skeleton.

Compound **3.1** was isolated as yellow amorphous solid with a positive optical rotation ($[\alpha]_D^{27} +42.5$). Its molecular formula was determined to be $C_{19}H_{23}NO_2$, based on HRESIMS data of the molecular ion at m/z 298.1793 ($[M+H]^+$, calcd for $C_{19}H_{24}NO_2^+$, 298.1802), corresponding to 9 degrees of unsaturation. The occurrence of amide N in **3.1** is supported by the presence of one IR band at $\nu_{max} = 3388\text{ cm}^{-1}$. By recrystallization from methanol, a crystal of sufficient quality enabled X-ray structural analysis (Figure 3.2; Table S4, Supplementary data). Compound **3.1** was assigned as a undescribed diterpenoid possessing a tetracyclic [5-7-6-5] core, which is similar to the guanacastane skeleton (Brady et al.; 2000, 2001; Markovic et al., 2015), except for a double bond between C-10 and C-11, as well as an additional 5-membered ring. Due to a methyl group missing at C-11, which distinguishes it from guanacastepenes, compound **3.1** is assigned as a *nor*-guanacastane diterpenoid.

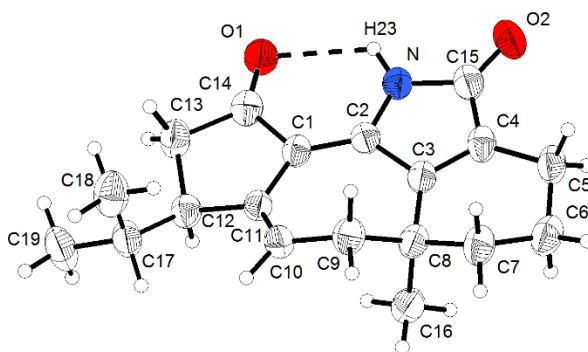


Figure 3.2. ORTEP drawing of pyromyxone A (**3.1**).

The guanacastane skeleton, which was first described in 1995 by Invernizzi et al. and named neodolastane, was then renamed by Brady et al. in 2000. This skeleton is characterized by a tricyclic [5-7-6] ring system as well as two methyl groups and one isopropyl group attached to C-8, C-11 and C-12, respectively (Brady et al., 2000, 2001; Markovic et al., 2015). Interestingly, the family of diterpenoids, so-called guanacastepenes, with this guanacastane skeleton were mostly isolated from fungal and marine resources (Brady et al., 2000, 2001; Invernizzi et al., 1995; Markovic et al., 2015).

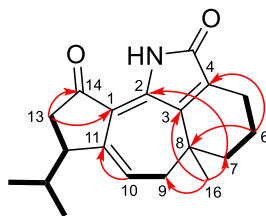


Figure 3.3. Key COSY (bold) and HMBC (arrow) correlations of pyromyxone A (**3.1**).

In agreement with the X-ray analysis, NMR studies on compound **3.1** revealed 19 carbon resonances, classified as three methyl groups, five aliphatic methylenes, three methines (one

olefinic and two aliphatic), and eight quaternary carbons (two carbonyl, five olefinic and one aliphatic). It is noteworthy that the C-2 carbon signal was not detected in methanol-d₄, but in pyridine-d₅. In addition, although signals of H-5 α & β , H-9 A&B, H-13 A&B and H-17 are overlapping, their chemical shifts were clearly assigned based on 1D TOCSY and HSQC experiments (Table 3.1).

Table 3.1. ¹H and ¹³C NMR data of pyromyxone A (**3.1**) including HMBC and NOE correlations (600/150 MHz, CD₃OD, δ in ppm).

Pos.	δ_C , type	δ_H , mult. (<i>J</i> in Hz)	3.1	
			HMBC	Key NOE
1	118.1, C	-		
2	142.8, C ^a	-		
3	152.8, C	-		
4	133.4, C	-		
5	21.1, CH ₂	α 2.40 ddd 19.0/4.8/2.3 ^b β 2.22 ddd 19.0/10.2/7.2 ^b	<i>d</i> <i>d</i>	
6	19.8, CH ₂	1.94 ^c	C-4, C-5, C-7, C-8	
7	38.1, CH ₂	α 1.61 br dt-like 13.3/3.5 β 1.52 ddd 13.3/11.6/5.2	C-2, C-3, C-5, C-6, C-8, C-16 C-5, C-6, C-8, C-9, C-16	16
8	35.3, C	-		
9	39.6, CH ₂	A 2.40 dt 16.5/3.8 ^b B 2.28 dd 16.5/8.9 ^b	<i>d</i> <i>d</i>	
10	122.9, CH	5.89 ddd 8.9/3.8/2.6	C-8, C-9, C-11, C-12	
11	143.0, C	-		
12	45.3, CH	α 3.01 m		13A,16,18
13	38.6, CH ₂	A 2.47 dd 18.9/9.5 B 2.27 dd 18.9/7.4	C-1, C-2, C-11, C-12, C-14, C-17 C-2, C-11, C-12, C-14, C-17	
14	209.5, C	-		
15	173.3, C	-		
16	23.0, CH ₃	1.11 s	C-3, C-7, C-8, C-9	12, 7 α
17	30.5, CH	2.28 septd 6.9/3.6 ^b	<i>d</i>	
18	21.8, CH ₃	1.01 d 6.9	C-12, C-17, C-19	
19	15.1, CH ₃	0.76 d 6.9	C-12, C-17, C-18	
NH		9.47 b rs ^e		

^a Measured in C₅D₅N. ^b Overlapping signals, chemical shifts were determined from 1D TOCSY. ^c Overlapping signals, chemical shifts were determined from ¹H, ¹³C-HSQC correlation peaks. ^d Not assignable due to overlapping signals. ^e Measured in CDCl₃.

Initial analysis of the COSY and 1D TOCSY spectra, as depicted in Figure 3.3, reveals the presence of an isopropyl moiety as well as a -CH₂-CH₂-CH₂- and an olefinic-CH-CH₂- spin system. The ¹H – ¹³C HMBC correlations from H-13 A&B to C-12, C-11, C-1 and C-14 confirm the presence of an isopropylpentenone moiety (ring A). Moreover, the ¹H – ¹³C HMBC correlations from H₃-16 to C-8, C-9, C-7 and C-3, as well as from the isochronous protons attached to C-6 to C-8, C-7, C-5, and C-4 indicate a methylcyclohexene moiety (ring C) connected to ring A through

C-10 – C-9. On the basis of the above analysis, the structure of **3.1** was determined, and named pyromyxone A (**3.1**).

Compound **3.2**, purified as yellow amorphous solid with a negative optical rotation ($[\alpha]_D^{26} - 32.2$), had the molecular formula $C_{19}H_{21}NO_2$, as deduced from HRESIMS data (m/z 296.1649 ($[M+H]^+$, calcd for $C_{19}H_{22}NO_2^+$, 296.1645). The 1D and 2D NMR spectroscopic data (Table 3.2) of **3.2** closely resemble those of **3.1**, except for the presence of an additional double bond between C-12 and C-13 (δ_H 6.13, s; δ_C 177.6 & 126.7). Additionally, the carbon signal of C-14 of **3.2** (δ_C 197.0) was shifted upfield compared to that of **3.1** (δ_C 209.5) confirming this ketone group of **3.2** to be conjugated to a double bond. HMBC correlations of H-13 with C-12 (δ_C 177.6), C-11 (δ_C 137.4), C-1 (δ_C 113.7) and C-14 (δ_C 197.0) support the presence of the double bond between C-12 and C-13. Thus, the structure of **3.2** was established as a dehydro derivative of **3.1**, and subsequently named pyromyxone B.

Table 3.2. 1H and ^{13}C NMR data of compounds **3.2-3.4** (600/150 MHz, CD_3OD , δ in ppm).

Pos.	δ_H , mult. (J in Hz)			δ_C		
	3.2	3.3	3.4^a	3.2	3.3	3.4^a
1	-	-	-	113.7	114.4	114.0
2	-	-	-	141.0	<i>n.d.^b</i>	148.3
3	-	-	-	152.3	152.1	157.2
4	-	-	-	134.5	136.6	130.5
5	α 2.42 ddd 9.0/5.6/1.6	α 2.40 ^c	α 2.54 dd 19.4/6.0	21.1	21.2	20.5
	β 2.23 ddd 19.0/10.8/7.0	β 2.21 ddd 19.2/10.9/6.9	β 2.31 ddd 19.4/11.1/6.8			
6	1.95 m ^c	1.93 m ^c	2.00 m; 1.90 m	19.5	19.7	18.4
7	α 1.68 ddd 13.1/3.3/3.3	α 1.64 ddd 13.2/3.4/3.4	α 1.68 ddd 13.3/3.4/3.4	38.1	38.3	36.7
	β 1.62 dt 13.1/13.1/4.3	β 1.53 ddd 13.2/13.2/4.3	β 1.56 ddd 13.3/13.4/3.5			
8	-	-	-	35.9	35.5	34.4
9	A 2.54 dd 16.8/3.6	A 2.39 ^c	A 2.51 dd 16.6/3.6	40.4	39.6	38.7
	B 2.45 dd 16.8/8.6	B 2.29 dd 16.7/8.8	B 2.38 dd 16.6/8.8			
10	6.38 dd 8.6/3.6	6.23 dd 8.8/3.5	6.21 dd 8.8/3.6	125.9	125.7	122.6
11	-	-	-	137.4	146.6	136.1
12	-	-	-	177.6	70.2	174.4
13	6.13 br s	3.65s	6.15 br s	126.7	57.2	127.4
14	-	-	-	197.0	199.3	191.5
15	-	-	-	173.4	<i>n.d.^b</i>	168.5
16	1.18 br s	1.12 br s	1.17 br s	24.5	23.3	23.8
17	3.03 septd 6.9/0.9	2.68 septd 6.8/0.9	2.91 septd 6.8/1.0	27.6	25.6	26.4
18	1.26 d 6.9	1.08 d 6.8	1.25 d 6.8	22.2	20.2	21.7
19	1.25 d 6.9	1.00 d 6.8	1.24 d 6.8	22.8	17.8	22.2
NH	9.29 br s ^a					

^a measured in $CDCl_3$. ^b *n.d.* = not detected. ^c Overlapping signals, chemical shifts were determined from 1H , ^{13}C -HSQC correlation peaks.

Compound **3.3** was obtained as yellow solid with a positive optical rotation ($[\alpha]_D^{24} +92.5$). The molecular formula of **3.3** was determined as $C_{19}H_{21}NO_3$ from HRESIMS data ($[M+H]^+$ at m/z

312.1593, calcd for $C_{19}H_{22}NO_3^+$, 312.1594). Comparison of 1H NMR data (Table 3.2) of **3.3** and **3.2** reveals a singlet at δ_H 3.65 ppm (s, H-13) instead of the olefinic singlet at δ_H 6.13 ppm (s, H-13) in **3.2**. Interestingly, in the standard HSQC experiment adjusted to a $^1J_{CH}$ coupling constant of 146 Hz, this singlet H-13 at δ_H 3.65 ppm shows no correlation. However, by decreasing the corresponding HSQC delay according to a coupling constant of 180 Hz, a correlation with the ^{13}C signal at δ_{C-13} 57.2 ppm (C-13) was detected (Figure S29, Supplementary data). This big $^1J_{CH}$ coupling constant but high field ^{13}C chemical shift unambiguously indicates that C-13 is a part of an epoxide ring. Therefore, the structure of **3.3** was assigned as an epoxidized derivative of **3.2**, and named pyromyxone C.

Compound **3.4**, purified as yellow solid with a positive optical rotation ($[\alpha]_D^{25} +28.3$), was determined as $C_{19}H_{20}O_3$ from HRESIMS data, which showed a positive ion peak $[M+H]^+$ at m/z 297.1480 (calcd for $C_{19}H_{21}O_3^+$, 297.1485). Furthermore, the 1D and 2D NMR spectroscopic data (Table 3.2) of **3.4** are very similar to those of **3.2**, except for the absence of an amide proton signal (δ_H 9.29 for **3.2**) and an upfield shift of the carbonyl carbon (C-15) of approximately 5 ppm (δ_C 168.5 for **3.4** and 173.4 for **3.2**). Thus, the structure of **3.4** bears in ring D a furan instead of a pyrrole moiety as in **3.2**, and was named pyromyxone D.

3.2.2 Assignment of relative and absolute configuration of compounds 3.1-3.4

The relative configuration of compound **3.1** was deduced from X-ray analysis and was reflected in the vicinal H-H coupling constants $J_{H,H}$ and NOESY correlations between H-12 and CH_3 -16, as well as between CH_3 -16 and the equatorial oriented proton H-7 α (1.61 br dt-like, J 13.3/3.5). Interestingly, no NOE correlation was detected between CH_3 -16 and the axially oriented proton H-7 β . These findings indicate an α -orientation of H-12 and CH_3 -16, consistent with guanacastepenes reported in the literature (Brady et al., 2000, 2001; Markovic et al., 2015).

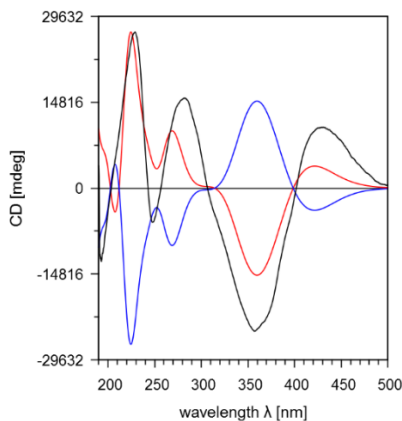


Figure 3.4. Calculated CD spectra of the 8*S*, 12*R* isomer (red) of compound **3.1** in comparison with the experimental one (black line) and its enantiomer (8*R*, 12*S*, blue). The best similarity factor ($S = 0.8969$) was found for $\sigma = 0.3$ eV and a shift of 21 nm. The similarity factor for the enantiomer is only 0.0269.

Compound **3.1** contains two chiral centers at C-8 and C-12, corresponding to four possible stereoisomers. In order to figure out the absolute configuration of **3.1**, the electronic circular dichroism (ECD) spectra of the four proposed isomers were calculated by quantum chemical methods, and compared with the experimental ECD spectrum. The one with *8S*, *12R* configurations was found to fit best with the experimental CD spectrum showing a similarity factor ($S = 0.8969$, $\sigma = 0.3$ eV and a shift of 21 nm), much higher than the similarity factors ($S \leq 0.3200$) for the other three isomers (Figure 3.4; Figure S16, Supplementary data). Therefore, the configuration of compound **3.1** was determined as *8S* and *12R*.

Similarly, to determine the absolute configurations of C-8 in **3.2** and **3.4**, NOE correlations were analyzed and energy-optimized conformers of the two possible isomers (*R* and *S*) were calculated. The analysis demonstrate that both compounds **3.2** and **3.4** have an *8S* configuration with an α -oriented methyl group CH₃-16 (Figures S25, S43, Supplementary data). Taking the common biosynthetic pathway of all four compounds **3.1-3.4** into consideration, the same conformer with *8S* configuration and an α -oriented methyl group CH₃-16 can be presumed for compound **3.3**. Furthermore, the absolute configurations of C-12 and C-13 in compound **3.3** were assigned by comparing calculated and experimental ECD spectra. Due to the three-membered epoxide moiety at ring A, the configurations of C-12 and C-13 were restricted to be either *SS* or *RR*. Thus, the possible number of stereoisomers is reduced from eight to four. The calculated ECD spectrum of the *8S*, *12R*, *13R*-configuration in **3.3** showed the best match with the experimental one, with the similarity of 79% (Figure S33, Supplementary data). This relatively low similarity might be caused by some impurities of the sample, but is obviously much higher than the similarities found for the other three isomers ($S \leq 44\%$) (Figure S34, Supplementary data). Therefore, compound **3.3** is determined to have *8S*, *12R*, *13R* -configuration.

3.2.3 Phylogenetic analyses

Closest BLAST matches of *C. pyromyxa* sequences presented only 91% sequence similarity (with an E value of 0.0). Interestingly, three matches correspond to unidentified sequences obtained from mass sequencing of soil/ root samples from Argentinian and Chilean *Nothofagus* forests (Table S3, Supplementary data). The most similar species identified by name were *Cortinarius olidoamarus* (NCBI accession version KJ421075.1) and *Cortinarius misermontii* (NR_130230.1), however, both belong to subgenus *Phlegmacium* and so far are known only from the Northern hemisphere. None of the 11 closest matches corresponds to subgenus *Myxacium* (Table S3, Supplementary data). As illustrated by the phylogenetic tree (Figure 3.5), compared to selected *Cortinarius* spp. from both hemispheres belonging to subgenus *Myxacium*, *Cortinarius pyromyxa* is monophyletic with 100% consensus support.

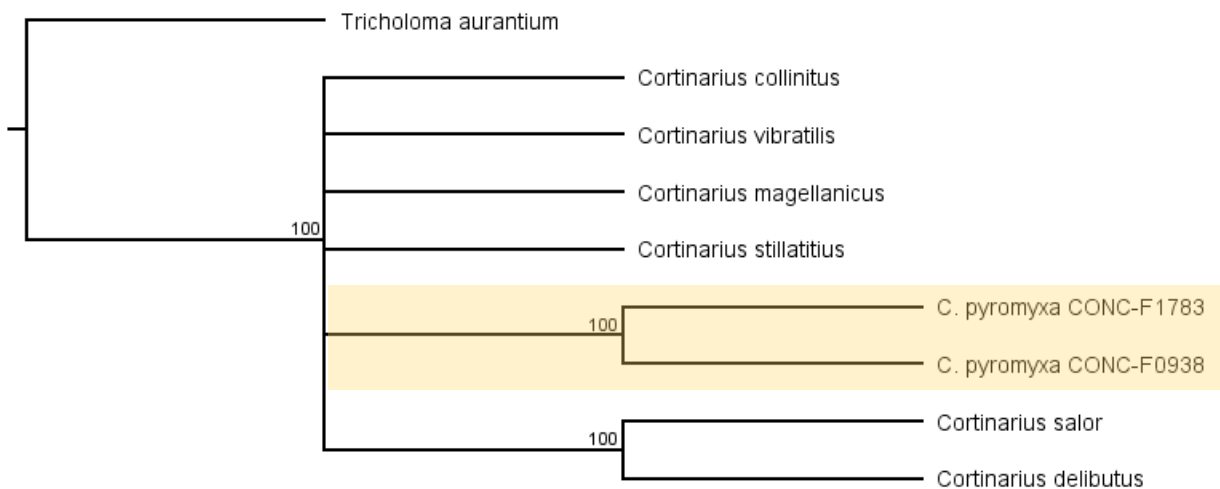


Figure 3.5. Phylogenetic tree of selected *Cortinarius* spp. belonging to subgenus *Myxacium* from both hemispheres based on ITS nucleotide sequences; branch labels show consensus support over 50% out of 1000 bootstrap resampling replicates; *Tricholoma aurantium* was employed as outgroup.

3.2.4 Biological evaluation

Isolated compounds **3.1**, **3.2** and **3.4** were examined towards their activity against the plant pathogenic fungi *Botrytis cinerea* (grey mold pathogen on many crops including strawberries and wine grapes) and *Septoria tritici* (causes septoria leaf blotch of wheat) as well as the oomycete *Phytophthora infestans* (causal agent of the late blight disease on potato and tomato) using a 96 well microtiter plate assay (Table S45, Supplementary data). 4-Oxohexadec-2-enoic acid was used as reference compound as described before (Teichert et al., 2005; Otto et al., 2017). Only compound **3.1** showed weak activity against *P. infestans*. Furthermore, compounds **3.1**, **3.2** and **3.4** were also tested for antibacterial activity against gram-positive *Bacillus subtilis* and gram-negative *Aliivibrio fischeri* (Figure S46, Supplementary data). Only compounds **3.1** and **3.2** show moderate growth inhibition activity of ca. 50% at 100 μ M against gram-negative *A. fischeri*, whereas pyromyxone D (**3.4**) inhibits bacterial growth around 30 % at 100 μ M. Growth inhibition of gram-positive *B. subtilis* was not observed.

3.3 Concluding remarks

In conclusion, the present study represents the first pigment chemical investigation of fruiting bodies of a species from suborder *Myxacium* in genus *Cortinarius*. Four undescribed pigments named pyromyxone A-D (**3.1-3.4**), responsible for the fire colored stem of the fruiting bodies of *C. pyromyxa* were isolated. Their structures were elucidated by means of X-ray crystallography, mass spectrometry and NMR spectroscopic methods. The absolute configurations of pyromyxones A-D (**3.1-3.4**) were assigned by comparing quantum chemical CD calculations to experimental spectra. Chemical, molecular and biological data support the isolated position of *C. pyromyxa*

within genus *Cortinarius* subgenus *Myxacium*. The isolated compounds were evaluated against gram-positive and gram-negative bacteria as well as phytopathogenic organisms but show only weak activity indicating that these pigments are probably not involved in the fungal pathogen defense.

3.4 Experimental

3.4.1 General experimental procedures

Column chromatography was performed on Sephadex LH 20 (Fluka, Germany), silica gel (0.040-0.063 mm, Merck, Germany), and silica gel 60 silanized (0.063-0.200 mm, Merck, Germany), whereas analytical TLC was performed on pre-coated silica gel F₂₅₄ aluminum sheets (Merck, Germany). Diaion HP20 was purchased from Supelco (USA). The compound spots were detected by their color and their absorbance at λ 254 nm. UV spectra were recorded on a Jasco V-560 UV/Vis spectrophotometer, CD spectra were obtained from a Jasco J-815 CD spectrophotometer. The specific rotation was measured with a Jasco P-2000 polarimeter. IR spectra were obtained from a Thermo Nicolet 5700 FT-IR spectrometer in ATR mode.

NMR spectra were recorded with an Agilent VNMRS 600 NMR spectrometer operating at a proton NMR frequency of 599.83 MHz using a 5-mm inverse detection cryoprobe. 2D NMR spectra were recorded using standard CHEMPACK 7.1 pulse sequences (s2pul, ¹H,¹H zTOCSY-1D, ¹H,¹H gDQCOSY, ¹H,¹H zTOCSY, ¹H,¹H ROESY(AD), ¹H,¹³C gHSQCAD, ¹H,¹³C gHMBCAD) implemented in Varian VNMRJ 4.2 spectrometer software. The mixing time for the TOCSY experiments was set to 80 msec, for the ROESY experiments was set to 400 msec (**3.1**) and 300 msec (**3.2**, **3.4**). The HSQC experiment was optimized for ¹J_{CH} = 146 Hz with DEPT-like editing and ¹³C-decoupling during acquisition time. The HMBC experiment was optimized for a long-range coupling of 8 Hz; a two-step ¹J_{CH} filter was used (130-165 Hz). ¹H chemical shifts are referenced to internal TMS (¹H δ = 0 ppm), ¹³C chemical shifts to CD₃OD (¹³C δ = 49.0 ppm), CDCl₃ (¹³C δ = 77.0 ppm) or C₅D₅N (¹³C δ = 123.5 ppm).

The positive ion high-resolution ESI mass spectra were obtained from an Orbitrap Elite mass spectrometer (Thermo Fisher Scientific, Germany) equipped with an HESI electrospray ion source (spray voltage 4.0 kV, capillary temperature 275 °C, source heater temperature 80 °C, FTMS resolution 100.000).

Spectroscopic data are available at RADAR (Lam et al., 2019).

The semi-preparative HPLC was performed on a Shimadzu prominence system which consists of a CBM-20A communications bus module, a SPD-M20A diode array detector, a FRC-10A fraction collector, a DGU-20A5R degassing unit, a LC-20AT liquid chromatograph, and a SIL-20A HT auto sampler, using a YMC Pack Pro C18 column (5 μ m, 120 Å, 150 x 10 mm I.D, YMC, USA) with H₂O (A) and CH₃CN (B) at a flow rate of 2.5 mL/min.

3.4.2 Fungal material

Fruiting bodies of *Cortinarius pyromyxa* M. M. Moser & E. Horak (Cortinariaceae) were collected during autumn in Chile, IX. Region Araucania, Province Malleco, District of Angol, Cordillera de Nahuelbuta, LS 37° 49' 42", LO 73° 00' 00", 1196 msnm, on soil and leaf litter under *Nothofagus dombeyi* (Mirb.) Oerst. on 11.05.2017 (collection CONC-F 1783, leg. N. Arnold, det. G. Palfner), and IX. Region Araucania, Province Malleco, District of Curacautin, Rio Blanco near Laguna Blanca, LS 38° 24' 18", LO 71° 41' 34", 1032 msnm, on soil and leaf litter under *Nothofagus dombeyi* on 20.04.2013 (collection CONC-F0938, leg. et det. G. Palfner). Voucher specimens are deposited in the Fungarium of Concepción University (CONC-F). A duplicate is deposited at the Leibniz Institute of Plant Biochemistry (IPB), Halle, Germany.

3.4.3 Molecular phylogenetic analyses

DNA was extracted from small pieces of dehydrated basidiomata of two collections of *Cortinarius pyromyxa* CONC-F1783, CONC-F0938 (Figure S1, Supplementary data) using the commercially available FastDNA™ SPIN kit for Soil and the FastPrep™ Instrument (MP Biomedicals, Santa Ana, CA, USA).

Amplification of the ribosomal internal transcribed spacer region (ITS) was carried out by PCR in a Veriti™ 96-well thermal cycler (Applied Biosystems, Foster City, CA, USA) in a 25 microliters reaction containing: KAPA Taq ReadyMix with dye containing 1.5 mM MgCl₂ (KAPA Biosystems, Wilmington, MA, USA), two microliters DNA and 0.2 μM each primer (ITS1: 5' TCCGTAGGTGAACCTGCGG; ITS4: 5' TCCTCCGCTTATTGATATGC), under the following amplification conditions: initial denaturation step at 95°C for 3 min; followed by 35 cycles at 95°C for 15 s, 54°C for 15 s and 72°C for 30 s; and a final step a 72°C for 7 min.

Products were visualized on a 1.5% agarose gel in 0.5 x TAE buffer and then purified and sequenced using Sanger methodology at Macrogen Korea, Seoul, Republic of Korea.

The obtained DNA sequences were submitted for closest matches to the NCBI nucleotide database using the Basic Local Alignment Search Tool (BLAST); subsequently, sequences were analysed, aligned and a phylogenetic tree was constructed with selected sequences available in NCBI nucleotide database of *Cortinarius* spp. in the same subgenus *Myxacium* from both hemispheres (Table S2, Supplementary data). Applying Geneious® 9.1.8 software (Kearse et al. 2012), we used the neighbor-joining method and the HKY genetic distance model, with 1000 bootstrap resampling replicates. *Tricholoma aurantium* was employed as outgroup to root the tree.

3.4.4 Extraction and isolation

Air-dried fruiting bodies of *Cortinarius pyromyxa* were crushed using a blender and subsequently extracted with EtOAc (3 x 2L), MeOH (3 x 2L); and 80% aqueous MeOH (3 x 2L) in an ultrasound bath for 1 h at room temperature. The yellow-brown solutions were evaporated *in vacuo* to dryness to give three crude extracts (EtOAc, MeOH, and aq. MeOH). The MeOH and aq. MeOH extracts

were then combined according to their TLC pattern and subjected to Diaion HP20 column, eluting with water followed by MeOH. The resulting MeOH fraction and the crude EtOAc extract were combined together to afford a residue (11.45 g). This residue was chromatographed on a Sephadex LH20 column, using CH₂Cl₂ – MeOH (1:1) as eluent to give six fractions (A1 – A6). Fraction A2 was separated on a silica gel 60 silanized column, eluting with *n*-hexane – EtOAc (5:1 → 1:1), which resulted in four fractions (A2a – A2d). Fraction A2a was first subjected to a silica gel column using *n*-hexane – EtOAc (10:1 → 1:2) as solvents, and then purified by semipreparative RP-C₁₈ HPLC (0 → 20 min, 30 → 100% solvent B) to afford **3.1** (*t*_R = 11.8 min, 8 mg). Likewise, fraction A2b was purified to obtain three yellow compounds **3.2** (*t*_R = 10.8 min, 5 mg), **3.3** (*t*_R = 10.3 min, 0.2 mg), and **3.4** (*t*_R = 10.2 min, 3 mg).

Pyromyxone A (3.1): yellow amorphous solid; TLC *R*_f 0.66 (*n*-hexane – EtOAc, 2:1); [α]_D²⁷ +42.5 (*c* 0.190, MeOH); UV (MeOH) λ_{\max} (log ϵ) 220 (1.87), 286 (1.78), 357 (1.52), 430 (1.71) nm; CD (MeOH) [θ]₂₂₉ +26939, [θ]₂₄₈ -5584, [θ]₂₈₁ +15555, [θ]₃₅₇ -24667, [θ]₄₃₁ +10529 deg cm² x dmol⁻¹; IR (ATR) ν_{\max} 3388 (w), 3014 (w), 2960 (w), 2297 (w), 2871 (w), 2362 (br, w), 1690 (s), 1624 (m), 1600 (m), 1464 (w), 1387 (w), 1369 (w), 1349 (w), 1274 (w), 1214 (m), 1177 (w), 1095(w), 1062 (w), 1033 (w), 1006 (w), 946 (w), 857 (w), 841 (w), 802 (w), 747 (s) cm⁻¹; ¹H NMR and ¹³C NMR see Table 1; HRESIMS *m/z* 298.1793 ([M+H]⁺, calcd for C₁₉H₂₄NO₂⁺, 298.1802).

Pyromyxone B (3.2): yellow amorphous solid; TLC *R*_f 0.48 (*n*-hexane – EtOAc, 2:1); [α]_D²⁶ -32.2 (*c* 0.190, MeOH); UV (MeOH) λ_{\max} (log ϵ) 267 (1.81), 314 (1.98) nm; CD (MeOH) [θ]₂₀₈ +14959, [θ]₂₂₉ +7121, [θ]₂₆₂ +17530, [θ]₃₃₀ -9552 deg cm² x dmol⁻¹; IR (ATR) ν_{\max} 3346 (br, w), 2977 (w), 2934 (w), 2987 (w), 2359 (w), 2342 (w), 1682 (s), 1634 (s), 1385 (m), 1268 (m), 1214 (m), 1075 (s), 1026 (s), 750 (s) cm⁻¹; ¹H NMR and ¹³C NMR see Table 2; HRESIMS *m/z* 296.1649 ([M+H]⁺, calcd for C₁₉H₂₂NO₂⁺, 296.1645).

Pyromyxone C (3.3): yellow solid; TLC *R*_f 0.60 (*n*-hexane – EtOAc, 2:1); [α]_D²⁴ +92.5 (*c* 0.019, MeOH); UV (MeOH) λ_{\max} (log ϵ) 218 (3.96), 331 (2.92) nm; CD (MeOH) [θ]₂₁₅₋₂₅₈₁₃, [θ]₂₃₉ +19043, [θ]₂₈₅ +4522, [θ]₃₂₉ -689 deg cm² x dmol⁻¹; ¹H NMR and ¹³C NMR see Table 2; HRESIMS *m/z* 312.1593 ([M+H]⁺, calcd for C₁₉H₂₂NO₃⁺, 312.1594).

Pyromyxone D (3.4): yellow solid; TLC *R*_f 0.35 (*n*-hexane – EtOAc, 2:1); [α]_D²⁵ +28.3 (*c* 0.145, MeOH); UV (MeOH) λ_{\max} (log ϵ) 214 (1.90), 344 (1.21) nm; CD (MeCN) [θ]₁₉₁₊₄₆₃, [θ]₁₉₉₊₅₈₈, [θ]₂₂₄₊₅₆₇₅, [θ]₂₅₂₊₂₂₀₉, [θ]₂₇₈₊₃₀₄₂, [θ]₃₂₆₋₁₅₄₈ deg cm² x dmol⁻¹; IR (ATR) ν_{\max} 3362 (br, w), 2930 (m), 2871 (m), 2358 (w), 1764 (m), 1687 (s), 1643 (m), 1628 (m), 1572 (w), 1455 (w), 1385 (w), 1264 (w), 1216 (m), 1168 (w), 1106 (w), 1083 (w), 1066 (w), 1025 (m), 980 (w), 939 (w), 850 (w), 808 (w), 781 (w), 748 (w), 722 (w), 705 (w), 695 (w) cm⁻¹; ¹H NMR and ¹³C NMR see Table 2; HRESIMS *m/z* 297.1480 ([M+H]⁺, calcd for C₁₉H₂₁O₃⁺, 297.1485).

3.4.5 X-ray crystallographic data of compound 3.1

C₁₉H₃₂NO₂, formula weight 297.38, monoclinic system, space group C2, a = 2074.70(19), b = 680.14(4) pm, c = 1240.91(12) pm, V = 1.5933(2) nm³, Z = 4, d = 1.240 Mg/m³, crystal size: 0.490

x 0.050 x 0.050 mm³, number of independent reflections = 2587, R(int) = 0.0693, completeness to $\theta = 24.993^\circ$: 99.3 %. The structure was solved by direct methods and refined by full-matrix least-squares on F^2 . Final R indices [$I > 2\sigma(I)$]: R1 = 0.0345, wR2 [all data] = 0.0565. Data set for the crystal structure was collected with a STOE-IPDS2 diffractometer. Programs used: structure solution and refinement SHELX (Sheldrick, 2008) and graphics Diamond (Diamond, 2017). Crystallographic data for **3.1** have been deposited with the Cambridge Crystallographic Data Centre (CCDC 1588663). Copies of these data can be obtained free of charge from the Cambridge Crystallographic Data Centre on application to the Director, CCDC, 12, Union Road, Cambridge CB2 1 EZ, UK (e-mail: deposit@ccdc.cam.uk).

3.4.6 Computational details

All possible stereoisomers of compounds **3.1-3.4** were constructed using the Molecular Operating Environment (MOE 2016) software and energy optimized using the MMFF94 molecular mechanics force field (Halgren, 1999). Conformational analysis was performed for the rotation of the isopropyl group, but it appeared later that the three alternative low energy conformations have only minor influences on calculated CD spectra. Furthermore, for the six-membered ring, an up and down conformations of the C-6 carbon atom was calculated. The DFT optimized structures with conformation other than the ones shown in figure S44 are energetically more than 4 kcal/mol less stable and were, therefore, not included in spectra calculations. Thus, here only the CD spectra are shown for the displayed conformations representing the lowest energy conformation of each compound and no Boltzmann distribution was taken into consideration. Subsequently all structures were again optimized by using the density functional theory (DFT) with BP86 functional and the def2-TZVPP basis set (Becke, 1988; Karton et al., 2008; Perdew, 1986; Schäfer et al., 1992; Weigend and Ahlrichs, 2005) implemented in the *ab initio* ORCA 3.0.3 program package (Neese et al., 2012). The influence of the solvent MeOH was included in the DFT calculations using the COSMO model (Sinnecker et al., 2006). For the simulation of the CD spectra, the first 50 excited states of each enantiomer were calculated by applying the long-range corrected hybrid functional TD CAM-B3LYP with the def2-TZVP(-f) and def2-TZVP/J basis sets (Karton et al., 2008; Schäfer et al., 1992; Weigend and Ahlrichs, 2005). The CD curves were visualized and compared with the experimental ones with the help of the software SpecDis 1.64 (Bruhn et al. 2013, 2014) from the calculated rotatory strength values using a Gaussian distribution function at a half-bandwidth of $\sigma = 0.3$ eV.

3.4.7 Antifungal assay

Compounds **3.1**, **3.2** and **3.4** were tested in a 96-well microtiter plate assay against *Botrytis cinerea* Pers., *Septoria tritici* Desm., and *Phytophthora infestans* (Mont.) De Bary as described earlier (Otto et al., 2016).

3.4.8 Antibacterial assay

The isolated compounds **3.1**, **3.2** and **3.4** (1 and 100 μM) were tested against the gram-negative *Aliivibrio fischerii* and the gram-positive *Bacillus subtilis*. Chloramphenicol (100 μM) was used as positive control and induced the complete inhibition of bacterial growth.

The assay against *Aliivibrio fischeri* was performed according to a procedure described by Stark (2016) using the gram-negative *A. fischeri* test strain DSM507 (batch no. 1209). Briefly, for each test run a fresh glycerol stock was incubated in 25 ml BOSS medium at 100 rpm and 23 °C for 16-18 h and was afterwards diluted with fresh BOSS medium to an appropriate cell number (luminescence value between 30.000 and 50.000 RLU). The assay was conducted on black flat bottom 96 well plates (Brand cell Grade™ premium, STERILE R) in a final volume of 200 μl of BOSS medium containing 1% DMSO in each well (100 μl diluted bacterial solution and 100 μl test solution). The plates were incubated in the dark at 23 °C and 100 % humidity without lid and without shaking for 24 h. The bioluminescence (obtained in relative luminescence units, RLU) is dependent on the cell density and was determined after 24 h using the microplate reader TecanSpark. Therefore, the whole wavelength range was detected for 1000 ms without preliminary shaking to avoid secondary oxygen effects. The results (mean value \pm standard deviation, $n = 6$) are given as relative values (% inhibition) in comparison to the negative control (bacterial growth, 1% DMSO, without test compound). Negative values indicate an elevation of luminescence /increase of bacterial growth.

The activity against *Bacillus subtilis* 168 (DSM 10) is determined in a turbidimetric assay. A preculture in 100 ml tryptone yeast (TY) broth was incubated at 37°C for 24 h with agitation (120 rpm). The assay was performed on clear flat bottom 96 well plates (Greiner Bio-one) in a final volume of 200 μl TY broth containing 1% DMSO in each well (100 μl diluted bacterial suspension and 100 μl test solution). The microbial density was adjusted to the absorption of the medium at $\lambda = 612$ nm. To eliminate the influence of colored compounds for each test sample color controls without bacteria were treated in the same manner. The plate with lid was incubated for 16 h at 37°C with shaking (80 rpm) and the absorption determined at 612 nm using the microplate reader TecanSpark. The results (mean value \pm standard deviation, $n = 6$) are given as relative values (% inhibition) in comparison to the negative control (bacterial growth, 1% DMSO, without test compound) after subtracting background absorption of color control samples.

3.5 References

- Becke, A. D., 1988. Density-functional exchange-energy approximation with correct asymptotic behavior. *Phys Rev A Gen Phys* 38, 3098-3100.
- Brady, S. F., Bondi, S. M., Clardy, J., 2001. The guanacastepenes: a highly diverse family of secondary metabolites produced by an endophytic fungus. *J Am Chem Soc* 123, 9900-9901.
- Brady, S. F., Singh, M. P., Janso, J. E., Clardy, J., 2000. Guanacastepene, a fungal-derived diterpene antibiotic with a new carbon skeleton. *J Am Chem Soc* 122, 2116-2117.

- Bruhn, T., Schaumlöffel, A., Hemberger, Y., Bringmann, G., 2013. SpecDis: quantifying the comparison of calculated and experimental electronic circular dichroism spectra. *Chirality* 25, 243-249.
- Bruhn, T., Schaumlöffel, A., Hemberger, Y., Bringmann, G., 2014. SpecDis. University of Würzburg, Germany.
- Chen, H. P., Liu, J. K., 2017. Secondary metabolites from higher fungi. In: Progress in the chemistry of organic natural products 106, Springer International Publishing AG, Cham, pp. 1-201.
- Diamond, 2017. Visual crystal structure information system. Crystal Impact GbR, Bonn.
- Elsworth, C., Gill, M., Giménez, A., Milanovic, N. M., Raudies, E., 1999. Pigments of fungi. Part 50.1 Structure, biosynthesis and stereochemistry of new dimeric dihydroanthracenones of the phlegmacin type from *Cortinarius sinapicolor* Cleland. *J Chem Soc Perkin Trans 1*, 119-126.
- Garnica, S., Schon, M. E., Abarenkov, K., Riess, K., Liimatainen, K., Niskanen, T., Dima, B., Soop, K., Froslev, T. G., Jeppesen, T. S., Peintner, U., Kuhnert-Finkernagel, R., Brandrud, T. E., Saar, G., Oertel, B., Ammirati, J. F., 2016. Determining threshold values for barcoding fungi: lessons from *Cortinarius* (Basidiomycota), a highly diverse and widespread ectomycorrhizal genus. *FEMS Microbiol Ecol* 92, fiw045.
- Garnica, S., Weiss, M., Oberwinkler, F., 2002. New *Cortinarius* species from *Nothofagus* forests in South Chile. *Mycologia* 94, 136-145.
- Garrido, N., 1988. Agaricales s.l. und ihre Mykorrhizen in den Nothofagus-Wäldern Mittelchiles. J. Cramer, Berlin, Stuttgart, Germany, pp. 1-520.
- Gill, M., 1994. Pigments of fungi (Macromycetes). *Nat Prod Rep* 11, 67-90.
- Gill, M., 1996. Pigments of fungi (Macromycetes). *Nat Prod Rep* 13, 513-528.
- Gill, M., 1999. Pigments of fungi (Macromycetes). *Nat Prod Rep* 16, 301-317.
- Gill, M., 2001. The biosynthesis of pigments in Basidiomycetes. *Aust J Chem* 54, 721-734.
- Gill, M., 2003. Pigments of fungi (Macromycetes). *Nat Prod Rep* 20, 615-639.
- Gill, M., Steglich, W., 1987. Pigments of fungi (Macromycetes). In: Herz, W., Grisebach, H., Kirby, G. W., Tamm, C. (Eds.), Progress in the chemistry of organic natural products 51. Springer-Verlag, Wien, New York, pp. 1-317.
- Halgren, T. A., 1999. MMFF VI. MMFF94s option for energy minimization studies. *J Comp Chem* 20, 720-729.
- Harrower, E., Bougher, N. L., Winterbottom, C., Henkel, T. W., Horak, E., Matheny, P. B., 2015. New species in *Cortinarius* section *Cortinarius* (Agaricales) from the Americas and Australasia. *MycKeys* 11, 1-21.
- Horak, E., Wood, A. E., 1990. *Cortinarius* Fr. (Agaricales) in Australasia. 1. Subgen. *Myxacium* and subgen. *Paramyxacium*. *Sydowia* 42, 88-168.
- Invernizzi, A. G., Vidari, G., Vita-Finzi, P., 1995. Trichoaurantianolide A, a new diterpene with an unprecedented carbon skeleton from *Tricholoma aurantium*. *Tetrahedron Lett* 36, 1905-1908.
- Jaenicke, L., Marnett, F.-J., 1986. The irones and their precursors. In: Herz, W., Grisebach, H., Kirby, G. W., Tamm, C. (Eds.), Fortschritte der Chemie organischer Naturstoffe / Progress in the chemistry of organic natural products, vol. 50. Springer, Vienna, 1-25.
- Jiang, M. Y., Feng, T., Liu, J. K., 2011. N-containing compounds of Macromycetes. *Nat Prod Rep* 28, 783-808.

- Karton, A., Tarnopolsky, A., Lamère, J.-F., Schatz, G. C., Martin, J. M. L., 2008. Highly accurate first-principles benchmark data sets for the parametrization and validation of density functional and other approximate methods. Derivation of a robust, generally applicable, double-hybrid functional for thermochemistry and thermochemical kinetics. *J Phys Chem A* 112, 12868-12886.
- Kearse, M., Moir, R., Wilson, A., Stones-Havas, S., Cheung, M., Sturrock, S., Buxton, S., Cooper, A., Markowitz, S., Duran, C., Thierer, T., Ashton, B., Meintjes, P., Drummond, A., 2012. Geneious Basic: an integrated and extendable desktop software platform for the organization and analysis of sequence data. *Bioinformatics* (Oxford, England) 28, 1647-1649.
- Kirk, P. M., Cannon, P. F., Minter, D. W., Stalpers, J. A., 2008. Dictionary of the fungi. CABI Wallingford, UK, pp. 1-784.
- Markovic, D., Kolym padi, M., Deguin, B., Poree, F. H., Turks, M., 2015. The isolation and synthesis of neodolastane diterpenoids. *Nat Prod Rep* 32, 230-255.
- Moser, M., 1985. The relevance of chemical characters for the taxonomy of Agaricales. *Proc Indian Acad Sci (Plant Sci)* 94, 381-386.
- Moser, M., Horak, E., 1975. Cortinarius Fr. und nahe verwandte Gattungen in Sudamerika. *Beih. Nov. Hed.* 52, pp. 1-628.
- Neese, F., 2012. The ORCA program system. *WIREs Comput Mol Sci* 2, 73-78.
- Otto, A., Porzel, A., Schmidt, J., Brandt, W., Wessjohann, L., Arnold, N., 2016. Structure and absolute configuration of pseudohygrophorones A¹² and B¹², alkyl cyclohexenone derivatives from *Hygrophorus abieticola* (Basidiomycetes). *J Nat Prod* 79, 74-80.
- Otto, A., Porzel, A., Westermann, B., Brandt, W., Wessjohann, L., Arnold, N., 2017. Structural and stereochemical elucidation of new hygrophorones from *Hygrophorus abieticola* (Basidiomycetes). *Tetrahedron* 73, 1682-1690.
- Peintner, U., Moncalvo, J. M., Vilgalys, R., 2004. Toward a better understanding of the infrageneric relationships in *Cortinarius* (Agaricales, Basidiomycota). *Mycologia* 96, 1042-1058.
- Perdew, J. P., 1986. Density-functional approximation for the correlation energy of the inhomogeneous electron gas. *Phys Rev B* 33, 8822-8824.
- Schäfer, A., Horn, H., Ahlrichs, R., 1992. Fully optimized contracted Gaussian basis sets for atoms Li to Kr. *J Chem Phys* 97, 2571-2577.
- Sheldrick, G. M., 2008. A short history of SHELX. *Acta cryst A* 64, 112-122.
- Sinnecker, S., Rajendran, A., Klamt, A., Diedenhofen, M., Neese, F., 2006. Calculation of solvent shifts on electronic g-tensors with the conductor-like screening model (COSMO) and its self-consistent generalization to real solvents (direct COSMO-RS). *J Phys Chem A* 110, 2235-2245.
- Stark, S., 2016. Utilization of the Ugi four-component reaction for the synthesis of lipophilic peptidomimetics as potential antimicrobials. Martin-Luther-University Halle-Wittenberg, Halle (Saale).
- Steglich, W., 1994. Mushrooms - seen through the eyes of an organic chemist. Ernst Schering Research Foundation, Berlin, Germany, pp. 1-23.
- Steglich, W., Steffan, B., Eizenhofer, T., Fugmann, B., Hermann, R., Klamann, J. D., 1990. Some problems in the structural elucidation of fungal metabolites. Ciba Foundation Symposium 154 -Bioactive Compounds from Plants John Wiley & Sons Ltd., Chichester, England, Bangkok, Thailand, pp. 56-65.
- Teichert, A., Lübken, T., Schmidt, J., Porzel, A., Arnold, N., Wessjohann, L., 2005. Unusual bioactive 4-oxo-2-alkenoic fatty acids from *Hygrophorus eburneus*. *Z Naturforsch B* 60, 25-32.

- Wang, F., Tan, J.-W., Liu, J.-K., 2004. Vibratilicin: a Novel Compound from the Basidiomycete *Cortinarius vibratilis*. *Helv Chim Acta* 87, 1912-1915.
- Weigend, F., Ahlrichs, R., 2005. Balanced basis sets of split valence, triple zeta valence and quadruple zeta valence quality for H to Rn: Design and assessment of accuracy. *Phys Chem Chem Phys* 7, 3297-3305.
- Zhou, Z.-Y., Liu, J.-K., 2010. Pigments of fungi (Macromycetes). *Nat Prod Rep* 27, 1531-1570.

3.6 Supplementary data

Supplementary data to this article (HRESIMS, NMR data, UV and CD spectra of **3.1-3.4**; initial morphological analysis of *Cortinarius pyromyxa* M. M. Moser & E. Horak) can be found online at <https://doi.org/10.1016/j.phytochem.2019.05.021>.

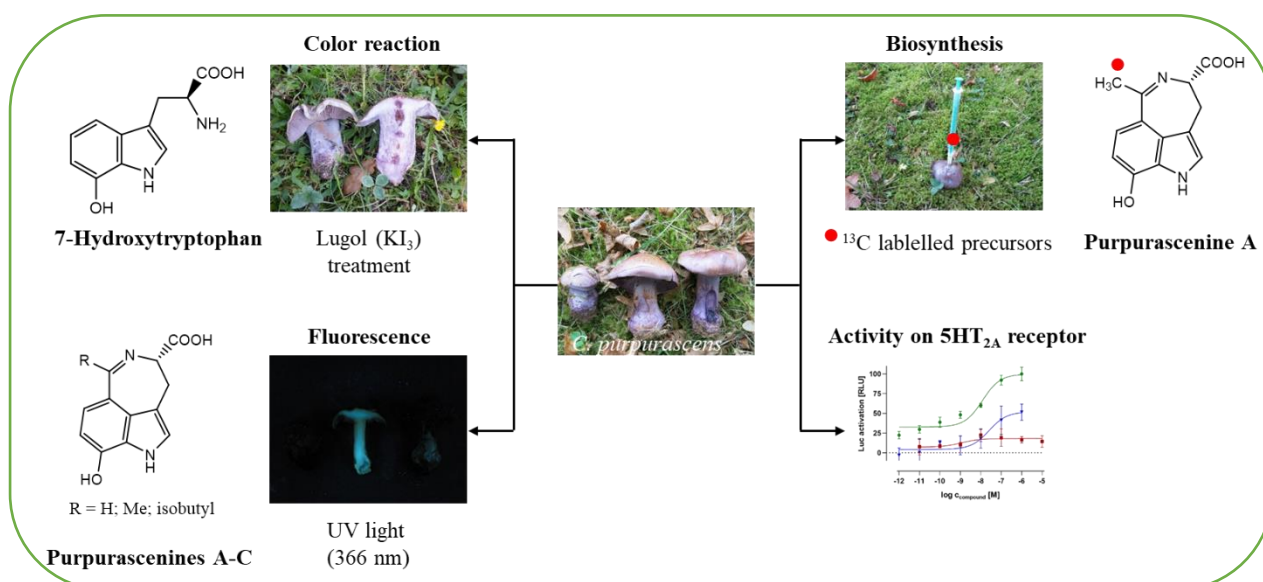
Chapter 4

Purpurascenines A-C, azepinoindole alkaloids from *Cortinarius purpurascens* Fr.: isolation, biosynthesis, and activity studies on 5-HT_{2A} receptor

This Chapter has been submitted as:

Yen T. H. Lam, Jana Hoppe, Dang N. Quang, Andrea Porzel, Alena Soboleva, Wolfgang Brandt, Robert Rennert, Hidayat Hussain, Mehdi D. Davari, Ludger Wessjohann and Norbert Arnold.

Graphical abstract



Highlights

- Three undescribed azepino-indole alkaloids were isolated from *Cortinarius purpurascens*.
- 7-hydroxytryptophan was isolated for the first time from a natural source (*C. purpurascens*).
- The biosynthesis of purpurascenines was proposed on the basis of *in vivo* feeding experiments on fruiting bodies of *C. purpurascens*.
- Purpurascenine A reduces a half of the maximal 5-HT dependent 5-HT_{2A} activation and antagonizes the constitutive activity of the 5-HT_{2A} receptor.

Abstract

Three undescribed azepino-indole alkaloids, named purpurascenines A-C (**4.1-4.3**), together with the new-to-nature 7-hydroxytryptophan (**4.4**) as well as two known compounds, adenosine (**4.5**) and riboflavin (**4.6**), were isolated from fruiting bodies of *Cortinarius purpurascens* Fr. (Cortinariaceae). The structures of **4.1-4.3** were elucidated based on extensive spectroscopic analyses and ECD calculations. Furthermore, the biosynthesis of purpurascenine A (**4.1**) was investigated by *in vivo* feeding experiments using ¹³C labeled samples of sodium pyruvate, alanine, and sodium acetate on fruiting bodies of *C. purpurascens*. The incorporation of ¹³C isotope into **4.1** was analyzed using 1D NMR and HRESIMS methods. In the experiments with [3-¹³C]-pyruvate, the dramatic enrichment of ¹³C was observed, compared to the abundance of ¹³C in unlabeled control and other labeled samples. Accordingly, a biosynthetic route via a direct Pictet-Spengler reaction between α -keto acids and 7-hydroxytryptophan (**4.4**) could be suggested for purpurascenines A-C (**4.1-4.3**). Compound **4.1** exhibited no anti-proliferative and cytotoxic effects against human prostate (PC-3), colorectal (HCT-116) and breast (MCF-7) cancer cells. Additionally, a new functional 5-HT_{2A} receptor activation assay was established showing the ability of purpurascenine A (**4.1**) to reduce the maximal 5-HT dependent 5-HT_{2A} activation by half and to antagonize the constitutive activity of the 5-HT_{2A} receptor.

Keywords: *Cortinarius purpurascens* Fr.; azepino-indole alkaloids; purpurascenines; 7-hydroxytryptophan; biosynthesis; Pictet-Spengler; constitutive activity; 5-HT_{2A} receptor

4.1 Introduction

Cortinarius Fr. (Basidiomycetes) is the largest genus in Agaricales comprising more than 5000 epithets occurring worldwide (Abdallah et al., 2018). Moreover, species in *Cortinarius* are rich sources of structurally diverse secondary metabolites such as terpenoids (Gill, 1999, 2003; Gill and Steglich, 1987; Lam et al., 2019), quinonoid pigments (Chen and Liu, 2017; Gill, 1999, 2003; Gill and Steglich, 1987), *N*-containing compounds (Chen and Liu, 2017; Jiang et al., 2011; Liu, 2005), sphingolipids (Jiang et al., 2011), as well as compounds based on a charge transfer complex between a phenol and a transition metal (Gill, 1999, 2003).

C. purpurascens Fr. belongs to *Cortinarius* subgenus Phlegmacium, section Purpurascetes. For Europe only 5 species within the section Purpurascetes are recognized: *Cortinarius collocandoides* Reumaux, *C. porphyropus* (Alb. & Schwein.) Fr., *C. subporphyropus* Pilat, *C. subpurpurascens* (Batsch) Fr., and *C. purpurascens* Fr. (Saar et al., 2014). All these taxa are well characterized by a slowly progressive violet-purple staining on air (*sic nomen*) when the basidiomata are cut or scratched (Saar et al., 2014). The discoloration can be accelerated by treating the flesh with Lugol solution (1 equiv. I₂, 2 equiv. KI in 100 mL H₂O), leading to a wine-red to violet-purple reaction (Figure B1, Appendix). In addition, the flesh in cross section of *C. purpurascens* showed blue-green fluorescence under UV light ($\lambda = 366$ nm) (Figure B1, Appendix). To the best of our knowledge, there is only one report about chemical constituents from a Chinese mushroom collection named *C. purpurascens*, thereby reporting the isolation of naphthalene–anthraquinone biaryl pigments together with known anthraquinoid pigments (Bai et al., 2013). However, this type of pigments is also characteristic of secondary metabolites from *C. rufo-olivaceus* (Gao et al., 2010; Gill and Steglich, 1987; Steglich and Oertel, 1984; Thiele et al., 2020), which is phylogenetically far distant from *C. purpurascens* (Garnica et al., 2005). Furthermore, quite recently, the occurrence of hydroxyl anthraquinones was described for mixing species names *C. caerulescens* and *C. pupurascens* (Song et al., 2022a), which were corrected to *Cortinarius* sp. soon after publishing (Song et al., 2022b).

Our present paper describes the isolation and structure elucidation of three previously unknown azepino-indole alkaloids from *C. purpurascens*, named purpurascenines A-C (**4.1-4.3**), together with the first report of 7-hydroxytryptophan (**4.4**) as a naturally occurring constituent, beside adenosine (**4.5**) and riboflavin (**4.6**). Compounds **4.1-4.3** and **4.6** are responsible for the fluorescence of the basidiomata under UV light ($\lambda = 366$ nm), while the TLC spot of compound **4.4** turns violet on air or by treating with Lugol solution (Figure B1, Appendix). The biosynthesis of purpurascenine A (**4.1**) was studied by extensive feeding experiments with proposed ¹³C-labeled precursors. Furthermore, the isolated compound **4.1** was examined for cytotoxic effects as well as its activity on the serotonin 5-HT_{2A} receptor.

4.2 Results and discussion

4.2.1 Isolation and structural elucidation of compounds 4.1-4.6

After repeated column chromatography of the methanol crude extract of *C. purpurascens* on Diaion HP20, silica gel, Sephadex LH20, and (semi)-preparative HPLC, compounds **4.1-4.6** could be isolated (Figure 4.1).

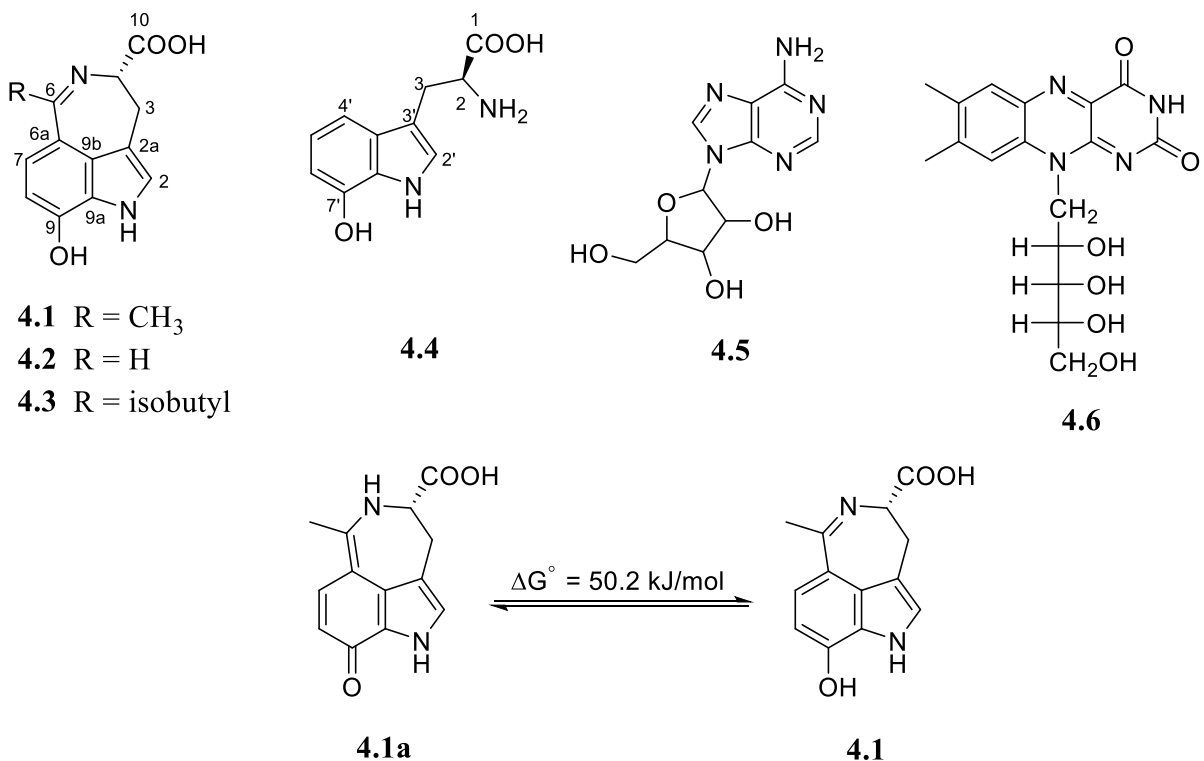


Figure 4.1. Structures of compounds **4.1-4.6**.

Compound **4.1**, purified as yellow amorphous solid, exhibited a strong green fluorescence on TLC plates under UV light ($\lambda = 366 \text{ nm}$). The UV spectrum showed absorption bands at $\lambda_{\text{max}} = 342 \text{ nm}$ and $\lambda_{\text{max}} = 413 \text{ nm}$. The molecular formula of **4.1** was determined to be C₁₃H₁₂O₃N₂ based on HRESIMS data of the protonated molecule at m/z 245.0912 ([M+H]⁺, calcd for C₁₃H₁₃O₃N₂⁺, 245.0921), corresponding to 9 degrees of unsaturation. HRESIMSⁿ analysis (Figure 4.2; Table S1, Supplementary data) in positive ion mode displayed two fragment ions at m/z 199 ([M+H-HCO₂H]⁺) and m/z 184 ([M+H-HCO₂H-CH₃]⁺) as the most abundant peaks in MS² and MS³ spectra, respectively, indicating the loss of a carboxylic functionality and a methyl group. Furthermore, the MS³ spectrum of the ([M+H-HCO₂H]⁺) ion shows two characteristic fragment ions: the ion at m/z 181 ([M+H-HCO₂H-H₂O]⁺) suggests the presence of a hydroxy group, whereas the ion at m/z 131 ([M+H-HCO₂H-HCN-CH₃CN]⁺) represents the hydroxyindan key ion resulting from an hydroxyindole derivative. Previously, such hydroxyindan moiety is also observed in the fragmentation of cimitrypazepine (Nikolić et al., 2012) and brunnein A (Teichert et al., 2007).

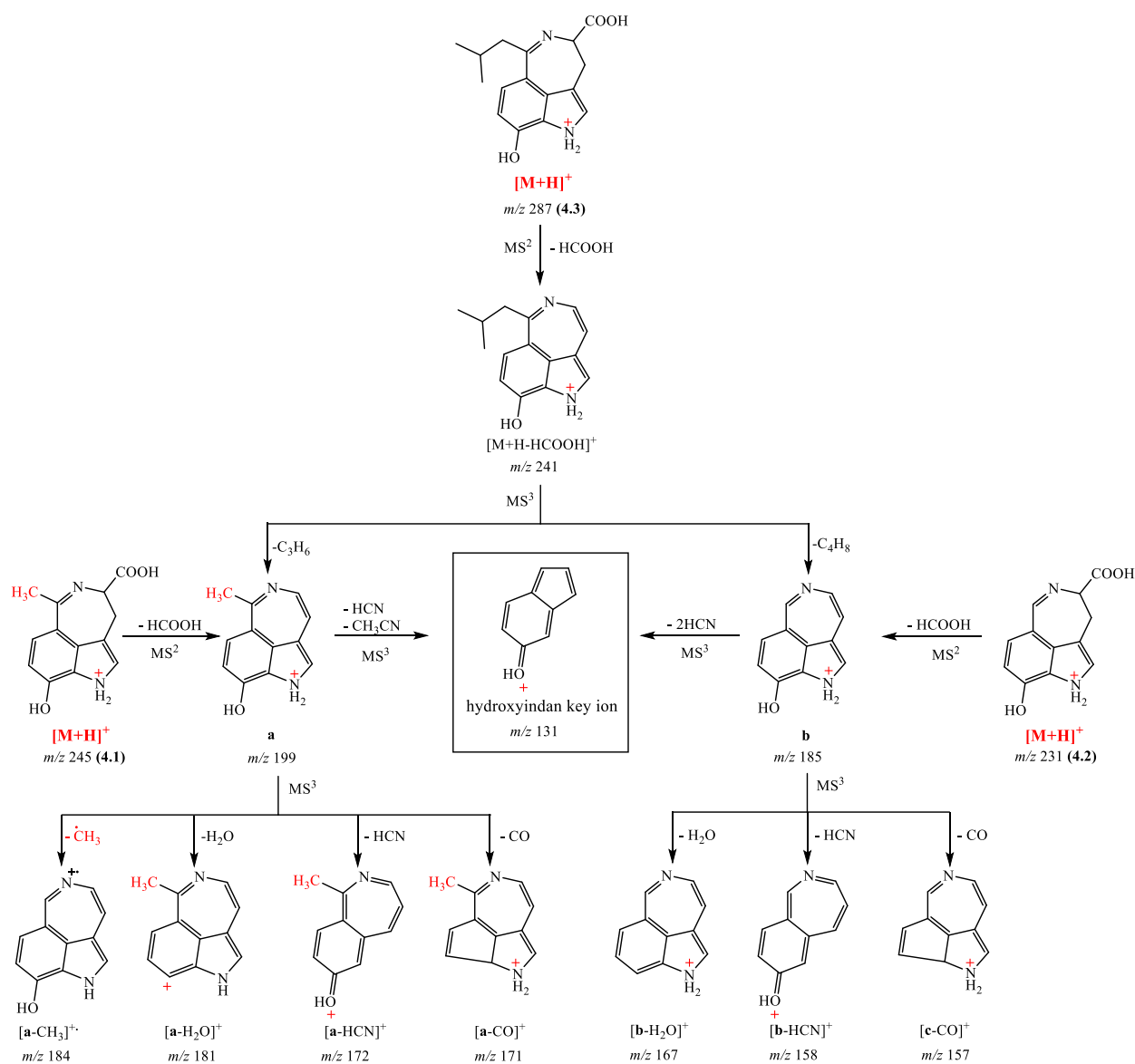


Figure 4.2. Fragmentation pattern of compounds 4.1-4.3.

The structure of **4.1** was further determined on the basis of detailed NMR analysis (Table 4.1, Figure 4.3; Table B2, Appendix). The ^{13}C NMR spectrum of **4.1** reveals 13 carbon resonances including two signals for carbonyl-like carbons at δ_C 171.4 and 178.5 ppm, eight signals for aromatic carbons assigned for the hydroxyindole moiety (δ_C 109-155 ppm), and three signals for high-field shifted carbons (δ_C 23.7, 30.9 and 61.4 ppm). The 1H NMR spectrum of **4.1** displays three resonances for aromatic protons including two ortho-coupling atoms at δ_H 7.95 ppm (1H, d, $J = 8.6$ Hz, H-7) and 6.84 ppm (1H, d, $J = 8.6$ Hz, H-8), together with a singlet at δ_H 7.42 ppm (1H, s, H-2) suggesting a 3,4-substituted hydroxyindole scaffold (indole numbering). This scaffold is confirmed by HMBC correlations from H-2 to C-2a, C-9a and C-9b, from H-7 to C-9 and C-9b, as well as from H-8 to C-6a and C-9a. The additional HMBC correlation from H-2 to C-9 (δ_C 154.6

ppm) supports the position of the hydroxy group at C-9, resulting in the presence of a 3,4-substituted 7-hydroxyindole scaffold (indole numbering).

In addition, an overlapping methine signal at δ_{H} 4.81 ppm (1H, H-4), a broad methylene signal at δ_{H} 3.52 ppm (2H, H₂-3), and a methyl singlet at 2.95 ppm (3H, s, H₃-11) were also detected based on the combination of ¹H NMR, TOCSY and HSQC spectra. The methyl signal showed HMBC correlations with carbons at δ_{C} 178.5 ppm (C-6) and 113.5 ppm (C-6a), allowing the partial structure CH₃-C- to be located at the C-4 position of the 3,4-substituted 7-hydroxyindole scaffold. Moreover, TOCSY spectrum showed that the methine and methylene groups form a spin system with the indole singlet proton at δ_{H} 7.42 ppm (H-2), which exhibits a HMBC correlation with the methylene carbon at δ_{C} 30.9 ppm (C-3). Unfortunately, no HMBC correlations of the methine and methylene protons could be detected despite our repeated NMR studies in different solvents. Nevertheless, by comparison to related structures (e.g. hyrtiazepine (Sauleau et al., 2006) and hyrtioreticulins (Yamanokuchi et al., 2012)), a partial structure -CH₂-CH- could be unambiguously established and assigned at the remaining – C-3 position of the 3,4-substituted 7-hydroxyindole nucleus.

Considering the molecular formula of **4.1**, the unsaturation degrees and the presence of a carboxylic group suggested by HRESIMS studies, as well as the aforementioned analysis, a remaining nitrogen atom is added. This nitrogen binds the quaternary carbon at δ_{C} 178.5 ppm (C-6) and the methine group (C-4), forming a tetrahydroazepine ring. In addition, a carboxylic group is assigned at C-4, also based on its comparable chemical shift with the same position of the close analogue hyrtiazepine (C-4, $\delta_{\text{H}}/\delta_{\text{C}}$ 4.81/61.4 ppm for **4.1**; 4.34/63.3 for hyrtiazepine) (Sauleau et al., 2006). Therefore, the structure of **4.1** was determined to be a new azepino[5,4,3-*cd*]indole derivative, and trivially named purpurascenine A (**4.1**).



Figure 4.3. Key HMBC (plain arrow), ROESY (dashed arrow) and TOCSY (bold) correlations of compound **4.1** and **4.1a**.

Interestingly, during storage of **4.1** in CD₃OD an unusual deuterium exchange phenomenon occurred. In the high field area of the methyl singlet at $\delta_{\text{H}}/\delta_{\text{C}}$ 2.70/22.57 ppm, there are additional “triplet-like” resonances (see Figure B53 and B54, Appendix), which have very close chemical shifts ($\delta_{\text{H}}/\delta_{\text{C}}$ 2.68/22.23 and 2.67/22.06 ppm) and exhibit the same HMBC correlations as the

methyl singlet (Figure B57, Appendix). After five months, both the methyl singlet and the additional “triplet-like” peaks disappeared, indicating that the deuterium exchange in **4.1** had been completed (Figure B58, Appendix). The deuterium exchange of alkyl protons is rarely observable and here is probably based on the effect of the highly conjugated system in **4.1** on its *exo*-methyl group, featuring acidic methyl protons in the α -position to a C=N (in **4.1**) or phenylogous carbonyl (in **4.1a**) group.

Table 4.1. NMR spectroscopic data (600/150 MHz, CH₃OD/D₂O = 5/1 (v/v)) for purpurascenine A in enol (**4.1**) and keto form (**4.1a**).

Position	4.1			4.1a		
	δ_C , type	δ_H (J in Hz)	HMBC	δ_C , type	δ_H (J in Hz)	HMBC
1-NH		11.28, br s ^a			11.16, br s ^a	
2	127.7, CH	7.42, s	2a, 3, 9, 9a, 9b	125.1, CH	7.27 s	2a, 3, 9a, 9b
2a	114.0, qC			116.5, qC		
3	30.9, CH ₂	3.52 ^b	<i>n.d.</i>	33.2, CH ₂	3.69 ^c 3.06 m	2, 2a, 4, 9b, 10 ^a
4	61.4, CH	4.81 ^c	<i>n.d.</i>	63.1, CH	4.06	2a, 3, 6, 10 ^a
6	178.5, qC			171.0, qC		
6a	113.5, qC			109.5, qC		
7	134.3, CH	7.95 d (8.6)	2a, 6, 6a, 9, 9a, 9b	135.4, CH	7.79 d (8.8)	2a, 6, 6a, 9, 9a, 9b
8	109.5, CH	6.84 d (8.6)	6a, 9, 9a	113.1, CH	6.61 d (8.8)	9 ^a ; 6a, 9a
9	154.6, qC			162.7, qC		
9a	126.3, qC			128.2, qC		
9b	130.0, qC			129.5, qC		
9-OH		9.40 br s ^a				
10-COOH	171.4, qC			170.2, qC		
11-CH ₃	23.7, CH ₃	2.95 s	6, 6a, 7	23.3, CH ₃	2.81 s	6, 6a, 7

^a detected in DMSO-*d*₆ measurement; ^b broad signal, chemical shift determined from 2D TOCSY; ^c overlapping signal, chemical shift determined from ¹H, ¹³C HSQC; *n.d.* = not detected.

Compound **4.1a**, obtained when avoiding any acidified solvents during its purification, exhibited identical physical properties [e.g. color, fluorescence under UV light ($\lambda = 366$ nm), R_f , and R_t] and mass spectroscopic data with **4.1**, suggesting that **4.1a** and **4.1** are isomers. While ¹H and ¹³C NMR spectra of **4.1a** are very similar to those of **4.1**, 2D NMR data for **4.1a** showed the major differences for C-6 and C-9. An upfield shift of C-6 (δ_C 171.0 ppm for **4.1a** and 178.5 ppm for **4.1**) and a downfield shift of C-9 (δ_C 162.7 ppm for **4.1a** and 154.6 ppm for **4.1**) confirmed that **4.1a** is the keto-isomer of **4.1**. Interestingly, all missing HMBC correlations of H₂-3 and H-4 in **4.1** could be detected in **4.1a** (Table 4.1, Figure 4.3; Table B2, Appendix). Quantum chemical calculation showed that the keto form (**4.1a**) is 12 kcal more stable than the enol form (**4.1**) (data not shown).

Compounds **4.2** and **4.3**, purified as yellow amorphous solids, exhibited strong green fluorescence on TLC plates under UV light ($\lambda = 366$ nm) and UV absorption bands similar to compound **4.1** (Figure B1, B27, B35, Appendix). The molecular formulas were determined to be

$C_{12}H_{10}O_3N_2$ for **4.2** ($[M+H]^+$ at m/z 231.0758, calcd for $C_{12}H_{11}O_3N_2^+$, 231.0757), and $C_{16}H_{18}O_3N_2$ for **4.3** ($[M+H]^+$ at m/z 287.1381, calcd for $C_{16}H_{19}O_3N_2^+$, 287.1390) established by HRESIMS in positive ion mode. As depicted in Figure 4.2, HRESIMSⁿ analysis of compounds **4.2** and **4.3** showed similar fragmentation patterns to that of purpurascenine A (**4.1**). Upon MS² fragmentation of compounds **4.1-4.3**, the base peak of each compound at m/z 199, 185, 241, respectively, is generated by the loss of a HCO₂H molecule (neutral loss of 46 Da), indicating the fact that they possess a carboxylic acid moiety in their structures. Those base peaks were used as precursor ions in further MSⁿ experiments, showing another common fragmentation feature of **4.1-4.3** that they share the characteristic loss of either a H₂O, HCN, or CO molecule (neutral loss of 18, 27 or 28 Da). Additionally, the key specific fragment at m/z 131, which represents the hydroxyindan key ion, was also detected upon MSⁿ experiments of **4.1-4.3**. Therefore, compounds **4.2** and **4.3** are assumed as close analogues of the new azepino[5,4,3-*cd*]indole alkaloid **4.1**.

Table 4.2. NMR spectroscopic data (600/150 MHz, CH₃OD) of purpurascenine B (**4.2**) and C (**4.3**).

Position	4.2			4.3		
	δ_C , type	δ_H (J in Hz)	HMBC	δ_C , type	δ_H (J in Hz)	HMBC
2	125.5, CH	7.27 s	2a, 3, 9a, 9b	124.4, CH	7.18 s	2a, 9b
2a	117.0, qC			116.8 qC		
3	33.2, CH ₂	3.82 d (15.4) 3.03 dd (15.4, 8.9)	2, 2a, 4, 9b, 10 ^a	33.9, CH ₂	3.74 2.93	<i>n.d.</i>
4	63.1, CH	4.04 d-like (8.8)	<i>n.d.</i>	62.7, CH	3.94	<i>n.d.</i>
6	159.8, CH	8.23 s	9b	171.0, qC		
6a	110.6, qC			<i>n.d.</i>		
7	138.8, CH	7.52 d (8.5)	2a, 6, 9a, 9b	135.6, CH	7.71 d (9.0)	2a, 6, 9a, 9b
8	113.3, CH	6.59 d (8.5)	6a, 9a	115.1, CH	6.48 d (9.0)	9b
9	<i>n.d.</i>			<i>n.d.</i>		
9a	128.0, qC			127.3, qC		
9b	130.6, qC			129.4, qC		
10-CO ₂ H	<i>n.d.</i>			<i>n.d.</i>		
11				45.5, CH ₂	3.12 m 2.70 m	<i>n.d.</i>
12				31.4, CH	2.09 m	<i>n.d.</i>
13				22.8, CH ₃	1.06 d (6.6)	11, 12, 14
14				22.4, CH ₃	1.02 d (6.6)	11, 12, 13

n.d. = not detected.

NMR spectroscopic data of compounds **4.2** and **4.3** (Table 4.2) also closely resemble that of **4.1** except the signals related to substituents at C-6. For compound **4.2**, the high-field singlet at δ_H 2.95 ppm (CH₃-11) is absent, while one additional aromatic resonance at δ_H 8.27 ppm (1H, s, H-6) occurs in the low-field of the ¹H NMR spectrum. This aromatic proton was shown to be involved in a spin system with two aromatic protons at δ_H 7.52 ppm (H-7) and δ_H 6.59 ppm (H-8) as well as saturated protons at δ_H 3.82 / 3.03 ppm (H₂-3) and δ_H 4.04 ppm (H-4) based on its TOCSY

correlations. Unfortunately, due to the low amount of **4.2**, the HMBC spectrum displayed only the correlation from H-6 to C-9b. Nonetheless, the interpretation of MS and NMR data clearly demonstrated that **4.2** is the demethylated derivative of **4.1**, and trivially named purpurascenine B (**4.2**).

Similarly, for compound **4.3**, the methyl singlet at δ_{H} 2.95 ppm (CH₃-11) in **4.1** is replaced by a group of resonances at δ_{H} 1.02-3.12 ppm representing an isobutyl (CH₃)₂CH-CH₂- substituent, which is established on the basis of COSY, TOCSY and HMBC experiments (Table 4.2; Figure B32-B34, Appendix). Therefore, the structure of compound **4.3** was also assigned as a new azepino[5,4,3-*cd*]indole alkaloid, and named purpurascenine C (**4.3**).

Up to now, azepino[5,4,3-*cd*]indole alkaloids form a small group of 30 natural products, roughly equally contributed by fungal cultures (i.e. *Claviceps* and *Penicillium*), plants (i.e. *Psychotria*, *Evodia* and *Cimifuga*) as well as the marine sponge *Hyrtios* spp. (Klein-Junior et al., 2020; Lindsay et al., 2018). Thus, the isolated purpurascenines **4.1-4.3** are the first azepinoindole alkaloids from fungal basidiocarps.

Compound **4.4** was isolated as a white, amorphous solid. HRESIMS studies of the [M+H]⁺ ion at *m/z* 221.0908 afforded the molecular formula C₁₁H₁₂O₃N₂ (calcd for C₁₁H₁₃O₃N₂⁺, 221.0921). Detailed analyses of 1D and 2D NMR spectroscopic data (Figure B39-B43, Appendix) confirmed the structure of **4.4** as 7-hydroxytryptophan. To the best of our knowledge, 7-hydroxytryptophan (**4.4**) was reported since 1990 as a synthetic product (Eich and Rochelmeyer, 1966; Gartz, 1985; van den Berg et al., 1990), but so far it was not found in any natural sources other than *C. purpurascens*. Given that the spot on TLC plate of **4.4** turned violet by exposing to the air or by treating with Lugol solution (Figure B1, Appendix), similar to the color reaction of the mushroom's flesh, we could assume that **4.4** is responsible for this characteristic color change of *C. purpurascens*.

Compound **4.5** was obtained as a white, amorphous solid. Deduced from positive ion high resolution MS studies of the [M+H]⁺ ion at *m/z* 268.1045 (calcd for C₁₀H₁₄O₄N₅⁺, 268.1040) as well as 1D NMR experiments (Figure B46-B48, Appendix), **4.5** was identified as adenosine. All spectroscopic data are in agreement with published data (Ciuffreda et al., 2007).

Compound **4.6**, purified as a yellow solid, exhibited strong green fluorescence on TLC plates under UV light (366 nm). The molecular formula of **4.6** was determined as C₁₇H₂₀O₄N₆ from HRESIMS data ([M+H]⁺ at *m/z* 377.1477, calcd for C₁₇H₂₁O₄N₆⁺, 377.1456). The mass spectroscopic as well as 1D and 2D NMR data (Figure B49-B51, Appendix) of **4.6** were in accordance with those of riboflavin (**4.6**) (Hu et al., 2013).

Among the isolated compounds, compounds **4.1-4.3** and **4.6** are responsible for the blue-green fluorescence of the mushroom under UV light ($\lambda = 366$ nm). Moreover, the first natural 7-hydroxytryptophan (**4.4**) is the chemical component behind the violet reaction of the flesh with Lugol solution and on air characterizing the section Purpurascenites.

The section Scauri, also placed in the section Purpurascentes by Moser (Moser, 1960) because of the same reaction with Lugol, differs in the absence of violet reaction of the flesh and the presence of green pigments in stipe, lamellae, velum and rhizomorphs. *C. scaurus* has been considered as sister species of *C. purpurascens* (Horak, 2005; Moser, 1983). The green pigments (scaurin A and B) of *C. scaurus* were identified as polyenes connected to glutamic acid (Gill, 1999), which can also react with Lugol. Furthermore, the molecular analyses by Garnica et al. suggested that *C. scaurus* belongs to the Scauri clade, whereas *C. purpurascens* is a part of the Purpurascentes clade. Therefore, phylogenetically the Purpurascentes and Scauri are closely related sister groups (Garnica et al., 2005). However, in the view of their chemical entities, they are far distant.

In addition, anthraquinones and specific anthraquinone-related pigments were not detected in *C. purpurascens*. Therefore, the isolation of such types of pigments from a Chinese collection of *C. purpurascens* (Bai et al., 2013) might be based on an incorrect identification of the investigated species.

4.2.2 Absolute configuration of compounds 4.1-4.4

The absolute configuration of compounds **4.1-4.4** was determined using quantum chemical methods. Since each compound has only one chiral center at C-4 (**4.1**, **4.1a**, **4.2**, and **4.3**) or C-1 (**4.4**), corresponding to two possible stereoisomers, the electronic circular dichroism (ECD) spectra of these two presumed isomers were calculated and compared with the experimental ECD spectrum. For compound **4.1**, a similarity factor $S = 0.7911$ (sigma 0.28 eV at 8 nm shift) was found for the *S*-configuration, while the *R*-configuration showed a much lower similarity $S = 0.1253$ (Figure 4.4). This clearly demonstrated that **4.1** has a 4*S* configuration. Likewise, compounds **4.1a**, **4.2-4.4** were shown to have the same *S*-configuration with the similarity factors $S = 0.8309, 0.7451, 0.6336$ and 0.9561 , respectively (Figure B21, B28, B36, B45, Appendix).

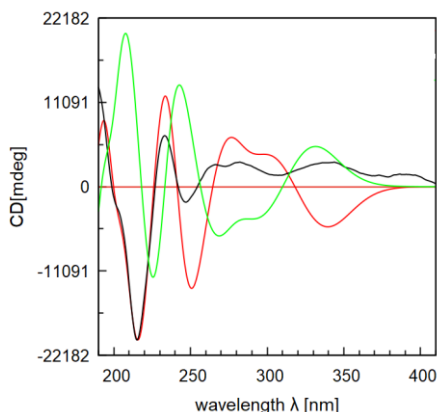


Figure 4.4. Calculated CD spectra of the 4*R* (green) and 4*S* (red) of compound **4.1** in comparison with the experimental one (black).

4.2.3 Biosynthesis of purpurascenines A-C

Owing to their intriguing structures and potential as pharmaceuticals, azepino[5,4,3-*cd*]indole alkaloids have inspired many synthetic studies as well as biosynthetic research (Lindsay et al., 2018). Among the known 30 natural azepino[5,4,3-*cd*]indole alkaloids (Figure 4.5), the plausible biosynthesis of fungi-derived products were investigated by enzyme-based experiments. The biosynthetic pathway of clavicipitic acid, a compound from submerged cultures of *Claviceps* species, was proven to involve 4-dimethylallyltryptophan (DMAT) catalyzed by an enzyme present in the extracted *Claviceps* species (Robbers et al., 1980; Saini et al., 1976). DMAT, an intermediate in ergot alkaloid biosynthesis, is formed via the prenylation of L-tryptophan with dimethylallyl pyrophosphate (DMAPP) catalyzed by dimethylallyl prenyltransferase (Lindsay et al., 2018). Likewise, the presumably decarboxylated derivative of clavicipitic acid, named aurantioclavine, isolated from *Penicillium aurantio-virens* seems to be also biosynthesized by DMAT (Lin et al., 2015). Aurantioclavine, together with tryptamine, was then approved as biosynthetic precursor of communesins (e.g. communesin A), a group of eight azepino-indole alkaloids derived from various *Penicillium* species (Lin et al., 2015). In contrast, the biosynthesis of azepino-indole alkaloids from the marine sponge *Hyrtios* was only proposed based on biomimetic synthetic studies, while the biosynthetic pathway of plant-extracted alkaloids remains untouched due to their fresh detection (Lindsay et al., 2018). In the following part we describe an *in vivo* study towards the biosynthesis of purpurascenine A (4.1).

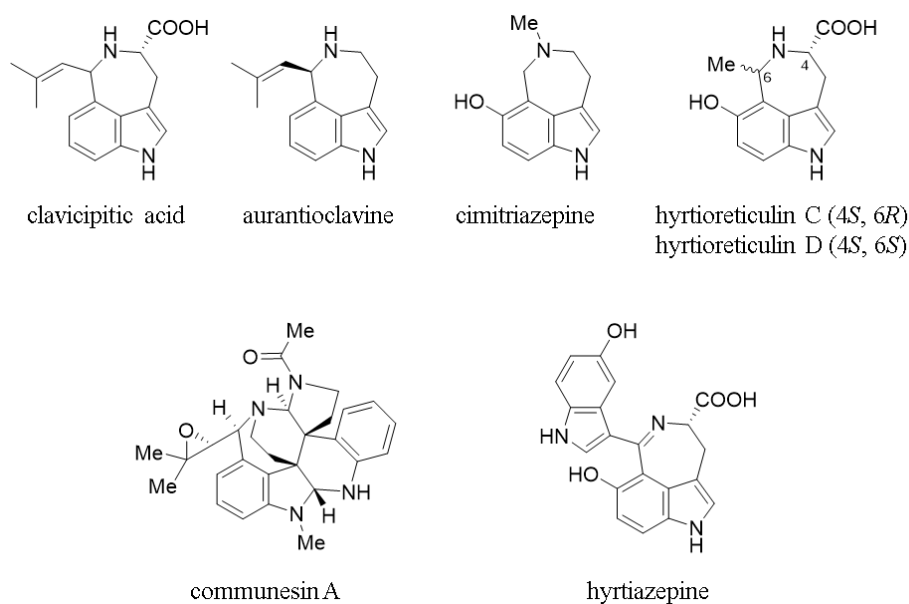
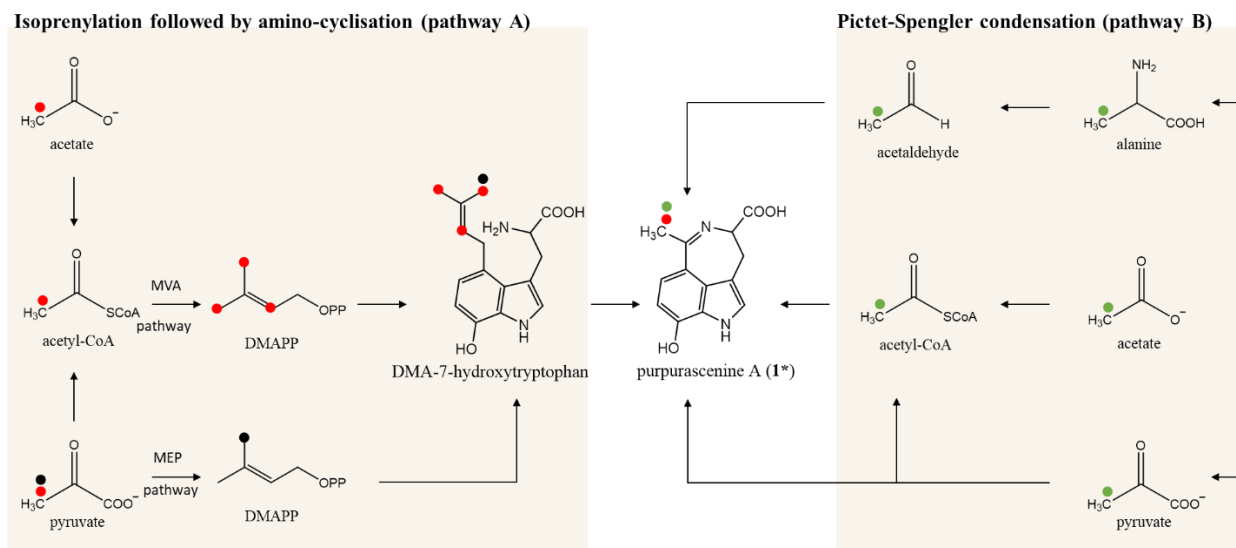


Figure 4.5. Selected azepino-indole alkaloids from different natural sources.

As depicted in Scheme 4.1, azepino[5,4,3-*cd*]indole alkaloids can be biosynthesized by the isoprenylation of tryptophan followed by the amino-cyclisation (pathway A), or via a Pictet-Spengler reaction between tryptophan and an aldehyde component (pathway B). Considering the

involvement of tryptophan as a precursor in the biogenetic synthesis of communesins in *Penicillium expansum* (Lin et al., 2015; Wigley et al., 2006; Wigley et al., 2008; Xu et al., 2014), it could be speculated that the azepinoindole moiety in **4.1** is derived from **4.4**, valid for both pathways A and B in Scheme 4.1.



Scheme 4.1. Possible biosynthesis pathways to purpurascenine A (**4.1***). (A) Isoprenylation followed by amino-cyclisation and predicted labeling pattern after feeding ^{13}C -labeled precursors; (●) position of ^{13}C via mevalonate (MVA) pathway, (●) position of ^{13}C via methylerythritol phosphate (MEP) pathway. (B) Pictet-Spengler condensation and predicted labeling pattern after feeding ^{13}C -labeled precursors (●).

On the one hand, it is possible that the isoprenylation of 7-hydroxytryptophan (**4.4**) with dimethylallylpyrophosphate (DMAPP) forms 4-dimethylallyl-7-hydroxytryptophan (DMA-7-hydroxytryptophan) in pathway A. The following amino-cyclisation afforded purpurascenine A (**4.1**). DMAPP can be achieved from the mevalonate (MVA) pathway via acetyl-CoA from pyruvate and acetate or from the methylerythritol phosphate (MEP) pathway via condensation of pyruvate and glyceraldehyde-3-phosphate (Yamazaki et al., 2004).

On the other hand, the biogenesis of **4.1** may also involve a Pictet-Spengler reaction in pathway B. The Pictet-Spengler condensation, enzymatically catalyzed by Pictet-Spenglerase, had been evidenced in different organisms in nature (Naoi et al., 2002; Stockigt et al., 2011). 7-hydroxytryptophan (**4.4**) acts as the amine precursor reacting with an aldehyde constituent to form purpurascenine A (**4.1**). The three possible aldehyde constituents could be pyruvate, acetyl-CoA or acetaldehyde. Acetyl-CoA is derived from acetate or pyruvate, whereas acetaldehyde is formed directly from alanine. Alanine itself may be formed from pyruvate via an aminotransferase.

To examine these putative biogenic pathways of purpurascenine A (**4.1**), feeding experiments on basidiocarps of *C. purpurascens* were carried out in the field. To guarantee efficient

incorporation of labelled precursors into **4.1***, young fruiting bodies were selected due to their high rate of secondary metabolic activity. For this purpose, aqueous solutions of [3-¹³C]-pyruvate, [3-¹³C]-alanine, or [2-¹³C]-acetate were separately injected using a syringe into the caps and stems of fruiting bodies of *C. purpurascens*. The basidiomata were harvested after seven to nine days after feeding. To evaluate the incorporation of fed precursors, intense ¹H NMR and HRESIMS studies were performed. As illustrated in Scheme 1, the methyl ¹³CH₃-11 group can be incorporated into **4.1*** from the labeled precursors with exception via MEP pathway (in pathway A). Successful incorporation of the labeled precursors would lead to an increase of the ¹³C satellites of the methyl signal CH₃-11 in the ¹H NMR spectrum as well as the enrichment of the isotope ions abundance in the HRESIMS spectrum.

Purpurascenine A (**4.1***) was isolated from the methanol extract of *C. purpurascens* using liquid-liquid partition, column chromatography on Sephadex LH20 followed by semi-preparative HPLC. Approximately 2.5 mg of **4.1*** was obtained from fruiting bodies of *C. purpurascens* fed [3-¹³C]-alanine or [2-¹³C]-acetate, but only 0.5 mg of **4.1*** could be isolated after feeding [3-¹³C]-pyruvate. The ¹H NMR and HRESIMS data of **4.1*** are in agreement with those of the unlabeled control **4.1**.

The ¹H NMR spectrum of **4.1*** displayed a singlet signal at δ_{H} 2.7-2.9 ppm representing the methyl ¹³CH₃-11 group. The ¹³C satellites ($J = 130$ Hz) of this methyl signal were confirmed by ¹H, ¹³C HSQC spectrum without ¹³C decoupling (Figure B56, Appendix). In each sample of compound **4.1***, the integration of the main peak of the methyl group ¹³CH₃-11 was set to 100 in order to calculate the integration of satellite signals (Figure B54, B61, B64, Appendix) allowing to evaluate the incorporation of ¹³C containing precursors into purpurascenine A (**4.1***).

As shown in Table 4.3, the satellite intensity was increased up to sevenfold in **4.1*** due to the incorporation of [3-¹³C]-pyruvate, and over twofold in **4.1*** fed [3-¹³C]-alanine or [2-¹³C]-acetate, compared to the unlabeled compound **4.1**. Since the dramatic enhancement of the satellite intensity was only observed after feeding [3-¹³C]-pyruvate, the biosynthesis of the azepine moiety in **4.1** through isoprenylation followed by amino-cyclisation (pathway A) can be excluded. Therefore, the biosynthesis of **4.1** via a direct Pictet-Spengler condensation of pyruvate is the most favored one.

Table 4.3. Incorporation of [3-¹³C]-pyruvate, [3-¹³C]-alanine, and [2-¹³C]-acetate into purpurascenine A (**4.1***) based on ¹H NMR spectroscopic data.

Position	Satellite intensity (%) ^c			
	unlabeled control ^a (4.1)	[3- ¹³ C]-pyruvate ^b (4.1*)	[3- ¹³ C]-alanine ^a (4.1*)	[2- ¹³ C]-acetate ^a (4.1*)
11-CH ₃	1.1 ^d	7.7	3.0	2.8

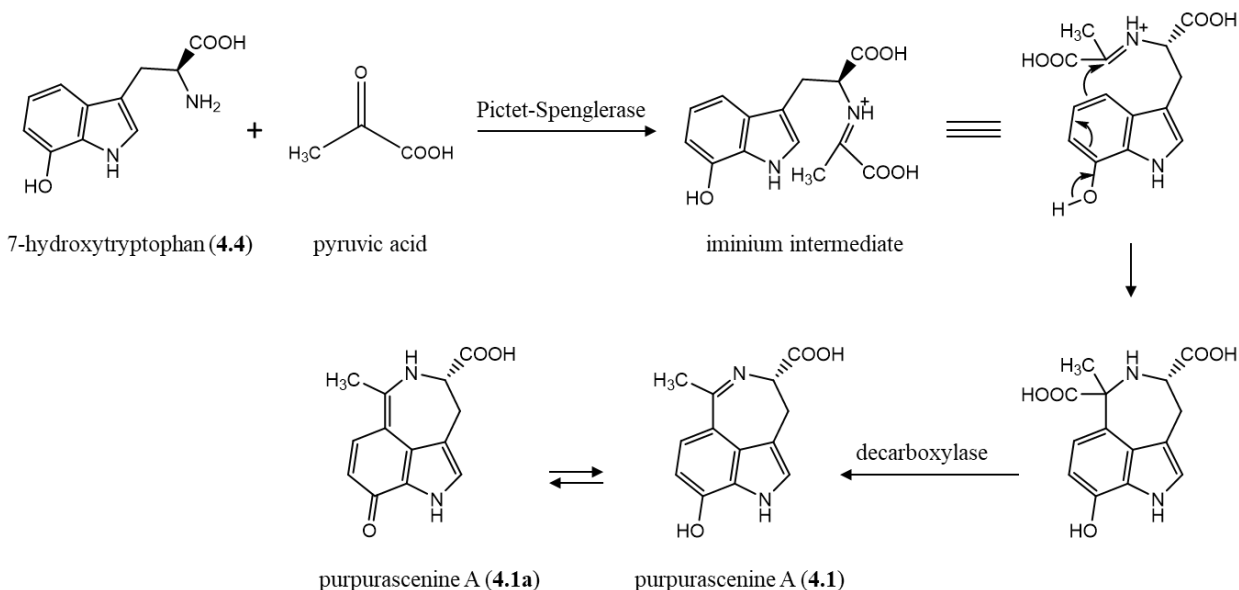
^a measured in CD₃OD/D₂O = 7/3 (v/v); ^b measured in CD₃OD; ^c percentage ratio of the ¹³C – ¹³C satellite area to the global NMR signal area of the methyl group; ^d not detected, value from natural abundance of ¹³C.

Additionally, the incorporation of ^{13}C labelled precursors in **4.1*** was corroborated by HRESIMS measurements displaying enhancement of the [M+1] and [M+2] ion abundances (Table 4.4). In accordance with NMR results, the relative intensity of isotope ions of **4.1*** increased significantly (almost twofold for [M+1] ion and threefold for [M+2] ion) after feeding [3- ^{13}C]-pyruvate, and slightly after feeding [3- ^{13}C]-alanine or [2- ^{13}C]-acetate, compared to the unlabeled control **4.1**.

Table 4.4. HRESIMS analyses of purpurascenine A (**4.1***) labeled with [3- ^{13}C]-pyruvate, [3- ^{13}C]-alanine, and [2- ^{13}C]-acetate.

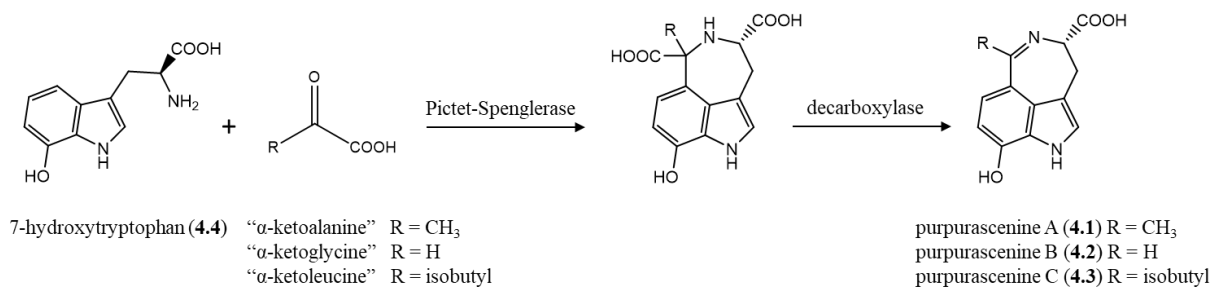
Ion		<i>m/z</i> , Relative intensity (%)			
		unlabeled control (4.1)	[3- ^{13}C]-pyruvate (4.1*)	[3- ^{13}C]-alanine (4.1*)	[2- ^{13}C]-acetate (4.1*)
$^{12}\text{C}_{13}\text{H}_{13}\text{O}_3\text{N}_2^+$	[M]	245.0918, 100.0	245.0920, 100.0	245.0921, 100.0	245.0918, 100.0
$^{12}\text{C}_{12}^{13}\text{C}_1\text{H}_{13}\text{O}_3\text{N}_2^+$	[M+1]	246.0952, 13.7	246.0954, 23.0	246.0954, 16.0	246.0952, 15.2
$^{12}\text{C}_{11}^{13}\text{C}_2\text{H}_{13}\text{O}_3\text{N}_2^+$	[M+2]	247.0987, 0.8	247.0989, 2.1	247.0987, 1.2	247.0988, 1.1
$^{12}\text{C}_{10}^{13}\text{C}_3\text{H}_{13}\text{O}_3\text{N}_2^+$	[M+3]	<i>n.d.</i>	<i>n.d.</i>	<i>n.d.</i>	<i>n.d.</i>

Based on ^1H NMR and HRESIMS analysis, the biogenetic pathway of purpurascenine A (**4.1**) is proposed as depicted in Scheme 4.2, which is at the same time in agreement with the absolute configurations of isolated compounds mentioned above.



Scheme 4.2. Suggested biosynthesis pathway of purpurascenine A (**4.1**) via iminium intermediate in a Pictet-Spengler reaction, considering the proposal of Yamanokuchi et al. (2012) and Naoi et al. (2002).

Considering pyruvic acid as “ α -ketoalanine”, we hypothesize that “ α -ketoglycine” (glyoxilic acid), and “ α -ketoleucine” (4-methyl-2-oxopentanoic acid) are the precursors for purpurascenines B (**4.2**) and C (**4.3**), respectively. Each α -keto acid can react with 7-hydroxytryptophan (**4.4**) in a Pictet-Spengler reaction as described in Scheme 4.3. In principle, α -keto acids can be formed from corresponding amino acids by the oxidative deamination *via* either amino acid dehydrogenase, L-amino oxidase or L-amino acid desaminase (Nshimiyimana et al., 2019). However, due to the observed less incorporation rate of fed ^{13}C alanine into **4.1***, it is most probably that the α -keto amino acids are formed through the reversible reaction catalyzed by amino acid dehydrogenase.



Scheme 4.3. Proposed biosynthesis pathway of purpurascenines A-C (**4.1-4.3**).

4.2.4 Purpurascenine A – Impact on cell viability

Purpurascenine A (**4.1**) was screened for possible anti-proliferative and cytotoxic effects, respectively, on three human cell lines, namely prostate adenocarcinoma (PC-3), colorectal adenocarcinoma (HCT-116) and breast cancer (MCF-7) cells. The compound’s impact on the cells’ growth and viability after 48 h of cell treatment was measured by using a fluorometric resazurin assay read-out. Purpurascenine A (**4.1**) was tested with concentrations up to 100 μM . Furthermore, serotonin (5-hydroxytryptamine, 5-HT), the native agonist of the 5-HT_{2A} serotonin receptor, was also tested for its impacts on cell viability since 5-HT was used as a reference in the functional 5-HT_{2A} reporter gene assay that was conducted to evaluate a potential modulatory function of the 5-HT_{2A} receptor by **4.1**.

Our results showed that neither **4.1** nor 5-HT were found to be cytotoxic and anti-proliferative, respectively, to any of the three tested human cell lines, even in higher concentration up to 100 μM (Figure B66, Appendix). The only sign for some cytotoxicity was detected with compound **4.1** in PC-3, where just the highest concentration of 100 μM reduced the PC-3 cell viability by ~ 30%. Therefore, the IC₅₀ value of **4.1** is estimated to be distinctly higher than 100 μM , making purpurascenine A (**4.1**) a quite inactive compound with respect to cytotoxicity towards human cells.

4.2.5 Effect of purpurascenine A on 5-HT_{2A} receptor activation

Due to its structural similarity to 5-HT as well as other known 5-HT_{2A} receptor modulators, e.g. agonists like ibogaine or tabernanthine (Zieba et al., 2021) or allosteric modulators like glaucine (Fasciani et al., 2020; Heng et al., 2019), the question arose whether purpurascenine A (**4.1**) could permit some functional effect on the 5-HT_{2A} serotonin receptor subtype. Thus, preliminary docking

studies were carried out demonstrating that purpurascenine A (**4.1**) can interact with 5-HT_{2A} serotonin receptor with an interaction energy of -33.4 kcal/mol (Figure B66, Appendix). The interaction is stabilized by hydrogen bonds of the formic acid side chain with the side chain of K223 and N343. Furthermore, hydrophobic interactions with F339, L362, V366 and L228 additionally support the docking arrangement (Figure 4.6A). Therefore, a functional reporter gene assay was conducted by using transiently co-transfected CHO-K1 cells overexpressing the 5-HT_{2A} receptor and Promega's reporter gene system pGL4.33 with a luciferase enzyme under the control of a serum response element (SRE) that becomes activated upon functional activation of a G_i/G_o-coupled receptor, e.g. the 5-HT_{2A} receptor.

As shown in Figure 4.6B, the transiently co-transfected CHO-K1 cells were treated with broad concentration ranges of (i) the native agonist ligand 5-HT as reference, (ii) purpurascenine A (**4.1**), and (iii) with a combination of 10⁻¹² – 10⁻⁶ M 5-HT plus a fixed concentration of 100 μM of **4.1**.

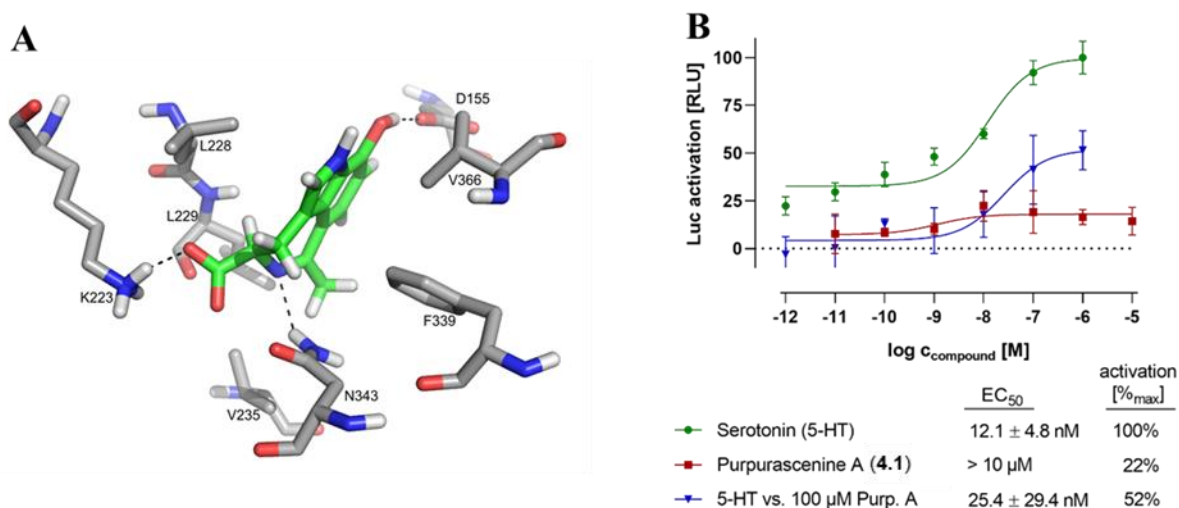


Figure 4.6. (A) Most favored docking arrangement of purpurascenine A (**4.1**) (in green) with the 5-HT_{2A} receptor. (B) EC₅₀ curves and values of the functional activation of the human 5-HT_{2A} receptor by serotonin (5-HT), purpurascenine A (**4.1**) and a co-treatment of both with fixed purpurascenine A (**4.1**) excess concentration of 100 μM. Dose-response curves were determined by using a functional SRE reporter gene assays in transiently co-transfected CHO-K1 cells. The maximal receptor activation (in percentage) was normalized to the maximal receptor activation by the native agonist serotonin (5-HT).

The native agonist serotonin activated the 5HT_{2A} receptor with an EC₅₀ value of approximately 12 nM, which nicely fits to EC₅₀ values published in the IUPHAR database of G protein-coupled receptors (Andrade et al., 2019), indicating the good performance of the functional reporter gene assay. Nevertheless, the lifted bottom plateau of the EC₅₀ curve – to a basal receptor activation level of around 25% – is noteworthy, and could be either explained by some constitutive activity of the 5-HT_{2A} receptor or some basal agonistic activity of the ligand 5-HT even with its lowest test

concentrations. Contrarily, purpurascenine A (**4.1**) by itself was found to be incapable to activate the 5-HT_{2A} receptor, at least up to a concentration of 10 μ M, and hence **4.1** is not able to act as 5-HT_{2A} agonist. However, the flat dose-response curve of **4.1** was detected very close to an activation level of 0%. Surprisingly, when 5-HT, applied with the same concentration range as reference treatment, was combined with 100 μ M of **4.1**, the bottom plateau of the EC₅₀ curve of the co-treatment was also close to 0% receptor activation. Furthermore, albeit the co-treatment activated the 5-HT_{2A} receptor, it allowed just a half-maximal activation (maximum activation 52%). The EC₅₀ of the co-treatment (in fact just due to the action of 5-HT) could be reduced by factor 2. However, the standard error is quite high for that EC₅₀ calculation.

These results of the functional 5-HT_{2A} receptor activation assay demonstrated that: (i) purpurascenine A (**4.1**) did not permit substantial agonistic 5-HT_{2A} activation, (ii) purpurascenine A (**4.1**) (100 μ M) reduced the maximal 5-HT dependent 5-HT_{2A} activation from 100% down to 50%, with only minor effect on the EC₅₀ of 5-HT, and (iii) purpurascenine A (**4.1**) seemed to inhibit putative constitutive 5-HT_{2A} activity. In fact, constitutive activity of the 5-HT_{2A} receptor is so far described to be relatively weak *in vitro*. However, it was observed that some experimental settings, e.g. overexpression of G-proteins or some methodologies for receptor amplification, can cause elevated constitutive activity of 5-HT_{2A} receptors (Berg et al., 2005; De Deurwaerdère et al., 2018). It might be that the co-transfection of the 5-HT_{2A} receptor, all the more as a fusion protein with EYFP for transfection control, with the SRE luciferase reporter, and the resulting strong overexpression of 5-HT_{2A} are the reasons for the substantial constitutive receptor activity observed in our assay. Nonetheless, also under these artificial assay conditions, purpurascenine A (**4.1**) seems to be able to antagonize those constitutive 5-HT_{2A} activity.

Purpurascenine A (**4.1**) does not act as a classical, competitive inhibitor at the 5-HT_{2A} receptor, since there seems to be no direct competition with the native ligand 5-HT at its receptor binding site. However, **4.1** could be a weak allosteric 5HT_{2A} antagonist, inhibiting primarily weaker constitutive 5HT_{2A} activity, and altering more the constitutive or agonist-induced activation height rather than the agonist's EC₅₀ value. On the other hand, purpurascenine A (**4.1**) could also primarily be a modulator of another 5-HT receptor subtype.

Based on these results, it could be worthwhile for specialists in the field to investigate the effects of purpurascenine A (**4.1**) and derivatives thereof on 5-HT_{2A} and other 5-HT receptor subtypes in more detail. All the more, since there is evidence that the 5-HT_{2A} receptor can display significant levels of constitutive activity *in vivo*, where the constitutive activity of the 5-HT_{2A} receptor acts to regulate associative learning through its ability to modulate the release of glutamate, acetylcholine, dopamine, and possibly other transmitters that, in turn, directly affect learning (Berg et al., 2008; Berg et al., 2005; De Deurwaerdere et al., 2020; Harvey, 2003; Harvey et al., 2004; Romano et al., 2006).

4.3 Concluding remarks

In summary, three new azepino-indole alkaloids, named purpurascenines A-C (**4.1-4.3**), together with the keto form of purpurascenine A (**4.1a**) and the new-to-nature 7-hydroxytryptophan (**4.4**) as well as two known compounds, adenosine (**4.5**) and riboflavin (**4.6**), were isolated from fruiting bodies of *Cortinarius purpurascens* Fr. (Cortinariaceae). The structures of **4.1-4.3** were elucidated based on extensive spectroscopic analyses and ECD calculations. Among the isolated compounds, purpurascenines A-C (**4.1-4.3**) and riboflavin (**4.6**) are responsible for the blue-green fluorescence of the mushroom under UV light ($\lambda = 366$ nm). Moreover, 7-hydroxytryptophan (**4.4**) is the chemical component behind the violet reaction of the flesh with Lugol solution and on air characterizing the section Purpurascentes.

Additionally, the biosynthesis of purpurascenine A (**4.1**) was investigated by *in vivo* feeding experiments using ^{13}C labeled samples of sodium pyruvate, alanine, and sodium acetate on fruiting bodies of *C. purpurascens*. The incorporation of ^{13}C isotope was analyzed using 1D NMR and HRESIMS methods. In the experiments with [$3\text{-}^{13}\text{C}$]-pyruvate, the dramatic enrichment of ^{13}C was observed, compared to the abundance of ^{13}C in unlabeled control and other labeled samples. Therefore, a biosynthetic route *via* a direct Pictet-Spengler reaction between pyruvic acid and 7-hydroxytryptophan (**4.4**) could be suggested for purpurascenine A (**4.1**) (Scheme 4.2). Considering pyruvic acid as “ α -ketoalanine”, “ α -ketoglycine” (glyoxilic acid), and “ α -ketoleucine” (4-methyl-2-oxopentanoic acid) were hypothesized as the precursors for purpurascenines B (**4.2**) and C (**4.3**), respectively. Consequently, the biosynthesis of purpurascenines A-C (**4.1-4.3**) was proposed as described in Scheme 4.3.

Furthermore, purpurascenine A (**4.1**) exhibited no anti-proliferative and cytotoxic effects against human prostate (PC-3), colorectal (HCT-116) and breast (MCF-7) cancer cells. In addition, a new functional 5-HT_{2A} receptor activation assay was established showing the ability of **4.1** to reduce the maximal 5-HT dependent 5-HT_{2A} activation by half and to antagonize the constitutive activity of the 5-HT_{2A} receptor.

4.4 Experimental

4.4.1 General experimental procedures

Column chromatography was performed on Sephadex LH20, Sephadex LH60, and Sephadex G25 (Fluka, Germany), whereas analytical TLC was performed on pre-coated silica gel F₂₅₄ aluminum sheets (Merck, Germany). The compound spots were detected by their color and their absorbance at $\lambda = 366$ nm. UV spectra were measured with a Jasco V-560 UV/Vis spectrophotometer, CD spectra were recorded on a Jasco J-815 CD spectrophotometer, and the specific rotation was obtained from a Jasco P-2000 polarimeter (Jasco, Pfungstadt, Germany).

NMR spectra were recorded with an Agilent VNMRs 600 system (Varian, Palo Alto, CA, USA) operating at 599.83 MHz (^1H) and 150.84 MHz (^{13}C), respectively, using a 5-mm inverse detection

cryoprobe. 2D NMR spectra were recorded using standard CHEMPACK 8.1 pulse sequences (s2pul, $^1\text{H}, ^1\text{H}$ zTOCSY, $^1\text{H}, ^1\text{H}$ ROESY(AD), $^1\text{H}, ^{13}\text{C}$ and $^1\text{H}, ^{15}\text{N}$ gHSQCAD, $^1\text{H}, ^{13}\text{C}$ gHMBCAD) implemented in Varian VNMRJ 4.2 spectrometer software. The mixing time for the TOCSY experiments was set to 80 msec, for the ROESY experiments was set to 300 msec. The HMBC experiment was optimized for a long-range coupling of 8 Hz. For measurements in DMSO-*d*₆, ^1H and ^{13}C chemical shifts are referenced to internal DMSO-*d*₆ (δ_{H} 2.51 ppm and δ_{C} 39.5 ppm), while for other measurements ^1H chemical shifts are referenced to internal TMS ($\delta_{\text{H}} = 0$ ppm), and ^{13}C chemical shifts are referenced to CD₃OD (δ_{C} 49.0 ppm).

The positive ion high-resolution electron spray ionization mass spectra (HRESIMS) were obtained from either an Orbitrap Elite mass spectrometer or an API 3200 Triple Quadrupole System. The Orbitrap Elite mass spectrometer (ThermoFisher Scientific, Bremen, Germany) is equipped with an ESI electrospray ion source (spray voltage 4.0 kV; capillary temperature 275 °C, source heater temperature 40 °C; FTMS resolution 60.000). The API 3200 Triple Quadrupole System (AB SCIEX, Framingham, MA, USA) has a turbo ion spray source, which performs ionization with an ion spray voltage on 70 eV. Nitrogen was used as sheath gas. The sample solutions were introduced continuously via a 500 μl Hamilton syringe pump with a flow rate of 5 $\mu\text{l}/\text{min}$. The instruments were externally calibrated by the Pierce® LTQ Velos ESI positive ion calibration solution (product number 88323). The data were evaluated by the Xcalibur software 2.7 SP1 or the Peakview software 2.2.0.11391. The collision induced dissociation (CID) MSⁿ measurements were performed using the relative collision energies given in Table B1 (Appendix).

The preparative HPLC was performed on a Shimadzu prominence system which consists of a CBM-20A communications bus module, a SPD-M20A diode array detector, a FRC-10A fraction collector, a DGU-20A5R degassing unit, a LC-20AT liquid chromatograph, and a SIL-20A HT auto sampler, using either ODS-A column 1 (5 μm , 120 Å, 150 x 10 mm ID, YMC Europe, Dinslaken, Germany) or ODS-A column 2 (5 μm , 120 Å, 150 x 20 mm ID, YMC Europe, Dinslaken, Germany). The following mobile phases were used: H₂O (A) + 0.1% trifluoroacetic acid and CH₃CN + 0.1% trifluoroacetic acid (B) (solvent system I); H₂O + 0.1% formic acid (A) and CH₃CN + 0.1% formic acid (B) (solvent system II); H₂O + 10 mmol/L ammonium formate (A) and CH₃CN + 0.1% formic acid (B) (solvent system III); H₂O (A) and CH₃CN (B) (solvent system IV).

The labeled precursors, sodium [3- ^{13}C]-pyruvate, [3- ^{13}C]-alanine, and sodium [2- ^{13}C]-acetate (all 99% ^{13}C abundance), were purchased from Sigma Aldrich (Steinheim, Germany).

4.4.2 Fungal materials

Fruiting bodies of *Cortinarius purpurascens* Fr. were collected under *Quercus* spec. at different places in the Campus area of University Bayreuth (49°55'43''N11°35'25''E; 49°55'47''N11°35'03''E; 49°55'44''N11°35'14''E), Bavaria, Germany in October 2016 and 2017 (leg./det. N. Arnold). A voucher specimen (coll. 2/2016) is deposited at the Leibniz Institute of Plant Biochemistry (IPB), Halle, Germany.

4.4.3 Extraction and isolation

The frozen fruiting bodies of *C. purpurascens* (1285 g) were macerated using a blender and extracted with methanol (3 x 3.5 L). The yellow-brown solution was evaporated *in vacuo* to dryness. The MeOH crude extract (41.54 g) was subsequently partitioned with CH₂Cl₂, *n*-BuOH and H₂O. According to TLC (UV, $\lambda = 366$ nm), the *n*-BuOH crude extract (2.24 g) contained most of the blue-green fluorescent compounds and therefore subjected to size exclusion chromatography using Sephadex LH20 (eluent: MeOH) to afford 8 fractions (B1-B8). Fraction B3 (0.16 g) was separated by preparative HPLC using column 2 with solvent system I, (4.5 mL/min; 0-10 min, 10-35% B, 10-30 min, 35-59% B) yielded **4.6** ($t_R = 15.6$ min, 1.4 mg). Fraction B4 (0.15 g) was chromatographed on Sephadex G25 (eluent: acetic acid 0.05M degassed and saturated with argon) to arise pure compound **4.4** (5.5 mg). Fraction B5 (0.89 g) was submitted to chromatography using Sephadex LH60 (eluent: MeOH) to give fractions C1-C50. The fractions C10-23 were combined according to their TLC pattern and separated by repeated semipreparative HPLC using column 1 with solvent system II (flow rate 2.5 mL/min; 0-18 min, 10-55% B) to afford **4.2** ($t_R = 7.5$ min, 0.4 mg), **4.1** ($t_R = 7.8$ min, 10.6 mg), and **4.3** ($t_R = 10.0$ min, 0.7 mg). The fractions C24-40 containing **4.5** were combined and finally purified by preparative HPLC using column 2 with solvent system III (15 mL/min; 0-10 min, 5-10% B) yielded **4.5** ($t_R = 6.2$ min, 12.8 mg). Fraction B6 (0.29 g) was separated by preparative HPLC using column 2 with solvent system IV (4 mL/min; 30%B, isocratic) to give **4.1a** ($t_R = 8.4$ min, 9.3 mg).

Purpurascenine A - enol form (4.1): yellow, amorphous solid; TLC $R_f = 0.41$ (*n*-BuOH/AcOH/H₂O, 4:1:1); $[\alpha]_D^{24} +54.7$ (*c* 0.100, MeOH/H₂O, 4:1); UV (MeOH/H₂O, 4:1) λ_{max} (log ϵ) 286 (1.57), 341 (1.64), 413 (2.15) nm; CD (MeOH/H₂O, 4:1) $[\theta]_{215} -20165$, $[\theta]_{233} +6709$, $[\theta]_{247} -2043$, $[\theta]_{267} +2904$, $[\theta]_{283} +3205$, $[\theta]_{344} +3192$, $[\theta]_{387} +1653$ deg cm² x dmol⁻¹; ¹H NMR and ¹³C NMR see Table 1; HRESIMS m/z 245.0912 ([M+H]⁺, calcd for C₁₃H₁₃O₃N₂⁺, 245.0921). HRESIMSⁿ see Table B1, Appendix.

Purpurascenine A – keto form (4.1a): yellow, amorphous solid; TLC $R_f = 0.41$ (*n*-BuOH/AcOH/H₂O, 4:1:1); $[\alpha]_D^{25} +48.0$ (*c* 0.100, MeOH/H₂O, 4:1); UV (MeOH/H₂O, 4:1) λ_{max} (log ϵ) 285 (1.45), 342 (1.53), 413 (2.08) nm; CD (MeOH/H₂O, 4:1) $[\theta]_{227} -14800$, $[\theta]_{234} +5464$, $[\theta]_{247} -2113$, $[\theta]_{266} +1637$, $[\theta]_{280} +1708$, $[\theta]_{347} +2487$, $[\theta]_{396} +1164$ deg cm² x dmol⁻¹; ¹H NMR and ¹³C NMR see Table 1; HRESIMS m/z 245.0919 ([M+H]⁺, calcd for C₁₃H₁₃O₃N₂⁺, 245.0921). HRESIMSⁿ see Table B1, Appendix.

Purpurascenine B (4.2): yellow amorphous solid; TLC $R_f = 0.43$ (*n*-BuOH/AcOH/H₂O, 4:1:1); $[\alpha]_D^{22} -7.2$ (*c* 0.040, MeOH); UV (MeOH) λ_{max} (log ϵ) 251 (1.61), 288 (1.40), 344 (1.66), 404 (2.15) nm; CD (MeOH) $[\theta]_{217} -6068$, $[\theta]_{233} +2108$, $[\theta]_{251} -1557$, $[\theta]_{336} +2114$ deg cm² x dmol⁻¹; ¹H NMR and ¹³C NMR see Table 1; HRESIMS m/z 231.0758 ([M+H]⁺, calcd for C₁₂H₁₁O₃N₂⁺, 231.0757). HRESIMSⁿ see Table B1, Appendix.

Purpurascenine C (4.3): yellow amorphous solid; TLC R_f 0.57 (*n*-BuOH/AcOH/H₂O, 4:1:1); $[\alpha]_D^{25} -9.2$ (*c* 0.070, MeOH); UV (MeOH) λ_{max} (log ϵ) 341 (1.12), 415 (1.40) nm; CD (MeOH)

$[\theta]_{216}$ -2107, $[\theta]_{234}$ +1110 deg cm² x dmol⁻¹; ¹H NMR and ¹³C NMR see Table 1; HRESIMS m/z 287.1381 ($[M+H]^+$, calcd for C₁₆H₁₉O₃N₂⁺, 287.1390). HRESIMSⁿ see Table B1, Appendix.

7-hydroxytryptophan (4.4): white, amorphous solid; TLC R_f 0.43 (*n*-BuOH/AcOH/H₂O, 4:1:1); $[\alpha]_D^{23}$ -37.2 (*c* 0.450, H₂O); UV (H₂O) λ_{max} (log ϵ) 218 (1.50), 268 (0.70) nm; CD (H₂O) $[\theta]_{195}$ -15138, $[\theta]_{220}$ +8761 deg cm² x dmol⁻¹; ¹H NMR and ¹³C NMR in accordance with Van den Berg et al. (1990); HRESIMS m/z 221.0908 ($[M+H]^+$, calcd for C₁₁H₁₃O₃N₂⁺, 221.0921).

Adenosin (4.5): white, amorphous solid; TLC R_f 0.43 (*n*-BuOH/AcOH/H₂O, 4:1:1); ¹H NMR and ¹³C NMR in agreement with Ciuffreda et al. (2007); HRESIMS m/z 268.1045 ($[M+H]^+$, calcd for C₁₀H₁₄O₄N₅⁺, 268.1040).

Riboflavin (4.6): yellow, amorphous solid; TLC R_f 0.43 (*n*-BuOH/AcOH/H₂O, 4:1:1); ¹H NMR and ¹³C NMR in accordance with Hu et al. (2013); HRESIMS m/z 377.1520 ($[M+H]^+$, calcd for C₁₇H₂₁O₆N₄⁺, 377.1456)

4.4.4 Feeding experiments

Feeding experiments on fruiting bodies of *C. purpurascens* Fr. growing in the campus area of University of Bayreuth, Bayreuth, Germany were performed during October and November 2019 and 2020. For this purpose, 50 mg of each precursor was dissolved in 200 μ L water and injected via a syringe into the caps and stems of young fruiting bodies of *C. purpurascens*. To monitor mushroom growth, diameter of the cap was measured at the beginning and the end of the feeding experiment (Table 4.5). After seven to nine days, the fruiting bodies were harvested, immediately frozen in liquid nitrogen, and stored at -20 °C until isolation process.

Table 4.5. Experimental details of labelling studies and purification of purpurascenine A (**4.1***).

precursor	feeding experiments				weight of	
	number of fruit bodies	days to harvest	growth (cm)	fruiting bodies	crude extract	purified (4.1*)
[3- ¹³ C]-pyruvate	2	7	1.2 – 2.7	58.45 g	1.31 g	0.5 mg
[3- ¹³ C]-alanine	11	9	2.0 – 8.5	382.44 g	5.06 g	2.4 mg
[2- ¹³ C]-acetate	10	8	1.5 – 4.5	443.40 g	5.97 g	2.5 mg

4.4.5 Isolation procedure of purpurascenine A (**4.1***) after feeding experiments

Frozen fruiting bodies fed with respective labeled precursor were crushed using a blender and extracted with methanol (4 x 1 L) in an ultrasound bath for 1h at room temperature. The isolation procedure follows the same protocol as for unlabeled compound **4.1** (see Table 4.5).

4.4.6 Computational details

The initial molecular geometries of the compounds, including all possible stereoisomers, were built using Molecular Operating Environment (MOE) software (v2020.09, 2022). All structures and conformational analyses were performed with the MMFF94 force field (Halgren, 1999). The force field energy minimum structures were further optimized with DFT method (B3LYP/def2-TZVP) (Becke, 1993; Lee et al., 1988; Vosko et al., 1980) using the ORCA 5.0 program package (Neese, 2018) and the conductor-like polarizable continuum model (CPCM) solvent field for water and methanol (Barone and Cossi, 1998). Optimized structures were subsequently used for the CD spectra calculation using ORCA. The first 25 excited states of each compound and conformation were calculated employing TD B3LYP hybrid functional (Becke, 1993; Lee et al., 1988; Vosko et al., 1980) with the def2-TZVP basis set (Weigend and Ahlrichs, 2005) and CPCM model. To compare the calculated CD spectra with the experimental ones, the single spectra of the energetically relevant conformers were summed according to the Boltzmann factors derived from the single-point energies. The SpecDis software (version 1.71) (Bruhn et al., 2017) were applied to visualize and compare the calculated spectra with the experimental ones.

4.4.7 Molecular docking studies

The X-ray structure (pdb code 6A93) of the 5-HT_{2A} receptor in complex with risperidone was used for docking studies. (Kimura et al., 2019) First, the protons were added to the crystal structure by applying the protonate-3d tool implemented in MOE (v2019.0101, 2019). 100 docking poses were generated with the docking tool in MOE defining the position of risperidone as putative binding site for purpurascenine A (**4.1**). The 30 best scored docking arrangements of **4.1** to the 5-HT_{2A} receptor were analysed in detail. For this purpose, the docking poses were energy optimized using the Amber14:EHT force field with Born solvation. The backbone atoms of the receptor were fixed. Subsequently the interaction energies of the ligand with the receptor were calculated.

4.4.8 Assay materials and reagents

The three human cancer cell lines under investigation – PC-3 (prostate adenocarcinoma), HCT-116 (colorectal adenocarcinoma), and MCF-7 (breast ductal carcinoma) – were purchased from ATCC (Manassas, USA). Media and supplements for cell culturing, namely RPMI 1640 and DMEM basal media, FCS, L-glutamine, non-essential amino acids (NEAA), sodium pyruvate, PBS and trypsin/EDTA, were purchased from Capricorn Scientific GmbH (Ebsdorfergrund, Germany). The reagents for the reporter gene assay were purchased from the following vendors: 5-hydroxytryptamine (5-HT, serotonin) and BSA from Sigma-Aldrich (Taufkirchen, Germany), ONE-Glo™ reagent and the reporter gene vector pGL4.33 from Promega GmbH (Mannheim, Germany), Metafectene® Pro transfection reagent from Biontix Laboratories GmbH (Martinsried, Germany). White/clear bottom 96-well plates were purchased from Corning (Corning, USA). All other multi-well plates, culture flasks and further cell culture plastics were purchased from TPP (Trasadingen, Switzerland) and Greiner Bio-One GmbH (Frickenhausen, Germany), respectively.

4.4.9 Cell culture

The prostate cancer cell line PC-3, as well as the Chinese hamster ovary cell line CHO-K1 for the reporter gene assay, were cultured in RPMI 1640 medium supplemented with 10% heat-inactivated FCS and 2 mM L-glutamine. For MCF-7 breast cancer cells RPMI 1640 medium supplemented with 10% heat-inactivated FCS, 2 mM L-glutamine, 1 mM sodium pyruvate and 0.2% (v/v) NEAA was used. HCT-116 colorectal cancer cell were cultured in DMEM supplemented with 10% not heat-inactivated FCS and 2 mM L-glutamine. All cells were routinely cultured in T-75 flasks in a humidified atmosphere with 5% CO₂ at 37°C to reach subconfluency (~ 70-80%) prior to subsequent sub-culturing or assay usage. The adherent cells were rinsed with PBS and detached by using trypsin/EDTA (0.05% in PBS) prior to cell passaging and seeding (Khan et al., 2020).

4.4.10 *In vitro* cell viability assay

Anti-proliferative and cytotoxic effects, respectively, of the compounds were investigated by performing a fluorometric resazurin-based cell viability assay (Sigma-Aldrich, Taufkirchen, Germany) (Kufka et al., 2019). For that purpose, cancer cells were seeded in low densities in 96-well plates – namely 4,000 cells/well (PC-3) and 6,000 cells/well (HCT-116 and MCF-7) – to yield a seeding confluency of ~ 10%, and were allowed to adhere for 24 h. Subsequently, the cells were treated for 48 h with purpurascenine A (**4.1**) and serotonin (5-HT), respectively using concentrations up to 100 µM. For control measures, cells were treated in parallel with 1% DMSO (negative control, representing the final DMSO content of the highest concentrated test compound concentration) and 100 µM digitonin (positive control, for data normalization set to 0% cell viability), both in the respective standard growth medium. As soon as the 48 h incubation was finished, the incubation medium was discarded, and cell were rinsed once with PBS. Resazurin solution in RPMI 1640 without phenol red and other supplements was prepared freshly prior to use, and added to the cells in a final resazurin concentration of 50 µM. Subsequently, the cells were incubated under standard growth conditions for further 2 hours. Finally, the conversion of resazurin to resorufin by viable, metabolically active cells was measured with 540 nm excitation and 590 nm emission settings by using a SpectraMax M5 multiwell plate reader (Molecular Devices, San Jose, USA). Data were determined in biological and technical triplicates. For data analyses, GraphPad Prism version 8.0.2 and Microsoft Excel 2013 were used.

4.4.11 *In vitro* functional 5-HT_{2A} receptor activation assay

Due to its structural similarity to 5-hydroxytryptamine (5-HT; serotonin), purpurascenine A (**4.1**) was evaluated for its possible ability to modulate the function of the 5-HT_{2A} G protein-coupled receptor by conducting a functional reporter gene assay. For that purpose, CHO-K1 cells were transiently co-transfected with an expression vector encoding for a fusion protein comprising the human 5-HT_{2A} receptor with a N-terminal HA tag and a C-terminally fused enhanced yellow fluorescent protein (EYFP) (expression vector HA-5HT_{2A}-EYFP-pVitro2; kindly provided by OntoChem GmbH (Halle (Saale), Germany) and the commercial reporter gene vector pGL4.33 (Promega GmbH, Mannheim, Germany) containing a luciferase under the control of a serum

response element (SRE) allowing the functional investigation of G_i/G₀-coupled G protein-coupled receptors, as 5-HT_{2A} is, by using luminescence read-out. For transient cell transfection, 2.5·10⁶ CHO-K1 cells were seeded per 25 cm² cell culture flask and allowed to adhere and grow to reach a cell confluency of ~ 80% overnight. Subsequently, co-transfection of the cells was done by using 8 µg 5-HT_{2A} expression vector, 4 µg pGL4.33 reporter vector and 24 µL of Metafectene[®] Pro transfection reagent (Biontex Laboratories GmbH, Martinsried, Germany) per culture flask. Reconstitution and preparation of the transfection mixture was done in RPMI 1640 basal medium without any supplements following the manufacturer's guideline of the transfection reagent. After 6 hours transfection incubation of the cells under standard growth conditions, the transfection solution was discarded, transfected cells were harvested by using 0.01% Trypsin/EDTA in PBS, and seeded with fresh CHO-K1 medium in white/clear bottom 96-well plates (90,000 cells/100µL/well). To allow receptor and reporter gene expression, cells were cultured for 24 hours under standard growth conditions. Subsequently, the transfection medium was discarded, cells were washed once and then starved for 60 min with RPMI 1640 basal medium supplemented with 0.2% (w/v) BSA (incubation medium). Then cells were incubated with (i) 10⁻¹²-10⁻⁶ M of serotonin (5-HT), (ii) 10⁻¹¹-10⁻⁵ M of purpurascenine A (**4.1**), and (iii) 10⁻¹²-10⁻⁶ M of serotonin (5-HT) plus 10⁻⁴ M (100 µM) of purpurascenine A (**1**) as co-treatment. After 5.5 hours of cell incubation at 37°C incubation media were removed and 60 µL/96-well of Promega's ONE-Glo[™] reagent (1:1 in PBS, v/v) were added. After 60 min incubation at room temperature the reporter gene generated luminescence signal was measured by using a SpectraMax M5 multiwell plate reader (Molecular Devices, San Jose, USA). Data were determined in triplicates. For data analyses, GraphPad Prism version 8.0.2 and Microsoft Excel 2013 were used.

4.5 References

- Abdallah, M. F., Krska, R., Sulyok, M., 2018. Occurrence of ochratoxins, fumonisin B2 , aflatoxins (B1 and B2), and other secondary fungal metabolites in dried date palm fruits from Egypt: a mini-survey. *J Food Sci* 83, 559-564.
- Andrade, R., Barnes, N. M., Baxter, G., Bockaert, J., Branchek, T., Butler, A., Cohen, M. L., Dumuis, A., Eglen, R. M., Göthert, M., Hamblin, M., Hamon, M., Hartig, P. R., Hen, R., Hensler, J., Herrick-Davis, K., Hills, R., Hoyer, D., Humphrey, P. P. A., Latté, K. P., Maroteaux, L., Martin, G. R., Middlemiss, D. N., Mylecharane, E., Neumaier, J., Peroutka, S. J., Peters, J. A., Roth, B., Saxena, P. R., Sharp, T., Sleight, A., Villalon, C. M., Yocca, F., 2019. - 5-Hydroxytryptamine receptors (version 2019.4) in the IUPHAR/BPS Guide to Pharmacology Database.
- Bai, M. S., Wang, C., Zong, S. C., Lei, M., Gao, J. M., 2013. Antioxidant polyketide phenolic metabolites from the edible mushroom *Cortinarius purpurascens*. *Food Chem* 141, 3424-3427.
- Barone, V., Cossi, M., 1998. Quantum calculation of molecular energies and energy gradients in solution by a conductor solvent model. *J Phys Chem A* 102, 1995-2001.
- Becke, A. D., 1993. Density-functional thermochemistry. III. The role of exact exchange. *J Chem Phys* 98, 5648-5652.

- Berg, K., Harvey, J., Spampinato, U., Clarke, W., 2008. Physiological and therapeutic relevance of constitutive activity of 5-HT_{2A} and 5-HT_{2C} receptors for the treatment of depression. *Prog Brain Res* 172, 287-305.
- Berg, K. A., Harvey, J. A., Spampinato, U., Clarke, W. P., 2005. Physiological relevance of constitutive activity of 5-HT_{2A} and 5-HT_{2C} receptors. *Trends Pharmacol Sci* 26, 625-630.
- Bruhn, T., Schaumlöffel, A., Hemberger, Y., Pecitelli, G., 2017. SpecDis version 1.71. Berlin, Germany.
- Chen, H. P., Liu, J. K., 2017. Secondary metabolites from higher fungi. In: Progress in the chemistry of organic natural products 106, Springer International Publishing AG, Cham, pp. 1-201.
- Ciuffreda, P., Casati, S., Manzocchi, A., 2007. Complete (1)H and (13)C NMR spectral assignment of alpha- and beta-adenosine, 2'-deoxyadenosine and their acetate derivatives. *Magn Reson Chem* 45, 781-784.
- De Deurwaerdere, P., Bharatiya, R., Chagraoui, A., Di Giovanni, G., 2020. Constitutive activity of 5-HT receptors: Factual analysis. *Neuropharmacology* 168, 107967.
- De Deurwaerdère, P., Drutel, G., Di Giovanni, G., 2018. Pharmacological analysis in favour of a physiological role for the constitutive activity of 5-HT_{2A} receptors in learning. In: Guiard, B., Di Giovanni, G. (Eds.), 5-HT_{2A} receptors in the central nervous system. The receptors, vol. 32. Humana Press, Cham, pp. 3-29.
- Eich, E., Rochelmeyer, H., 1966. Über die präparative Anwendung der radikalischen Hydroxylierung von Indol. *Pharmac Acta Helvetia* 41, 109.
- Fasciani, I., Petragano, F., Aloisi, G., Marampon, F., Carli, M., Scarselli, M., Maggio, R., Rossi, M., 2020. Allosteric modulators of G protein-coupled dopamine and serotonin receptors: a new class of atypical antipsychotics. *Pharmaceuticals* (Basel) 13.
- Gao, J. M., Qin, J. C., Pescitelli, G., Di Pietro, S., Ma, Y. T., Zhang, A. L., 2010. Structure and absolute configuration of toxic polyketide pigments from the fruiting bodies of the fungus *Cortinarius rufolivaceus*. *Org Biomol Chem* 8, 3543-3551.
- Garnica, S., Weiß, M., Oertel, B., Oberwinkler, F., 2005. A framework for a phylogenetic classification in the genus *Cortinarius* (Basidiomycota, Agaricales) derived from morphological and molecular data. *Can J Bot* 83, 1457-1477.
- Gartz, J., 1985. Untersuchungen zur Radikalischen Hydroxylierung von Tryptophan und Tryptamin. *Pharmazie* 11, 811.
- Gill, M., 1999. Pigments of fungi (Macromycetes). *Nat Prod Rep* 16, 301-317.
- Gill, M., 2003. Pigments of fungi (Macromycetes). *Nat Prod Rep* 20, 615-639.
- Gill, M., Steglich, W., 1987. Pigments of fungi (Macromycetes). In: Herz, W., Grisebach, H., Kirby, G. W., Tamm, C. (Eds.), Progress in the chemistry of organic natural products 51. Springer-Verlag, Wien, New York, pp. 1-317.
- Halgren, T. A., 1999. MMFF VI. MMFF94s option for energy minimization studies. *J Comput Chem* 20, 720-729.
- Harvey, J. A., 2003. Role of the serotonin 5-HT_{2A} receptor in learning. *Learn Mem* 10, 355-362.
- Harvey, J. A., Quinn, J. L., Liu, R., Aloyo, V. J., Romano, A. G., 2004. Selective remodeling of rabbit frontal cortex: relationship between 5-HT_{2A} receptor density and associative learning. *Psychopharmacology* (Berl) 172, 435-442.

- Heng, H. L., Chee, C. F., Thy, C. K., Tee, J. T., Chin, S. P., Herr, D. R., Buckle, M. J. C., Paterson, I. C., Doughty, S. W., Abd Rahman, N., Chung, L. Y., 2019. *In vitro* functional evaluation of isolaureline, dicentrine and glaucine enantiomers at 5-HT₂ and α_1 receptors. *Chem Biol Drug Des* 93, 132-138.
- Horak, E., 2005. Röhrlinge und Blätterpilze in Europa. Elsevier GmbH, München, pp. 1-555.
- Hu, Y., Wang, K., MacMillan, J. B., 2013. Hunanamycin A, an antibiotic from a marine-derived *Bacillus hunanensis*. *Org Lett* 15, 390-393.
- Jiang, M. Y., Feng, T., Liu, J. K., 2011. N-containing compounds of Macromycetes. *Nat Prod Rep* 28, 783-808.
- Khan, M. F., Nasr, F. A., Noman, O. M., Alyhya, N. A., Ali, I., Saoud, M., Rennert, R., Dube, M., Hussain, W., Green, I. R., Basudan, O. A. M., Ullah, R., Anazi, S. H., Hussain, H., 2020. Cichorins D–F: three new compounds from *Cichorium intybus* and their biological effects. *Molecules* 25, 4160.
- Kimura, K. T., Asada, H., Inoue, A., Kadji, F. M. N., Im, D., Mori, C., Arakawa, T., Hirata, K., Nomura, Y., Nomura, N., Aoki, J., Iwata, S., Shimamura, T., 2019. Structures of the 5-HT_{2A} receptor in complex with the antipsychotics risperidone and zotepine. *Nat Struct Mol Biol* 26, 121-128.
- Klein-Junior, L. C., Cretton, S., Vander Heyden, Y., Gasper, A. L., Nejad-Ebrahimi, S., Christen, P., Henriques, A. T., 2020. Bioactive azepine-indole alkaloids from *Psychotria nemorosa*. *J Nat Prod* 83, 852-863.
- Kufka, R., Rennert, R., Kaluderovic, G. N., Weber, L., Richter, W., Wessjohann, L. A., 2019. Synthesis of a tubugi-1-toxin conjugate by a modulizable disulfide linker system with a neuropeptide Y analogue showing selectivity for hY1R-overexpressing tumor cells. *Beilstein J Org Chem* 15, 96-105.
- Lam, Y. T. H., Palfner, G., Lima, C., Porzel, A., Brandt, W., Frolov, A., Sultani, H., Franke, K., Wagner, C., Merzweiler, K., Wessjohann, L. A., Arnold, N., 2019. Nor-guanacastepene pigments from the Chilean mushroom *Cortinarius pyromyxa*. *Phytochemistry* 165, 112048.
- Lee, C., Yang, W., Parr, R. G., 1988. Development of the Colle-Salvetti correlation-energy formula into a functional of the electron density. *Phys Rev B* 37, 785-789.
- Lin, H. C., Chiou, G., Chooi, Y. H., McMahon, T. C., Xu, W., Garg, N. K., Tang, Y., 2015. Elucidation of the concise biosynthetic pathway of the communesin indole alkaloids. *Angew Chem Int Ed Engl* 54, 3004-3007.
- Lindsay, A. C., Kim, S. H., Sperry, J., 2018. Non-monoterpenoid azepinoindole alkaloids. *Nat Prod Rep* 35, 1347-1382.
- Liu, J. K., 2005. N-containing compounds of Macromycetes. *Chem Rev* 105, 2723-2744.
- Moser, M., 1960. Die Gattung Phlegmacium (Schleimköpfe). In: Die Pilze Mitteleuropas IV. Verlag Julius Klinkhardt. Bad Heilbrunn, Germany, pp. 1-440.
- Moser, M., 1983. Kleine Kryptogamenflora, Band II b/2, Basidiomyceten: Die Röhrlinge und Blätterpilze, Kleine Kryptogamenflora. Gustav Fischer Verlag, Stuttgart, New York, pp. 1-532.
- Naoi, M., Maruyama, W., Akao, Y., Yi, H., 2002. Dopamine-derived endogenous N-methyl-(R)-salsolinol: its role in Parkinson's disease. *Neurotoxicol Teratol* 24, 579-591.
- Neese, F., 2018. Software update: the ORCA program system, version 4.0. *WIREs Comput Mol Sci* 8, e1327.
- Nikolić, D., Gödecke, T., Chen, S.-N., White, J., Lankin, D. C., Pauli, G. F., van Breemen, R. B., 2012. Mass spectrometric dereplication of nitrogen-containing constituents of black cohosh (*Cimicifuga racemosa* L.). *Fitoterapia* 83, 441-460.

- Nshimiyimana, P., Liu, L., Du, G., 2019. Engineering of L-amino acid deaminases for the production of α -keto acids from L-amino acids. *Bioengineered* 10, 43-51.
- Robbers, J. E., Otsuka, H., Floss, H. G., Arnold, E. V., Clardy, J., 1980. Clavicipitic acid: its structure, biosynthesis, and role in ergot alkaloid formation. *J Org Chem* 45, 1117-1121.
- Romano, A. G., Quinn, J. L., Liu, R., Dave, K. D., Schwab, D., Alexander, G., Aloyo, V. J., Harvey, J. A., 2006. Effect of serotonin depletion on 5-HT_{2A}-mediated learning in the rabbit: evidence for constitutive activity of the 5-HT_{2A} receptor *in vivo*. *Psychopharmacology* (Berl) 184, 173-181.
- Saar, G., Dima, B., Schmidt-Stohn, G., Brandrud, T. E., Bellù, F., Frøslev, T. G., Oertel, B., Soop, K., 2014. *Cortinarius* Untergattung Phlegmacium Sektion Purpurascenes in Europa. *J JEC* 14, 140 – 161.
- Saini, M. S., Cheng, M., Anderson, J. A., 1976. Conversion of 4- γ,γ -dimethylallyltryptophan to clavicipitic acid. Some properties of the enzyme. *Phytochemistry* 15, 1497-1500.
- Sauleau, P., Martin, M. T., Dau, M. E., Youssef, D. T., Bourguet-Kondracki, M. L., 2006. Hyrtiazepine, an azepino-indole-type alkaloid from the Red Sea marine sponge *Hyrtios erectus*. *J Nat Prod* 69, 1676-1679.
- Song, C., Wu, M., Zhang, Y., Li, J., Yang, J., Wei, D., Li, H., Guo, L., Qin, J., 2022a. Bioactive monomer and polymer polyketides from edible mushroom *Cortinarius caerulescens* as glutamate dehydrogenase inhibitors and antioxidants. *J Agric Food Chem* 70, 804-814.
- Song, C., Wu, M., Zhang, Y., Li, J., Yang, J., Wei, D., Li, H., Guo, L., Qin, J., 2022b. Correction to bioactive monomer and polymer polyketides from edible mushroom *Cortinarius caerulescens* as glutamate dehydrogenase inhibitors and antioxidants. *J Agric Food Chem* 70, 1747-1747.
- Steglich, W., Oertel, B., 1984. Untersuchungen zur Konstitution und Verbreitung der Farbstoffe von *Cortinarius*, Untergattung Phlegmacium (Agaricales). *Sydowia Ann Mycol* 37, 284-295.
- Stockigt, J., Antonchick, A. P., Wu, F., Waldmann, H., 2011. The Pictet-Spengler reaction in nature and in organic chemistry. *Angew Chem Int Ed Engl* 50, 8538-8564.
- Teichert, A., Schmidt, J., Porzel, A., Arnold, N., Wessjohann, L., 2007. Brunneins A-C, beta-carboline alkaloids from *Cortinarius brunneus*. *J Nat Prod* 70, 1529-1531.
- Thiele, W., Froede, R., Steglich, W., Muller, M., 2020. Enzymatic formation of rufoschweinitzin, a binaphthalene from the basidiomycete *Cortinarius rufoolivaceus*. *Chembiochem* 21, 1423-1427.
- v2019.0101, M. O. E., 2019. Molecular Operating Environment v2019.0101. Chemical Computing Group Inc., Montreal, QC, Canada.
- v2020.09, M. O. E. M., 2022. Chemical Computing Group ULC. 1010 Sherbooke St. West, Suite #910, Montreal, QC, Canada.
- van den Berg, E. M. M., Jansen, F. J. H. M., de Goede, A. T. J. W., Baldew, A. U., Lugtenburg, J., 1990. Chemo-enzymatic synthesis and characterization of L-tryptophans selectively ¹³C-enriched or hydroxylated in the six-membered ring using transformed *Escherichia coli* cells. *Recl Trav Chim Pays-Bas* 109, 287-297.
- Vosko, S. H., Wilk, L., Nusair, M., 1980. Accurate spin-dependent electron liquid correlation energies for local spin density calculations: a critical analysis. *Can J Phys* 58, 1200-1211.
- Weigend, F., Ahlrichs, R., 2005. Balanced basis sets of split valence, triple zeta valence and quadruple zeta valence quality for H to Rn: Design and assessment of accuracy. *Phys Chem Chem Phys* 7, 3297-3305.
- Wigley, L. J., Mantle, P. G., Perry, D. A., 2006. Natural and directed biosynthesis of communesin alkaloids. *Phytochemistry* 67, 561-569.

- Wigley, L. J., Perry, D. A., Mantle, P. G., 2008. An experimental strategy towards optimising directed biosynthesis of communesin analogues by *Penicillium marinum* in submerged fermentation. *Mycol Res* 112, 131-137.
- Xu, W., Gavia, D. J., Tang, Y., 2014. Biosynthesis of fungal indole alkaloids. *Nat Prod Rep* 31, 1474-1487.
- Yamanokuchi, R., Imada, K., Miyazaki, M., Kato, H., Watanabe, T., Fujimuro, M., Saeki, Y., Yoshinaga, S., Terasawa, H., Iwasaki, N., Rotinsulu, H., Losung, F., Mangindaan, R. E., Namikoshi, M., de Voogd, N. J., Yokosawa, H., Tsukamoto, S., 2012. Hyrtioreticulins A-E, indole alkaloids inhibiting the ubiquitin-activating enzyme, from the marine sponge *Hyrtios reticulatus*. *Bioorg Med Chem* 20, 4437-4442.
- Yamazaki, Y., Kitajima, M., Arita, M., Takayama, H., Sudo, H., Yamazaki, M., Aimi, N., Saito, K., 2004. Biosynthesis of camptothecin. In silico and in vivo tracer study from [1-¹³C]glucose. *Plant Physiol* 134, 161-170.
- Zieba, A., Stepnicki, P., Matosiuk, D., Kaczor, A. A., 2021. Overcoming Depression with 5-HT_{2A} Receptor Ligands. *Int J Mol Sci* 23, 10.

Chapter 5

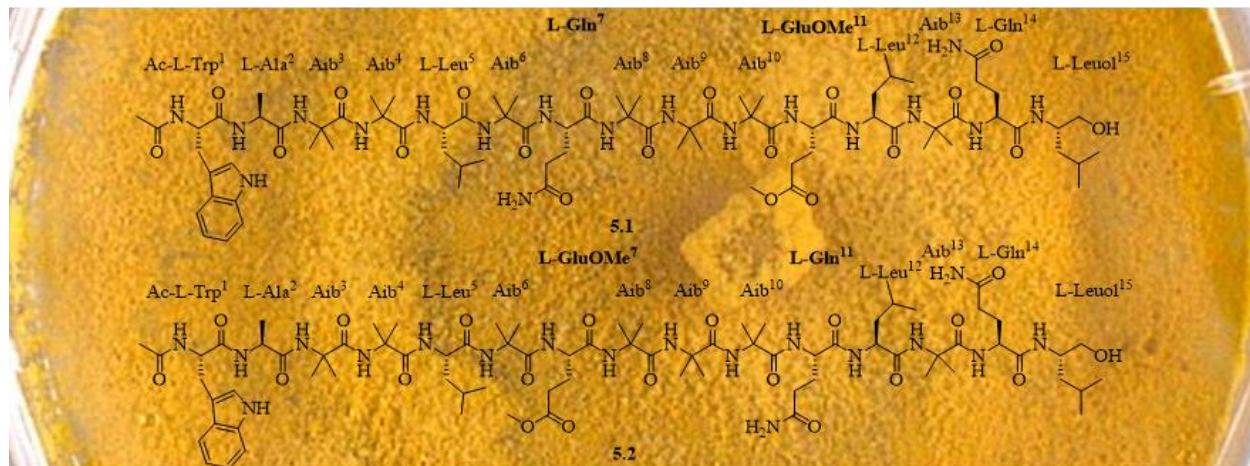
Rare glutamic acid methyl ester peptaibols from *Sepedonium ampullosporum* Damon KSH 534 exhibit promising antifungal and anticancer activity

This Chapter has been published as:

Yen T. H. Lam, Manuel G. Ricardo, Robert Rennert, Andrej Frolov, Andrea Porzel, Wolfgang Brandt, Pauline Stark, Bernhard Westermann and Norbert Arnold. *Int J Mol Sci* **2021**, 22(23), 12718, DOI: 10.3390/ijms222312718*

*Reprinted (adapted) with permission from MDPI, according to the Creative Commons Attribution License

Graphical abstract



Highlights

- Two undescribed peptaibols and five known peptides were isolated from *S. ampullosporum*.
- The novel peptaibols were synthesized on solid-phase establishing all chiral amino acids as L.
- Ampullosporin A, F and G exhibit strong antifungal and anticancer activity.
- Molecular docking study explains the structure-activity correlation of the ampullosporins.

Abstract

Fungal species of genus *Sepedonium* are rich sources of diverse secondary metabolites (e.g., alkaloids, peptaibols), which exhibit variable biological activities. Herein, two new peptaibols, named ampullosporin F (**5.1**) and ampullosporin G (**5.2**), together with five known compounds, ampullosporin A (**5.3**), peptaibolin (**5.4**), chrysosporide (**5.5**), c(Trp-Ser) (**5.6**) and c(Trp-Ala) (**5.7**), have been isolated from the culture of *Sepedonium ampullosporum* Damon strain KSH534. The structures of **5.1** and **5.2** were elucidated based on ESI-HRMSⁿ experiments and intense 1D and 2D NMR analyses. The sequence of ampullosporin F (**5.1**) was determined to be Ac-Trp¹-Ala²-Aib³-Aib⁴-Leu⁵-Aib⁶-Gln⁷-Aib⁸-Aib⁹-Aib¹⁰-GluOMe¹¹-Leu¹²-Aib¹³-Gln¹⁴-Leuol¹⁵, while ampullosporin G (**5.2**) differs from **5.1** by exchanging the position of Gln⁷ with GluOMe¹¹. Furthermore, the total synthesis of **5.1** and **5.2** was carried out on solid-phase to confirm the absolute configuration of all chiral amino acids as L. In addition, ampullosporin F (**5.1**) and G (**5.2**) showed significant antifungal activity against *B. cinerea* and *P. infestans*, but were inactive against *S. tritici*. Cell viability assays using human prostate (PC-3) and colorectal (HT-29) cancer cells confirmed potent anticancer activities of **5.1** and **5.2**. Furthermore, a molecular docking study was performed *in silico* as an attempt to explain the structure-activity correlation of the characteristic ampullosporins (**5.1–5.3**).

Keywords: *Sepedonium ampullosporum*; peptaibols; ampullosporin; glutamic acid methyl ester; solid-phase peptide synthesis; antifungal; anticancer; molecular docking.

5.1 Introduction

Filamentous fungi from saprophytic genera, e.g. *Acremonium*, *Trichoderma/Hypocrea* and *Sepedonium*, are known for a high abundance of nonribosomal-peptide-synthetase (NRPS)-derived metabolites, so-called peptaibols (Degenkolb and Brückner, 2008). This class of compounds is defined as linear peptides with 5–20 amino acid (AA) residues including *i*) a high proportion of the non-proteinogenic α,α -dialkylated amino acid α -aminoisobutyric acid (Aib); *ii*) an *N*-acetyl terminus; *iii*) and a *C*-terminal AA reduced into amino alcohol such as leucinol (Leuol) or phenylalaninol (Pheol) (Degenkolb and Brückner, 2008). Peptaibols are intriguing not only because of the structural variability generated by varying amino acid building blocks but also due to their broad range of bioactivities i.e. cytotoxic (Ayers et al., 2012; Carroux et al., 2013; Du et al., 2017; Liu et al., 2015; Mohamed-Benkada et al., 2016; Neumann et al., 2015; Rivera-Chavez et al., 2017; Sica et al., 2017; van Bohemen et al., 2021; Wu et al., 2021), antibacterial (Ayers et al., 2012; Kimonyo and Bruckner, 2013; Mohamed-Benkada et al., 2016; Neumann et al., 2015; Panizel et al., 2013; van Bohemen et al., 2021; Wu et al., 2021), antiviral (Kai et al., 2018; Stadler, 2001), antileishmanial (Fragiadaki et al., 2018), antifungal (Mohamed-Benkada et al., 2016; Neumann et al., 2015; Otto et al., 2016a; Otto et al., 2015; Otto et al., 2016b), plant root growth inhibiting (Shi et al., 2016), insecticidal (Du et al., 2017), and anthelmintic activity (Ayers et al., 2012). Furthermore, ampullosporin A (5.3), a peptaibol isolated from *Sepedonium ampullosporum* Damon, had been shown to permit neuroleptic-like activity in mice (Kronen et al., 2001; Ritzau et al., 1997), whereby a more targeted interaction with the glutamatergic system, namely the NMDA receptor (Berek et al., 2009).

These biological activities appear to be related to the strong foldameric capacity of Aib, so that peptaibols would adopt helical structures in artificial bilayers and natural membranes (Speckbacher and Zeilinger, 2018). Consequently, the amphipathic voltage-dependent helices can act as ion channels throughout the cell membrane causing cytoplasmic leakage and cellular breakdown (Milov et al., 2016; Speckbacher and Zeilinger, 2018).

The genus *Sepedonium* (teleomorph *Hypocrea*, Ascomycota), which was established by H.F. Link and restricted to mold-like fungal parasites, is characterized by the occurrence of two synanamorphs, i.e., aleurioconidia (for persistence) and phialoconidia (for fast propagation). *Sepedonium* species were mostly found to live on basidiocarps of Boletales s.l. (Sahr, 1999). Unlike the systematically studied genus *Trichoderma/Hypocrea*, there are only few reports on secondary metabolites isolated from *Sepedonium* spp. So far, compounds belonging to tropolones (Divekar et al., 1965; Divekar and Vining, 1964), anthraquinones (mono-, dimeric) (Shibata et al., 1957), isoquinoline alkaloids (Quang et al., 2010), azaphilones (Closse and Hauser, 1973), cyclopeptides (Laub et al.; Mitova et al., 2006), and peptaibols (Dornberger et al., 1995; Hulsmann et al., 1998; Kronen et al., 2001; Mitova et al., 2008; Neuhof et al., 2007; Otto et al., 2016a; Otto et al., 2015; Otto et al., 2016b; Ritzau et al., 1997; Stadler, 2001) are recognized from this genus. Therefore, further studies on chemical components of *Sepedonium* species are promising for novel bioactive compounds, especially for new peptaibols.

During our ongoing work to study secondary metabolites from *Sepedonium* species, the culture broth and mycelial MeOH extract of *S. ampullosporum* Damon strain KSH 534 was investigated. So far, the chemical studies on *S. ampullosporum* have resulted in the isolation of characteristic 15-residue peptaibols, named ampullosporins A-D and E1-E4 (Kronen et al., 2001; Ritzau et al., 1997), together with peptaibolin (Hulsmann et al., 1998) and ampullosine (Quang et al., 2010).

The present paper describes the MS-guided isolation, structural elucidation, and total synthesis of two new linear 15-residue peptaibols, named ampullosporin F (**5.1**) and G (**5.2**), together with five known compounds including two linear peptaibols, ampullosporin A (**5.3**) and peptaibolin (**5.4**), as well as three cyclic peptides, chrysosporide (**5.5**), c(Trp-Ser) (**5.6**), and c(Trp-Ala) (**5.7**), from the semi-solid culture of *S. ampullosporum* strain KSH 534. The absolute configuration of compounds **5.1** and **5.2** was determined by comparing with their synthesized counterparts. Moreover, the linear 15-residue peptaibols **5.1-5.3** were evaluated for their biological activity against the plant-pathogenic organisms *Botrytis cinerea* Pers., *Septoria tritici* Desm., and *Phytophthora infestans* (Mont) de Bary, as well as their anticancer effects against human prostate (PC-3) and colorectal (HT-29) cancer cells. Additionally, the relationship between change in amino acid sequence and activity of compounds **5.1-5.3** could be explained using a chemoinformatic molecular docking approach.

5.2 Results and Discussion

5.2.1 Isolation and structural elucidation of compounds 5.1-5.7

The chromatographic separation of the culture broth and mycelial crude extract using Diaion HP 20 and Sephadex LH 20 in combination with (semi)preparative HPLC yielded seven compounds (**5.1-5.7**) (Figure 5.1).

Compound **5.1** was isolated as a white, amorphous solid. The amino acid sequence of **5.1** was determined based on positive and negative ion ESI-HRMSⁿ studies, which showed diagnostic fragments of the b and y series (Figure 5.2 and 5.33; Table 5.1; Table S1, Supplementary data). The signal of the [M+2H]²⁺ ion at *m/z* 819.4849 (calcd for C₇₈H₁₃₀N₁₈O₂₀²⁺ 819.4849) was the most intense one in the positive mode full scan spectrum of **5.1**, followed by the signal for the [M+H]⁺ ion at *m/z* 1637.9608 (calcd for C₇₈H₁₂₉N₁₈O₂₀²⁺ 1637.9625), both corresponding to the molecular formula C₇₈H₁₂₈N₁₈O₂₀.

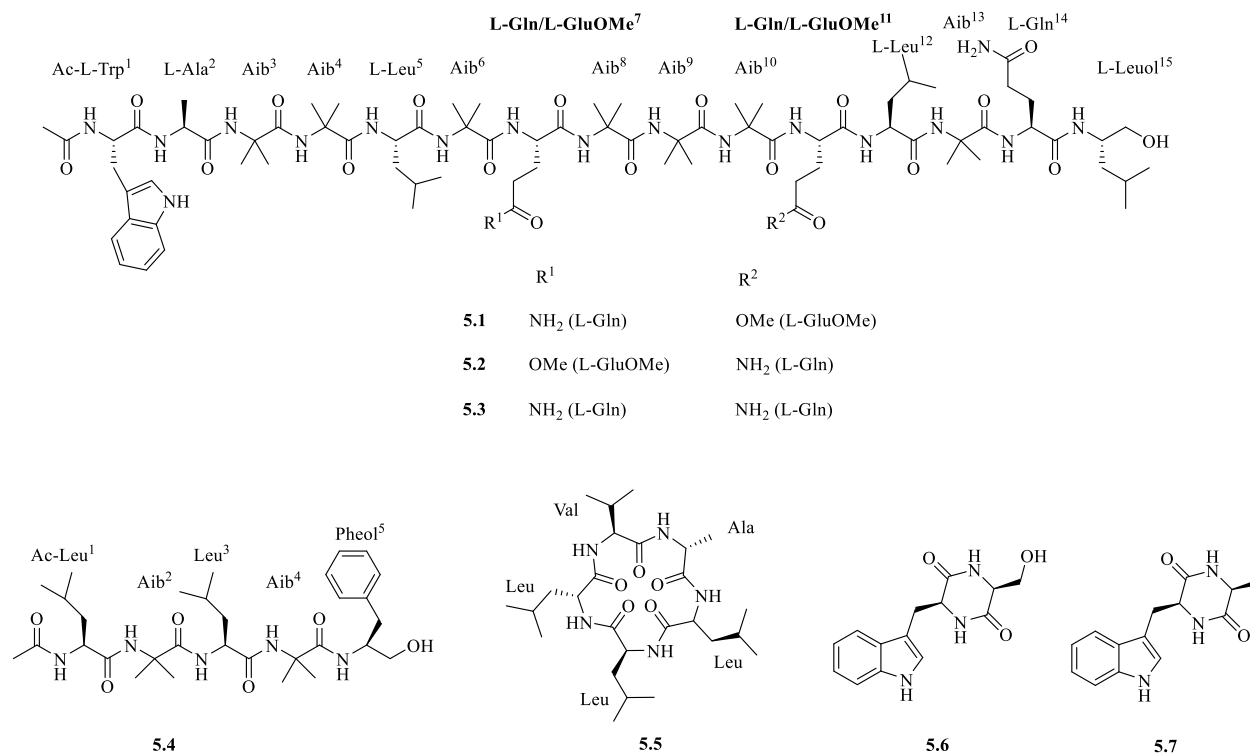


Figure 5.1. Structures of compounds **5.1–5.7**.

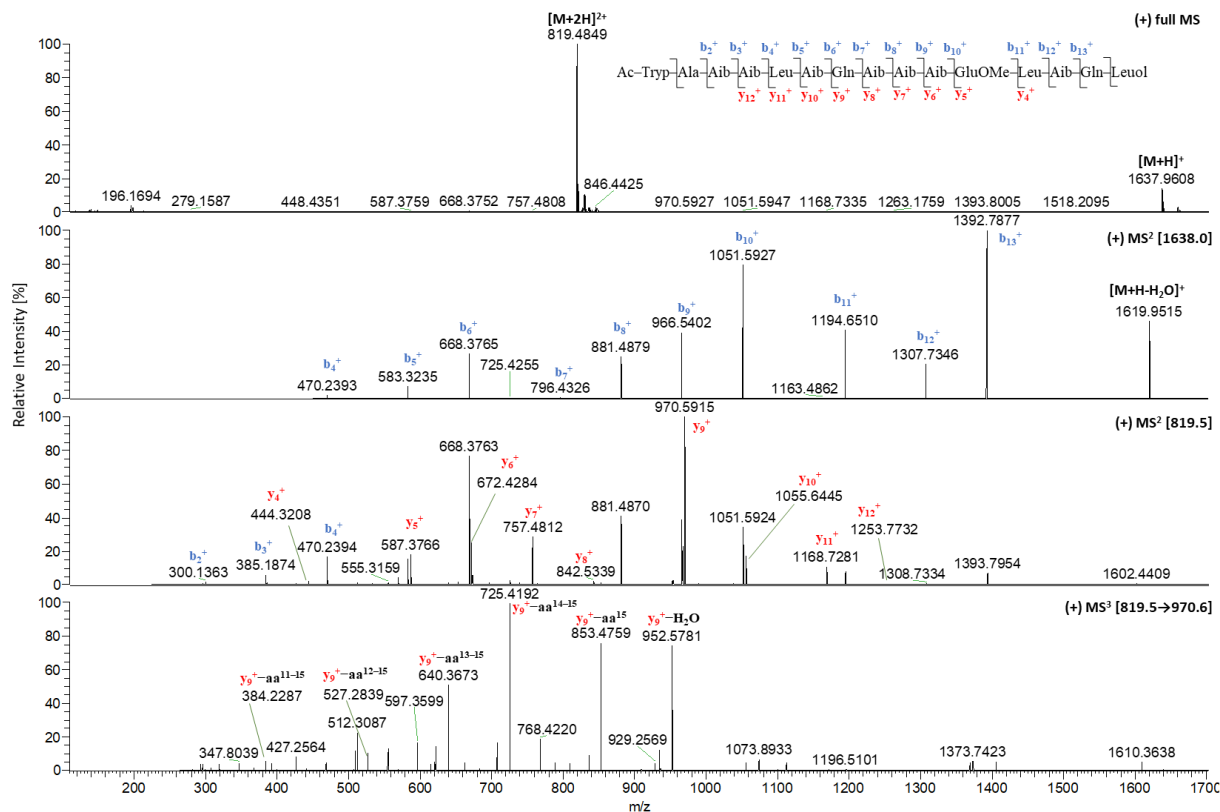


Figure 5.2. Positive ion ESI-HRMSⁿ spectra of ampullosporin F (**5.1**).

Fragmentation of the $[M+H]^+$ ion generated a series of product ions b_4^+ to b_{13}^+ , providing successive losses of Lxx^5 , Aib^6 , Gln^7 , Aib^8 , Aib^9 , Aib^{10} , $GluOMe^{11}$, Lxx^{12} and Aib^{13} . The MS^2 spectrum of the $[M+2H]^{2+}$ ion displayed further *N*-terminal *b* ions b_2^+ and b_3^+ corresponding to Aib^3 and Aib^4 . The negative ion MS^2 spectrum of the $[M-H]^-$ yielded diagnostic fragment ions y_{13}^- and y_{14}^- representing Ala^2 and $Ac-Trp^1$ as the acetylated *N*-terminal amino acid. In addition, the observed series of *C*-terminal ions y_4^+ to y_{12}^+ and y_9^- to y_{12}^- fully supported the sequence deduced from *b* series. Thus, the *N*-terminal peptide part was shown to be $Ac-Trp^1-Ala^2-Aib^3-Aib^4-Lxx^5-Aib^6-Gln^7-Aib^8-Aib^9-Aib^{10}-GluOMe^{11}-Lxx^{12}-Aib^{13}$.

Table 5.1. Diagnostic fragment ions $[m/z]$ of ampullosporin F (**5.1**) and ampullosporin G (**5.2**) from ESI-HRMSⁿ experiments in positive and negative ion modes.

	5.1	5.2		5.1	5.2
t_R (min)	11.62	11.54	y_{11}^+	1168.7280	1168.7294
$[M+2H]^{2+}$	819.4849	819.4864	y_{12}^+	<i>n.d.</i>	<i>n.d.</i>
$[M+H]^+$	1637.9608	1637.9646	y_{13}^+	<i>n.d.</i>	<i>n.d.</i>
b_1^+	229.0977	229.0978	y_{14}^+	<i>n.d.</i>	<i>n.d.</i>
b_2^+	300.1361	300.1345	y_9^+	970.5923	970.5915
b_3^+	385.1870	385.1874	$y_9^+-aa^{15}$	853.4770	853.4781
b_4^+	470.2393	470.2400	$y_9^+-aa^{14-15}$	725.4192	725.4180
b_5^+	583.3235	583.3235	$y_9^+-aa^{13-15}$	640.3662	640.3654
b_6^+	668.3765	668.3763	$y_9^+-aa^{12-15}$	527.2811	527.2847
b_7^+	796.4326	811.4340	$y_9^+-aa^{11-15}$	<i>n.d.</i>	399.2281
b_8^+	881.4879	896.4871	$y_9^+-aa^{10-15}$	<i>n.d.</i>	<i>n.d.</i>
b_9^+	966.5402	981.5396	$y_9^+-aa^{9-15}$	<i>n.d.</i>	<i>n.d.</i>
b_{10}^+	1051.5927	1066.5923	$y_9^+-aa^{8-15}$	<i>n.d.</i>	<i>n.d.</i>
b_{11}^+	1194.6510	1194.6440	$[M-H]^-$	1635.9458	1635.9453
b_{12}^+	1307.7346	1307.7357	y_2^-	<i>n.d.</i>	<i>n.d.</i>
b_{13}^+	1392.7877	1392.7875	y_3^-	<i>n.d.</i>	<i>n.d.</i>
b_{14}^+	<i>n.d.</i>	<i>n.d.</i>	y_4^-	<i>n.d.</i>	<i>n.d.</i>
y_1^+	<i>n.d.</i>	<i>n.d.</i>	y_5^-	<i>n.d.</i>	570.3615
y_2^+	<i>n.d.</i>	246.1820	y_6^-	<i>n.d.</i>	655.4136
y_3^+	<i>n.d.</i>	<i>n.d.</i>	y_7^-	<i>n.d.</i>	740.4655
y_4^+	444.3214	444.3169	y_8^-	<i>n.d.</i>	825.5215
y_5^+	587.3766	572.3767	y_9^-	968.5731	968.5756
y_6^+	672.4281	657.4289	y_{10}^-	1053.6372	1053.6267
y_7^+	757.4816	742.4813	y_{11}^-	1166.7102	1166.7143
y_8^+	842.5358	827.5331	y_{12}^-	1251.7668	1251.7572
y_9^+	970.5923	970.5915	y_{13}^-	1336.8179	1336.8088
y_{10}^+	1055.6453	1055.6426	y_{14}^-	1407.8525	1407.8543

Furthermore, the MS^3 spectrum of the *C*-terminal ion y_9^+ displayed the characteristic mass differences of 117 amu ($y_9^+-aa^{15}$, m/z 853.4759) and 245 amu ($y_9^+-aa^{14-15}$, m/z 725.4192) corresponding to isoleucinol/leucinol ($Lxxol^{15}$) as a *C*-terminal amino acid, and hence revealed the presence of Gln^{14} . Based on the above mass spectrometric analyses, the tentative sequence of **5.1**

was proposed to be Ac-Trp¹-Ala²-Aib³-Aib⁴-Lxx⁵-Aib⁶-Gln⁷-Aib⁸-Aib⁹-Aib¹⁰-GluOMe¹¹-Lxx¹²-Aib¹³-Gln¹⁴-Lxxol¹⁵.

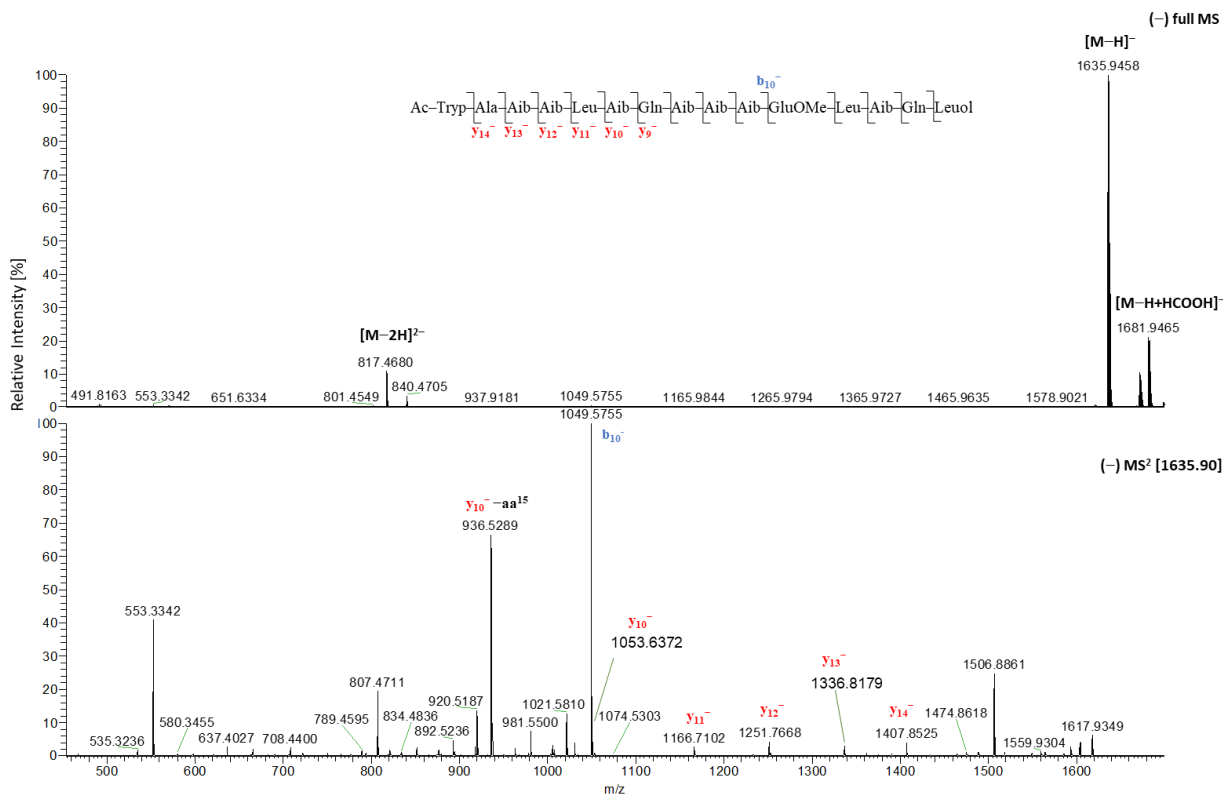


Figure 5.3. Negative ion ESI-HRMSⁿ spectra of ampullosporin F (**5.1**).

The sequence of **5.1** resulting from mass spectrometry fragmentations was confirmed by 1D & 2D NMR data, which simultaneously specified the isomeric residues Leu and Ile.

The ¹H spectrum of **5.1** (Table 5.2) displayed resonances of twenty exchangeable amide protons in the range of 6.7-11 ppm, including one broad low-field singlet (δ_{H} 10.86, Trp¹), eight doublets, seven singlets representing seven Aib, as well as four broad singlets displaying two side-chain N-H₂ (δ_{H} 7.12 and 6.75, Gln⁷; δ_{H} 7.13 and 6.73, Gln¹⁴), which were assigned in combination with ¹H-¹⁵N HSQC data. In addition, five aromatic protons (δ_{H} 7.22, 7.56, 7.33, 7.05 and 6.96, Trp¹) characterized the indole ring of tryptophan. In the high-field, multiple broad singlets between 1.30-1.50 ppm for Aib residues and a doublet for Ala² (δ_{H} 1.27, d, 7.4 Hz) were observed, while six characteristic doublets (δ_{H} 0.93, 0.86 (x2), 0.84, 0.83 and 0.81; each $J = 6.6$ Hz) were unambiguously assigned to CH₃ groups of Leu⁵, Leu¹² and Leuol¹⁵.

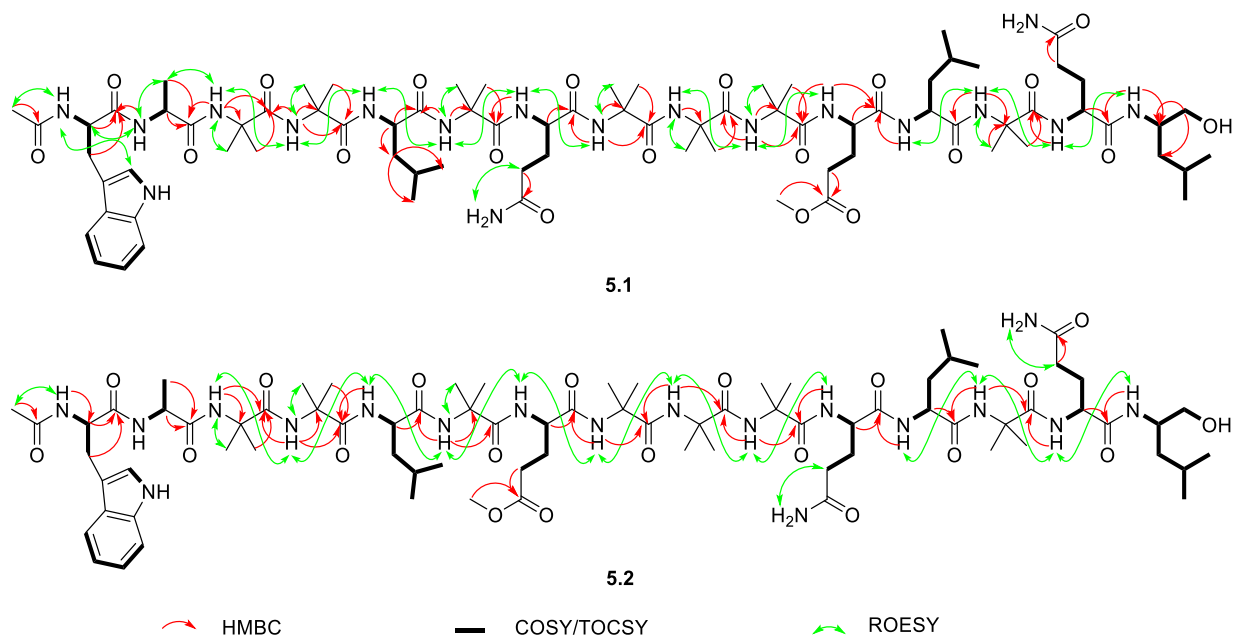


Figure 5.4. Key HMBC (H to C), COSY, ROE correlations of ampullosporin F (**5.1**) and G (**5.2**).

As depicted in Figure 5.4, ^1H - ^1H correlations from TOCSY and COSY spectra allowed defining eight N-H doublet peaks as part of eight spin systems, of which five correspond to one Ala, two Leu, and two Gln residues. Another leucine-related coupling system showing additional hydroxymethylene signals at δ_{H} 3.30/3.18, (δ_{C} 63.5) and a hydroxyl resonance at δ_{H} 4.50 bound to its methine at δ_{H} 3.78 (δ_{C} 48.2), demonstrated the presence of the reduced C-terminal Leuol residue. An additional moiety was pointed out by ^1H - ^1H TOCSY correlations between the N-H amide group at δ_{H} 8.38, the methine at δ_{H} 4.40 (δ_{C} 54.4), and the methylene at δ_{H} 3.12/2.98, (δ_{C} 26.8). ^1H - ^{13}C HMBC correlations demonstrated that this methylene carbon is linked to protons of the indole ring. Additionally, the ROESY correlation between the above amide at δ_{H} 8.38 and the acetyl CH_3 group at δ_{H} 1.86 (δ_{C} 22.2), which showed HMBC correlation to a carbonyl carbon at δ_{C} 170.2, clearly resulted in the characterization of an acetylated N-terminal Trp residue. Finally, the δ -methylene of a glutamine-related spin system exhibited HMBC correlation to a carbonyl carbon at δ_{C} 173.0, which itself showed the strong HMBC correlations with a methoxy group at δ_{H} 3.55 (δ_{C} 50.8), supporting the presence of a glutamic acid δ -methyl ester residue.

Seven N-H singlets (δ_{H} 8.46, 8.06, 7.99, 7.96, 7.87, 7.57, and 7.45) were assigned for seven Aib residues due to their HMBC correlations to seven characteristic quaternary C- α carbons (δ_{C} 55.1-56.0) and seven carbonyl carbons (δ_{C} 173.4-176.3), as well as their ROESY interactions with methyl broad singlet peaks (δ_{H} 1.30-1.50 ppm/ δ_{C} 22.0-26.2).

Detailed analysis of HMBC interactions of N-H resonances with carbonyl and C- α signals coupled with ROESY correlation peaks between neighboring proton signals afforded the sequence establishment as in accordance with mass spectrometry fragmentations. Therefore, the structure of

5.1 was confirmed to be Ac-Trp¹-Ala²-Aib³-Aib⁴-Leu⁵-Aib⁶-Gln⁷-Aib⁸-Aib⁹-Aib¹⁰-GluOMe¹¹-Leu¹²-Aib¹³-Gln¹⁴-Leuol¹⁵, and named as ampullosporin F (**5.1**) consistent with the ampullosporin series reported by Ritzau et al. in 1997 (Ritzau et al., 1997) and Kronen et al. in 2001 (Kronen et al., 2001).

Compound **5.2** was obtained as a white, amorphous solid. ESI-HRMS studies showed that **5.2** exhibited the same molecular formula (C₇₈H₁₂₈N₁₈O₂₀) as ampullosporin F (**5.1**). Positive and negative ion ESI-HRMSⁿ investigations (Table 5.1; Table S1, Supplementary data) clearly revealed that **5.2** is an isomer of **5.1**. The only difference between **5.1** and **5.2** is the positional exchange of Gln⁷/GluOMe¹¹ in **5.1** by GluOMe⁷/Gln¹¹ in **5.2**. Likewise, NMR data of **5.2** (Table 5.3, Figure 5.4) are closely resemble that of **5.1**, including the strong correlation between the methoxy singlet at δ_{H} 3.54 (δ_{C} 51.1) and a carbonyl carbon at δ_{C} 172.2 confirming the glutamic acid methyl ester moiety. Thus, the structure of **5.2** was determined as Ac-Trp¹-Ala²-Aib³-Aib⁴-Leu⁵-Aib⁶-GluOMe⁷-Aib⁸-Aib⁹-Aib¹⁰-Gln¹¹-Leu¹²-Aib¹³-Gln¹⁴-Leuol¹⁵, and trivially named ampullosporin G (**5.2**).

The δ -methyl ester of glutamic acid is rarely recognized in natural peptaibols, with only five examples of the over 1450 peptaibiotics reported in literature so far (Abdalla and McGaw, 2018; Iijima et al., 2017; Jiao et al., 2018; Katoch et al., 2019; Kim et al., 2021; Marik et al., 2018; Momose et al., 2019; Neumann et al., 2015; Ojo et al., 2018; Rawa et al., 2021a; Rawa et al., 2021b; Rivera-Chavez et al., 2017; Sica et al., 2017; Singh et al., 2018; Touati et al., 2018; van Bohemen et al., 2021; Wu et al., 2021; Zhang et al., 2021). The first occurrence was in four peptaibols Trichorzianines (TA) 1896, TA1924, TA1910, and TA1924a isolated from *Trichoderma atroviride* by Panizel et al. in 2013 (Panizel et al., 2013). The second was reported for Glu(OMe)¹⁸-alamethicin F50 isolated from *Trichoderma arundinaceum* by Rivera-Chávez et al. in 2017 (Rivera-Chavez et al., 2017). Consequently, the isolation and characterization of compounds **5.1** and **5.2** represents the third report of glutamic acid methyl ester containing peptaibols isolated from natural sources, and the first from a *Sepedonium* species.

Compound **5.3**, isolated as a white, amorphous solid, has the molecular formula C₇₇H₁₂₇N₁₉O₁₉ as deduced from ESI-HRMS studies of the protonated ion at m/z 1622.9646. The structure of **5.3** was identified as the ampullosporin A (**5.3**, Ac-Trp¹-Ala²-Aib³-Aib⁴-Leu⁵-Aib⁶-Gln⁷-Aib⁸-Aib⁹-Aib¹⁰-Gln¹¹-Leu¹²-Aib¹³-Gln¹⁴-Leuol¹⁵) based on MS studies in positive mode as well as 1D NMR experiments (Figures S29-S30, Table S2, Supplementary data).

Compound **5.4** was obtained as a white, amorphous solid. On the basis of ESI-HRMS studies, the molecular formula C₃₁H₅₁N₅O₆ was determined from the [M+H]⁺ ion's signal at m/z 590.3892. Mass fragmentation analyses coupled with 1D and 2D NMR investigations (Figures S31-S33, Table S2, Supplementary data) established **5.4** as peptaibolin (**5.4**, Ac-Leu¹-Aib²-Leu³-Aib⁴-Pheol⁵), the shortest peptaibol with only five amino acid residues. Both compounds ampullosporin A (**5.3**) and peptaibolin (**5.4**) were previously isolated from cultures of *S. ampullosporum* HKI-0053 (Hulsmann et al., 1998; Ritzau et al., 1997).

Compound **5.5** was obtained as a white, amorphous solid. ESI-HRMS analysis of the signal at m/z 510.3649 ($[M+H]^+$, calcd for $C_{26}H_{48}N_5O_5^+$ 510.3650) resulted in the molecular formula $C_{26}H_{47}N_5O_5$. Deduced from mass fragmentation analyses as well as 1D NMR investigations (Figures S34, Table S2, Supplementary data) compound **5.5** was identified as the cyclic pentapeptide chrysosporide (**5.5**).

Compound **5.6** was obtained as an amorphous solid, and exhibited the molecular formula $C_{14}H_{15}N_3O_3$ based on ESI-HRMS analyses of the $[M-H]^-$ ion at m/z 272.1042 (Figures S35, Supplementary data). 1D NMR spectroscopic data (Figures S36-S37, Supplementary data) of **5.6** were in accordance with those of c(Trp-Ser) (**5.6**), which was reported as a synthetic product in 2006 (Tullberg et al., 2006) and later isolated from several fungus like *Oidiodendron truncatum* GW3-13 (Li et al., 2012), *Acrostalagmus luteoalbus* SCSIO F457 (Wang et al., 2012), and *Rheinheimera aquimaris* QSI02 (Sun et al., 2016).

Compound **5.7** was obtained as a white, amorphous solid. On the basis of ESI-HRMS studies, the molecular formula $C_{14}H_{15}N_3O_2$ was deduced from the $[M-H]^-$ ion at m/z 256.1089 (Figures S38, Supplementary data), indicating the absence of one oxygen atom in **5.7** compared to **5.6**. 1D NMR spectroscopic data data (Figures S39-S40, Supplementary data) of **5.7** were in agreement with those of c(Trp-Ala) (**5.7**), which was synthesized in 1998 (Caballero et al., 1998) and later recognized in different fungal sources such as *Eurotium* sp. (Zhao et al., 2018) and *Eurotium chevalieri* MUT 2316 (Bovio et al., 2019). To the best of our knowledge, this is the first detection of c(Trp-Ser) (**5.6**) and c(Trp-Ala) (**5.7**) in a *Sepedonium* species.

Table 5.2. NMR data of ampullosporin F (**5.1**) (600/150 MHz, DMSO-*d*₆, δ in ppm).

Pos.	δ_H , Mult. <i>J</i> (Hz)	δ_C/δ_N	Pos.	δ_H , Mult. <i>J</i> (Hz)	δ_C/δ_N	Pos.	δ_H , Mult. <i>J</i> (Hz)	δ_C/δ_N
Ac			β	1.77 ^a ; 1.58 ^a	38.4	C=O		173.0
CH ₃	1.86 s	22.2	γ	1.72 ^a	23.8	α	3.95 m	54.4
C=O		170.2	δ_1	0.84 d 6.6	20.8	β	2.07 ^a ; 2.00 ^a	25.3
Trp ¹			δ_2	0.93 d 6.6	22.0	γ	2.60 m; 2.45 m	29.6
NH	8.38 d 6.5	125.3	Aib ⁶			C=O		172.5
C=O		173.0	NH	7.87 s	127.9	O-CH ₃	3.55 s	50.8
α	4.40	54.4	C=O		175.5	Leu ¹²		
β	3.12 dd 14.6/3.6 2.98 dd 14.6/9.4	26.8	α	1.48	55.4	NH	7.42 d 7.3	115.4
1-NH	10.86 br s	131.2	β	1.36 s	22.6	C=O		172.8
2	7.22 d 2.4	123.4	γ	1.48 s	26.1	α	4.08 m	52.5
3		109.8	Gln ⁷			β	1.67 ^a ; 1.59 ^a	38.4
3a		127.1	NH	7.41 d 6.2	112.9	γ	1.73 ^a	23.7
4	7.56 d 8.1	117.9	C=O		173.1	δ_1	0.86 d 6.6	22.2
5	6.96 t 7.5	117.7	α	3.82 m	55.7	δ_2	0.83 d 6.6	20.6
6	7.05 ^a	120.5	β	2.00 ^a ; 1.91 ^a	25.8	Aib ¹³		
7	7.33 d 8.1	111.0	γ	2.22 ^a ; 2.07 ^a	31.0	NH	7.45 s	126.5
7a		136.0	C=O		172.9	C=O		173.4
Ala ²			N-H ₂	7.12 br s 6.75 br s	107.7	α		56.0
NH	8.52 ^a	121.9	Aib ⁸			β	1.38 s	23.7
C=O		174.0	NH	7.99 s	128.5	γ	1.41 s	25.4
α	4.04 ^a	50.1	C=O		175.0	Gln ¹⁴		
β	1.27 d 7.4	15.5	α		55.1	NH	7.19 d 7.7	109.2
Aib ³		132.1	β	1.31 s	22.0	C=O		173.1
NH	8.46 s	174.6	γ	1.43 s	25.3	α	3.98 m	52.9
C=O		55.4	Aib ⁹			β	2.05 ^a ; 1.81 ^a	26.7
α		25.3	NH	7.96 s	125.2	γ	2.18 ^a ; 2.08 ^a	31.2
β	1.38 s	22.6	C=O		175.0	C=O		173.5
γ	1.35 s	22.6	α		55.3	N-H ₂	7.13 br s 6.73 br s	107.9
Aib ⁴			β	1.39 s	26.0	Leuol ¹⁵		
NH	8.06 s	124.3	γ	1.32 s	22.0	NH	7.06 ^a	118.8
C=O		176.3	Aib ¹⁰			α	3.78 m	48.2
α		55.3	NH	7.57 s	125.1	β	1.35 ^a	39.4
β	1.38 s	26.2	C=O		175.8	γ	1.66 ^a	23.5
γ	1.36 s	22.0	α		55.4	δ_1	0.86 d 6.6	23.2
Leu ⁵			β	1.39 s	22.3	δ_2	0.81 d 6.6	21.2
NH	7.71 d 4.1	114.8	γ	1.49 s	26.1	β'	3.30 ^a ; 3.18 m	63.5
C=O		173.7	GluOMe ¹¹			O-H	4.50 t 6.0	
α	3.90 m	54.1	NH	7.76 d 6.6	111.2			

Chemical shifts of quaternary carbons were determined from ¹H, ¹³C HMBC correlation peaks; ^a overlapping signals, chemical shifts were determined from ¹H, ¹⁵N or ¹H, ¹³C HSQC correlation peaks.

Table 5.3. NMR data of ampullosporin G (**5.2**) (600/150 MHz, DMSO-*d*₆, δ in ppm).

Pos.	δ_H , Mult. <i>J</i> (Hz)	δ_C/δ_N	Pos.	δ_H , Mult. <i>J</i> (Hz)	δ_C/δ_N	Pos.	δ_H , Mult. <i>J</i> (Hz)	δ_C/δ_N
Ac			β	1.55 ^a ; 1.76 ^a	38.7	α	3.93 m	55.0
CH ₃	1.85 br s	22.3	γ	1.70 ^a	24.3	β	1.94 ^a ; 2.00 ^a	26.3
C=O		170.4	δ_1	0.833 d 6.6	21.1	γ	2.13 m; 2.34 m	31.5
Trp¹			δ_2	0.914 d 6.6	22.1	C=O		173.2
NH	8.30 ^a	125.2	Aib⁶			N-H ₂	7.12 br s	107.6
C=O		173.0	NH	7.85 s	127.8		6.70 br s	
α	4.39 m	54.4	C=O		176.0	Leu¹²		
β	3.11 dd 14.4/4.2		α		55.6	NH	7.77 d 6.6	115.2
	2.98 dd 14.4/9.6	26.8	β	1.35 s	22.2	C=O		173.2
1-NH	10.84 br s	131.1	γ	1.45 s	26.2	α	4.07 m	52.6
2	7.21 d 2.4	123.5	GluOMe⁷			β	1.58 ^a & 1.67 ^a	38.5
3		109.6	NH	7.47 d 6.0	111.8	γ	1.70 ^a	23.9
3a		126.9	C=O		172.8	δ_1	0.85 d 6.6	22.3
4	7.55 d 7.8	118.0	α	3.87 m	55.2	δ_2	0.82 d 6.6	20.7
5	6.95 t-like 7.2	117.9	β	1.96 ^a ; 2.03 ^a	25.4	Aib¹³		
6	7.06 t-like 7.8	120.7	γ	2.49 ^a ; 2.39 m	29.7	NH	7.48 s	126.7
7	7.33 d 8.1	111.1	C=O		172.2	C=O		173.7
7a		135.9	O-CH ₃	3.54 s		α		56.0
Ala²			Aib⁸			β	1.37 s	23.8
NH	8.30 ^a	121.6	NH	7.97 s	128.7	γ	1.41 s	25.6
C=O		174.0	C=O		175.0	Gln¹⁴		
α	4.01 m	50.3	α		55.4	NH	7.22 d 8.4	109.3
β	1.25 d 7.2	15.7	β	1.34 s	22.4	C=O		170.6
Aib³			γ	1.42 s	25.4	α	3.98 m	53.0
NH	8.33 s	131.9	Aib⁹			β	1.80 ^a & 2.05 ^a	26.6
C=O		174.7	NH	7.87 s	125.0	γ	2.09 ^a & 2.18 ^a	31.3
α		55.4	C=O		175.0	C=O		173.8
β	1.33 s	23.0	α		55.4	N-H ₂	7.17 br s	108.2
γ	1.37 s	25.4	β	1.31 s	22.0		6.73 br s	
Aib⁴			γ	1.37 s	26.1	Leuol¹⁵		
NH	8.06 s	124.4	Aib¹⁰			NH	7.07 d 8.4	119.1
C=O		176.4	NH	7.56 s	125.1	α	3.76 m	48.4
α		55.4	C=O		175.9	β	1.34 ^a	39.5
β	1.32 s	22.0	α		55.5	γ	1.64 ^a	23.7
γ	1.37 s	26.5	β	1.38 s	22.6	δ_1	0.85 d 6.6	23.2
Leu⁵			γ	1.48 s	26.2	δ_2	0.81 d 6.6	21.3
NH	7.65 d 5.4	114.8	Gln¹¹			β'	3.18 m, 3.30 m	63.6
C=O		173.8	NH	7.74 d 5.4	111.9	O-H	4.54 t-like	
α	3.88 ^a	54.2	C=O		173.5			

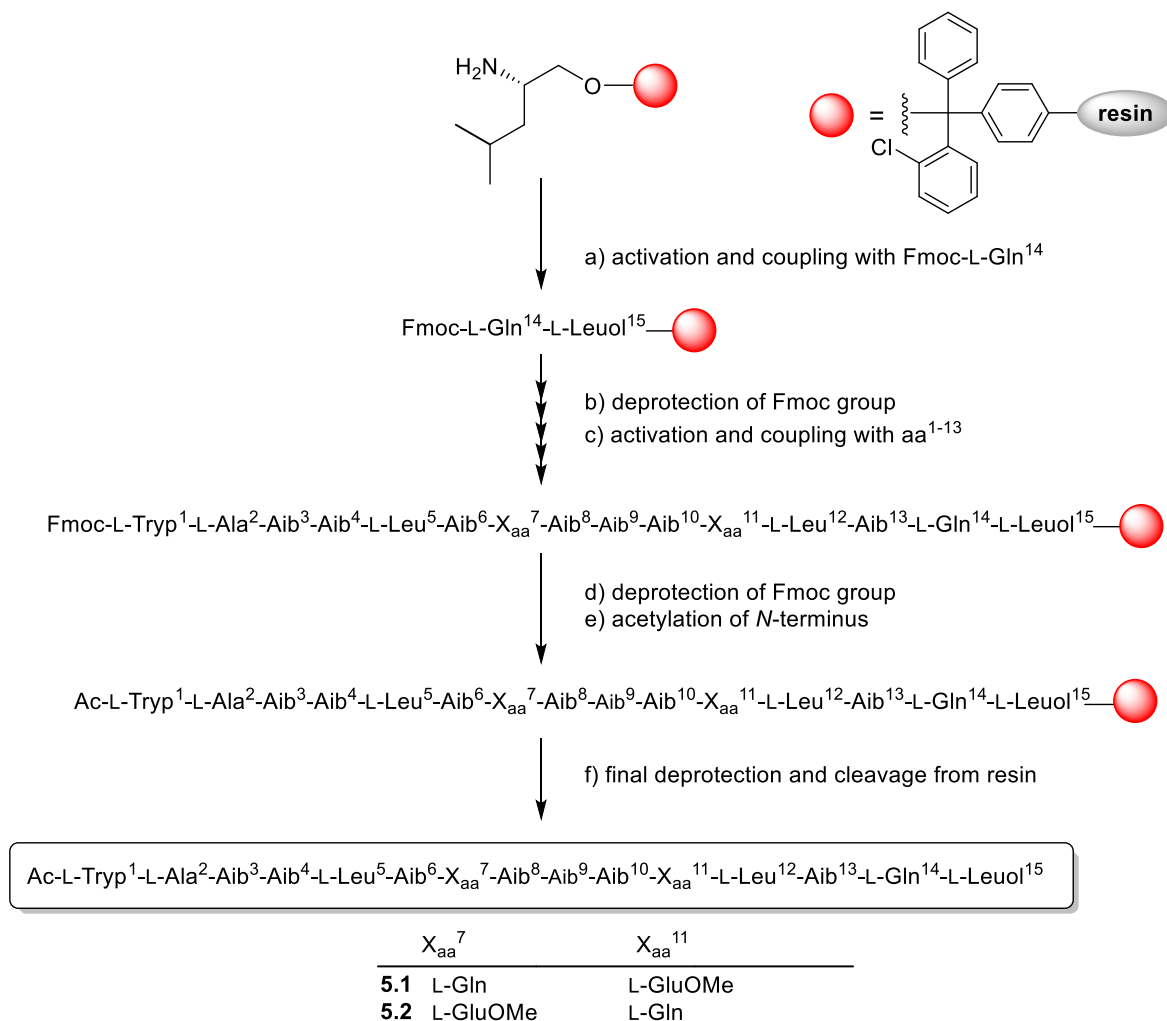
Chemical shifts of quaternary carbons were determined from ¹H, ¹³C HMBC correlation peaks; ^a overlapping signals, chemical shifts were determined from ¹H, ¹⁵N or ¹H, ¹³C HSQC correlation peaks.

5.2.2 *In situ* chemical analysis

Because ampullosporin F (**5.1**) and G (**5.2**) were isolated as minor compounds with similar structures as ampullosporin A (**5.3**), the dominant component of *S. ampullosporum*, a question may arise with regard to the authenticity of these new compounds **5.1** and **5.2**. Are the isolated ampullosporins **5.1** and **5.2** biosynthesized by fungus itself or are they artefacts formed during extraction, fractionation and/or the purification processes using methanol?

In order to answer this question, a crude extract from cultivated *S. ampullosporum* was prepared using ethanol, instead of methanol, and investigated using LC-HRMS screening approach. From an enriched fraction of the ethanol crude extract of *S. ampullosporum*, the ampullosporin F (**5.1**) and G (**5.2**) as well as ampullosporin A (**5.3**) could be unambiguously detected by their characteristic mass (Figure S43, Supplementary data). Therefore, ampullosporin F (**5.1**) and G (**5.2**) are native constituents of *S. ampullosporum* Damon strain KSH 534.

5.2.3 Solid phase synthesis and absolute configuration of ampullosporin F and G



Scheme 5.1. Solid-phase peptide synthesis of ampullosporin F (**5.1**) and G (**5.2**).

The absolute configuration of **5.1** and **5.2** was established based on solid-phase peptide synthesis using Fmoc protected, L-configured amino acids (except the achiral Aib) and tetramethylfluorom-amidinium hexafluorophosphate (TFFH) as coupling reagent (Scheme 5.1).

The combined manual and automated synthesis was carried out on L-Leucinol 2-chlorotriptyl polystyrene resin. The first four amino acid residues were incorporated by automated synthesis using the standard PyBOP (benzotriazol-1-yloxytripyrrolidinophosphonium hexafluorophosphate) strategy, while the rest of the synthesis was performed manually using TFFH or HATU (1-[bis(dimethylamino)methylene]-1H-1,2,3-triazolo[4,5-b]pyridinium 3-oxide hexafluorophosphate) activations. *N*-terminal acetylation was achieved after complete peptide assembly by treating the resin with Ac₂O, followed by solid-phase cleavage and deprotection using TFA. The synthesized peptides **5.1** and **5.2** were purified by size exclusion column chromatography using LH20 in combination with preparative HPLC. The ESI-HRMSⁿ, 1D NMR, and CD spectra of the synthetic peptaibols **5.1** and **5.2** were consistent with those of the natural ampullosporin F (**5.1**) and ampullosporin G (**5.2**) (Figures S17-S28, Supplementary data). Consequently, all chiral amino acids naturally present in **5.1** and **5.2** possess the L-configuration, which is typical for the particular class of ampullosporins (Hulsmann et al., 1998; Ritzau et al., 1997).

5.2.4 Evaluation of antifungal activities

Isolated peptaibols **5.1-5.3** were examined for their antifungal activities against plant pathogenic ascomycetous fungi *Botrytis cinerea* (grey mold pathogen on many crops, e.g. strawberries and wine grapes) and *Septoria tritici* (causes septoria leaf blotch of wheat) as well as the oomycete *Phytophthora infestans* (causal agent of the late blight disease on potato and tomato) using a 96-well microtiter plate assay. The commercially available fungicides epoxiconazole and terbinafine were used as positive controls.

Table 5.4. Biological activity of ampullosorin F (**5.1**), G (**5.2**) and A (**5.3**) (IC₅₀, μM).

Compound	Toxicity ^a		Antifungal Activity ^b		
	HT29	PC3	<i>B. cinerea</i>	<i>S. tritici</i>	<i>P. infestans</i>
5.1	5.90 ± 0.65	3.62 ± 0.49	7.27 ± 0.95	>125	14.75 ± 1.89
5.2	6.04 ± 0.64	3.35 ± 0.89	4.59 ± 0.34	>125	14.79 ± 2.84
5.3	10.45 ± 1.18	6.68 ± 1.67	11.41 ± 1.48	>125	19.49 ± 4.29
Epoxiconazole ^c			<1.5	<1.5	
Terbinafine ^c					48.30 ± 0.2

^a Data represent biological quadruplicates (*n* = 4), each comprising technical triplicates. ^b The experiment was carried out in triplicates (*n* = 3), each comprising technical triplicates. ^c Used as positive control.

All three compounds **5.1-5.3** showed strong activity against *B. cinerea* and only slightly lower inhibitory effects against *P. infestans*, but were inactive against *S. tritici*. Interestingly, the growth-inhibitory effects against both *B. cinerea* and *P. infestans* increased with the presence of GluOMe in ampullosporin F (**5.1**) and G (**5.2**), compared to ampullosporin A (**5.3**) (Table 5.4; Figures S41, Supplementary data).

5.2.5 Evaluation of anticancer activities

The peptaibols **5.1** – **5.3** were tested for their effects on the viability of two different human cancer cell lines, namely prostate PC-3 adenocarcinoma cells and colorectal HT-29 adenocarcinoma cells. The cell viability and cytotoxicity assay was conducted by using resazurin and fluorometric read-out after 48 h cell treatment. The saponin digitonin (100 μM), a very potent permeabilizer of cell membranes, was used as positive control compromising the cells to yield 0% cell viability after 48 h. As negative control, representing 100% cell viability for data normalization, medium with 0.5% (v/v) DMSO supplementation (highest final DMSO concentration in test item samples) was measured.

The peptaibols **5.1** – **5.3** were tested with concentrations in the range of 0.195 – 100 μM (factor 2 dilutions) in order to determine IC_{50} values that have been calculated to be $\sim 3 - 6 \mu\text{M}$ for both novel ampullosporins F (**5.1**) and G (**5.2**), with twofold higher activity in prostate PC-3 cancer cells compared to the colorectal cancer cells HT-29. Furthermore, in both cancer cell lines, **5.1** and **5.2** were found with twofold lower IC_{50} s compared to the already known ampullosporin A (**5.3**) (Figure 5.5), indicating that the GluOMe modifications at the amino acid positions 7 and 11, respectively, enhance not only the antifungal but also the anticancer activity of the ampullosporins. Summarized results are shown in Table 5.3.

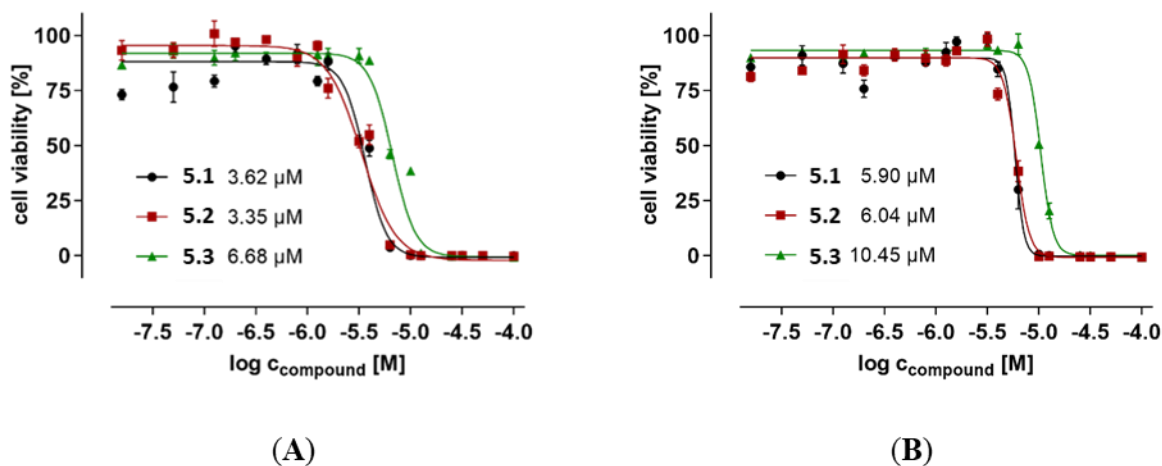


Figure 5.5. Cell viability of (A): prostate cancer PC-3 cells, and (B): colon cancer HT-29 cells treated for 48 h with the peptaibols **5.1** (●), **5.2** (■), and **5.3** (▲), respectively, as determined by resazurin-based fluorimetric assay. Data represent biological quadruplicates ($n = 4$), each comprising technical triplicates.

5.2.6 *In silico* NMDA receptor docking

In 2009, Berek et al. investigated the neuroleptic-like activity of ampullosporin A (**5.3**) in mice. Thereby, they described a complete suppression of the effects of the *N*-methyl-D-aspartate (NMDA) receptor antagonist MK-801, and alteration of the activity of those glutamate receptors

(Berek et al., 2009), indicating NMDA receptors as potential biological target molecules of ampullosporin A (5.3). Recently, Lu et al. (2017) investigated the interplay of MK-801 and NMDA receptor in more detail using cryo-EM structural analyses, explaining the allosteric antagonistic action of MK-801 (pdb-code 5UOW) (Lu et al., 2017). Based on those results, we decided to proof the hypothesis of NMDA receptor binding of our ampullosporins (5.1-5.3) by using a chemoinformatic molecular docking approach based on two protein databank entries (5UOW and 6IRA). While 5UOW includes the MK-801 inhibitor but reflects the situation at non-human NMDA receptor proteins, 6IRA comprises the human GluN1/GluN2A ligand binding domain as the relevant part of the human NMDA receptor (Zhang et al., 2018).

Based on the protein databank entry 5UOW, a putative binding site on the trimeric NMDA receptor GluN1/GluN2A/GluN2B was indicated by the cryo-EM-based localization of the inhibitor MK-801 in structure 5UOW (Figure 5.6). Moreover, our *in silico* docking approach based on 5UOW highlighted a very good docking of 5.3 in very close proximity to MK-801, as also shown in Figure 5.6. The indicated binding site is located in a hydrophobic cleft that is formed by several helices of both NMDA receptor subunits GluN1 and GluN2A. This theoretical colocalization of ampullosporin A (5.3) and the allosteric NMDA receptor antagonist MK-801 could explain the complete suppression of MK-801 effects caused by the peptaibol (5.3).

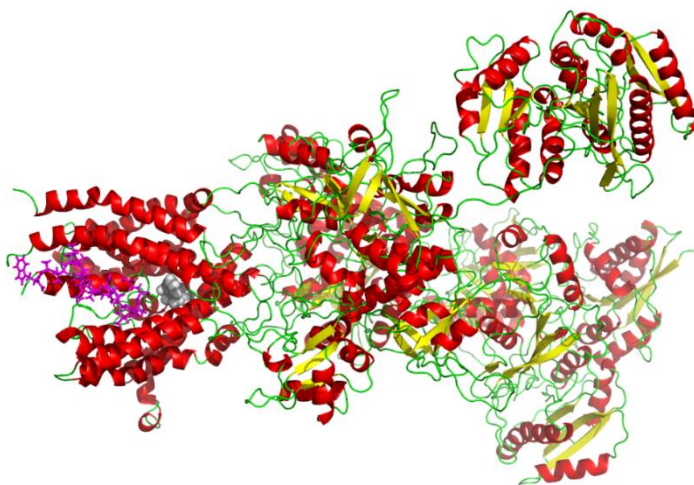


Figure 5.6: The complete structure of the non-human trimeric NMDA receptor GluN1/GluN2A/GluN2B (based on protein databank entry 5UOW) with docked ampullosporin A (5.3) (magenta atoms, left site). The position of a proposed allosteric binding site is given by the cryo-EM structure-based position of the inhibitor MK-801 (drawn in grey) in structure 5UOW.

In addition, compounds 5.1-5.3 were tested for their antiproliferative effects in PC-3 prostate and HT-29 colorectal human cancer cells, which, to some extent, express the NMDA receptor proteins GluN1 and GluN2A (according to mRNA expression data; analyzed by using the Genevestigator software, data base: HS_mRNASeq_HUMAN_GL-1; data not shown). Therefore, we also investigated the ampullosporins' binding *in silico* based on protein databank entry 6IRA

representing the human GluN1/GluN2A NMDA receptor complex that, however, do not include MK-801. Indeed, also in our 6IRA-based *in silico* model the peptaibols **5.1-5.3** were docked with best scores at the same position in the hydrophobic cleft between GluN1 and GluN2A (Figure 5.7).

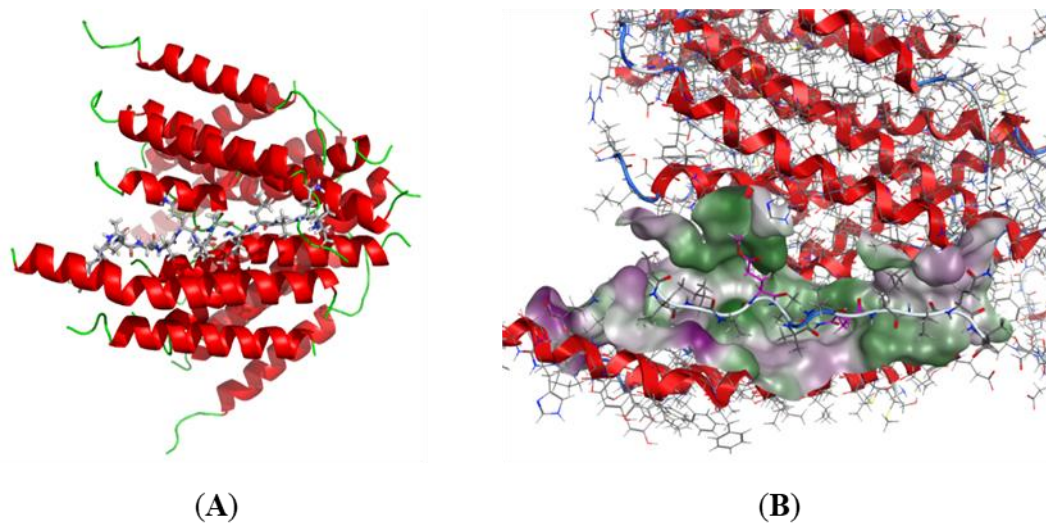


Figure 5.7. (A) Ampullosporins (**5.1-5.3**) dock with best docking scores into cleft formed by several helices of human NMDA receptor subunits GluN1 and GluN2A. (B) The hydrophobic potential blot –hydrophobic (in green)/ hydrophilic (in lilac)– indicates the primarily hydrophobic character of the binding site.

Our *in silico* results, coupled with the observations by Berek et al. (Berek et al., 2009), led to the hypothesis that this hydrophobic cleft at the interphase between GluN1 and GluN2A could be the binding site for the very hydrophobic peptaibols **5.1-5.3**, causing their biological effects. To shed more light on the molecular ampullosporins binding mode and especially to investigate consequences of the sequence modifications in the novel ampullosporin F (**5.1**) and G (**5.2**), further docking studies were performed to validate this hydrophobic cleft as potential binding site of compounds **5.1-5.3**.

As illustrated in Figure 5.8 and Figure S43 (Supplementary data), all compounds **5.1-5.3** fit nicely into the described hydrophobic cleft and seem to be stabilized by numerous hydrophobic interactions to hydrophobic receptor side chains. Accordingly, for ampullosporin A (**5.3**) an interaction energy of -92.0 kcal/mol was calculated. However, replacement of each of Gln residues (Gln⁷ and Gln¹¹) in ampullosporin A (**5.3**) by GluOMe resulted in additional hydrophobic interactions of ampullosporin F (**5.1**; GluOMe¹¹) and ampullosporin G (**5.2**; GluOMe⁷) with hydrophobic receptor residues. In case of **5.1**, enhanced hydrophobic interactions to the receptor residues V820, I824 and F637 elevates the calculated interaction energy to be -94.5 kcal/mol. In case of **5.2**, the molecular docking indicates additional hydrophobic interactions of its GluOMe⁷ modification with the hydrophobic receptor residues W608 and W611. The calculated interaction energy (-92.9 kcal/mol) for **5.2** is slightly enhanced compared to **5.3**. Based on these calculated

interaction energies, the binding of both ampullosporin F (**5.1**) and G (**5.2**) should outperform the binding of ampullosporin A (**5.3**).

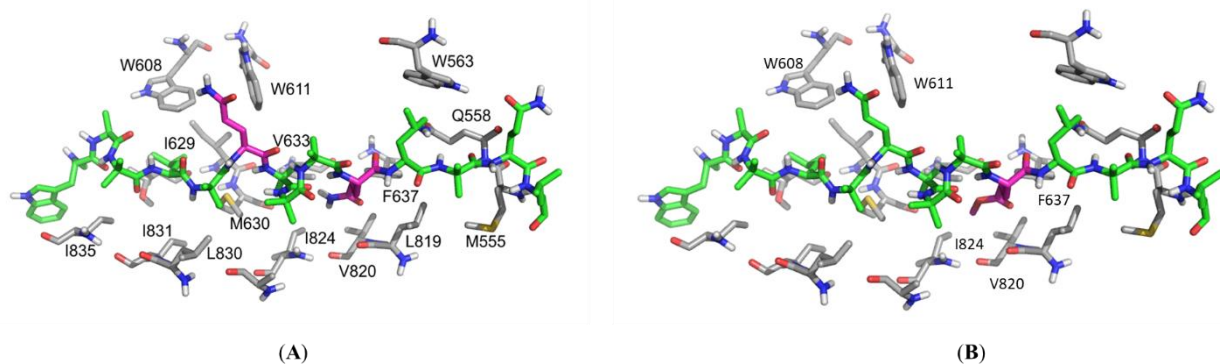


Figure 5.8. Docking arrangements of (A) ampullosporin A (**5.3**), and (B) ampullosporin F (**5.1**) in the proposed binding site in the hydrophobic cleft between NMDA receptor subunits GluN1 and GluN2A, as modeled based on protein databank entry 6IRA.

Interestingly, the determined antiproliferative activities of compounds **5.1–5.3** (Figure 5.5) correlate very well with the proposed enhanced binding of both novel ampullosporins (**5.1** and **5.2**). The antiproliferative IC_{50} values in the anticancer assay were detected to be by twofold better for ampullosporin F (**5.1**) and G (**5.2**) than for ampullosporin A (**5.3**).

Whether or not the NMDA receptor is really the relevant molecular target explaining the observed antiproliferative effects of the ampullosporins on human cancer cells, further investigations are necessary. However, considering the well-published neuroleptic-like activities of ampullosporin A (**5.3**) (Berek et al., 2009; Nguyen et al., 2002; Ritzau et al., 1997), that can be easily attributed to NMDA receptor pathways, it would be of very high interest to test our novel ampullosporins F (**5.1**) and G (**5.2**), with presumed improved NMDA receptor binding, for their neuroleptic activity, e.g. *in vivo* in mice.

5.3 Concluding remarks

In conclusion, the present study represents the chemical investigation of semi-solid culture of *Sepedonium ampullosporum* Damon strain KSH 534. There are seven constituents including two new 15-residue linear peptaibols, named ampullosporin F (**5.1**) and G (**5.2**), as well as two known linear peptaibols, ampullosporin A (**5.3**) and peptaibolin (**5.4**), together with three previously described cyclic peptides, chrysosporide (**5.5**), c(Trp-Ser) (**5.6**), and c(Trp-Ala) (**5.7**). The authenticity of peptaibols **5.1** and **5.2** was approved by using LC-HRMS approach. Additionally, the total synthesis of **5.1** and **5.2** was performed on solid-phase synthesis establishing the L-configuration of all chiral amino acids. Furthermore, peptaibols **5.1–5.3** showed significant anti-phytopathogenic activity against *B. cinerea* and *P. infestans*, but no activity against *S. tritici*. Moreover, compounds **5.1–5.3** exhibited strong anticancer activities against human prostate (PC-

3) and colorectal (HT-29) cancer cells. Interestingly, for both antifungal and anticancer assays, the activities of ampullosporin F (**5.1**) and G (**5.2**) were found to be twofold higher than the structurally similar ampullosporin A (**5.3**), demonstrating the effect of a GluOMe moiety on biological activity. Our molecular docking data on NMDA receptors suggests the better hydrophobic interaction of **5.1** and **5.2** than **5.3** with the hydrophobic cleft of the receptor, which might lead to the higher inhibitory effects of the new compounds **5.1** and **5.2** compared to **5.3**.

5.4 Experimental

5.4.1 General Experimental Procedures

Column chromatography was carried out on Sephadex LH 20 (Fluka, Steinheim, Germany), while analytical TLC was performed on precoated silica gel F₂₅₄ aluminum sheets (Merck, Darmstadt, Germany). Peptaibols were detected on TLC plates using ninhydrin reagent as described in literature (Otto et al., 2015). Diaion HP 20 was purchased from Supelco (Bellefonte, PA, USA). UV spectra were recorded on a Jasco V-770 UV-Vis/NIR spectrophotometer (Jasco, Pfungstadt, Germany), meanwhile CD spectra were obtained from a Jasco J-815 CD spectropolarimeter (Jasco, Pfungstadt, Germany). The specific rotation was measured with a Jasco P-2000 digital polarimeter (Jasco, Pfungstadt, Germany).

NMR spectra were obtained from an Agilent DD2-400 and an Agilent VNMRS 600 system (Varian, Palo Alto, CA, USA) using a 5-mm inverse detection cryoprobe. Compounds were dissolved in DMSO-*d*₆ (99.96% D for **5.1** and **5.2**, 99.80% D for **5.3-5.7**). The spectra were recorded at 399.82/599.83 MHz (¹H) and 100.54/125.80 (¹³C), respectively. 2D NMR spectra were recorded using standard CHEMPACK 8.1 pulse sequences (s2pul, ¹H,¹H gDQCOSY, ¹H,¹H zTOCSY, ¹H,¹H ROESY(AD), ¹H,¹³C and ¹H,¹⁵N gHSQCAD, ¹H,¹³C gHMBCAD) implemented in Varian VNMRJ 4.2 spectrometer software. The mixing time for the TOCSY experiments was set to 80 msec, for the ROESY experiments was set to 250 msec. The HMBC experiment was optimized for a long-range coupling of 8 Hz. ¹H and ¹³C chemical shifts were referenced to internal DMSO-*d*₆ (δ_{H} 2.51 ppm and δ_{C} 39.5 ppm), whereas ¹⁵N chemical shifts were given relative to liquid NH₃ (δ_{N} 0 ppm).

The solid phase synthesis was partly carried out on a ResPep SL peptide synthesizer (Intavis Bioanalytical Instruments, Germany). The L-configured Fmoc-amino acids Fmoc-Trp(Boc)-OH, Fmoc-Ala-OH, Fmoc-Leu-OH, Fmoc-Gln(Trt)-OH and Fmoc-Glu(OMe)-OH were purchased from Carbolution Chemicals (Ingbert, Germany), while L-Leucinol 2-chlorotrityl polystyrene resin were obtained from Iris Biotech GmbH (Marktredwitz, Germany). TFFH was supplied Carbolution Chemicals (Ingbert, Germany). Piperidine, Ac₂O, DIPEA, and DMF were purchased from Sigma-Aldrich (Steinheim, Germany).

The high resolution mass spectra in positive and negative modes were obtained from an Orbitrap Elite mass spectrometer (ThermoFisher Scientific, Bremen, Germany) equipped with an ESI

electrospray ion source (spray voltage 4.0 kV; capillary temperature 275 °C, source heater temperature 40 °C; FTMS resolution 60.000). Nitrogen was used as sheath gas. The sample solutions were introduced continuously via a 500 µl Hamilton syringe pump with a flow rate of 5 µl/min. The instrument was externally calibrated by the Pierce® LTQ Velos ESI positive ion calibration solution (product number 88323) and Pierce® ESI negative ion calibration solution (product number 88324) from Thermofisher Scientific (Rockford, IL, 61105 USA). The data were evaluated by the Xcalibur software 2.7 SP1 (Thermofisher Scientific, Waltham, MA, USA). The collision induced dissociation (CID) MSⁿ measurements were performed using the relative collision energies given in Table S1 (Supplementary data).

The preparative HPLC was performed on a Shimadzu prominence system (Kyoto, Japan) which consists of a CBM-20A communications bus module, a SPD-M20A diode array detector, a FRC-10A fraction collector, a DGU-20A5R degassing unit, a LC-20AT liquid chromatograph, and a SIL-20A HT auto sampler, using either column 1 (ODS-A, 5 µm, 120 Å, 150 x 20 mm I.D; YMC, Devens, MA, USA) or column 2 (ODS-A, 5 µm, 120 Å, 150 x 10 mm I.D; YMC, Devens, MA, USA). The mobile phases were H₂O (A) and CH₃CN (B), with 0.1% formic acid contained in both solvents, using a gradient system.

5.4.2 Extraction and Isolation

The fungal strain *Sepedonium ampullosporum* KSH 534 was isolated in August 1999, from *Boletus calopus* in Crista Acri near Cosenza, Italy (leg./det. C. Lavorato). A voucher specimens is deposited at the herbarium of the University Regensburg. The fungal culture of *S. ampullosporum* KSH 534 was stored on malt peptone agar (MPA) plates and transferred periodically. The up-scaled semi-solid cultures, used for isolation, were grown in 31 Erlenmeyer flasks (size 1 L) each containing 1.5 g of cotton wool and 250 ml of malt peptone medium (2.5 g malt and 0.625 g peptone in 250 ml deionized water), resulting in a total volume of 7.75 L. Each culture flask was inoculated with a 10 x 10 mm agar plug of colonized fungus and incubated for 14 days at room temperature without agitation.

5.4.3 Extraction and Isolation

The mycelia were separated from the culture broth by vacuum filtration, frozen with liquid nitrogen and subsequently extracted with EtOAc (2 x 2L) and MeOH (2 x 2L) to yield two crude extracts (EtOAc, 2.20 g and MeOH, 8.98 g, respectively). Meanwhile, activated Diaion HP 20 (50 g) was added to the culture broth and agitated for 12 hours at room temperature. Diaion HP 20 was then removed by vacuum filtration, washed with H₂O, eluted with MeOH to give a yellow solution, which was then evaporated *in vacuo* to dryness. This dryness (3.44 g) from culture broth was combined with the EtOAc extract from mycelia according to their LC-MS profiles. The resulting residue (5.64 g) was chromatographed on a Sephadex LH 20 column, using aq. MeOH 60% as eluent to afford 140 fractions (8 ml each). Based on ESI-MS spectra, fractions 26-38 were combined (1.91 g), which were first separated by size exclusion column chromatography (using

Sephadex LH 20, eluent: MeOH), then subjected to preparative HPLC using column 1 at a flow rate of 4.5 mL/min (0-30 min, 30-80% B; 31-50 min, 80-100% B) to afford **5.3** (ampullosporin A, $t_R = 34.0$ min, 100.9 mg), **5.1** (ampullosporin F, $t_R = 37.5$ min, 4.7 mg), and **5.2** (ampullosporin G, $t_R = 40.5$ min, 3.8 mg). In addition, the combination of fractions 39-48 (311.7 mg) was purified by semipreparative HPLC using column 2 at a flow rate of 2.2 mL/min (0-12 min, 30-100% B; 12-17 min, 100% B) to afford **5.4** (peptaibolin, $t_R = 12.7$ min, 1.4 mg) and **5.5** (chrysosporide, $t_R = 14.5$ min, 0.3 mg). Similarly, fractions 61-74 (85.4 mg) were combined and finally purified by semipreparative HPLC using column 2 at a flow rate of 2.2 mL/min (0-20 min, 10-100% B) to afford **5.6** (c(Trp-Ser), $t_R = 10.6$ min, 8.1 mg) and **5.7** (c(Trp-Ala), $t_R = 11.2$ min, 7.3 mg).

5.4.4 Sample preparation for LC-MS screening

For the preparation of the enriched fraction for the LC-HRMS screening, one stored deep frozen agar plate cultures of *S. ampullosporum* KSH534 was crushed in small pieces and extracted with EtOH 96% (2 x 250 mL) in an ultrasonic bath at room temperature. The resulted yellow solution was evaporated *in vacuo* to dryness. The dried crude extract was redissolved in EtOH 96%/H₂O (1:2, v/v) to a concentration of 50 mg/mL. The resulting solution was separated on SPE cartridges Chromabond® C18 (loading 200 mg/3 mL, particle size 45 μ m, Macherey-Nagel, Düren, Germany), targeted peptaibols **5.1-5.3** were eluted with EtOH 96%. After evaporation to dryness *in vacuo*, the enriched fraction was redissolved in CH₃CN and submitted to LC-HRMS.

5.4.5 Solid-phase peptide synthesis

Compounds **5.1** and **5.2** were synthesized by combining manual and automated synthesis. The protocol was based on a Fmoc/*t*-butyl strategy in a 0.1 mmol scale starting from L-Leucinol 2-chlorotriyl resin (200–400 mesh, loading 0.67 mmol/g resin). The first four amino acids residues, were incorporated by automated synthesis using the standard method based in PyBOP/NMM activation. The rest of the synthesis was performed manually using 4 equiv. of the amino acids and DMF as a solvent. For all the Aib residues the coupling cycle protocol was based on activation with TFFH (4 equiv.) and NMM (*N*-methylmorpholine, 4 equiv.) for 12 min and coupling time of 120 min. The rest of the amino acids were coupled using activation with HATU (4 equiv.) and NMM (4 equiv.) for 5 min and a coupling time of 120 min. Fmoc removals were carried out using a solution of 20% piperidine in DMF for two cycles of 10 min. *N*-terminal acetylation was performed after complete peptide assembly by treating the resin with Ac₂O (10 equiv.) and DIPEA (10 equiv.) in DMF for 30 min. Solid-phase cleavage and global deprotection was achieved by treating the resin with 5 mL of TFA/H₂O/TIPS (95:2.5:2.5, v/v/v) for 120 min. The cleavage mixture was concentrated under reduced pressure, suspended in a mixture of CH₃CN 50% in water and lyophilized.

For the peptide **5.1**, the crude peptide mixture (183.8 mg) obtained after lyophilizing was redissolved in MeOH, and subjected to column chromatography (360 x 30 mm) using Sephadex LH20, eluting with MeOH to afford 30 fractions (8mL each). Fractions 6 and 7 were combined

(78.6 mg) and purified by preparative HPLC using column 1 (0-2 min, 30-70% B; 3-15 min, 70-100% B; 10 mL/min) to give **5.1** in 7.0% total yield ($t_R = 15.6$ min, 11.5 mg).

For the peptide **5.2**, the crude peptide mixture (201.7 mg) obtained after lyophilizing was redissolved in MeOH, and separated by column chromatography (360 x 30 mm) on Sephadex LH20, using MeOH as eluent to give 30 fractions (8mL each). Fractions 1-5 were combined (95.6 mg) and purified by preparative HPLC using column 1 (0-2 min, 30-80% B; 3-15 min, 80-100% B; 10 mL/min) to give **5.2** in 7.7% total yield ($t_R = 16.2$ min, 12.6 mg).

Natural ampullosporin F (5.1): white, amorphous solid; TLC R_f 0.34 (*n*-BuOH/AcOH/H₂O 4:1:1); $[\alpha]_D^{22}$ -15.6 (*c* 0.100, MeOH); CD (MeOH) $[\theta]_{208}$ -120119, $[\theta]_{224}$ -103881 deg cm² x dmol⁻¹; UV (MeOH) λ_{max} (log ϵ) 290 (23.56) nm; ¹H NMR and ¹³C NMR see Table 5.2; ESI-HRMS m/z 819.4849 ([M+2H]²⁺, calcd for C₇₈H₁₃₀N₁₈O₂₀²⁺ 819.4849); ESI-HRMSⁿ see Table 5.1, and Table S1 (Supplementary data).

Synthetic ampullosporin F (5.1): white, amorphous solid; CD (MeOH) $[\theta]_{208}$ -232819, $[\theta]_{224}$ -208346 deg cm² x dmol⁻¹; ¹H NMR and ¹³C NMR in accordance with data of natural **5.1**; ESI-HRMS m/z 819.4855 ([M+2H]²⁺, calcd for C₇₈H₁₃₀N₁₈O₂₀²⁺ 819.4859); ESI-HRMSⁿ in agreement with natural **5.1**.

Natural ampullosporin G (5.2): white, amorphous solid; TLC R_f 0.44 (*n*-BuOH/AcOH/H₂O 4:1:1); $[\alpha]_D^{23}$ -17.1 (*c* 0.080, MeOH); CD (MeOH) $[\theta]_{208}$ -150953, $[\theta]_{223}$ -125977 deg cm² x dmol⁻¹; UV (MeOH) λ_{max} (log ϵ) 281 (1.88), 290 (1.81) nm; ¹H NMR and ¹³C NMR see Table 5.3; ESI-HRMS m/z 819.4860 ([M+2H]²⁺, calcd for C₇₈H₁₃₀N₁₈O₂₀²⁺ 819.4849); ESI-HRMSⁿ see Table 5.1, and Table S1 (Supplementary data).

Synthetic ampullosporin G (5.2): white, amorphous solid; CD (MeOH) $[\theta]_{207}$ -246393, $[\theta]_{222}$ -205061 deg cm² x dmol⁻¹; ¹H NMR and ¹³C NMR in accordance with data of natural **5.2**; ESI-HRMS m/z 819.4848 ([M+2H]²⁺, calcd for C₇₈H₁₃₀N₁₈O₂₀²⁺ 819.4859); ESI-HRMSⁿ in agreement with natural **5.2**.

Natural ampullosporin A (5.3): white, amorphous solid; TLC R_f 0.26 (*n*-BuOH/AcOH/H₂O 4:1:1); ¹H NMR and ¹³C NMR in agreement with data of Ritzau et al. (1997); ESI-HRMS m/z 811.9851 ([M+2H]²⁺, calcd for C₇₇H₁₂₉N₁₉O₁₉²⁺ 811.9851); ESI-HRMSⁿ see Table S2, Supplementary data.

Natural peptaibolin (5.4): white, amorphous solid; TLC R_f 0.88 (*n*-BuOH/AcOH/H₂O 4:1:1); ¹H NMR and ¹³C NMR in agreement with data of Hulsmann et al. (1998); ESI-HRMS m/z 590.3892 ([M+H]⁺, calcd for C₃₁H₅₂N₅O₆⁺ 590.3912); ESI-HRMSⁿ see Table S2, Supplementary data.

Natural chrysosporide (5.5): white, amorphous solid; TLC R_f 0.68 (*n*-BuOH/AcOH/H₂O 4:1:1); ¹H NMR and ¹³C NMR in agreement with data of Mitova et al. (2006); ESI-HRMS m/z 510.3649 ([M+H]⁺, calcd for C₂₆H₄₈N₅O₅⁺ 510.3650); ESI-HRMSⁿ see Table S2, Supplementary data.

Natural cyclic-(Trp-Ser) (5.6): white, amorphous solid; TLC R_f 0.66 (*n*-BuOH/AcOH/H₂O 4:1:1); ¹H NMR and ¹³C NMR in agreement with data of Tullberg et al. (2006); ESI-HRMS *m/z* 272.1042 ([M+H]⁺, calcd for C₁₄H₁₄N₃O₃⁻ 272.1041).

Natural cyclic-(Trp-Ala) (5.7): white, amorphous solid; TLC R_f 0.76 (*n*-BuOH/AcOH/H₂O 4:1:1); ¹H NMR and ¹³C NMR in agreement with data of Zhao et al. (2018); ESI-HRMS *m/z* 256.1089 ([M+H]⁺, calcd for C₁₄H₁₄N₃O₂⁻ 256.1092).

5.4.6 Antifungal assay

Compounds **5.1-5.3** were tested in a 96-well microtiter plate assay against *Botrytis cinerea* Pers., *Septoria tritici* Desm., and *Phytophthora infestans* (Mont.) de Bary as described earlier (Otto et al., 2016b). The experiment was carried out in triplicates (*n* = 3), each comprising technical triplicates. For data analyses, GraphPad Prism version 8.0.2 (GraphPad Software, San Diego, CA, USA), SigmaPlot 14.0 (Systat Software, San Jose, CA, USA) and Microsoft Excel 2013 (Microsoft, Redmond, WA, USA) were used.

5.4.7 *In vitro* cell proliferation assay – anticancer activity

The prostate cancer cell line PC-3 (ATCC, Manassas, VA, USA) and the colon cancer cell line HT-29 (ATCC, Manassas, VA, USA) were cultured in RPMI 1640 medium supplemented with 2 mM L-glutamine and 10% heat-inactivated FCS. The cells were routinely grown in a humidified atmosphere with 5% CO₂ at 37°C to reach subconfluency (~ 70-80%) prior to subsequent usage or subculturing. The adherent cells were rinsed with PBS and detached by using trypsin/EDTA (0.05% in PBS) prior to cell passaging and seeding. RPMI 1640 basal medium, FCS, L-glutamine, PBS and trypsin/EDTA for cell culturing were purchased from Capricorn Scientific GmbH (Ebsdorfergrund, Germany). The culture flasks, multi-well plates and further cell culture plastics were purchased from TPP (Trasadingen, Switzerland) and Greiner Bio-One GmbH (Frickenhausen, Germany), respectively.

Antiproliferative and cytotoxic effects, respectively, of the compounds **5.1 – 5.3** were investigated by performing a fluorimetric resazurin-based cell viability assay (Sigma-Aldrich, Taufkirchen, Germany). For that purpose, prostate PC-3 and colorectal HT-29 cancer cells were seeded in low densities into 96-well plates (3,000 – 6,000 cells per well; seeding confluency ~ 10%), and were allowed to adhere for 24 h. Subsequently, the cells were treated for 48 h with compound concentrations up to 100 μM. For control measures, cells were treated in parallel with 0.5% DMSO (negative control, representing the final DMSO content of the highest concentrated test compound concentration) and 100 μM digitonin (positive control, for data normalization set to 0% cell viability), both in standard growth medium. As soon as the 48 h incubation was finished, the incubation medium was discarded, and cell were rinsed once with PBS. Resazurin solution in RPMI 1640 without phenol red and other supplements was prepared freshly prior to use, and added to the cells in a final resazurin concentration of 50 μM. Subsequently, the cells were incubated under standard growth conditions for further 2 hours. Finally, the conversion of resazurin to resorufin by viable, metabolically active cells was measured with 540 nm excitation and 590 nm

emission settings by using a SpectraMax M5 multiwell plate reader (Molecular Devices, San Jose, USA). Data were determined in biological quadruplicates, each with technical triplicates. For data analyses GraphPad Prism version 8.0.2 (GraphPad Software, San Diego, CA, USA) and Microsoft Excel 2013 (Microsoft, Redmond, WA, USA) were used.

5.4.8 Computational details

The X-ray structures of the human GluN1/GluN2A NMDA receptor in the glutamate/glycine-bound state at pH 7.8 (pdb-code 6IRA) (Zhang et al., 2018) and non-human (frog and mouse) trimeric NMDA receptor GluN1/GluN2A/GluN2B in complex with glycine, glutamate, the uncompetitive NMDA receptor antagonist MK-801 and a GluN2B-specific Fab, at pH 6.5 (pdb-code 5UOW) (Lu et al., 2017) were downloaded from the protein databank (Berman et al., 2000) and used for *in silico* docking analyses of compounds **5.1-5.3**.

All theoretical investigations were performed using the molecular modelling software package MOE (molecular operating environment) (2019). The X-ray structure was prepared for docking studies by adding the missing hydrogen atoms using the 3D-protonate module implemented in MOE. The structures of all three peptaibols were constructed in MOE and force field optimized with AMBER-14:EHT which is also implemented in MOE.

The putative active site of the enzyme is indicated by the co-crystallized inhibitor MK-801 (Figure 5.6, left site). By closer inspection of this site, an almost complete hydrophobic cleft formed by several helices could be detected, which led to the hypothesis that this could be a perfect binding site for the very hydrophobic peptaibols due to multiple Aib amino acid containing residues. Therefore, docking studies were performed defining this as a binding site. For each of the three peptaibols, ampullosporin A (**5.3**), F (**5.1**), and G (**5.2**), 30 poses were generated using the triangle matcher for fast placement, the London dG as fitness function with subsequent induced fit relaxation of the binding site. The best scored docking poses are displayed and discussed.

5.5 References

- Abdalla, M. A., McGaw, L. J., 2018. Natural cyclic peptides as an attractive modality for therapeutics: a mini review. *Molecules* 23, 2080.
- Ayers, S., Ehrmann, B. M., Adcock, A. F., Kroll, D. J., Carcache de Blanco, E. J., Shen, Q., Swanson, S. M., Falkinham, J. O., 3rd, Wani, M. C., Mitchell, S. M., Pearce, C. J., Oberlies, N. H., 2012. Peptaibols from two unidentified fungi of the order Hypocreales with cytotoxic, antibiotic, and anthelmintic activities. *J Pept Sci* 18, 500-510.
- Berek, I., Becker, A., Schroder, H., Hartl, A., Hollt, V., Grecksch, G., 2009. Ampullosporin A, a peptaibol from *Sepedonium ampullosporum* HKI-0053 with neuroleptic-like activity. *Behav Brain Res* 203, 232-239.
- Berman, H. M., Westbrook, J., Feng, Z., Gilliland, G., Bhat, T. N., Weissig, H., Shindyalov, I. N., Bourne, P. E., 2000. The protein data bank. *Nucleic Acids Res* 28, 235-242.

- Bovio, E., Garzoli, L., Poli, A., Lukanini, A., Villa, P., Musumeci, R., McCormack, G. P., Cocuzza, C. E., Gribaudo, G., Mehiri, M., Varese, G. C., 2019. Marine fungi from the sponge *Grantia compressa*: biodiversity, chemodiversity, and biotechnological potential. *Mar Drugs* 17, 220.
- Caballero, E., Avendaño, C., Menéndez, J. C., 1998. Stereochemical issues related to the synthesis and reactivity of pyrazino[2',1'-5,1]pyrrolo[2,3-b]indole-1,4-diones. *Tetrahedron: Asymmetry* 9, 967–981.
- Carroux, A., Van Bohemen, A. I., Roullier, C., Robiou du Pont, T., Vansteelandt, M., Bondon, A., Zalouk-Vergnoux, A., Pouchus, Y. F., Ruiz, N., 2013. Unprecedented 17-residue peptaibiotics produced by marine-derived *Trichoderma atroviride*. *Chem Biodivers* 10, 772-786.
- Closse, A., Hauser, D., 1973. Isolierung und Konstitutionsermittlung von Chrysodin. *Hel Chim Acta* 56, 2694-2698.
- Degenkolb, T., Brückner, H., 2008. Peptaibiotics: towards a myriad of bioactive peptides containing α -dialkylamino acids? *Chem Biodivers* 5, 1817-1843.
- Divekar, P. V., Raistrick, H., Dobson, T. A., Vining, L. C., 1965. Studies in the biochemistry of microorganisms part 117. Sepedonin, a tropolone metabolite of *Sepedonium chrysospermum* Fries. *Can J Chem* 43, 1835-1848.
- Divekar, P. V., Vining, L. C., 1964. Reaction of anhydrosepedonin with alkali synthesis of a degradation product and some related dimethylhydroxybenzoic acids. *Can J Chem* 42, 63-68.
- Dornberger, K., Ihn, W., Ritzau, M., Grafe, U., Schlegel, B., Fleck, W. F., Metzger, J. W., 1995. Chrysospermins, new peptaibol antibiotics from *Apiocrea chrysosperma* Ap101. *J Antibiot (Tokyo)* 48, 977-989.
- Du, L., Risinger, A. L., Mitchell, C. A., You, J., Stamps, B. W., Pan, N., King, J. B., Bopassa, J. C., Judge, S. I. V., Yang, Z., Stevenson, B. S., Cichewicz, R. H., 2017. Unique amalgamation of primary and secondary structural elements transform peptaibols into potent bioactive cell-penetrating peptides. *Proc Natl Acad Sci USA* 114, E8957-E8966.
- Fragiadaki, I., Katogiritis, A., Calogeropoulou, T., Bruckner, H., Scoulica, E., 2018. Synergistic combination of alkylphosphocholines with peptaibols in targeting *Leishmania infantum* in vitro. *Int J Parasitol Drugs Drug Resist* 8, 194-202.
- Hulsmann, H., Heinze, S., Ritzau, M., Schlegel, B., Grafe, U., 1998. Isolation and structure of peptaibolin, a new peptaibol from *Sepedonium* strains. *J Antibiot (Tokyo)* 51, 1055-1058.
- Iijima, M., Amemiya, M., Sawa, R., Kubota, Y., Kunisada, T., Momose, I., Kawada, M., Shibasaki, M., 2017. Acremopeptin, a new peptaibol from *Acremonium* sp. PF1450. *J Antibiot (Tokyo)* 70, 791-794.
- Jiao, W. H., Khalil, Z., Dewapriya, P., Salim, A. A., Lin, H. W., Capon, R. J., 2018. Trichodermides A-E: new peptaibols isolated from the Australian termite nest-derived fungus *Trichoderma virens* CMB-TN16. *J Nat Prod* 81, 976-984.
- Kai, K., Mine, K., Akiyama, K., Ohki, S., Hayashi, H., 2018. Anti-plant viral activity of peptaibols, trichorzins HA II, HA V, and HA VI, isolated from *Trichoderma harzianum* HK-61. *J Pestic Sci* 43, 283-286.
- Katoch, M., Singh, D., Kapoor, K. K., Vishwakarma, R. A., 2019. *Trichoderma lixii* (IIM-B4), an endophyte of *Bacopa monnieri* L. producing peptaibols. *BMC Microbiol* 19, 98.
- Kim, C. K., Krumpke, L. R. H., Smith, E., Henrich, C. J., Brownell, I., Wendt, K. L., Cichewicz, R. H., O'Keefe, B. R., Gustafson, K. R., 2021. Roseabol A, a new peptaibol from the fungus *Clonostachys rosea*. *Molecules* 26, 3594.

- Kimonyo, A., Bruckner, H., 2013. Sequences of metanicins, 20-residue peptaibols from the ascomycetous fungus CBS 597.80. *Chem Biodivers* 10, 813-826.
- Kronen, M., Kleinwachter, P., Schlegel, B., Hartl, A., Grafe, U., 2001. Ampullosporines B, C, D, E1, E2, E3 and E4 from *Sepedonium ampullosporum* HKI-0053: structures and biological activities. *J Antibiot* (Tokyo) 54, 175-178.
- Laub, A., Lam, Y. T. H., Mendez, Y., Vidal, A. V., Porzel, A., Schmidt, J., Wessjohann, L. A., Westermann, B., Arnold, N., Identification and total synthesis of two new cyclic pentapeptides from *Sepedonium microspermum* Besl. Manuscript in submission.
- Li, L., Li, D., Luan, Y., Gu, Q., Zhu, T., 2012. Cytotoxic metabolites from the antarctic psychrophilic fungus *Oidiodendron truncatum*. *J Nat Prod* 75, 920-927.
- Liu, D., Lin, H., Proksch, P., Tang, X., Shao, Z., Lin, W., 2015. Microbacterins A and B, new peptaibols from the deep sea actinomycete *Microbacterium sediminis* sp. nov. YLB-01(T). *Org Lett* 17, 1220-1223.
- Lu, W., Du, J., Goehring, A., Gouaux, E., 2017. Cryo-EM structures of the triheteromeric NMDA receptor and its allosteric modulation. *Science* 355, 1282.
- Marik, T., Tyagi, C., Racic, G., Rakk, D., Szekeres, A., Vagvolgyi, C., Kredics, L., 2018. New 19-Residue Peptaibols from *Trichoderma* clade Viride. *Microorganisms* 6, 85.
- Milov, A. D., Tsvetkov, Y. D., Raap, J., De Zotti, M., Formaggio, F., Toniolo, C., 2016. Conformation, self-aggregation, and membrane interaction of peptaibols as studied by pulsed electron double resonance spectroscopy. *Biopolymers* 106, 6-24.
- Mitova, M. I., Murphy, A. C., Lang, G., Blunt, J. W., Cole, A. L., Ellis, G., Munro, M. H., 2008. Evolving trends in the dereplication of natural product extracts. 2. The isolation of chrysaibol, an antibiotic peptaibol from a New Zealand sample of the mycoparasitic fungus *Sepedonium chrysospermum*. *J Nat Prod* 71, 1600-1603.
- Mitova, M. I., Stuart, B. G., Cao, G. H., Blunt, J. W., Cole, A. L., Munro, M. H., 2006. Chrysosporide, a cyclic pentapeptide from a New Zealand sample of the fungus *Sepedonium chrysospermum*. *J Nat Prod* 69, 1481-1484.
- Mohamed-Benkada, M., Francois Pouchus, Y., Verite, P., Pagniez, F., Caroff, N., Ruiz, N., 2016. Identification and biological activities of long-chain peptaibols produced by a marine-derived strain of *Trichoderma longibrachiatum*. *Chem Biodivers* 13, 521-530.
- Momose, I., Onodera, T., Doi, H., Adachi, H., Iijima, M., Yamazaki, Y., Sawa, R., Kubota, Y., Igarashi, M., Kawada, M., 2019. Leucinostatin Y: a peptaibiotic produced by the entomoparasitic fungus *Purpureocillium lilacinum* 40-H-28. *J Nat Prod* 82, 1120-1127.
- Neuhof, T., Berg, A., Besl, H., Schwecke, T., Dieckmann, R., von Dohren, H., 2007. Peptaibol production by *Sepedonium* strains parasitizing Boletales. *Chem Biodivers* 4, 1103-1115.
- Neumann, N. K., Stoppacher, N., Zeilinger, S., Degenkolb, T., Bruckner, H., Schuhmacher, R., 2015. The peptaibiotics database - a comprehensive online resource. *Chem Biodivers* 12, 743-751.
- Nguyen, H.-H., Imhof, D., Kronen, M., Schlegel, B., Ha, A., Gera, L., Reissmann, S., 2002. Synthesis and biological evaluation of analogues of the peptaibol ampullosporin A. *J Med Chem* 45, 2781-2787.
- Ojo, O. S., Nardone, B., Musolino, S. F., Neal, A. R., Wilson, L., Lebl, T., Slawin, A. M. Z., Cordes, D. B., Taylor, J. E., Naismith, J. H., Smith, A. D., Westwood, N. J., 2018. Synthesis of the natural product descurainolide and cyclic peptides from lignin-derived aromatics. *Org Biomol Chem* 16, 266-273.

- Otto, A., Laub, A., Haid, M., Porzel, A., Schmidt, J., Wessjohann, L., Arnold, N., 2016a. Tulasporins A-D, 19-residue peptaibols from the mycoparasitic fungus *Sepedonium tulasneanum*. *Nat Prod Commun* 11, 1821-1824.
- Otto, A., Laub, A., Porzel, A., Schmidt, J., Wessjohann, L., Westermann, B., Arnold, N., 2015. Isolation and total synthesis of albupeptins A-D: 11-residue peptaibols from the fungus *Gliocladium album*. *Eur J Org Chem* 2015, 7449-7459.
- Otto, A., Laub, A., Wendt, L., Porzel, A., Schmidt, J., Palfner, G., Becerra, J., Kruger, D., Stadler, M., Wessjohann, L., Westermann, B., Arnold, N., 2016b. Chilenopeptins A and B, peptaibols from the Chilean *Sepedonium* aff. *chalcipori* KSH 883. *J Nat Prod* 79, 929-938.
- Panizel, I., Yarden, O., Ilan, M., Carmeli, S., 2013. Eight new peptaibols from sponge-associated *Trichoderma atroviride*. *Mar Drugs* 11, 4937-4960.
- Quang, D. N., Schmidt, J., Porzel, A., Wessjohann, L., Haid, M., Arnold, N., 2010. Ampullosine, a new isoquinoline alkaloid from *Sepedonium ampullosporum* (Ascomycetes). *Nat Prod Commun* 5, 869-872.
- Rawa, M. S. A., Nogawa, T., Okano, A., Futamura, Y., Nakamura, T., Wahab, H. A., Osada, H., 2021a. A new peptaibol, RK-026A, from the soil fungus *Trichoderma* sp. RK10-F026 by culture condition-dependent screening. *Biosci Biotechnol Biochem* 85, 69-76.
- Rawa, M. S. A., Nogawa, T., Okano, A., Futamura, Y., Wahab, H. A., Osada, H., 2021b. Zealpeptaibolin, an 11-mer cytotoxic peptaibol group with 3 Aib-Pro motifs isolated from *Trichoderma* sp. RK10-F026. *J Antibiot* (Tokyo) 74, 485-495.
- Ritzau, M., Heinze, S., Dornberger, K., Berg, A., Fleck, W., Schlegel, B., Hartl, A., Grafe, U., 1997. Ampullosporin, a new peptaibol-type antibiotic from *Sepedonium ampullosporum* HKI-0053 with neuroleptic activity in mice. *J Antibiot* (Tokyo) 50, 722-728.
- Rivera-Chavez, J., Raja, H. A., Graf, T. N., Gallagher, J. M., Metri, P., Xue, D., Pearce, C. J., Oberlies, N. H., 2017. Prelamethicin F50 and related peptaibols from *Trichoderma arundinaceum*: Validation of their authenticity via in situ chemical analysis. *RSC Adv* 7, 45733-45751.
- Sahr, T. A., H.; Besl, H.; Fischer, M., 1999. AmericaInfrageneric classification of the boleticolous genus *Sepedonium*: species delimitation and phylogenetic relationships. *Mycologia* 91, 935-943.
- Shi, W. L., Chen, X. L., Wang, L. X., Gong, Z. T., Li, S., Li, C. L., Xie, B. B., Zhang, W., Shi, M., Li, C., Zhang, Y. Z., Song, X. Y., 2016. Cellular and molecular insight into the inhibition of primary root growth of *Arabidopsis* induced by peptaibols, a class of linear peptide antibiotics mainly produced by *Trichoderma* spp. *J Exp Bot* 67, 2191-2205.
- Shibata, S., Shoji, J., Ohta, A., Watanabe, M., 1957. Metabolic products of fungi. XI. Some observation on the occurrence of skyrin and rugulosin in mold metabolites, with a reference to structural relationship between Penicillipsin and Skyrin. *Pharm Bull* 5, 380-382.
- Sica, V. P., Rees, E. R., Raja, H. A., Rivera-Chavez, J., Burdette, J. E., Pearce, C. J., Oberlies, N. H., 2017. In situ mass spectrometry monitoring of fungal cultures led to the identification of four peptaibols with a rare threonine residue. *Phytochemistry* 143, 45-53.
- Singh, V. P., Yedukondalu, N., Sharma, V., Kushwaha, M., Sharma, R., Chaubey, A., Kumar, A., Singh, D., Vishwakarma, R. A., 2018. Lipovelutibols A-D: cytotoxic lipopeptaibols from the himalayan cold habitat fungus *Trichoderma velutinum*. *J Nat Prod* 81, 219-226.
- Speckbacher, V., Zeilinger, S., 2018. Secondary Metabolites of Mycoparasitic Fungi. In: Vijayakumar, R., Raja, S. (Eds.), Secondary metabolites-sources and applications. Intechopen, London, UK, pp. 37-55.

- Stadler, M. S., S.; Müller, H.; Henkel, T.; Lagojda, A.; Kleymann, G., 2001. New antiviral peptaibols from the mycoparasitic fungus *Sepedonium microspermum*. Irseer Naturstofftage der DECHEMA, Germany.
- Sun, S., Dai, X., Sun, J., Bu, X., Weng, C., Li, H., Zhu, H., 2016. A diketopiperazine factor from *Rheinheimera aquimaris* QSI02 exhibits anti-quorum sensing activity. *Sci Rep* 6, 39637.
- Touati, I., Ruiz, N., Thomas, O., Druzhinina, I. S., Atanasova, L., Tabbene, O., Elkahoui, S., Benzekri, R., Bouslama, L., Pouchus, Y. F., Limam, F., 2018. Hyporientalin A, an anti-Candida peptaibol from a marine *Trichoderma orientale*. *World J Microbiol Biotechnol* 34, 98.
- Tullberg, M., Grøtli, M., Luthman, K., 2006. Efficient synthesis of 2,5-diketopiperazines using microwave assisted heating. *Tetrahedron* 62, 7484-7491.
- v2019.0101, M. O. E., 2019. Molecular Operating Environment v2019.0101. Chemical Computing Group Inc., Montreal, QC, Canada.
- van Bohemen, A. I., Ruiz, N., Zalouk-Vergnoux, A., Michaud, A., Robiou du Pont, T., Druzhinina, I., Atanasova, L., Prado, S., Bodo, B., Meslet-Cladiere, L., Cochereau, B., Bastide, F., Maslard, C., Marchi, M., Guillemette, T., Pouchus, Y. F., 2021. Pentadecaibins I-V: 15-residue peptaibols produced by a marine-derived *Trichoderma* sp. of the *Harzianum* clade. *J Nat Prod* 84, 1271-1282.
- Wang, F. Z., Huang, Z., Shi, X. F., Chen, Y. C., Zhang, W. M., Tian, X. P., Li, J., Zhang, S., 2012. Cytotoxic indole diketopiperazines from the deep sea-derived fungus *Acrostalagmus luteoalbus* SCSIO F457. *Bioorg Med Chem Lett* 22, 7265-7267.
- Wu, G., Dentinger, B. T. M., Nielson, J. R., Peterson, R. T., Winter, J. M., 2021. Emerimicins V-X, 15-residue peptaibols discovered from an *Acremonium* sp. through integrated genomic and chemical approaches. *J Nat Prod* 84, 1113-1126.
- Zhang, J. B., Chang, S., Xu, P., Miao, M., Wu, H., Zhang, Y., Zhang, T., Wang, H., Zhang, J., Xie, C., Song, N., Luo, C., Zhang, X., Zhu, S., 2018. Structural basis of the proton sensitivity of human GluN1-GluN2A NMDA receptors. *Cell Rep* 25, 3582-3590
- Zhang, S. H., Yang, J., Ma, H., Yang, Y., Zhou, G. F., Zhao, X., Xu, R., Nie, D., Zhang, G. G., Shan, J. J., Cui, C. B., Li, C. W., 2021. Longibramides A-E, peptaibols isolated from a mushroom derived fungus *Trichoderma longibrachiatum* Rifai DMG-3-1-1. *Chem Biodivers* 18.
- Zhao, D., Cao, F., Guo, X.-J., Zhang, Y.-R., Kang, Z., Zhu, H.-J., 2018. Antibacterial indole alkaloids and anthraquinones from a sewage-derived fungus *Eurotium* sp. *Chem Nat Compd* 54, 399-401.

5.6 Supplementary data

Supplementary data to this article (ESI-HRMS², NMR data, as well as CD spectra of natural and synthetic **5.1-5.2**; UV spectra of natural **5.1-5.2**; NMR data of **5.3-5.5**; ESI-HRMS and 1D NMR data of **5.6-5.7**; ESI-HRMSⁿ data of **5.1-5.5**; antifungal activity of **5.1-5.3**; docking arrangements of **5.2**) can be found online at <https://www.mdpi.com/article/10.3390/ijms222312718/s1>.

Chapter 6

General discussion

Cortinarius is one of the most species-rich genera in Agaricales, with more than 5,600 epithets recorded worldwide, whereas 58 epithets were named for genus *Sepedonium* to date (<http://www.indexfungorum.org>). However, according to our statistical analysis using the two global citation databases Scifinderⁿ (<https://scifinder-n.cas.org>) and Web of Science (<https://www.webofscience.com>), it turns out that the two genera have not yet been well studied in contrast to their number of epithets (Table 6.1). A maximum of 904 publications refer to *Cortinarius* and 196 publications mention *Sepedonium*. Of these, less than 15 % deal with secondary metabolites from genus *Cortinarius*, and less than 35% are chemical investigations in genus *Sepedonium*. Although being chemically untapped, both genera have been proven as producers of structurally intriguing compounds that display a variety of biological activities. Thus, the main objective of our research work was to isolate and identify new fungal natural products, in order to find potential lead compounds for drug development and agricultural fungicides. Therefore, the present thesis describes studies on fruiting bodies of basidiomycete genus *Cortinarius* and cultures of the ascomycete genus *Sepedonium* in a polythetic approach based on chemical, molecular and biological data.

Table 6.1. Number of publications about *Cortinarius* and *Sepedonium* species found in public databases (last access 13.04.2022).

Context	Scifinder ⁿ	Web of Science
<i>Cortinarius</i>	904 (100%)	740 (100%)
Chemistry-related	116 ^a (13%)	87 ^{a'} (12%)
<i>Sepedonium</i>	196 (100%)	74 (100%)
Chemistry-related	54 ^b (28%)	25 ^{b'} (34%)

^a Selected context: new natural product; mycotoxins; 2,2'-dipyridyl; pigments, biological.

^{a'} Selected context: chemistry multidisciplinary; chemistry medicinal; chemistry organic; chemistry applied; chemistry analytical; spectroscopy; engineering chemical.

^b Selected context: fungicides; antibiotics; magnetic resonance spectroscopy; peptides; anti-bacterial agents; antitumor agents; peptaibols; new natural products; molecular structure, natural product; spectrum analysis; steroids.

^{b'} Selected context: chemistry multidisciplinary; chemistry medicinal; chemistry organic; chemistry applied; chemistry analytical; engineering chemical; neurosciences.

Two species of genus *Cortinarius* were studied under various aspects like chemistry, biosynthesis, phylogeny, and biological activity (Chapter 3 and 4). The first investigation on the Chilean mushroom *Cortinarius pyromyxa* afforded four new diterpenoid pigments, named

pyromyxones A-D (**3.1-3.4**) (Chapter 3). The pyromyxones A-D (**3.1-3.4**) do not only possess an undescribed *nor*-guanacastane skeleton, but also represent the first occurrence of diterpenoids in the genus *Cortinarius*. The pyromyxones A-D (**3.1-3.4**) belong to a group of almost 60 guanacastane diterpenoids (other name: neodolastane diterpenoids), which also include guanacastepenes, heptemerones, plicatilisins, radianspenes, dahlianes, 2,15-epoxy-5,13-dihydroxyneodolast-3-en-14-one and sphaerostanol (Figure 6.1.) (Markovic et al., 2015; Wu et al., 2016; Yin et al., 2014; Zhang and Feng, 2022).

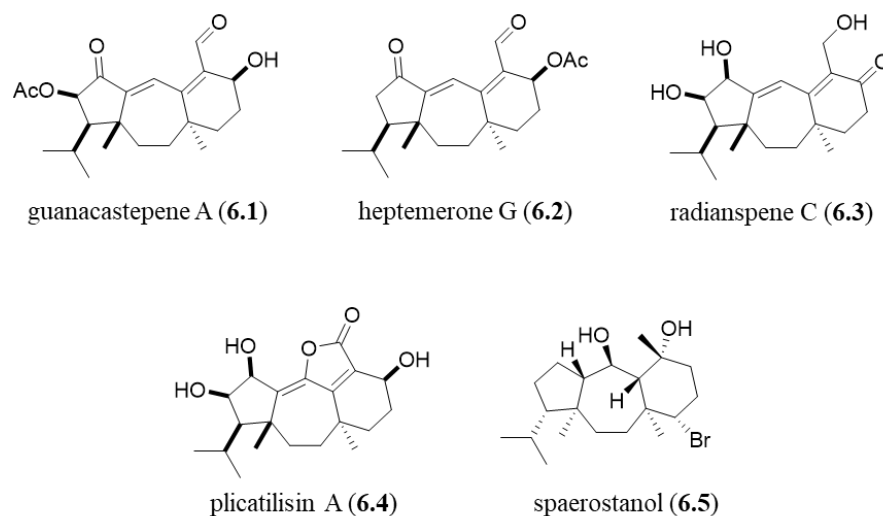


Figure 6.1. Selected structures of guanacastane diterpenoids from natural sources.

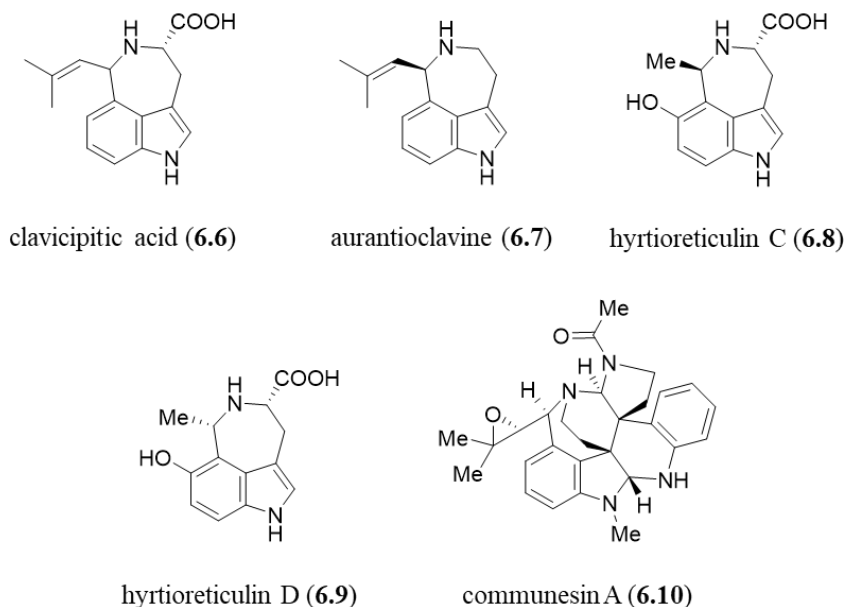


Figure 6.2. Selected structures of azepino[5,4,3-*cd*]indole alkaloids from natural sources.

From fruiting bodies of *Cortinarius purpurascens* Fr. (Cortinariaceae), three new azepino[5,4,3-*cd*]indole alkaloids, named purpurascenines A-C (**4.1-4.3**), together with the new-to-nature 7-

hydroxytryptophan (**4.4**) and the known compounds, adenosine (**4.5**) and riboflavin (**4.6**), were isolated (Chapter 4). Up to now, azepino[5,4,3-*cd*]indole alkaloids is a small group of 30 natural products, roughly equally contributed by fungal cultures (i.e. *Claviceps* and *Penicillium*), plants (i.e. *Psychotria*, *Evodia* and *Cimifuga*) as well as the marine sponge *Hyrtios* spp. (Figure 6.2) (Klein-Junior et al., 2020; Lindsay et al., 2018). Thus, the isolated purpurascenines A-C (**4.1-4.3**) are the first azepinoindole alkaloids from fungal basidiocarps.

A crucial purpose of natural product research is to understand the biosynthetic origin of the targeted compounds. The pyromyxones A-D (**3.1-3.4**) possess a *nor*-guanacastane skeleton that is related to the guanacastane skeleton, and hence also to the dolabellane or dolastane skeletons. The biosynthesis of those guanacastane, dolabellane or dolastane diterpenoids was not studied yet, however, it was proposed by Hiersemann and Helmboldt (2005) as a series of enzyme catalyzed ring closures and Wagner-Meerwein migrations from geranylgeranyl pyrophosphate (GGPP) (Hiersemann and Helmboldt, 2005). GGPP is the common precursor of diterpenoids, which could be generated from either dimethylallyl pyrophosphate (DMAPP) or farnesyl pyrophosphate (FPP) together with isopentenyl pyrophosphate (IPP) (Zhang and Feng, 2022). Based on this knowledge, a biosynthetic route could be also presumed for pyromyxones A-D (**3.1-3.4**) (Figure 6.3).

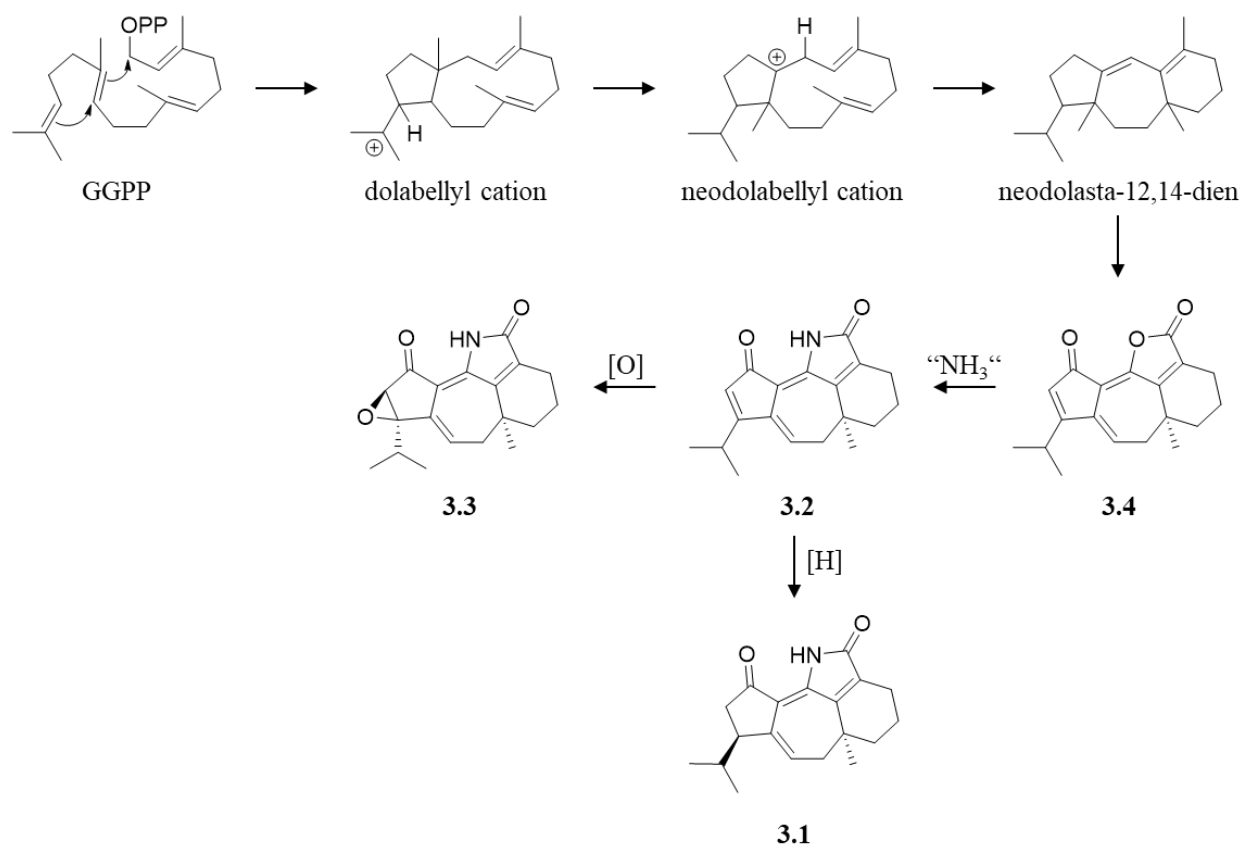


Figure 6.3. Proposed biosynthesis of pyromyxones A-D (**3.1-3.4**), adapted from Hiersemann et al. (2005).

This may be a suggestion to study the biosynthesis of the pyromyxones A-D (**3.1-3.4**) by feeding ^{13}C -labeled samples of either GGPP or its precursors to the fruiting bodies of *C. pyromyxa* in the field. In addition, the conversion of the γ -lactone ring (in **3.4**) to the γ -lactam ring (in **3.1-3.3**) may be verified by feeding ^{15}N -labeled samples (e.g. $^{15}\text{NH}_3$ or ^{15}N -amino acids) also to the basidiocarps of *C. pyromyxa*. To the best of our knowledge, the biosynthesis of γ -lactams is yet to be published (Caruano et al., 2016); however, such conversion was successfully obtained under *in vitro* conditions by using NH_3 or amines even in an one-step reaction at room temperature (Caruano et al., 2016; Rankic et al., 2017).

Such isotopic labeling experiments have been successfully broadened human knowledge of biosynthesis of secondary metabolites (Rinkel and Dickschat, 2015). In natural product chemistry, the use of stable, i.e. non-radioactive, isotopes such as ^{13}C and ^2H has become favored over the radioactive nuclei like ^{14}C and ^3H thanks to the development of suitable NMR and MS methods. Furthermore, the labelling experiments were performed on fungal fruiting bodies including *Cortinarius* species (e.g. Elsworth et al., 1999; Müller et al., 2004; Spiteller et al., 2000), leading to the proposal of plausible biosynthetic pathways of different compound classes. The efficiency of feeding experiments to study fungal secondary metabolite biosynthesis was thus clearly demonstrated.

Moreover, among the known 30 natural azepino[5,4,3-*cd*]indole alkaloids, only fungal culture-derived products were investigated into their biosynthesis by enzyme-based experiments (Lindsay et al., 2018). Therefore, a highlight of the present thesis is the *in vivo* study towards the biosynthesis of purpurascenine A (**4.1**) using ^{13}C labeled precursors. To study the biosynthetic pathway of purpurascenine A (**4.1**), feeding experiments using separately [3- ^{13}C]-pyruvate, [3- ^{13}C]-alanine, and [2- ^{13}C]-acetate were performed on fruiting bodies of *C. purpurascens*. Tryptophan was proven as a biogenetic precursor of the azepino[5,4,3-*cd*]indole alkaloids named communesins, e.g. communesin A (**6.10**), in *Penicillium expansum* (Lin et al., 2015; Wigley et al., 2006; Wigley et al., 2008; Xu et al., 2014), and hence 7-hydroxytryptophan (**4.4**), an isolated compound from *C. purpurascens*, was speculated to be involved in the biosynthesis of purpurascenines (**4.1-4.3**). Furthermore, the results of our *in vivo* feeding experiments reveals the participation of pyruvate in biosynthetic pathway of **4.1**. Thus, the biosynthesis of purpurascenine A (**4.1**) was proposed to involve pyruvic acid and 7-hydroxytryptophan (**4.4**) in a Pictet-Spengler reaction condensation enzymatically catalyzed by Pictet-Spenglerase, which had been evidenced in different organisms in nature (Naoi et al., 2002; Stockigt et al., 2011). Moreover, considering pyruvic acid as “ α -ketoalanine”, “ α -ketoglycine” (glyoxilic acid), and “ α -ketoleucine” (4-methyl-2-oxopentanoic acid) were hypothesized as the precursors for purpurascenines B (**4.2**) and C (**4.3**), respectively. Consequently, a biosynthesis of purpurascenines (**4.1-4.3**) could be proposed (Figure 6.4).

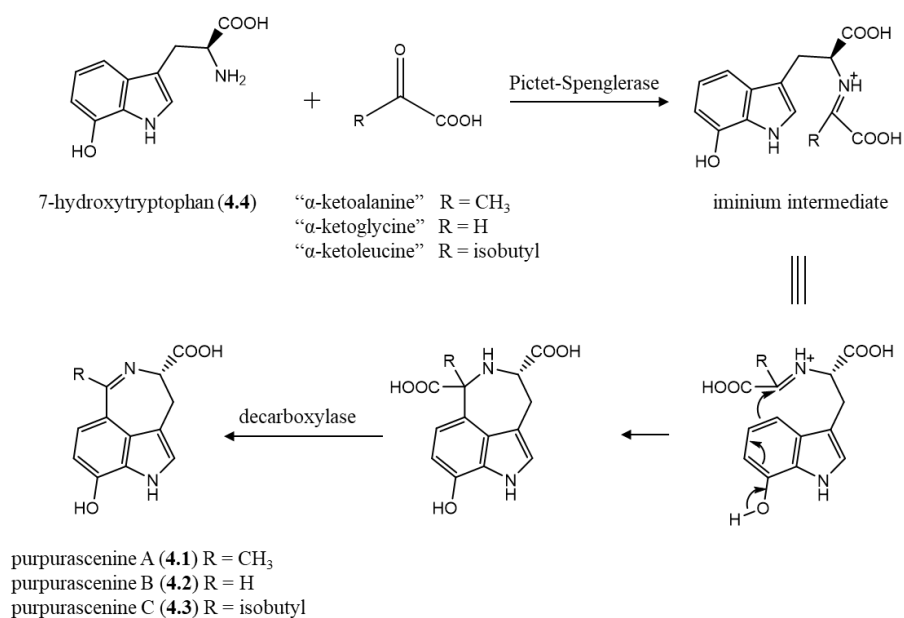


Figure 6.4. Proposed biosynthesis of purpurascenines A-C (**4.1-4.3**), considering the proposal of Yamanokuchi et al. (2012) and Naoi et al. (2002).

Furthermore, the ultimate goal of our research was to evaluate the potential of isolated compounds for pharmaceutical and agricultural use. Thus, selected pyromyxones and purpurascenines were subjected to biological studies. Pyromyxones A (**3.1**), B (**3.2**) and D (**3.4**) were evaluated for their antifungal and antibacterial activity, showing only weak inhibitory effects against the organisms tested (Chapter 3). The weak antibacterial activities were also reported for other close analogues like guanacastepene A (**6.1**) and heptemerones, e.g. heptemerone G (**6.2**) (Kettering et al., 2005; Markovic et al., 2015; Singh et al., 2000). Nonetheless, Kettering and coworkers observed that the antifungal activities of heptemerones depend largely on the assay medium (Kettering et al., 2005). In water, the inhibition of those heptemerones occurred at 5 to 10 fold lower concentration than in medium, showing their potent inhibition of fungal germination in water. Furthermore, the pyromyxone-related analogues, namely radianspenes, plicatilisins, heptemerones and sphaerostanol were also evaluated for their cytotoxicities against different tumor cell lines (Markovic et al., 2015). Among them, radianspene C (**6.3**) exhibited the most significant effect with an IC₅₀ of 0.91 μM against the human breast carcinoma MDA-MB-435 cell line (Ou et al., 2012). Therefore, it would be more than worse to perform comprehensive biological assays or studies concerning structure-activity relationships on the pyromyxones as well as other guanacastane diterpenoids.

Additionally, purpurascenine A (**4.1**) was examined for its activation with a G protein-coupled receptor subtype, namely 5-HT_{2A} (Chapter 4). The structure of **4.1** is very similar to 5-hydroxytryptamine (5-HT; serotonin) and other known 5-HT_{2A} receptor modulators, e.g. agonists like ibogaine or tabernanthine (Zieba et al., 2021) or allosteric modulators like glaucine (Fasciani et al., 2020; Heng et al., 2019). Moreover, the possible interaction of purpurascenine A (**4.1**) with

the 5-HT_{2A} serotonin receptor was also suggested by our preliminary docking studies. Thus, a new functional reporter gene assay was established, which demonstrated that: (i) **4.1** did not permit substantial agonistic 5-HT_{2A} activation, (ii) **4.1** (at 100 µM) reduced the maximal 5-HT dependent 5-HT_{2A} activation from 100% down to 50%, with only minor effect on the EC₅₀ of 5-HT, and (iii) **4.1** seemed to inhibit putative constitutive 5-HT_{2A} activity. In fact, constitutive activity of the 5-HT_{2A} receptor is so far described to be relatively weak *in vitro*. However, it was observed that some experimental settings, e.g. overexpression of G-proteins or some methodologies for receptor amplification, can cause elevated constitutive activity of 5-HT_{2A} receptors (Berg et al., 2005; De Deurwaerdère et al., 2018). A future perspective would thus be to investigate the effects of purpurascenine A (**4.1**) and its derivatives on 5-HT_{2A} and other 5-HT receptor subtypes in more detail.

Besides the chemical, biosynthetic and biological investigations, a preliminary molecular biological study was also carried out that reveals the monotypic position of *C. pyromyxa* in subgenus Myxacium, genus *Cortinarius*, which is also demonstrated by the chemical pigments. Accordingly, our studies also demonstrate the integration of morphological, molecular and chemical data as a powerful tool to estimate phylogenetic relationships in fungal taxa, especially in such phylogenetically complicated genus like *Cortinarius*.

The further part of the present thesis was to study the chemical constituents of the fungicolous species *Sepedonium ampullosporum* Damon (KSH 534), which yielded in total 7 natural products (Chapter 5). Beside the known peptaibols, ampullosporin A (**5.3**) and peptaibolin (**5.4**), two new 15-residue peptaibols, named ampullosporins F (**5.1**) and G (**5.2**), were isolated from semi-solid cultures of *S. ampullosporum*. Both ampullosporin F (**5.1**) and G (**5.2**) bear in their structures a δ -methyl ester of glutamic acid residue, which is rarely recognized in natural peptaibols, with only five examples of the over 1,450 peptaibiotics reported in literature so far (Chapter 5). Consequently, they represent the third report of glutamic acid methyl ester containing peptaibols isolated from natural sources, and the first from the whole genus *Sepedonium*. The small amounts of compounds **5.1** - **5.2** proved a challenge of isolation works, and hence, probably led to the rare observation of this compound class. In contrast to peptaibols – the characteristic components of *Sepedonium* spp. – cyclopeptides were hardly recognized from this genus. The known *cyclo*(Trp-Ser) (**5.6**) and *cyclo*(Trp-Ala) (**5.7**), isolated from *S. ampullosporum*, record only the second occurrence of this compound class in the genus *Sepedonium* after chrysosporide (**5.5**), isolated from *S. chrysospermum* and *S. ampullosporum*. The biosynthesis of non-ribosomal peptides like peptaibols (e.g. **5.1-5.4**) and cyclic peptides (e.g. **5.5-5.7**) has been proven to involve the giant multi-domain enzymes so-called non-ribosomal peptide synthetases (NPRS), which produce the peptides in one by one steps (Chapter 2).

In natural product research, synthesis plays an important role as it does not only support the identification and biological studies of compounds isolated in minor amounts, but also improve the utilization of natural products (e.g. in pharmacy and agriculture) by derivatization. Therefore, the synthesis of the ampullosporins F (**5.1**) and G (**5.2**) in solid phase was accomplished (Chapter 5).

The ESI-HRMSⁿ, 1D NMR, and CD spectra of the synthetic peptaibols **5.1** and **5.2** were consistent with those of the natural ampullosporin F (**5.1**) and ampullosporin G (**5.2**), consequently establishing the L-configuration for all chiral amino acids in the natural peptaibols.

Besides the chemical and synthetic studies, it would be also worthwhile to determine the biological effects of the isolated compounds. The ampullosporins (**5.1-5.3**) exhibited strong antifungal activity against *Botrytis cinerea* and *Phytophthora infestans*, but were inactive against *Septoria tritici*. These results are in agreement with the reports of Otto and coworkers that the anti-phytopathogenic activity of peptaibols may lie in their chain length (Otto et al., 2016a; Otto et al., 2015; Otto et al., 2016b). Among the twelve tested peptaibols, the most potent anti-phytopathogenic effects were recorded for the long-chain (19-residue) peptaibols tulasporins A-D (**2.92-2.95**), followed by significant activity of the medium-chain (15-residue) chilenopeptins A-B (**2.75-2.76**) and tylopeptins A-B (**2.77-2.78**). However, the short-chain (11-residue) albupeptins A-D (**6.11-6.14**; Table A2, Appendix) exhibited only modest antifungal activity. In fact, many peptaibols, e.g. the long-chain (20-residue) alamethicin (**2.97**), were reported to have antimicrobial activities (e.g. Chapter 2 and 5). Interestingly, the α -helical molecules of alamethicin (**2.97**) are 34 Å in length, which is sufficient to span lipid bilayers, and hence able to form channels in various lipid molecules (Chugh and Wallace, 2001). The mechanism behind amphipathic channel formation of alamethicin (**2.97**) was proven to follow the “barrel-stave model” (Chapter 2). The shorter peptaibols may have similar membrane activity, however, they can not span the membrane in the same way like the longer ones. Indeed, it was shown that the medium-chain ampullosporin A (**5.3**) is not strongly anchored to the membrane surfaces as found for alamethicin (**2.97**), so the barrel-stave pores are likely not formed by the medium chain peptaibol (Bortolus et al., 2016). Instead, two other mechanisms were proposed for the medium- and short-chain peptaibols. On the one hand, within the bilayer they could form end-to-end bundles, effectively doubling their length perpendicular to the bilayer. On the other hand, those peptaibols could also form membrane-associated aggregates, surface-associated “carpets” membrane spanning circular channels or act via a detergent-like mechanism (Fuente-Núñez et al., 2013).

Our cell viability assays using human prostate (PC-3) and colorectal (HT-29) cancer cells confirmed potent anticancer activities of ampullosporins (**5.1-5.3**). It was observed that ampullosporins F (**5.1**) and G (**5.2**) exhibited antifungal and cytotoxic effects at roughly twofold lower concentrations than that of ampullosporin A (**5.3**) despite their very similar structures. The new peptaibols **5.1-5.2** only differ from the known **5.3** one by replacing either Gln¹¹ or Gln⁷ by GluOMe. Thus, it was proposed that this slight modification either changes the peptaibol spatial structures or increases the lipophilicity of **5.1-5.2**, and hence enhances the membrane permeability as well as their biological effects.

Peptaibols are smaller but share a number of common features with larger protein channels (e.g. potassium and sodium channels) including: *i*) the nature of their lumen, formed from carbonyl groups of the polypeptide backbone or polar side chains; *ii*) their ability to form pores in correct sizes for specific ion transport; and *iii*) the occurrence of aromatic amino acids in their sequences

that can stabilize the structures within membranes (Chugh and Wallace, 2001). These features together with their exponentially risen number of natural peptaibol sequences make the “small” compounds particularly good model systems for computational simulations of ion binding and translocations, and eventually shed more light into the complex processes involved in transport across membranes. In our studies, a preliminary docking calculation was performed to validate the binding capacity of ampullosporins (**5.1–5.3**) with the *N*-methyl-D-aspartate (NMDA) receptor, which was indicated as potential biological target molecule of ampullosporin A (**5.3**) (Chapter 5). Our *in silico* results showed that replacement of each of Gln residues (Gln⁷ and Gln¹¹) in ampullosporin A (**5.3**) by GluOMe resulted in additional hydrophobic interactions of ampullosporin F (**5.1**; GluOMe¹¹) and ampullosporin G (**5.2**; GluOMe⁷) with hydrophobic receptor residues, and thus causing higher biological effects of the new peptaibols. From this point of view, a future perspective would be promising to test our new ampullosporins F (**5.1**) and G (**5.2**) for their neuroleptic activity, which was reported for ampullosporin A (**5.3**). Also, it is very interesting to synthesize other derivatives of **5.3** by replacing partly/totally three Gln residues in its sequence with GluOMe and evaluate their biological activities, e.g. antifungal and anticancer activities, which might lead to the potential candidate for pharmaceutical and agricultural products.

In conclusion, valuable contributions have been made to the investigation of secondary metabolites regarding their identification, biosynthesis, total synthesis, and biological activity. This work also demonstrates the important role of new fungal natural products as leading compounds for the development of pharmaceutical and agricultural products, as well as the potential of fungi, including both basidiomycetes and ascomycetes, as a great but untapped source of new bioactive compounds.

References

- Berg, K. A., Harvey, J. A., Spampinato, U., Clarke, W. P., 2005. Physiological relevance of constitutive activity of 5-HT_{2A} and 5-HT_{2C} receptors. *Trends Pharmacol Sci* 26, 625-630.
- Bortolus, M., Dalzini, A., Formaggio, F., Toniolo, C., Gobbo, M., Maniero, A. L., 2016. An EPR study of ampullosporin A, a medium-length peptaibiotic, in bicelles and vesicles. *Phys Chem Chem Phys* 18, 749-760.
- Caruano, J., Muccioli, G. G., Robiette, R., 2016. Biologically active γ -lactams: synthesis and natural sources. *Org Biomol Chem* 14, 10134-10156.
- Chugh, J. K., Wallace, B. A., 2001. Peptaibols: models for ion channels. *Biochem Soc Trans* 29, 565-570.
- De Deurwaerdère, P., Drutel, G., Di Giovanni, G., 2018. Pharmacological analysis in favour of a physiological role for the constitutive activity of 5-HT_{2A} receptors in learning. In: Guiard, B., Di Giovanni, G. (Eds.), 5-HT_{2A} receptors in the central nervous system. The receptors, vol. 32. Humana Press, Cham, pp. 3-29.
- Elsworth, C., Gill, M., Giménez, A., Milanovic, N. M., Raudies, E., 1999. Pigments of fungi. Part 50.1 Structure, biosynthesis and stereochemistry of new dimeric dihydroanthracenones of the phlegmacin type from *Cortinarius sinapicolor* Cleland. *J Chem Soc, Perkin Trans 1*, 119–125.

- Fasciani, I., Petragnano, F., Aloisi, G., Marampon, F., Carli, M., Scarselli, M., Maggio, R., Rossi, M., 2020. Allosteric modulators of G protein-coupled dopamine and serotonin receptors: A new class of atypical antipsychotics. *Pharmaceuticals* (Basel) 13, 388.
- Fuente-Núñez, C. d. l., Whitmore, L., Wallace, B. A., 2013. Chapter 22 - Peptaibols. In: Kastin, A. J. (Ed.), *Handbook of biologically active peptides* (second edition). Academic Press, Boston, pp. 150-156.
- Heng, H. L., Chee, C. F., Thy, C. K., Tee, J. T., Chin, S. P., Herr, D. R., Buckle, M. J. C., Paterson, I. C., Doughty, S. W., Abd Rahman, N., Chung, L. Y., 2019. *In vitro* functional evaluation of isolaureline, dicentrine and glaucine enantiomers at 5-HT₂ and α_1 receptors. *Chem Biol Drug Des* 93, 132-138.
- Hiersemann, M., Helmboldt, H., 2005. Recent progress in the total synthesis of dolabellane and dolastane diterpenes. In: Mulzer, J. H. (Ed.), *Natural Product Synthesis I*, vol. 243. Springer, Berlin, Heidelberg, pp. 73-136.
- Kettering, M., Valdivia, C., Sterner, O., Anke, H., Thines, E., 2005. Heptemerones A~G, seven novel diterpenoids from *Coprinus heptemerus*: producing organism, fermentation, isolation and biological activities. *J Antibiot* 58, 390-396.
- Klein-Junior, L. C., Cretton, S., Vander Heyden, Y., Gasper, A. L., Nejad-Ebrahimi, S., Christen, P., Henriques, A. T., 2020. Bioactive azepine-indole alkaloids from *Psychotria nemorosa*. *J Nat Prod* 83, 852-863.
- Lin, H. C., Chiou, G., Chooi, Y. H., McMahon, T. C., Xu, W., Garg, N. K., Tang, Y., 2015. Elucidation of the concise biosynthetic pathway of the communesin indole alkaloids. *Angew Chem Int Ed Engl* 54, 3004-3007.
- Lindsay, A. C., Kim, S. H., Sperry, J., 2018. Non-monoterpenoid azepinoindole alkaloids. *Nat Prod Rep* 35, 1347-1382.
- Markovic, D., Kolypadi, M., Deguin, B., Pore, F.-H., Turks, M., 2015. The isolation and synthesis of neodolastane diterpenoids. *Nat Prod Rep* 32, 230-255.
- Müller, M., Lamottke, K., Steglich, W., Busemann, S., Reichert, M., Bringmann, G., Spiteller, P., 2004. Biosynthesis and stereochemistry of phlegmacin-type fungal pigments. *Eur J Org Chem* 2004, 4850-4855.
- Naoi, M., Maruyama, W., Akao, Y., Yi, H., 2002. Dopamine-derived endogenous *N*-methyl-(*R*)-salsolinol: Its role in Parkinson's disease. *Neurotoxicol Teratol* 24, 579-591.
- Otto, A., Laub, A., Haid, M., Porzel, A., Schmidt, J., Wessjohann, L., Arnold, N., 2016a. Tulasporins A-D, 19-residue peptaibols from the mycoparasitic fungus *Sepedonium tulasneanum*. *Nat Prod Commun* 11, 1821-1824.
- Otto, A., Laub, A., Porzel, A., Schmidt, J., Wessjohann, L., Westermann, B., Arnold, N., 2015. Isolation and total synthesis of albupeptins A-D: 11-residue peptaibols from the fungus *Gliocladium album*. *Eur J Org Chem* 2015, 7449-7459.
- Otto, A., Laub, A., Wendt, L., Porzel, A., Schmidt, J., Palfner, G., Becerra, J., Kruger, D., Stadler, M., Wessjohann, L., Westermann, B., Arnold, N., 2016b. Chilenopeptins A and B, peptaibols from the Chilean *Sepedonium* aff. *chalcipori* KSH 883. *J Nat Prod* 79, 929-938.
- Ou, Y. X., Li, Y. Y., Qian, X. M., Shen, Y. M., 2012. Guanacastane-type diterpenoids from *Coprinus radians*. *Phytochemistry* 78, 190-196.
- Rankic, D. A., Stiff, C. M., am Ende, C. W., Humphrey, J. M., 2017. Protocol for the direct conversion of lactones to lactams mediated by 1,5,7-triazabicyclo[4.4.0]dec-5-ene: synthesis of pyridopyrazine-1,6-diones. *J Org Chem* 82, 12791-12797.

- Rinkel, J., Dickschat, J. S., 2015. Recent highlights in biosynthesis research using stable isotopes. *Beilstein J Org Chem* 11, 2493-2508.
- Singh, M. P., Janso, J. E., Luckman, S. W., Brady, S. F., Clardy, J., Greenstein, M., Maiese, W. M., 2000. Biological activity of guanacastepene, a novel diterpenoid antibiotic produced by an unidentified fungus CR115. *J Antibiot* 53, 256-261.
- Spiteller, P., Ruth, M., von Nussbaum, F., Steglich, W., 2000. Detection of a 2,3-aminomutase in the mushroom *Cortinarius violaceus*. *Angew Chem Int Ed Engl* 39, 2754-2756.
- Stockigt, J., Antonchick, A. P., Wu, F., Waldmann, H., 2011. The Pictet-Spengler reaction in nature and in organic chemistry. *Angew Chem Int Ed Engl* 50, 8538-8564.
- Wigley, L. J., Mantle, P. G., Perry, D. A., 2006. Natural and directed biosynthesis of communesin alkaloids. *Phytochemistry* 67, 561-569.
- Wigley, L. J., Perry, D. A., Mantle, P. G., 2008. An experimental strategy towards optimising directed biosynthesis of communesin analogues by *Penicillium marinum* in submerged fermentation. *Mycol Res* 112, 131-137.
- Wu, F.-B., Li, T.-X., Yang, M.-H., Kong, L.-Y., 2016. Guanacastane-type diterpenoids from the insect-associated fungus *Verticillium dahliae*. *J Asian Nat Prod Res* 18, 117-124.
- Xu, W., Gavia, D. J., Tang, Y., 2014. Biosynthesis of fungal indole alkaloids. *Nat Prod Rep* 31, 1474-1487.
- Yin, X., Feng, T., Li, Z.-H., Leng, Y., Liu, J.-K., 2014. Five new guanacastane-type diterpenes from cultures of the fungus *Psathyrella candolleana*. *Nat Prod Bioprospect* 4, 149-155.
- Zhang, F.-L., Feng, T., 2022. Diterpenes specially produced by fungi: structures, biological activities, and biosynthesis (2010-2020). *J Fungi* 8, 244.
- Zieba, A., Stepnicki, P., Matosiuk, D., Kaczor, A. A., 2021. Overcoming depression with 5-HT_{2A} receptor ligands. *Int J Mol Sci* 23, 10.

Appendix

A Peptaibol sequences

Table A1. Sequences of peptaibols isolated from *Sepedonium* species (*)

source/peptaibol	1	2	3	4	5	6	7	8	9	10	11	12	13	14	15	16	17	18	19
<i>S. ampullosporum</i>																			
peptaibolin (2.64)	Ac	Leu	Aib	Leu	Aib	Pheol													
ampullosporin A (2.65)	Ac	Trp	Ala	Aib	Aib	Leu	Aib	Gln	Aib	Aib	Aib	Gln	Leu	Aib	Gln	Leuol			
ampullosporin B (2.66)	Ac	Trp	Ala	Aib	Aib	Leu	Aib	Gln	Ala	Aib	Aib	Gln	Leu	Aib	Gln	Leuol			
ampullosporin C (2.67)	Ac	Trp	Ala	Aib	Aib	Leu	Aib	Gln	Aib	Ala	Aib	Gln	Leu	Aib	Gln	Leuol			
ampullosporin D (2.68)	Ac	Trp	Ala	Aib	Aib	Leu	Aib	Gln	Aib	Aib	Ala	Gln	Leu	Aib	Gln	Leuol			
ampullosporin E ₁ (2.69)	Ac	Trp	Ala	Aib	Aib	Leu	Aib	Gln	Ala	Aib	Aib	Gln	Leu	Ala	Gln	Leuol			
ampullosporin E ₂ (2.70)	Ac	Trp	Ala	Aib	Aib	Leu	Aib	Gln	Aib	Ala	Ala	Gln	Leu	Aib	Gln	Leuol			
ampullosporin E ₃ (2.71)	Ac	Trp	Ala	Aib	Aib	Leu	Aib	Gln	Aib	Aib	Ala	Gln	Leu	Ala	Gln	Leuol			
ampullosporin E ₄ (2.72)	Ac	Trp	Ala	Aib	Aib	Leu	Aib	Gln	Ala	Ala	Aib	Gln	Leu	Aib	Gln	Leuol			
<i>S. chalcipori</i>																			
chalcipori A (2.73)	Ac	Trp	Val	Aib	Val	Ala	Gln	Ala	Aib	Ser	Leu	Ala	Leu	Aib	Gln	Leuol			
chalcipori B (2.74)	Ac	Trp	Val	Aib	Val	Ala	Gln	Ala	Aib	Gln	Aib	Ala	Leu	Aib	Gln	Leuol			
tylopeptin A (2.75)	Ac	Trp	Val	Aib	Iva	Ala	Gln	Ala	Aib	Ser	Aib	Ala	Leu	Aib	Gln	Leuol			
tylopeptin B (2.76)	Ac	Trp	Val	Aib	Aib	Ala	Gln	Ala	Aib	Ser	Aib	Ala	Leu	Aib	Gln	Leuol			
chilenopeptin A (2.77)	Ac	Aib	Ser	Trp	Aib	Pro	Leu	Aib	Aib	Gln	Aib	Aib	Gln	Aib	Leu	Pheol			
chilenopeptin B (2.78)	Ac	Aib	Ser	Phe	Aib	Pro	Leu	Aib	Aib	Gln	Aib	Aib	Gln	Aib	Leu	Pheol			

Table A1. (continued)

<i>S. chrysospermum</i>																				
chrysaibol (2.79)	Ac	Trp	Aib	Aib	Leu	Val	Gln	Aib	Aib	Aib	Gln	Leu	Aib	Pro	Gln	Alaol				
chrysospermin A (2.80)	Ac	Phe	Aib	Ser	Aib	Aib	Leu	Gln	Gly	Aib	Aib	Ala	Ala	Aib	Pro	Aib	Aib	Aib	Gln	Trpol
chrysospermin B (2.81)	Ac	Phe	Aib	Ser	Aib	Aib	Leu	Gln	Gly	Aib	Aib	Ala	Ala	Aib	Pro	Iva	Aib	Aib	Gln	Trpol
chrysospermin C (2.82)	Ac	Phe	Aib	Ser	Aib	Iva	Leu	Gln	Gly	Aib	Aib	Ala	Ala	Aib	Pro	Aib	Aib	Aib	Gln	Trpol
chrysospermin D (2.83)	Ac	Phe	Aib	Ser	Aib	Iva	Leu	Gln	Gly	Aib	Aib	Ala	Ala	Aib	Pro	Iva	Aib	Aib	Gln	Trpol
<i>S. microspermum</i>																				
microspermin A (2.84)	Ac	Trp	Aib	Ser	Aib	Iva	Trp	Gln	Gly	Aib	Aib	Ala	Ala	Aib	Pro	Aib	Aib	Aib	Gln	Leuol
microspermin B (2.85)	Ac	Trp	Aib	Ser	Aib	Aib	Trp	Gln	Gly	Aib	Aib	Ala	Ala	Aib	Pro	Aib	Aib	Iva	Gln	Leuol
microspermin C (2.86)	Ac	Trp	Iva	Ser	Aib	Iva	Trp	Gln	Gly	Aib	Aib	Ala	Ala	Aib	Pro	Aib	Aib	Aib	Gln	Leuol
microspermin D (2.87)	Ac	Trp	Aib	Ser	Aib	Iva	Trp	Gln	Gly	Aib	Aib	Ala	Ala	Aib	Pro	Aib	Aib	Iva	Gln	Leuol
microspermin E (2.88)	Ac	Trp	Iva	Ser	Aib	Iva	Trp	Gln	Gly	Aib	Aib	Ala	Ala	Aib	Pro	Aib	Aib	Iva	Gln	Leuol
microspermin F (2.89)	Ac	Trp	Iva	Ser	Aib	Iva	Leu	Gln	Gly	Aib	Aib	Ala	Ala	Aib	Pro	Aib	Aib	Aib	Gln	Leuol
microspermin G (2.90)	Ac	Trp	Aib	Ser	Aib	Iva	Leu	Gln	Gly	Aib	Aib	Ala	Ala	Aib	Pro	Aib	Aib	Iva	Gln	Leuol
microspermin F (2.91)	Ac	Trp	Iva	Ser	Aib	Iva	Leu	Gln	Gly	Aib	Aib	Ala	Ala	Aib	Pro	Aib	Aib	Iva	Gln	Leuol
<i>S. tulasneanum</i>																				
tulasporin A (2.92)	Ac	Phe	Aib	Ser	Aib	Aib	Leu	Gln	Gly	Aib	Aib	Gln	Ala	Aib	Pro	Aib	Aib	Aib	Gln	Trpol
tulasporin B (2.93)	Ac	Phe	Aib	Ser	Aib	Iva	Leu	Gln	Gly	Aib	Aib	Gln	Ala	Aib	Pro	Aib	Aib	Aib	Gln	Trpol
tulasporin C (2.94)	Ac	Phe	Aib	Ser	Aib	Aib	Leu	Gln	Ala	Aib	Aib	Gln	Ala	Aib	Pro	Aib	Aib	Aib	Gln	Trpol
tulasporin D (2.95)	Ac	Phe	Aib	Ser	Aib	Iva	Leu	Gln	Ala	Aib	Aib	Gln	Ala	Aib	Pro	Aib	Aib	Aib	Gln	Trpol

Table A2. Sequences of selected peptaibols from other species (*)

source/peptaibol	1	2	3	4	5	6	7	8	9	10	11	12	13	14	15	16	17	18	19	20	
<i>Trichoderma viride</i>																					
alamethicin (2.96)	Ac	Aib	Pro	Aib	Ala	Aib	Ala	Gln	Aib	Val	Aib	Gly	Leu	Aib	Pro	Val	Aib	Aib	Glu	Gln	Pheol
trichotoxin A50E (2.97)	Ac	Aib	Gly	Aib	Leu	Aib	Gln	Aib	Aib	Aib	Ala	Ala	Aib	Pro	Leu	Aib	Aib	Gln	Valol		
<i>Gliocladium album</i>																					
albupeptin A (6.11)	Ac	Aib	Aib	Val	Leu	Aib	Pro	Iva	Leu	Gln	Aib	Leuol									
albupeptin B (6.12)	Ac	Aib	Aib	Val	Leu	Iva	Pro	Iva	Leu	Gln	Aib	Leuol									
albupeptin C (6.13)	Ac	Iva	Aib	Val	Leu	Aib	Pro	Iva	Leu	Gln	Aib	Leuol									
albupeptin D (6.14)	Ac	Iva	Aib	Val	Leu	Iva	Pro	Iva	Leu	Gln	Aib	Leuol									

(*) Ac = acetyl; Aib = γ -aminoisobutyric acid; Ala = alanine; Gln = glutamine; Glu = glutamic acid; Gly = glycine; Iva = isovaline; Leu = leucine; Phe = phenylalanine; Pro = proline; Ser = serine; Trp = tryptophan; Val = valine.

B Supplementary data chapter 4

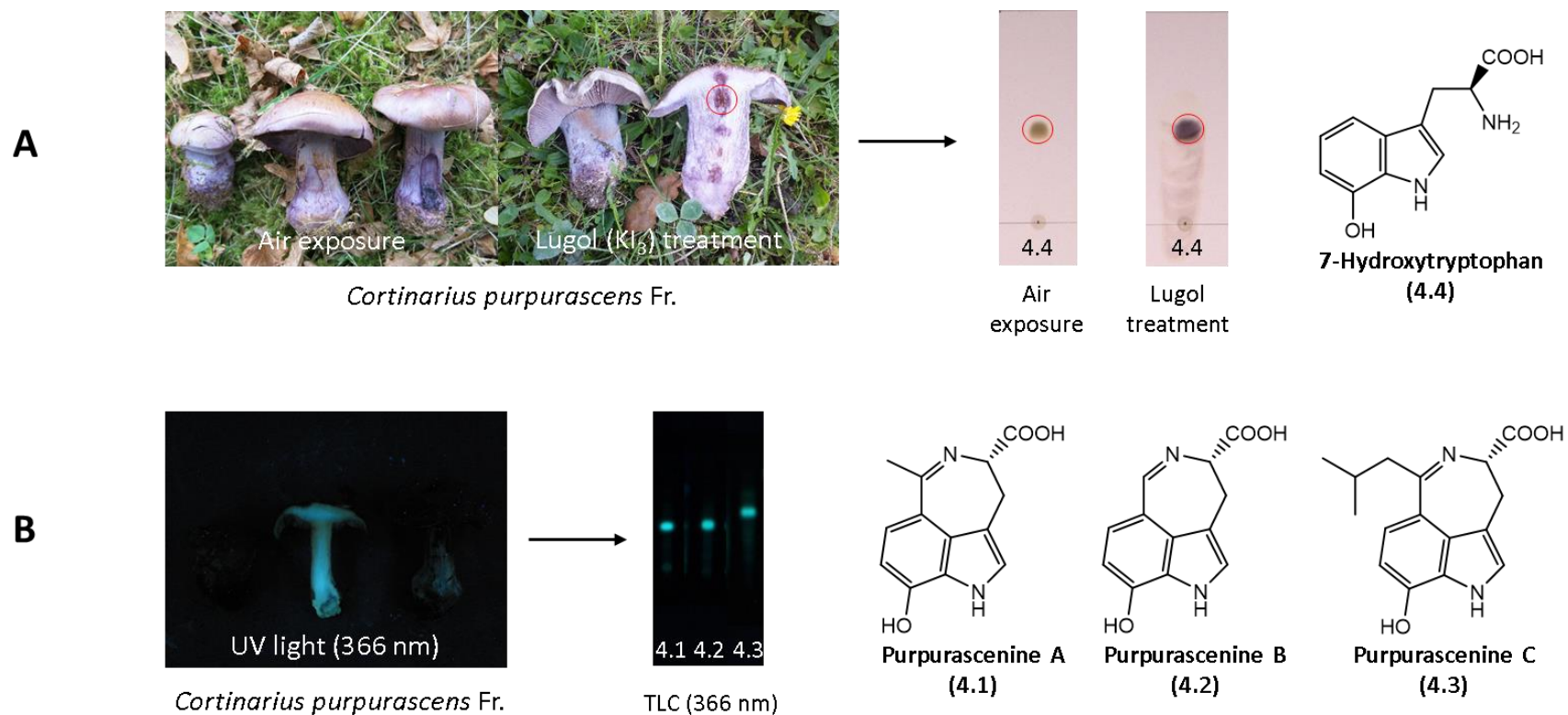


Figure B1. A: Characteristic violet-purple staining phenomenon; B: Blue-green fluorescence exhibited by *Cortinarius purpurascens* Fr. basidiomata and isolated compounds.

Figure B2. Positive ion HRESIMSⁿ spectra of purpurascenine A (**4.1**).

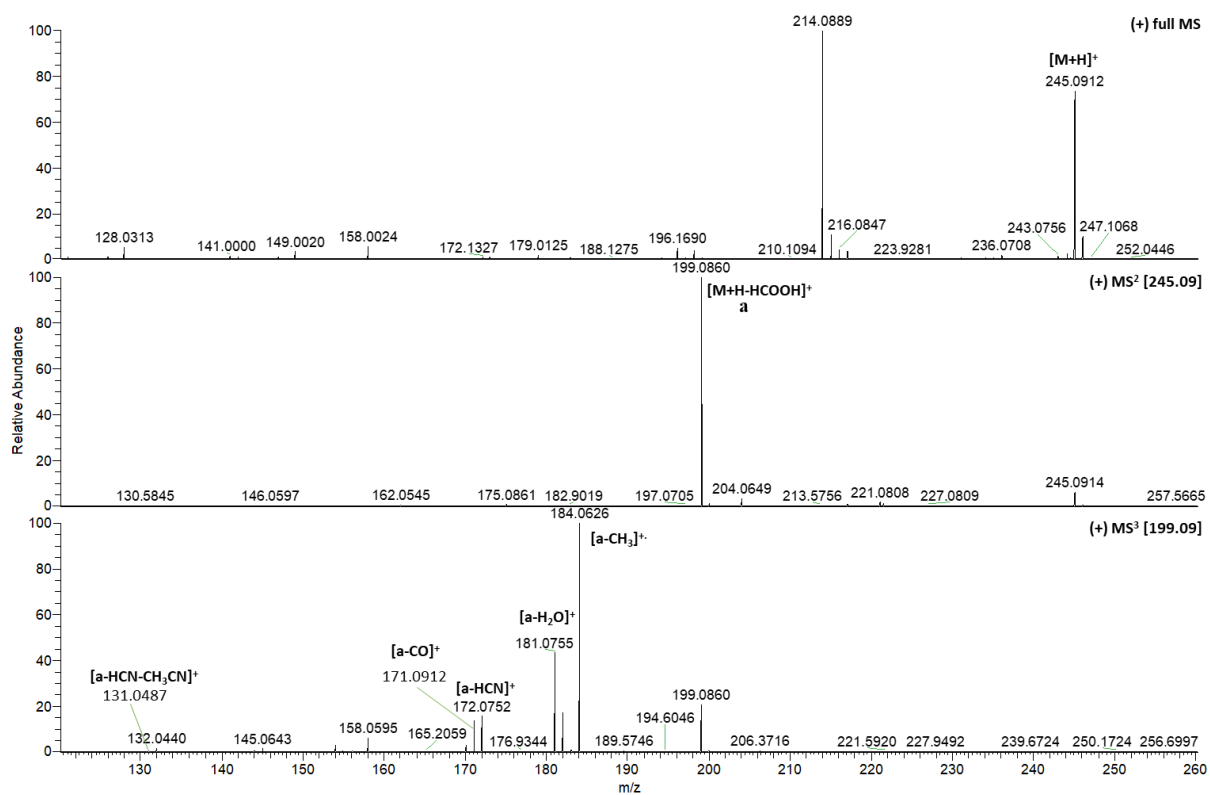


Figure B3. ^1H NMR spectrum (600 MHz, $\text{CD}_3\text{OD}/\text{D}_2\text{O} = 5/1$, v/v) of purpurascenine A (**4.1**).

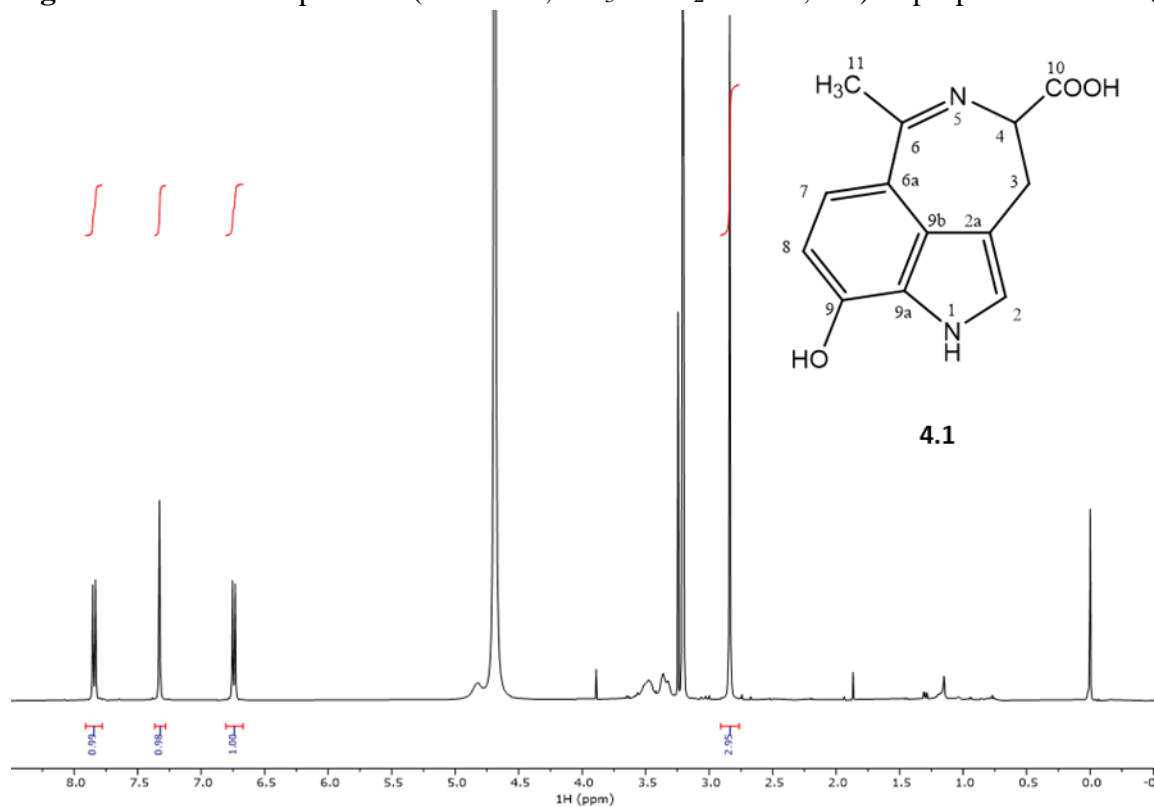


Figure B4. ^1H NMR spectrum (600 MHz, $\text{DMSO}-d_6$) of purpurascenine A (**4.1**).

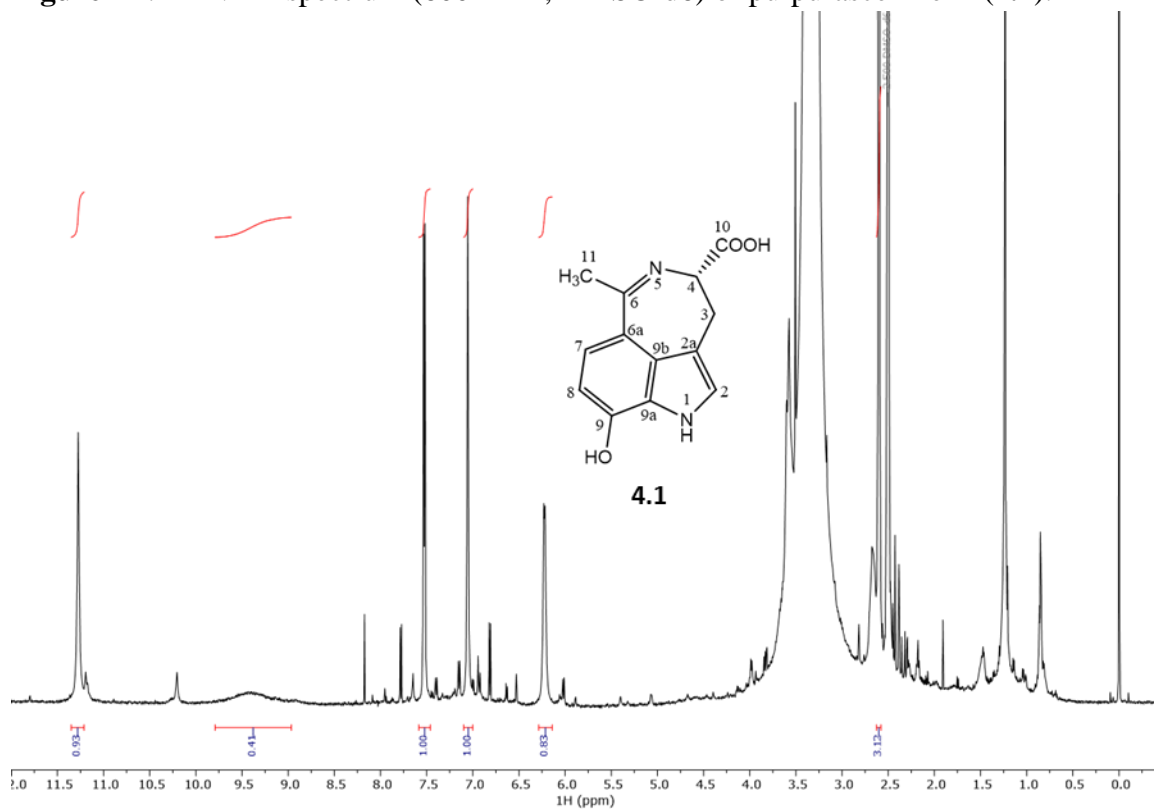


Figure B5. ^{13}C NMR spectrum (150 MHz, $\text{CD}_3\text{OD}/\text{D}_2\text{O} = 5/1, \text{v/v}$) of purpurascenine A (**4.1**).

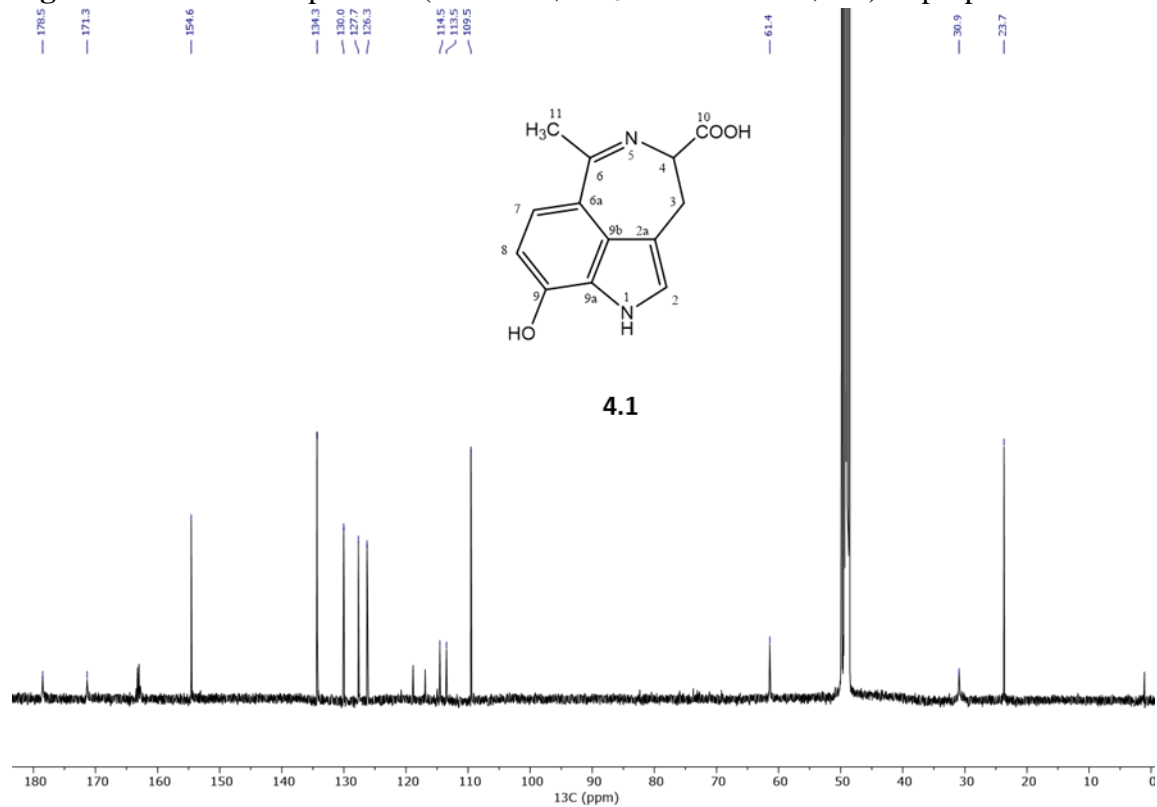


Figure B6. HSQC spectrum ($\text{CD}_3\text{OD}/\text{D}_2\text{O} = 5/1, \text{v/v}$) of purpurascenine A (**4.1**).

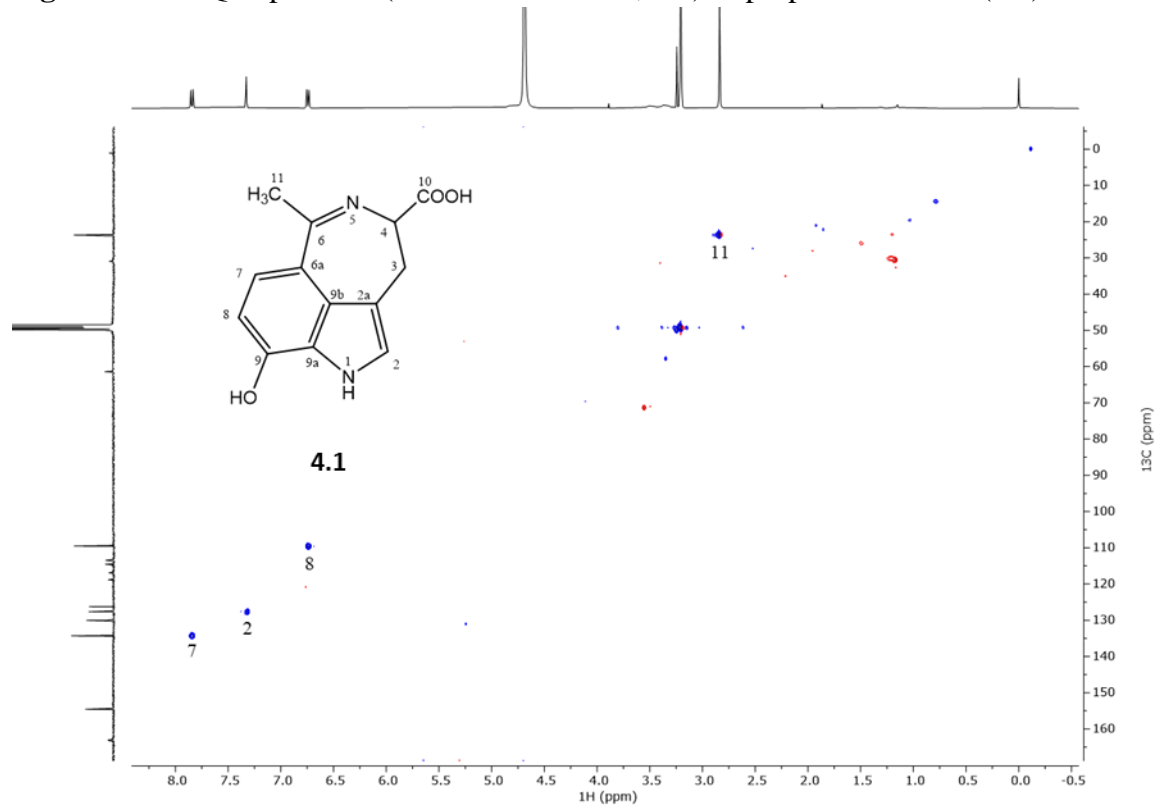


Figure B7. HSQC spectrum (DMSO-d₆) of purpurascenine A (**4.1**).

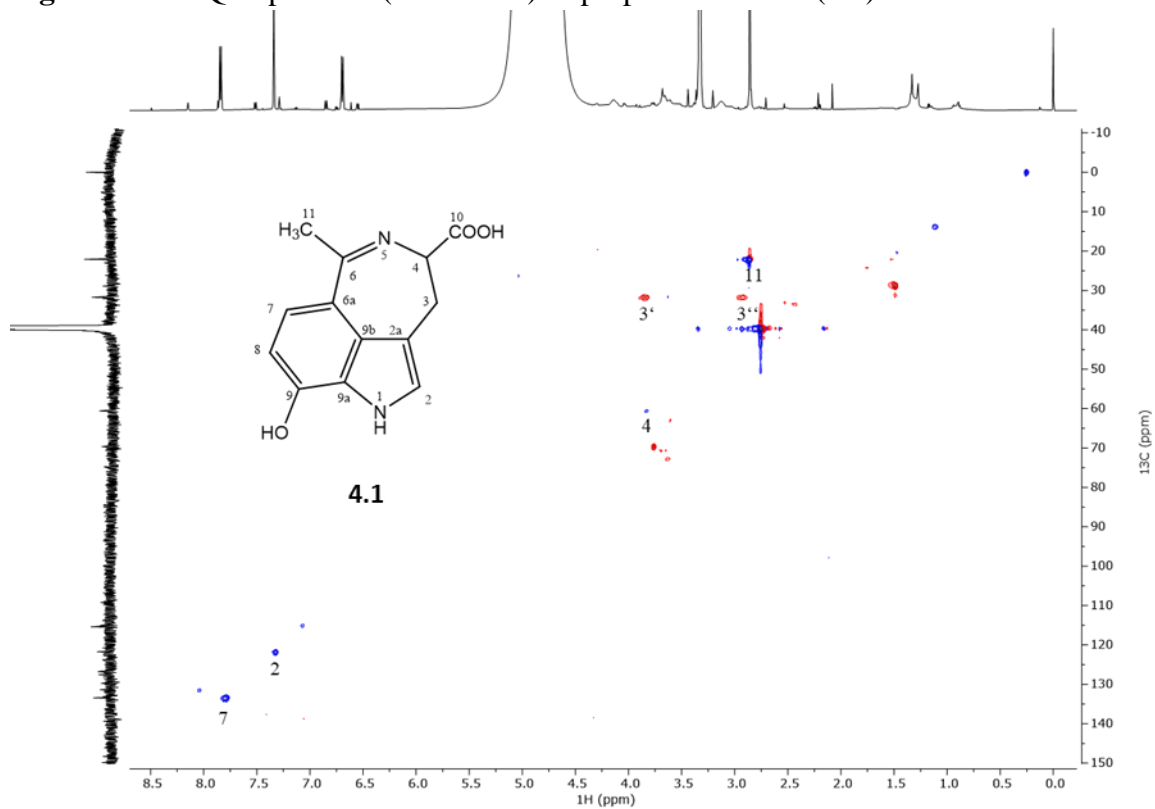


Figure B8. HMBC spectrum (CD₃OD/D₂O = 5/1, v/v) of purpurascenine A (**4.1**).

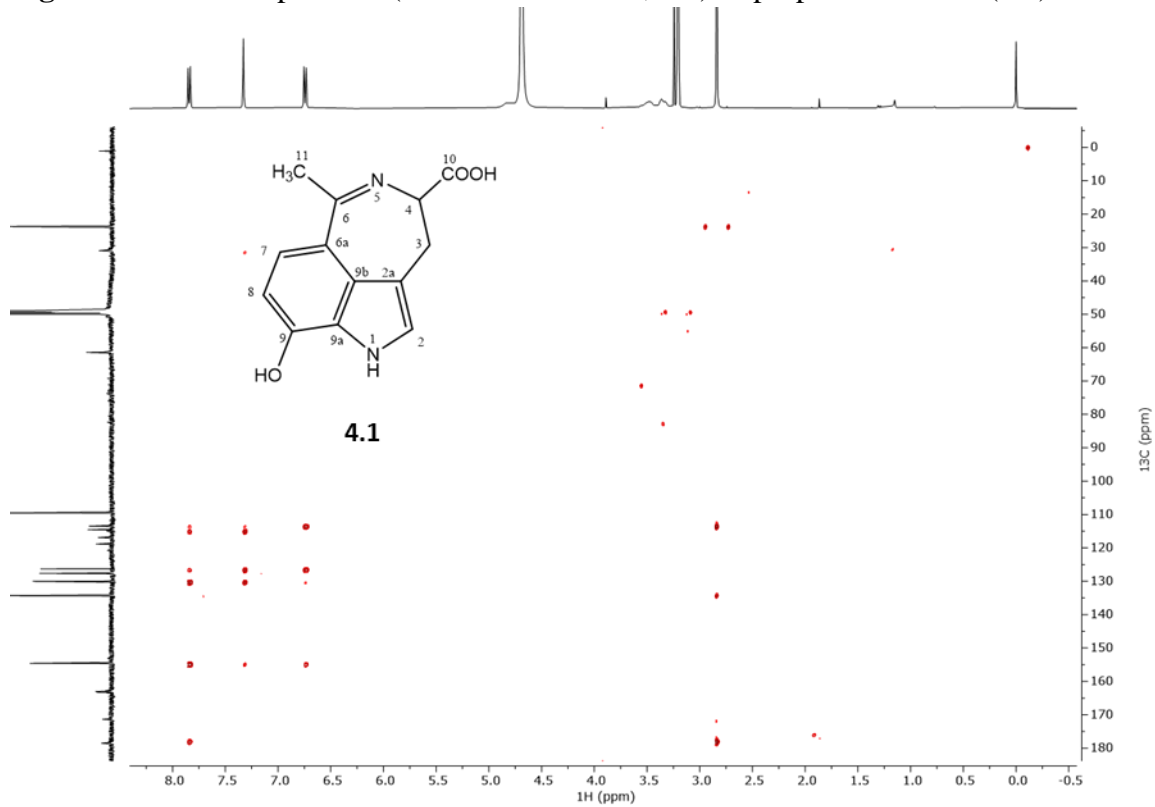


Figure B9. TOCSY spectrum ($\text{CD}_3\text{OD}/\text{D}_2\text{O} = 5/1, \text{v/v}$) of purpurascenine A (**4.1**).

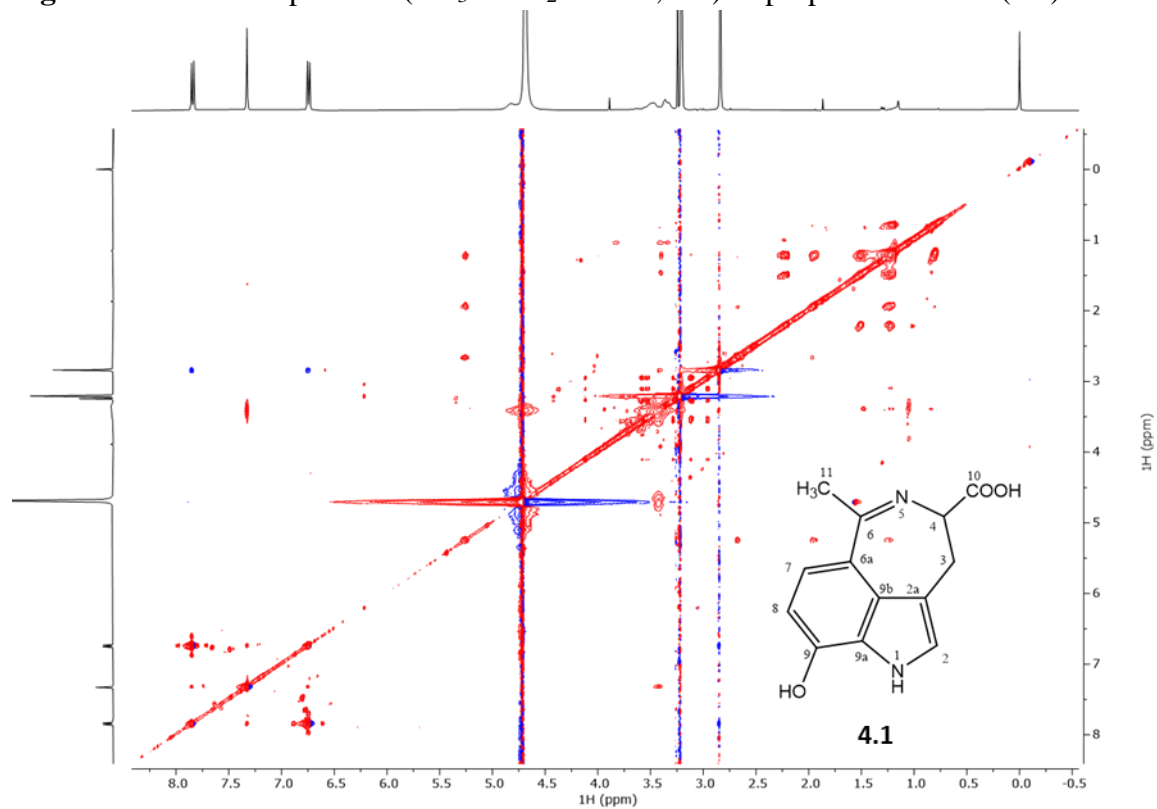


Figure B10. ROESY spectrum (DMSO-d_6) of purpurascenine A (**4.1**).

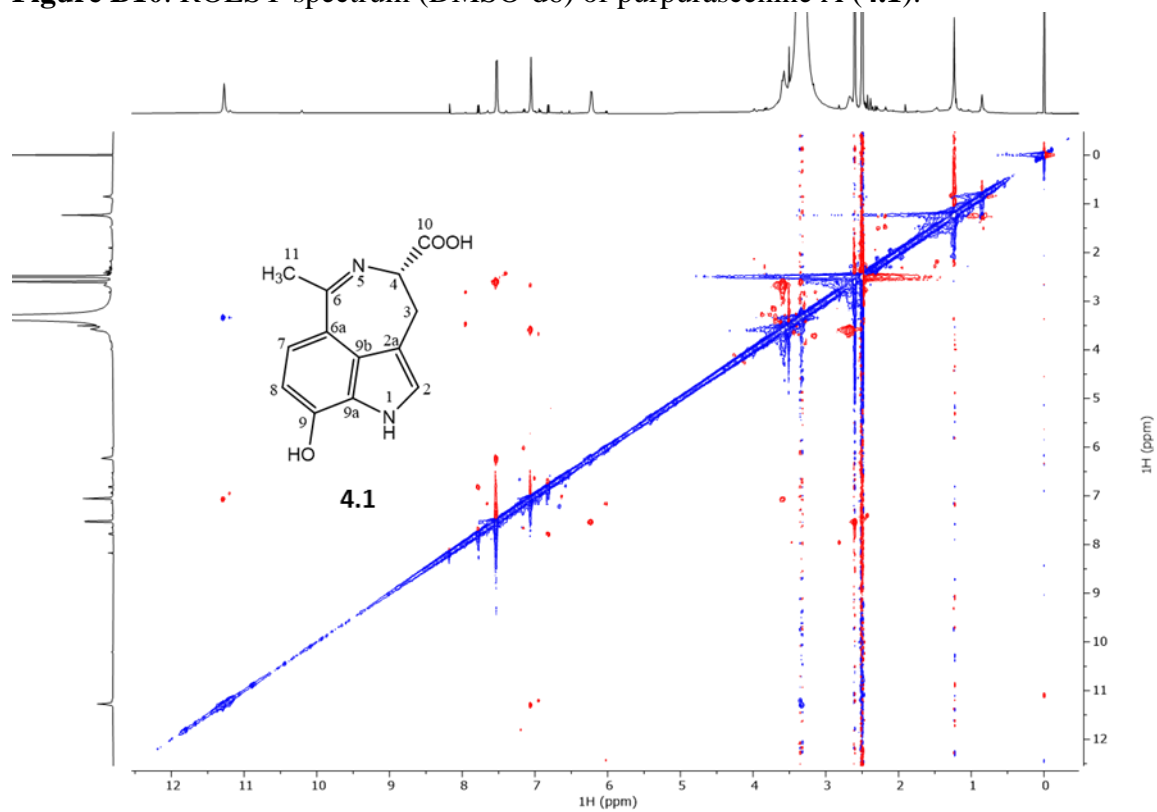


Figure B11. UV spectrum (MeOH/H₂O, 4:1) of purpurascenine A (**4.1**)

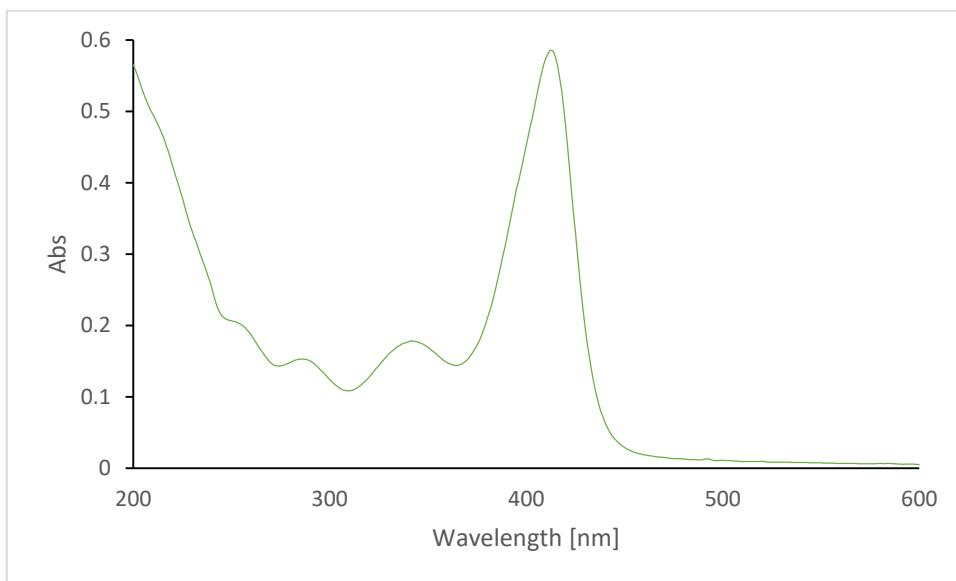


Figure B12. Positive ion HRESIMSⁿ spectrum of purpurascenine A **4.1a** (keto form).

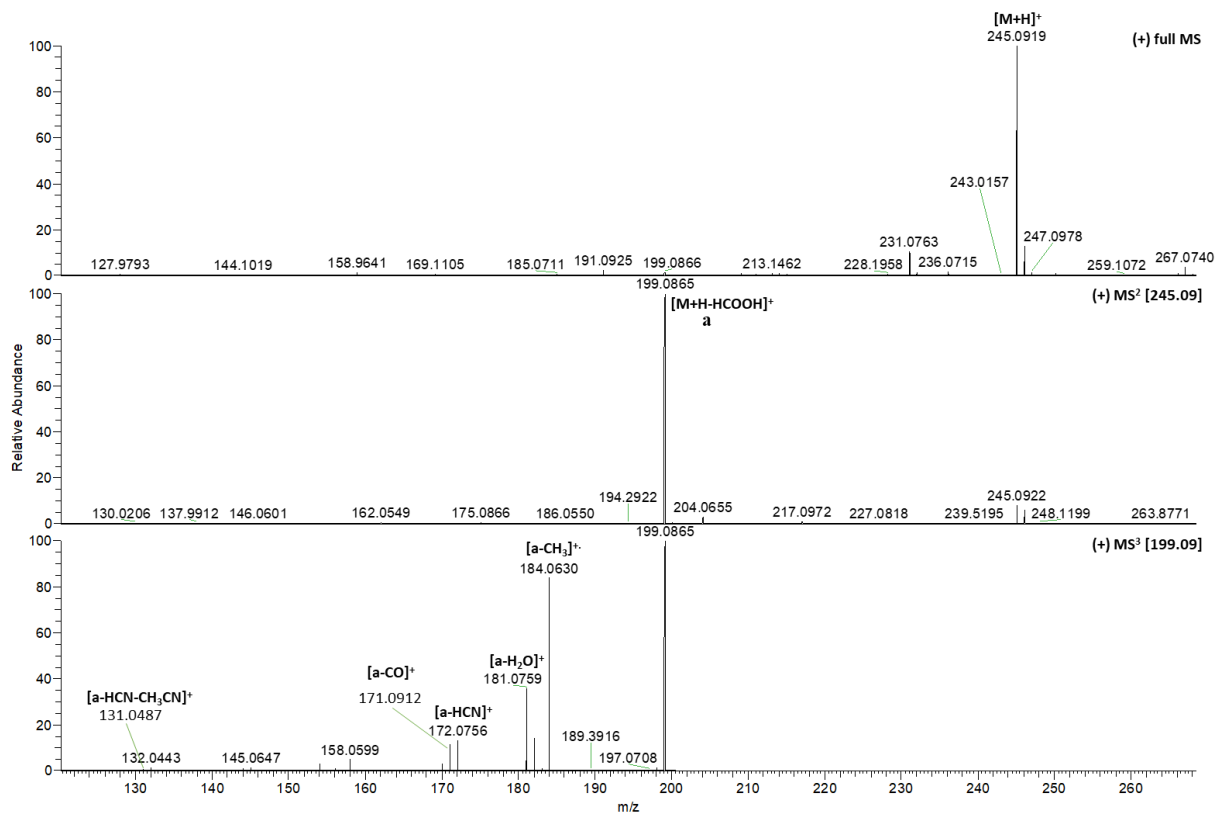


Figure B13. ^1H NMR spectrum (600 MHz, $\text{CD}_3\text{OD}/\text{D}_2\text{O} = 5/1$, v/v) of purpurascenine A **4.1a** (keto form).

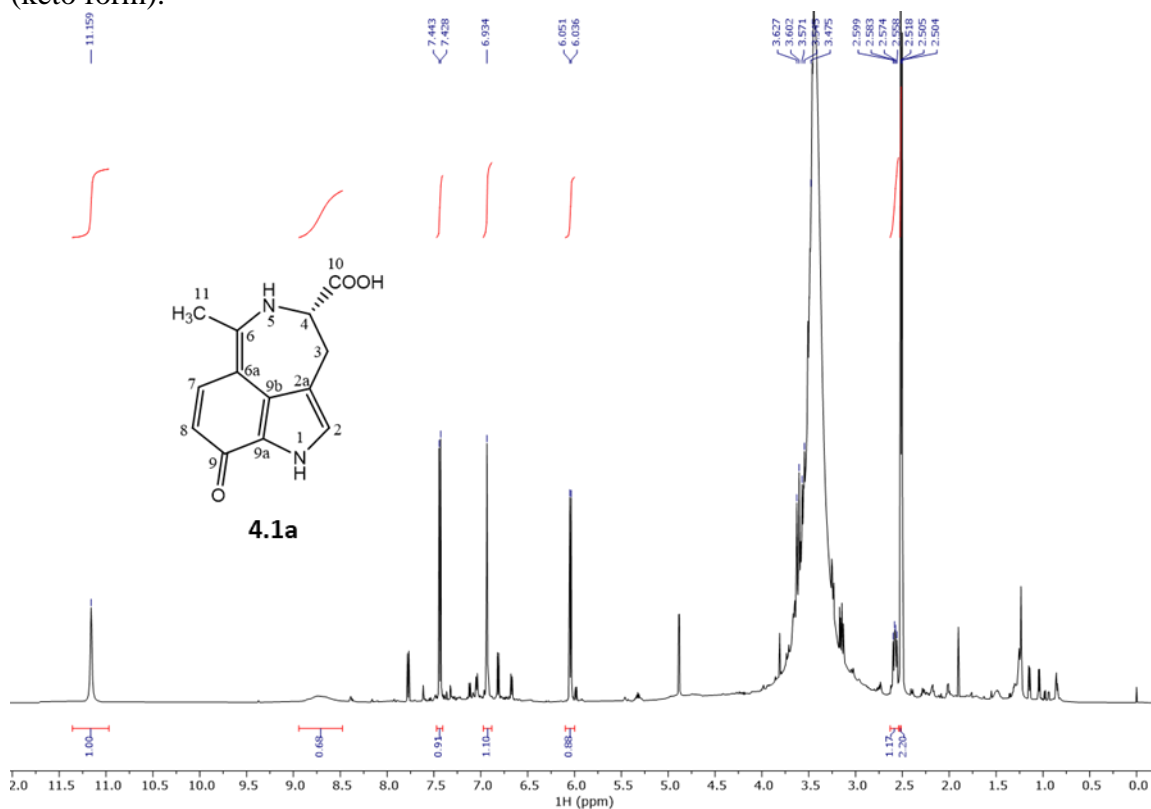


Figure B14. ^1H NMR spectrum (600 MHz, $\text{DMSO}-d_6$) of purpurascenine A **4.1a** (keto form).

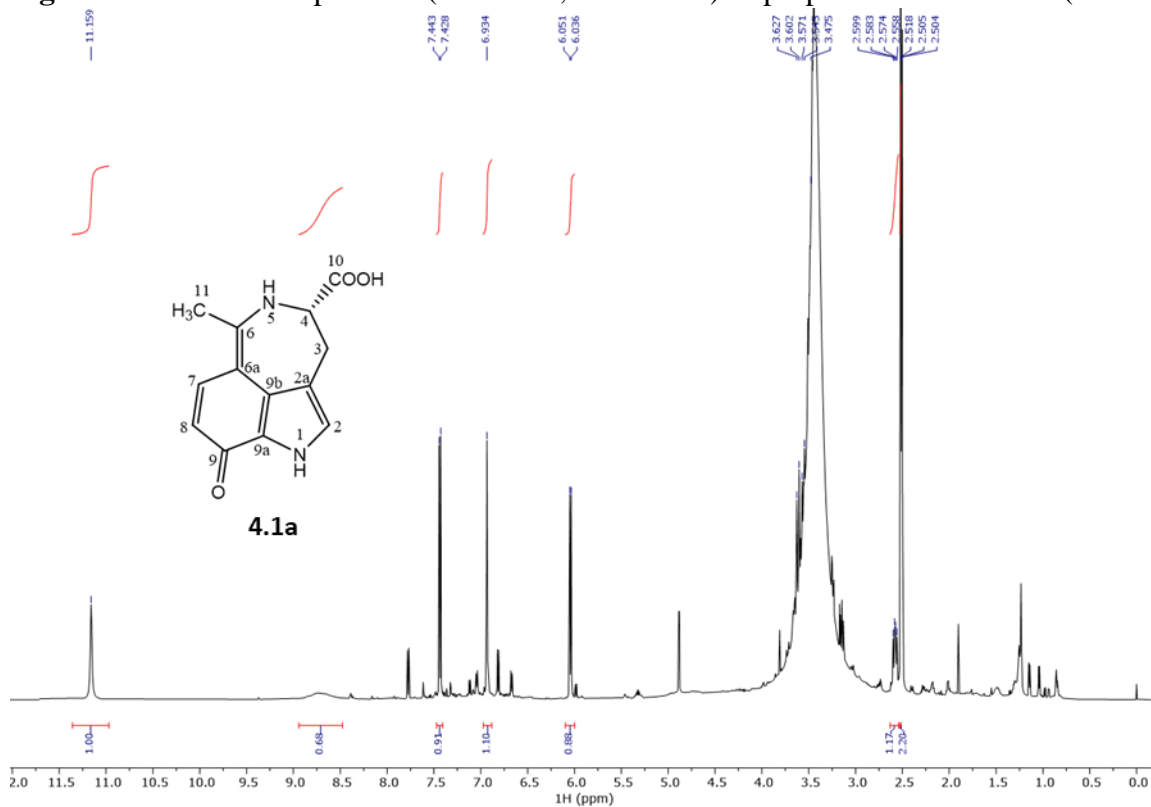


Figure B15. ^{13}C NMR spectrum (150 MHz, $\text{CD}_3\text{OD}/\text{D}_2\text{O} = 5/1$, v/v) of purpurascenine **4.1a** (keto form).

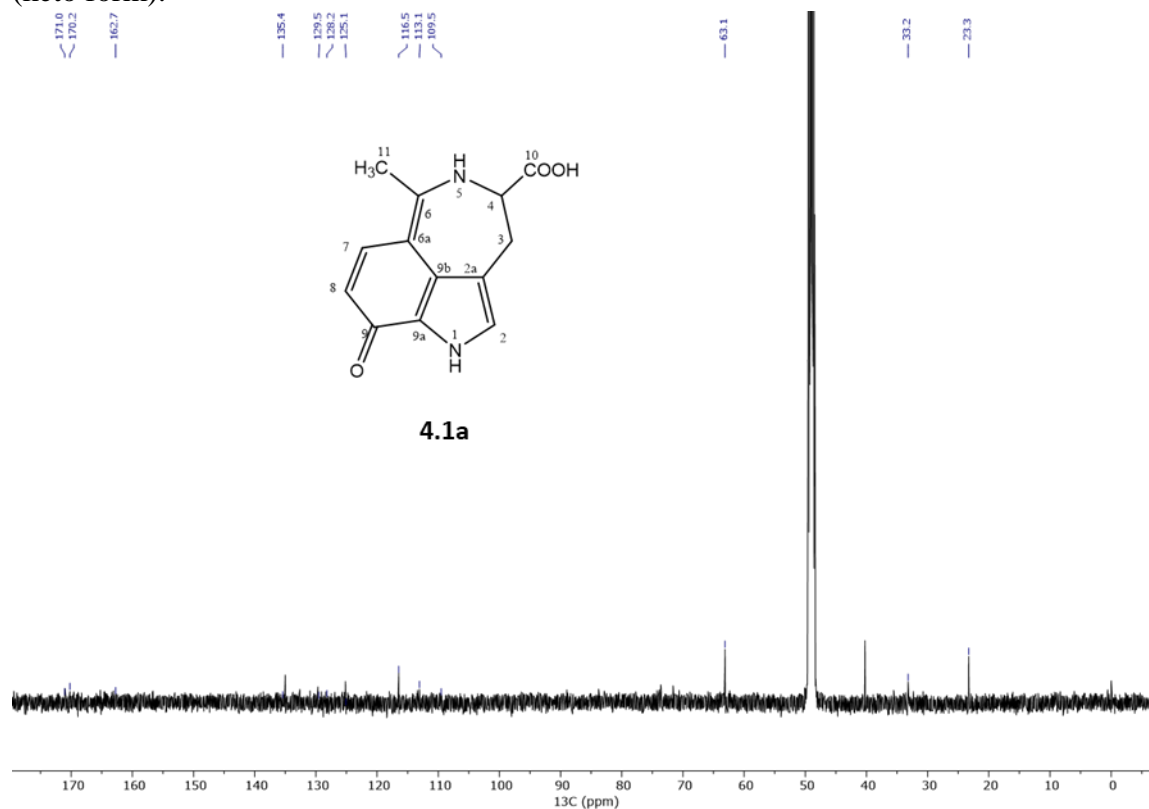


Figure B16. HSQC spectrum ($\text{CD}_3\text{OD}/\text{D}_2\text{O} = 5/1$, v/v) of purpurascenine A **4.1a** (keto form).

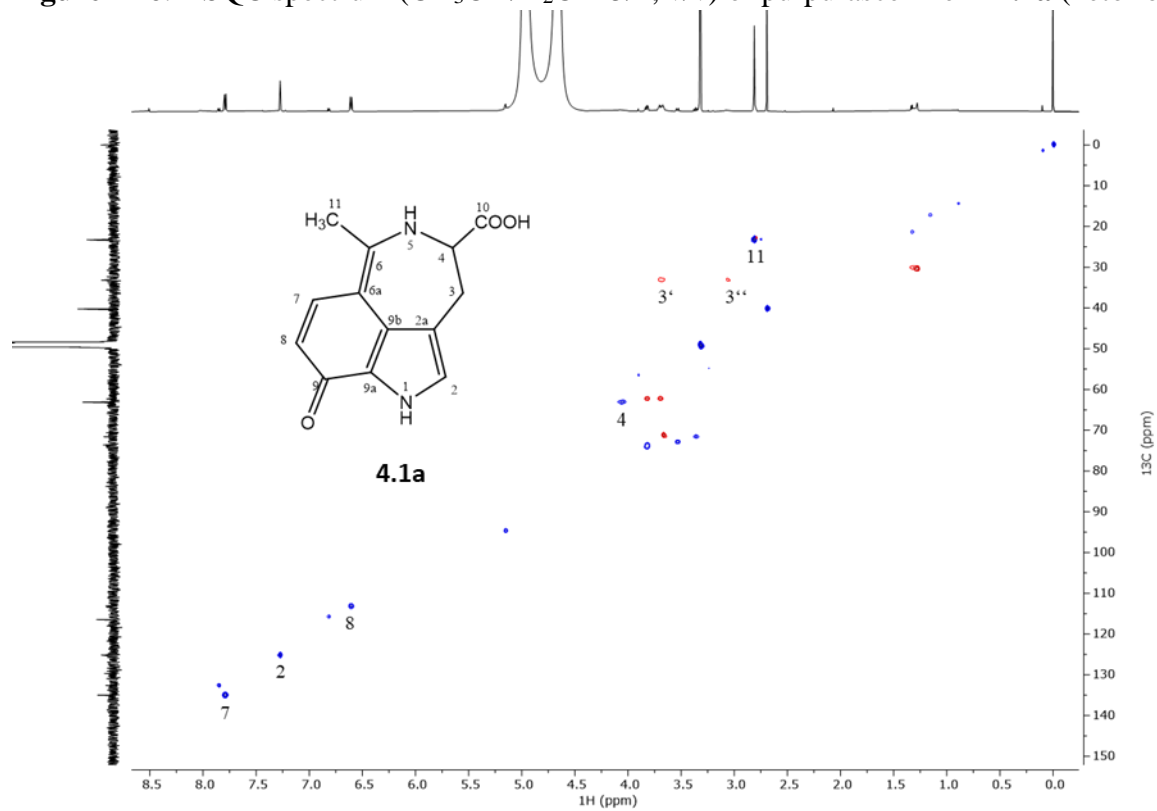


Figure B17. HMBC spectrum ($\text{CD}_3\text{OD}/\text{D}_2\text{O} = 5/1, \text{v/v}$) of purpurascenine A **4.1a** (keto form).

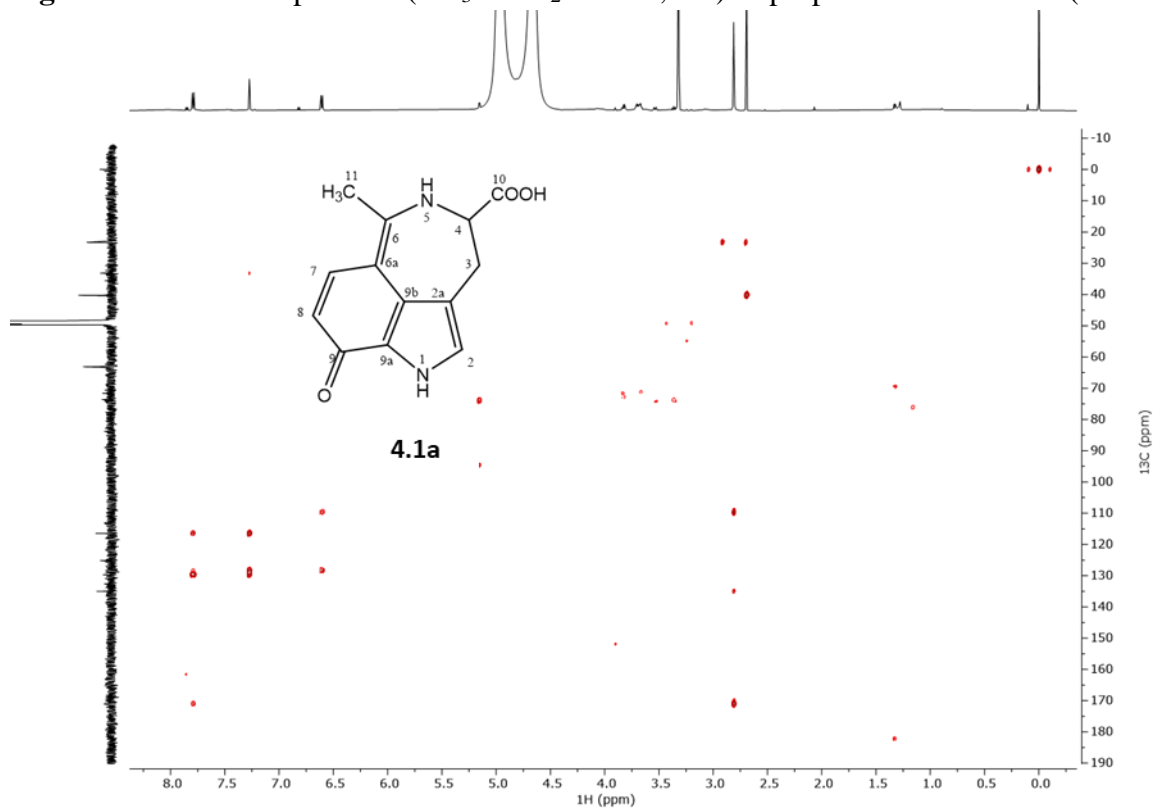


Figure B18. TOCSY spectrum ($\text{CD}_3\text{OD}/\text{D}_2\text{O} = 5/1, \text{v/v}$) of purpurascenine A **4.1a** (keto form).

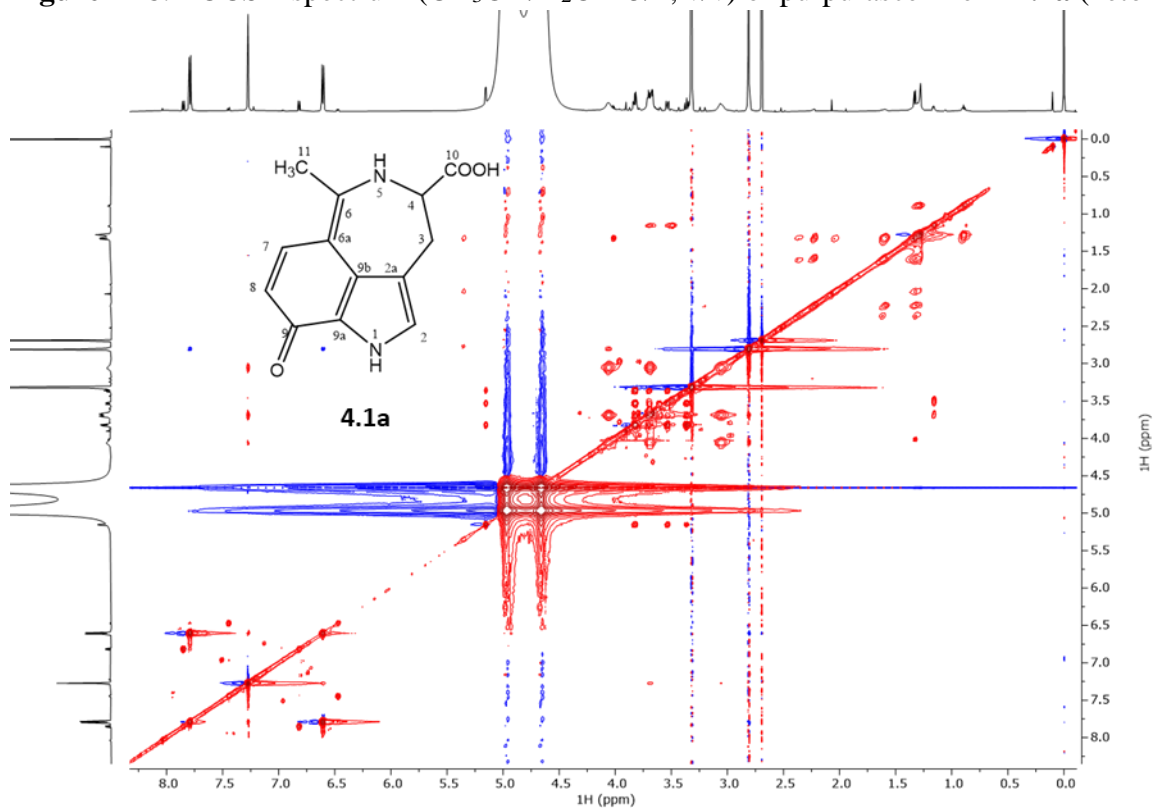


Figure B19. ROESY spectrum (600 MHz, DMSO-d₆) of purpurascenine A **4.1a** (keto form).

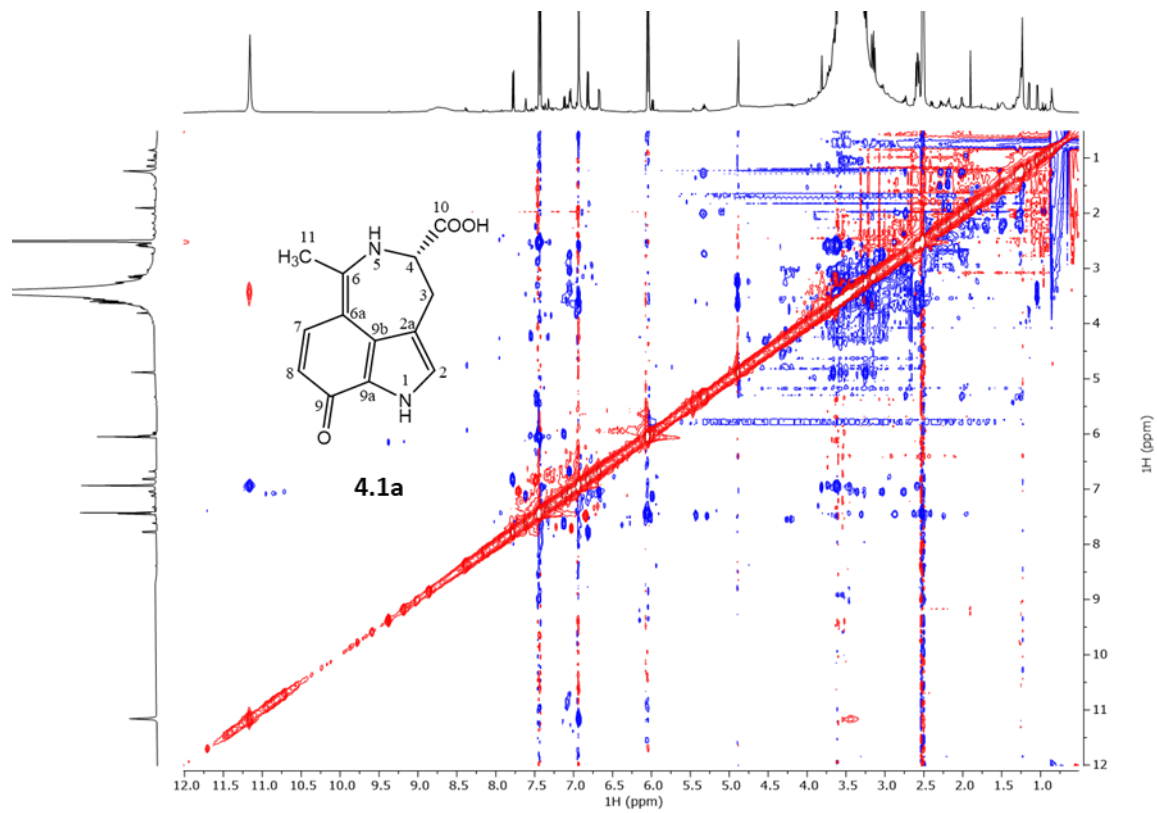


Figure B20. UV spectrum (MeOH/H₂O, 4:1) of purpurascenine A **4.1a** (keto form).

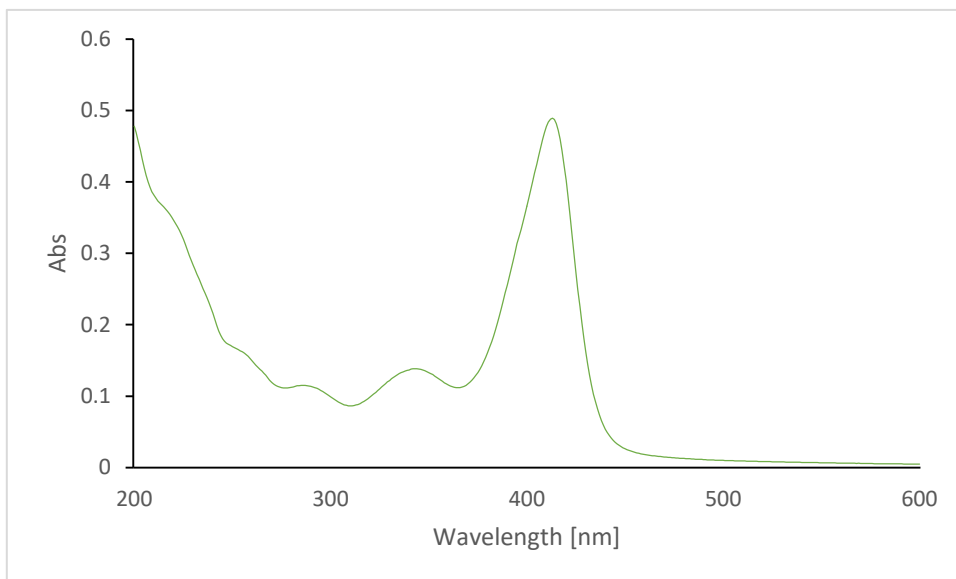


Figure B21. Calculated CD spectra of 4*R* (green) and 4*S* (red), compared with the experimental spectrum (black) of **4.1a**. The best similarity factor $S=0.8309$ was found for $\sigma=0.26$ eV and a shift of 10 nm. The similarity factor for the enantiomer is only 0.0098.

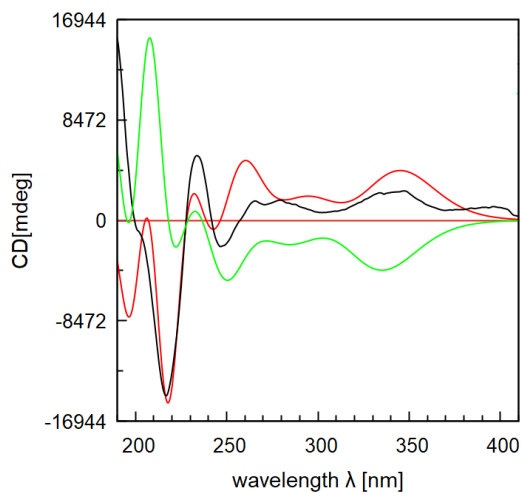


Figure B22. Positive ion HRESIMSⁿ spectra of purpurascenine B (**4.2**).

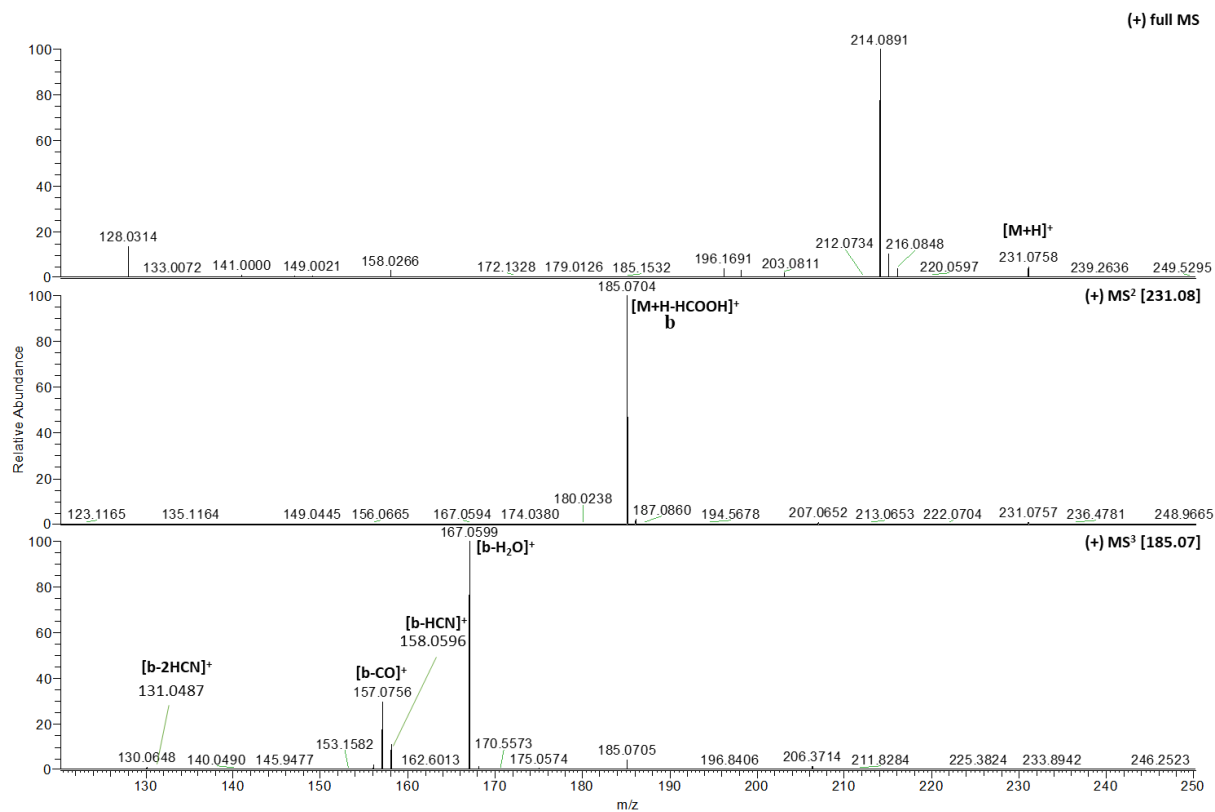


Figure B23. ^1H NMR spectrum (600 MHz, CD_3OD) of purpurascenine B (**4.2**).

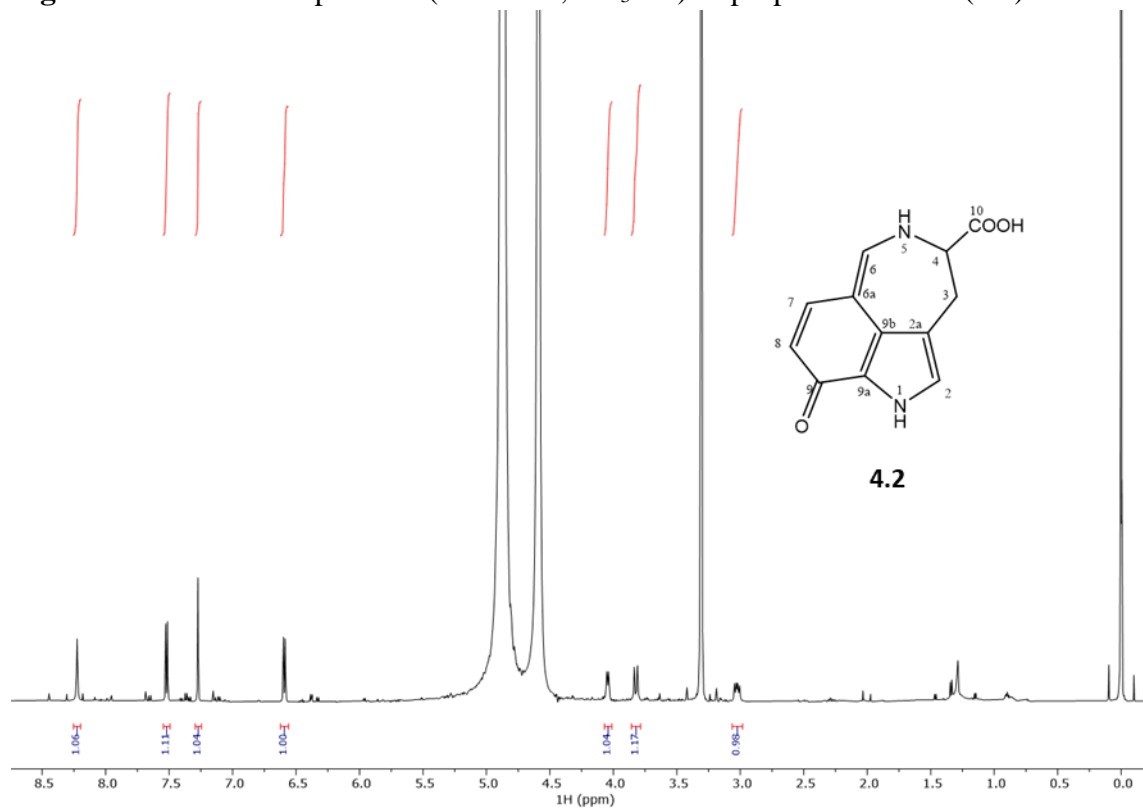


Figure B24. HSQC spectrum (600 MHz, CD_3OD) of purpurascenine B (**4.2**).

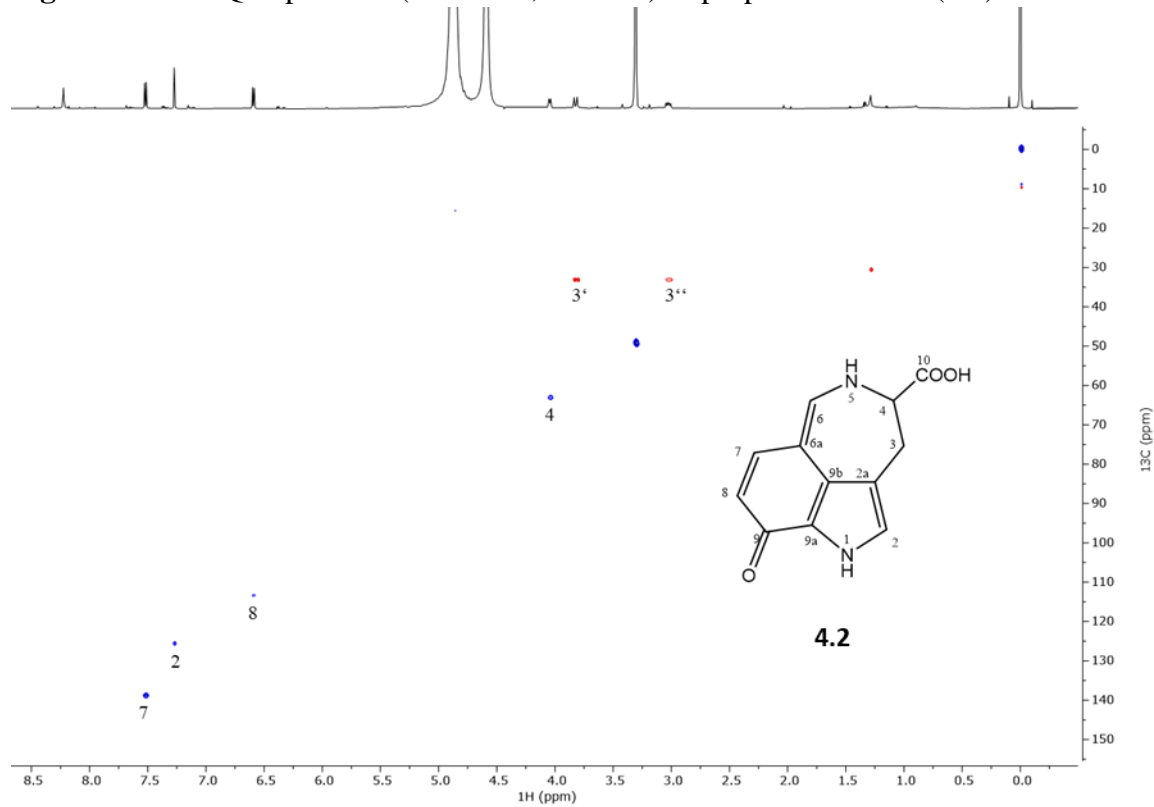


Figure B25. HMBC spectrum (600 MHz, CD₃OD) of purpurascenine B (**4.2**).

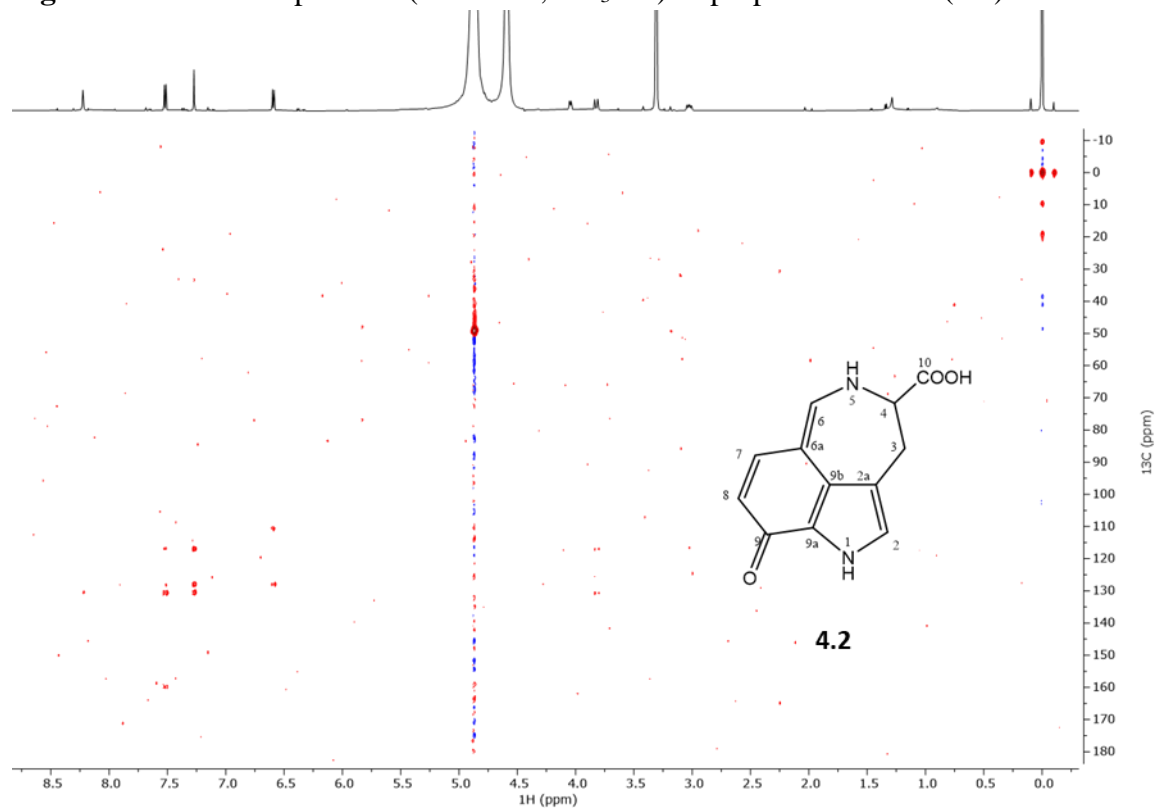


Figure S26. TOCSY spectrum (600 MHz, CD₃OD) of purpurascenine B (**4.2**).

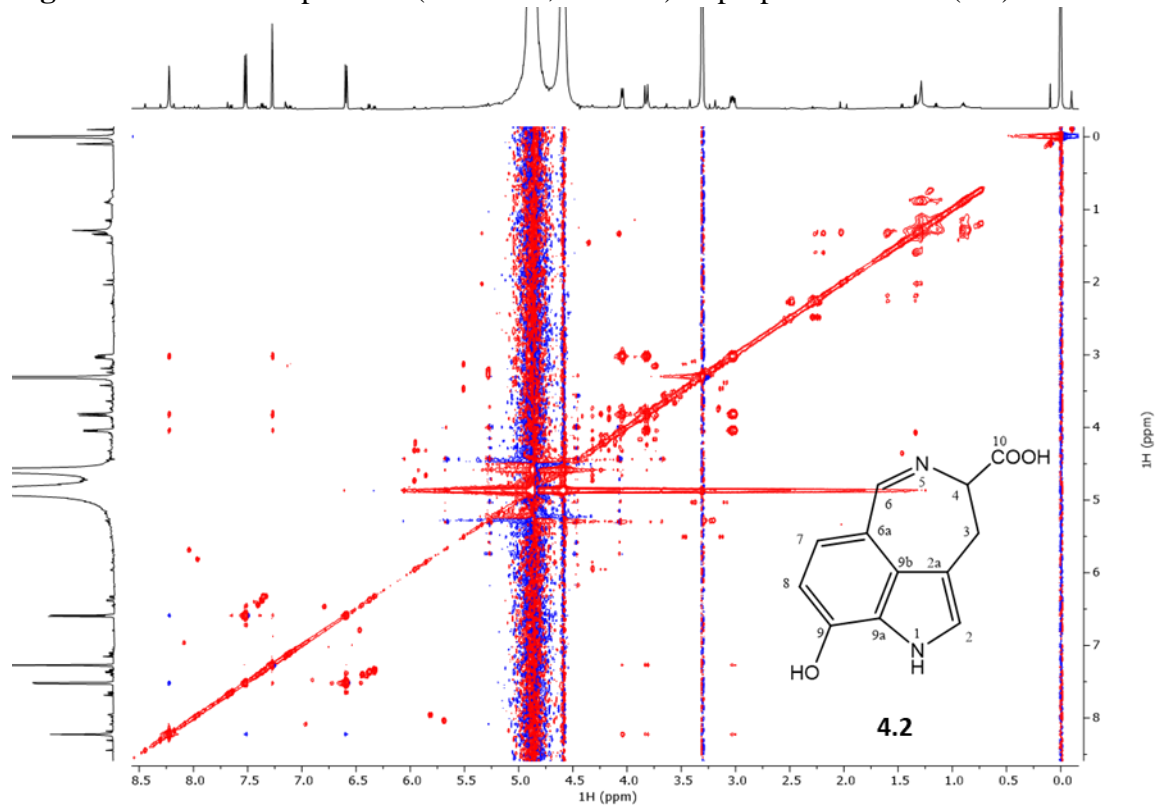


Figure B27. UV spectrum (MeOH) of purpurascenine B (**4.2**).

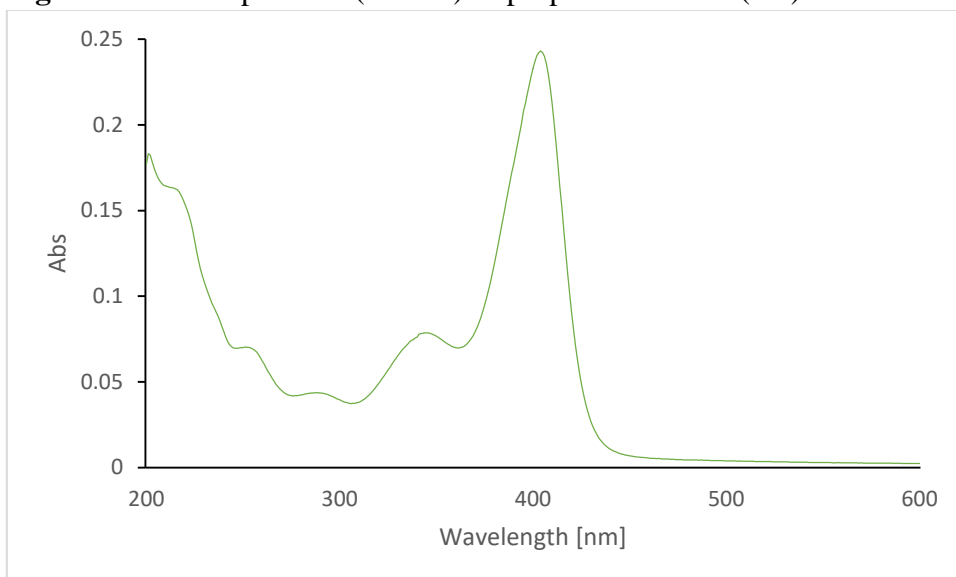


Figure B28. Calculated CD spectra of 4*R* (green) and 4*S* (red), compared with the experimental spectrum (black) of purpurascenine B (**4.2**). The best similarity factor $S=0.7451$ was found for $\sigma=0.27$ eV and a shift of -11 nm. The similarity factor for the enantiomer is only 0.0792.

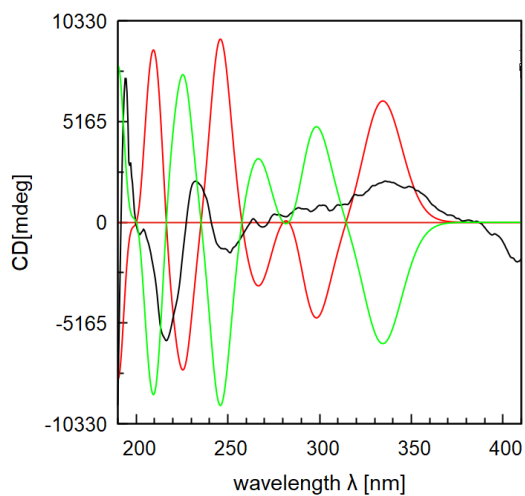


Figure B29. Positive ion HRESIMSⁿ spectra of purpurascenine C (**4.3**).

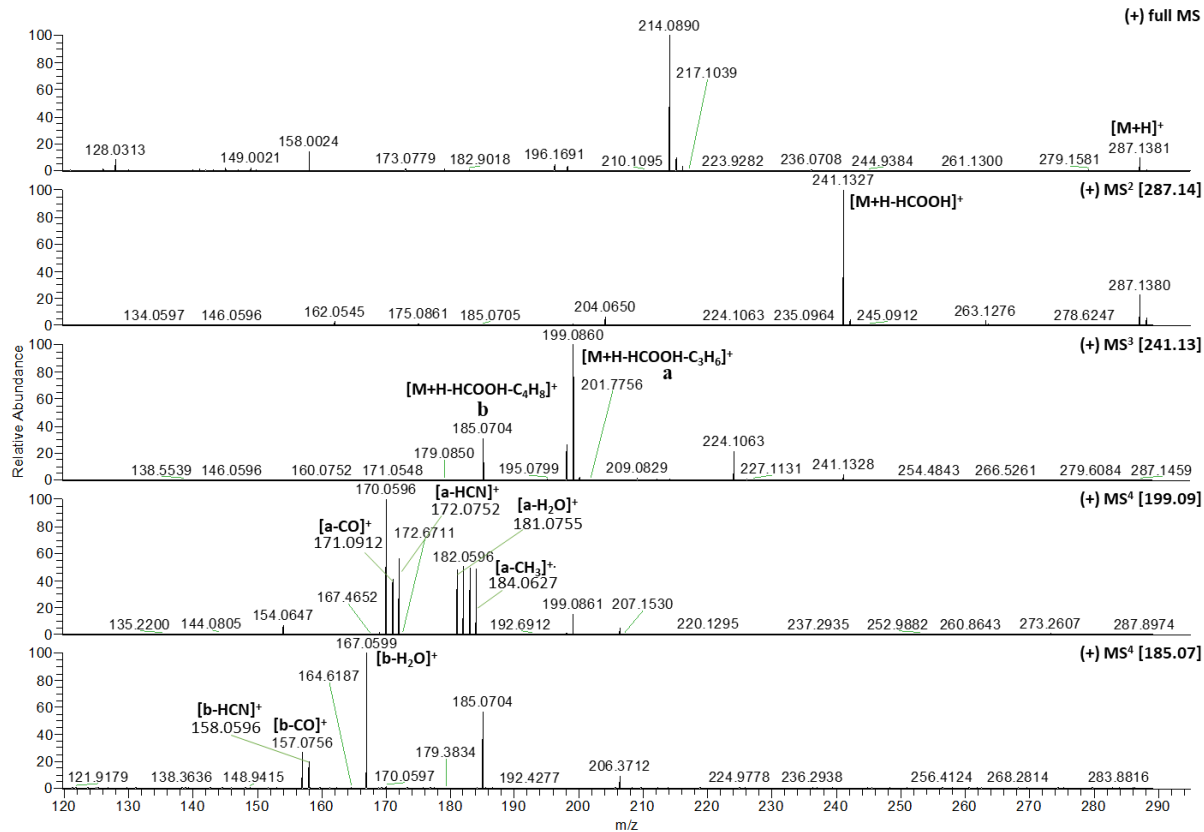


Figure B30. ^1H NMR spectrum (600 MHz, CD_3OD) of purpurascenine C (**4.3**).

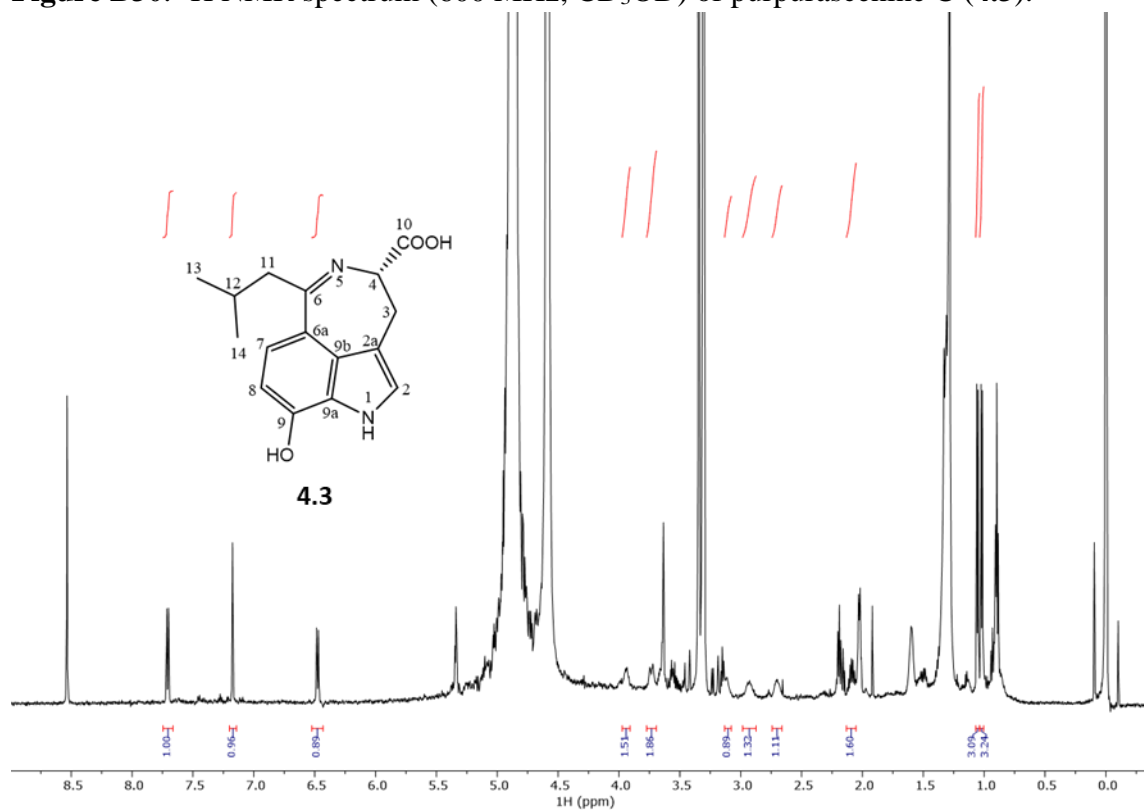


Figure B30. ^{13}C NMR spectrum (150 MHz, CD_3OD) of purpurascenine C (**4.3**).

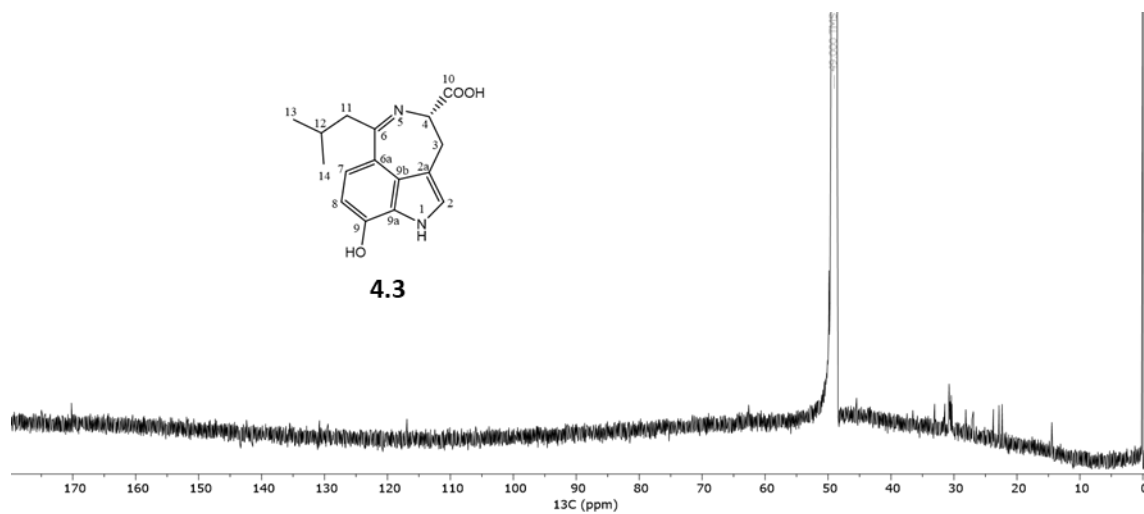


Figure B31. HSQC spectrum (600 MHz, CD₃OD) of purpurascenine C (**4.3**).

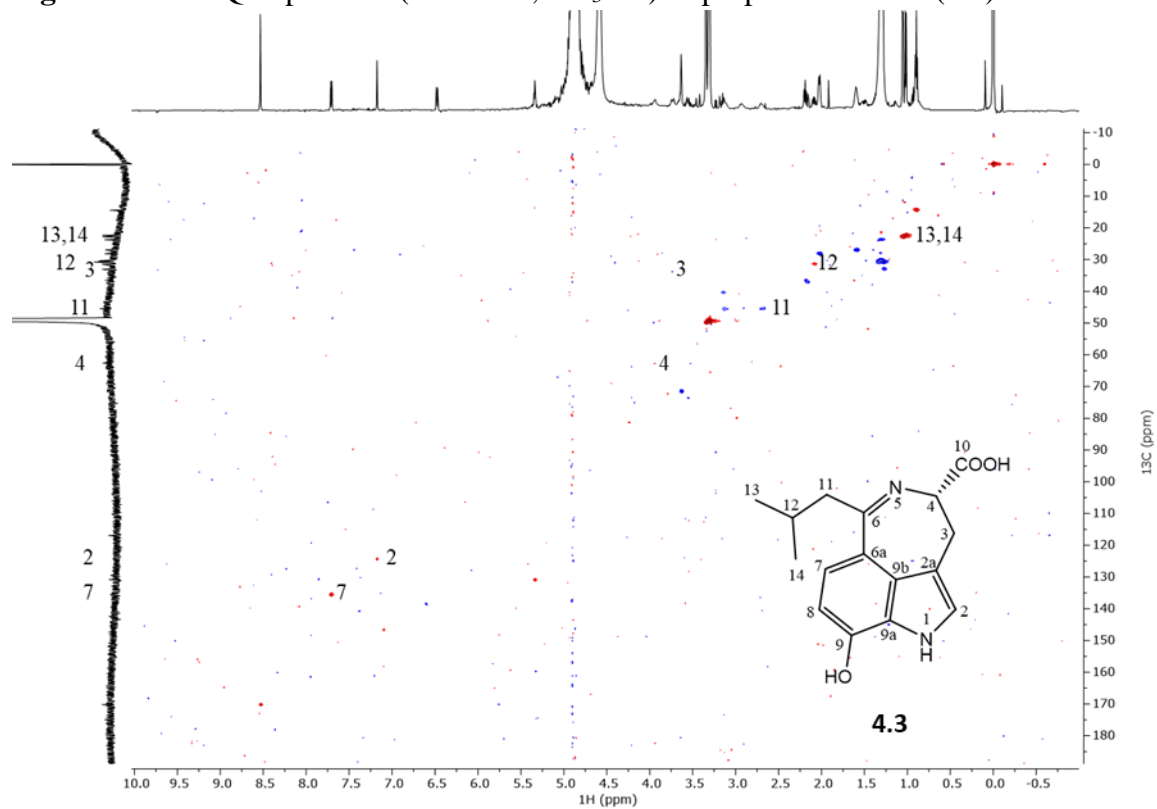


Figure B32. HMBC spectrum (600 MHz, CD₃OD) of purpurascenine C (**4.3**).

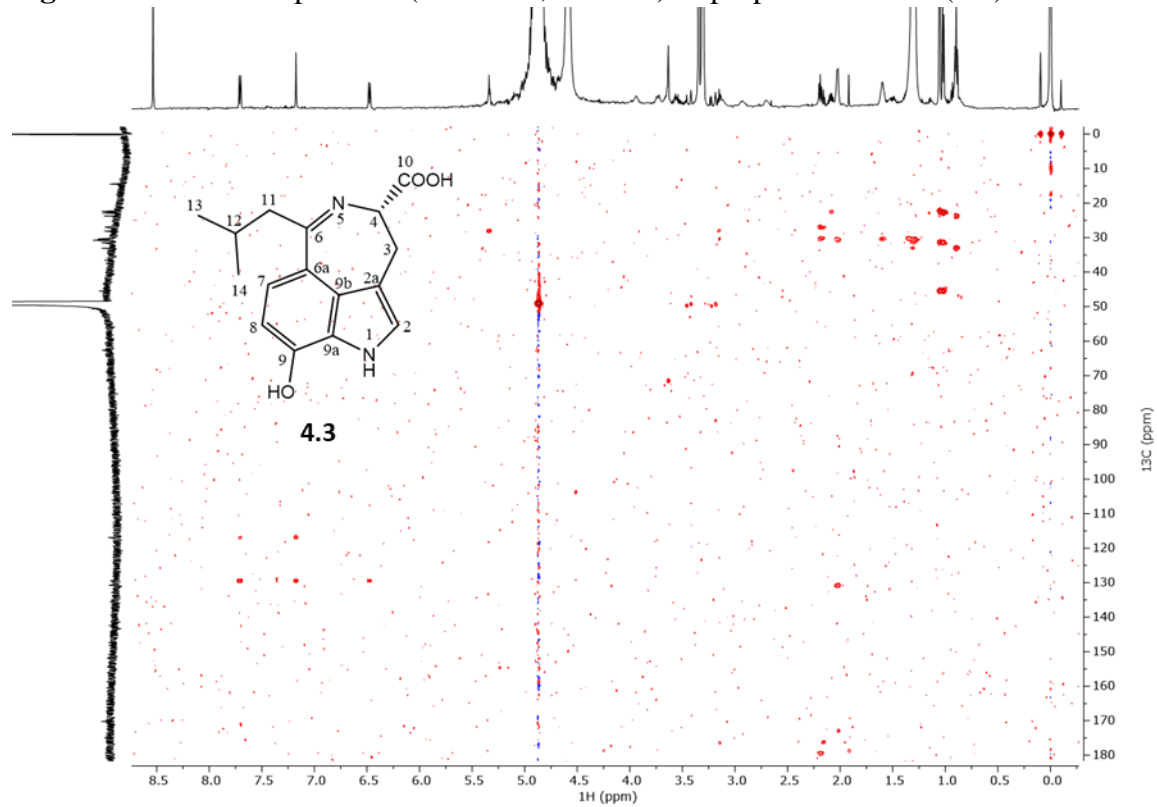


Figure B33. COSY spectrum (600 MHz, CD₃OD) of purpurascenine C (**4.3**).

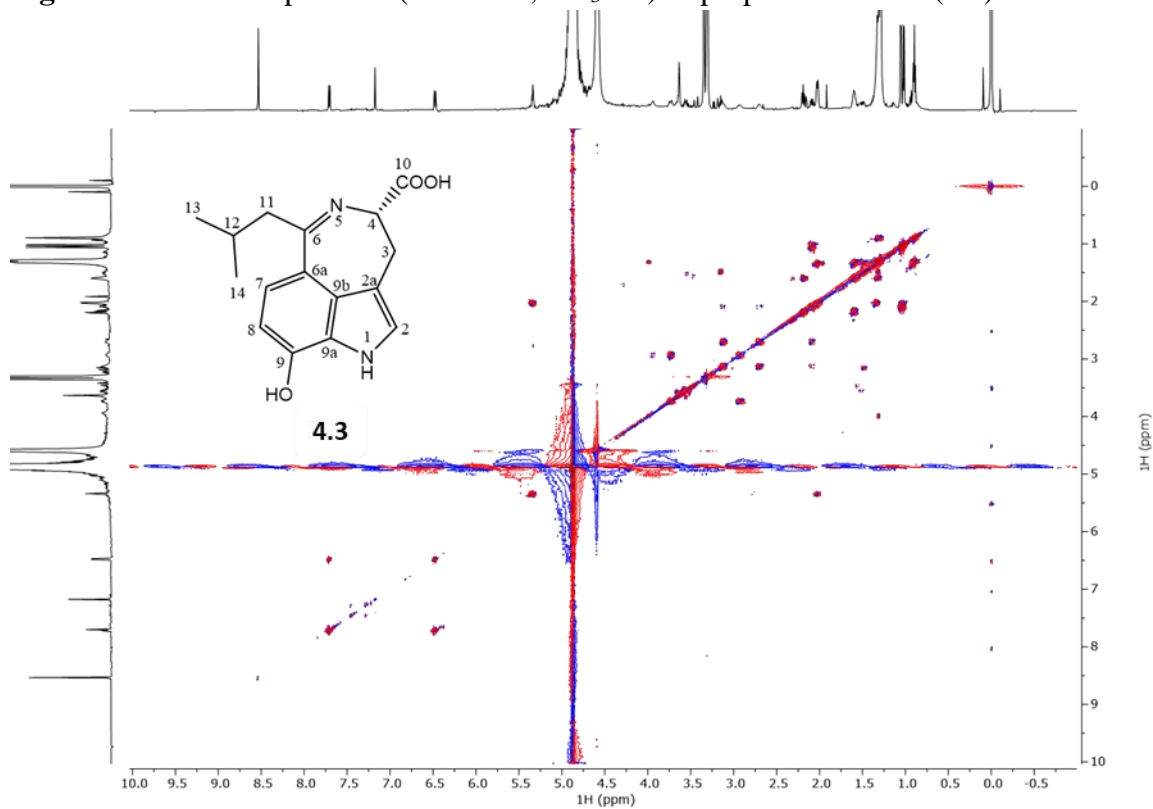


Figure B34. TOCSY spectrum (600 MHz, CD₃OD) of purpurascenine C (**4.3**).

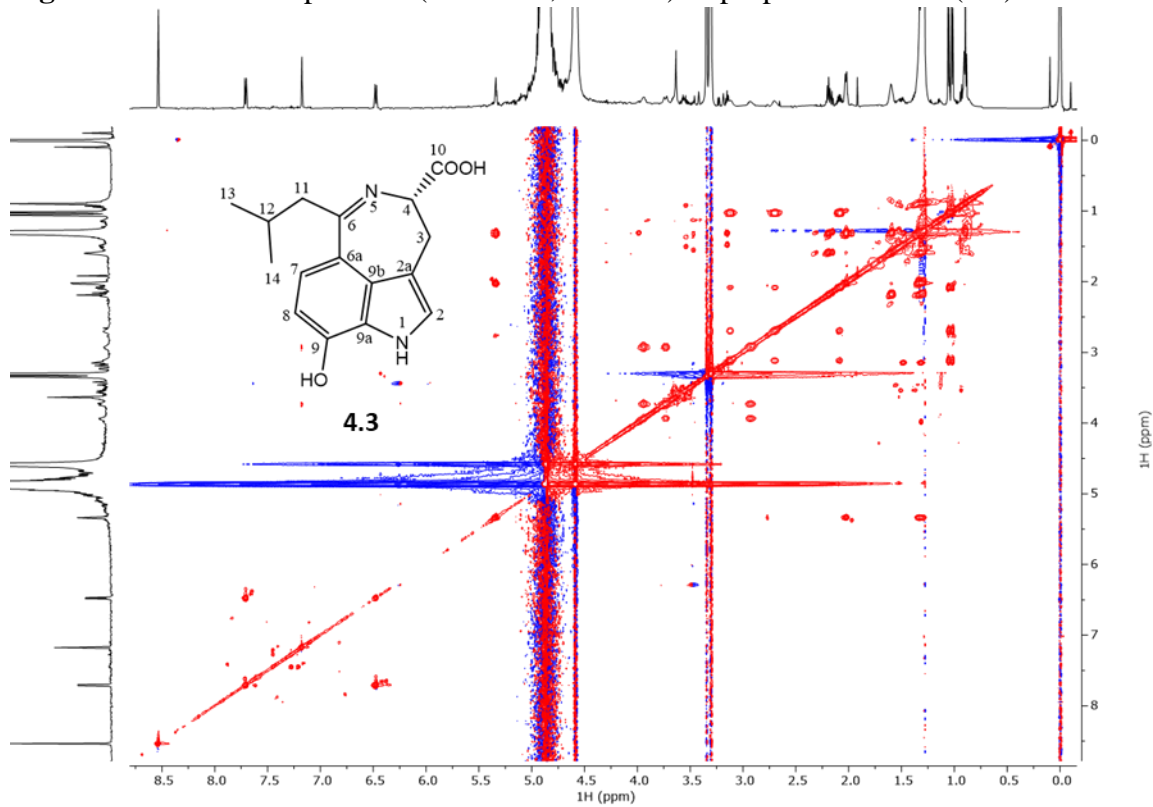


Figure B35. UV spectrum (MeOH) of purpurascenine C (**4.3**).

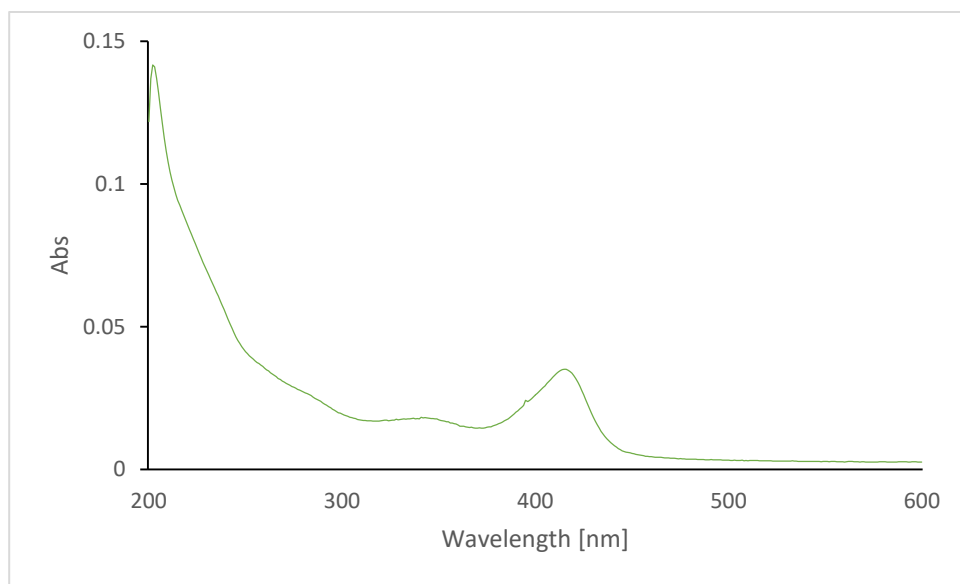


Figure B36. Calculated CD spectra of 4*R* (green) and 4*S* (red), compared with the experimental spectrum (black) of purpurascenine C (**4.3**). The best similarity factor $S = 0.6336$ was found for $\sigma = 0.25$ eV and a shift of -15 nm. The similarity factor for the enantiomer is only 0.0095.

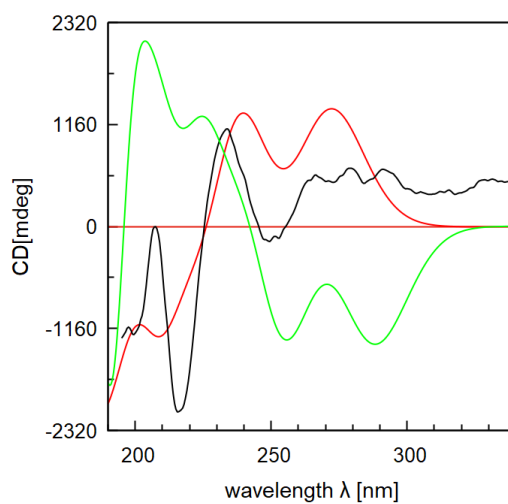
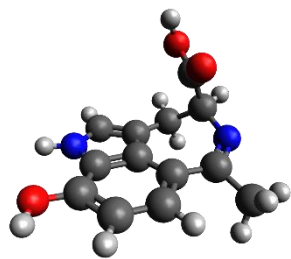
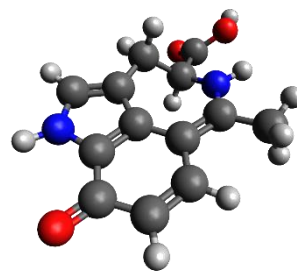


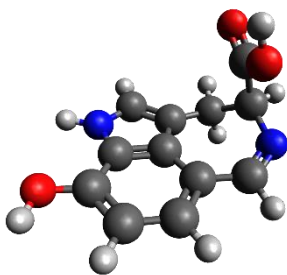
Figure B37. Energy optimized structures of compounds **4.1-4.4** and **4.1a**.



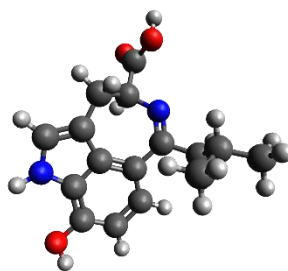
4.1



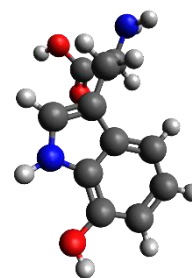
4.1a



4.2



4.3



4.4

Figure B38. Positive ion HRESIMS spectrum of 7-hydroxytryptophan (**4.4**).

THL020_C4M_6P5_fullScan#40 RT: 0.28 AV: 1 NL: 2.22E7
T: FTMS + p ESI Full ms [100.00-2000.00]

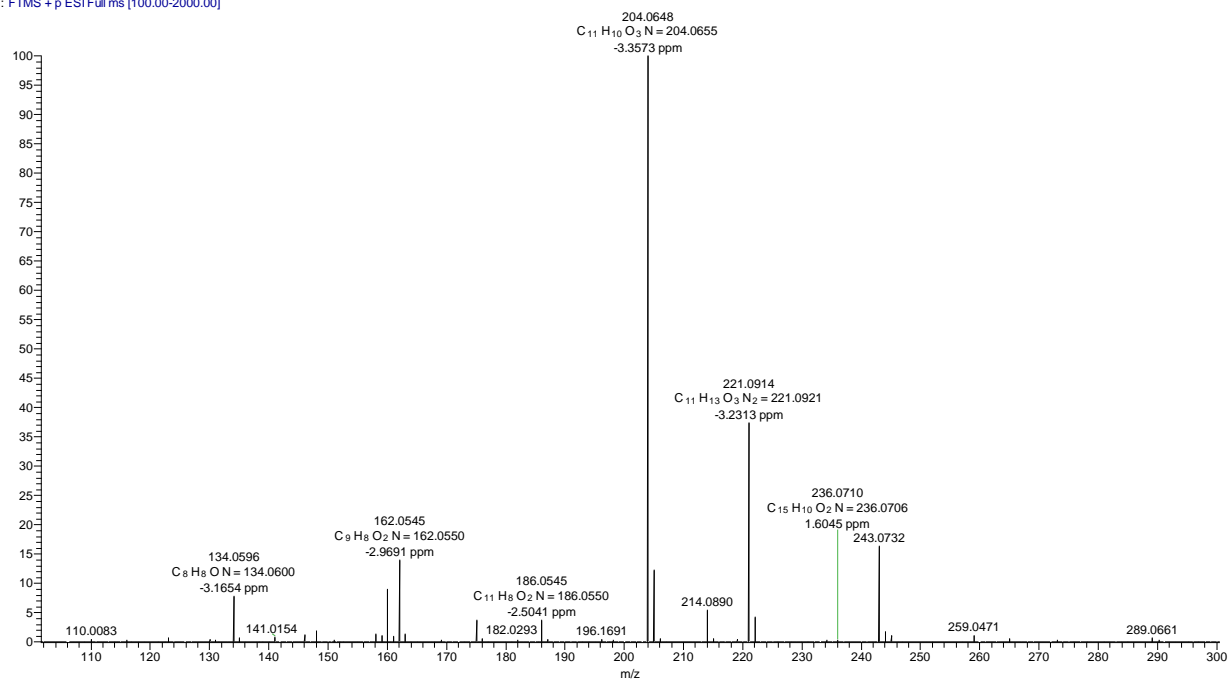


Figure B39. ^1H NMR spectrum (600 MHz, D_2O) of 7-hydroxytryptophan (**4.4**).

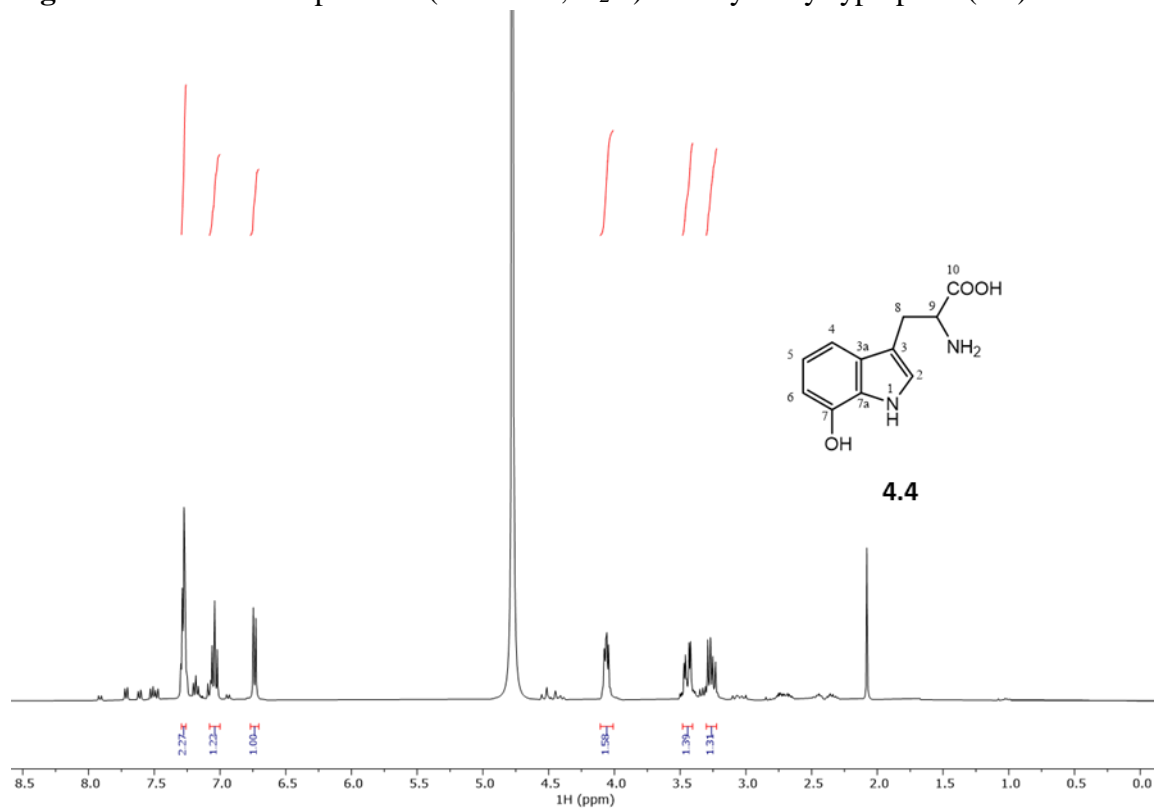


Figure B40. ^{13}C NMR spectrum (150 MHz, D_2O) of 7-hydroxytryptophan (**4.4**).

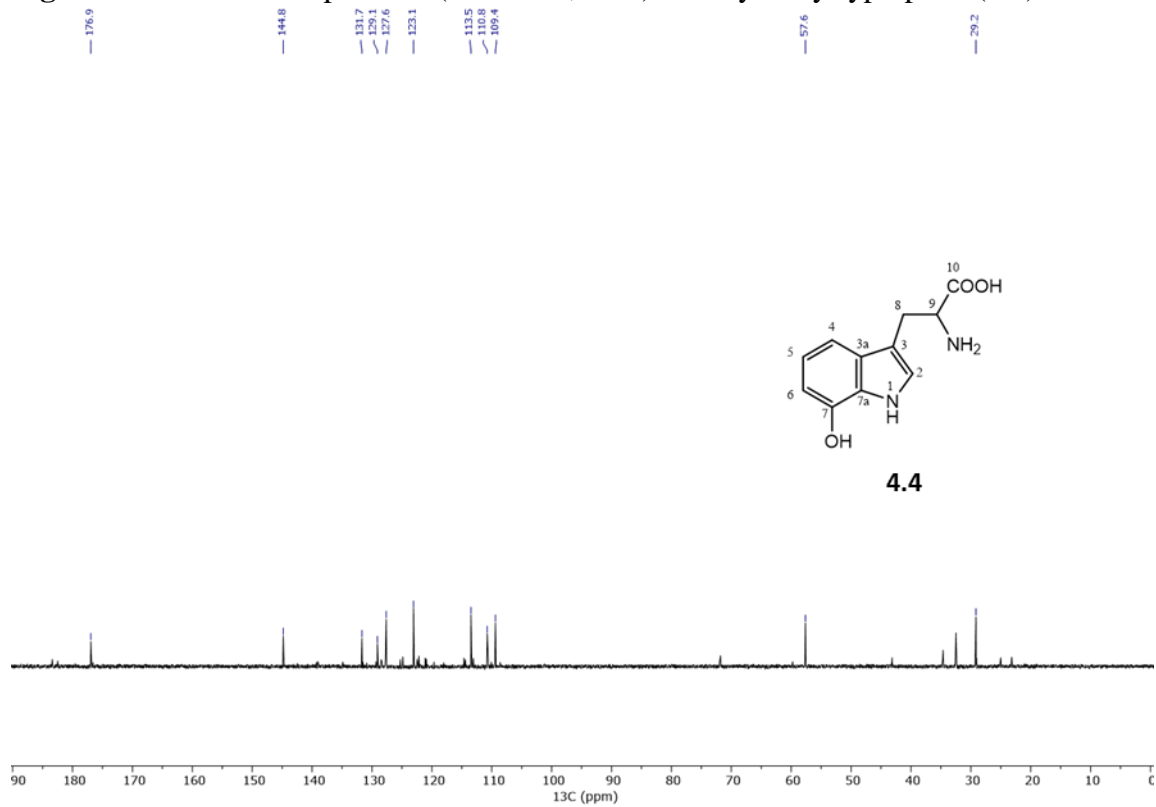


Figure B41. HSQC spectrum of 7-hydroxytryptophan (**4.4**).

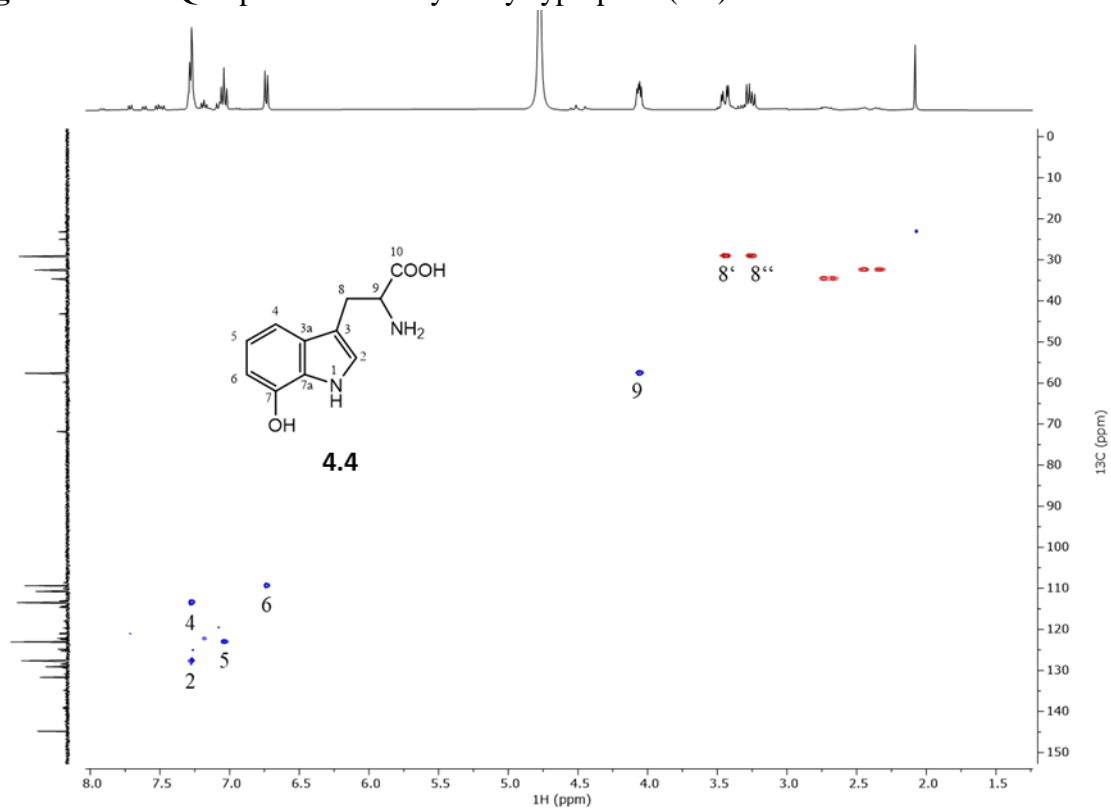


Figure B42. HMBC spectrum of 7-hydroxytryptophan (**4.4**).

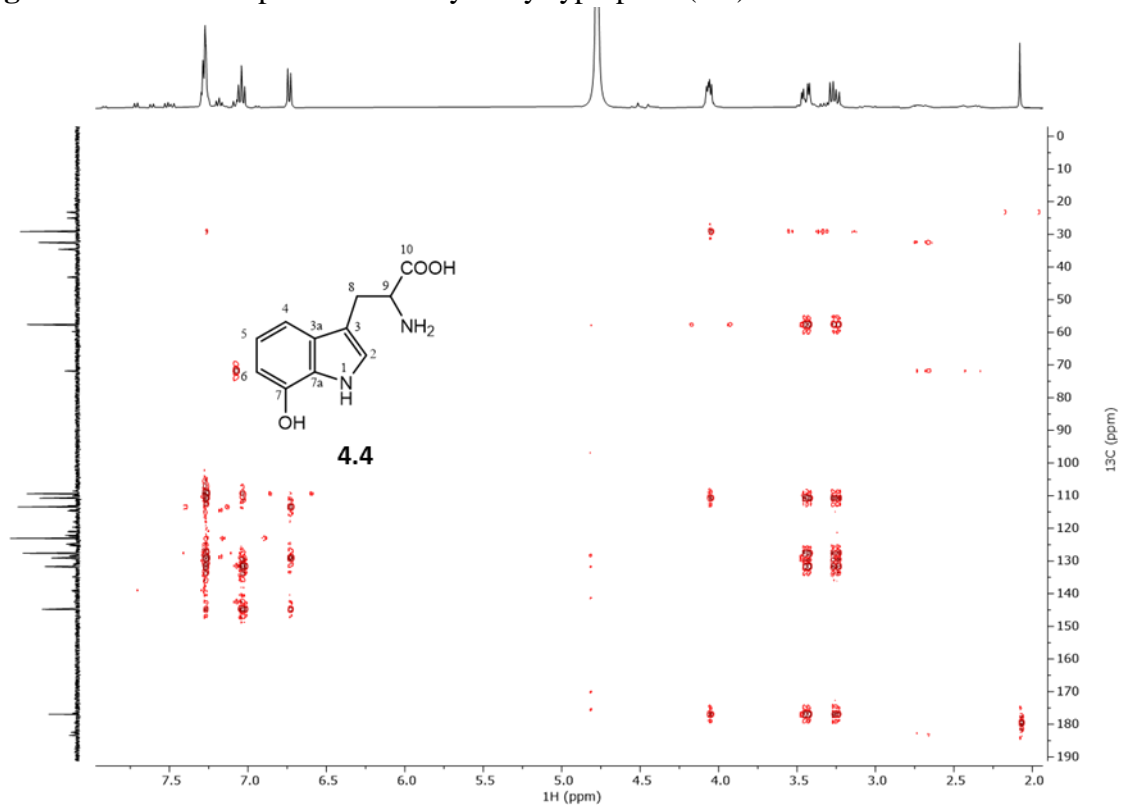


Figure B43. TOCSY spectrum of 7-hydroxytryptophan (**4.4**).

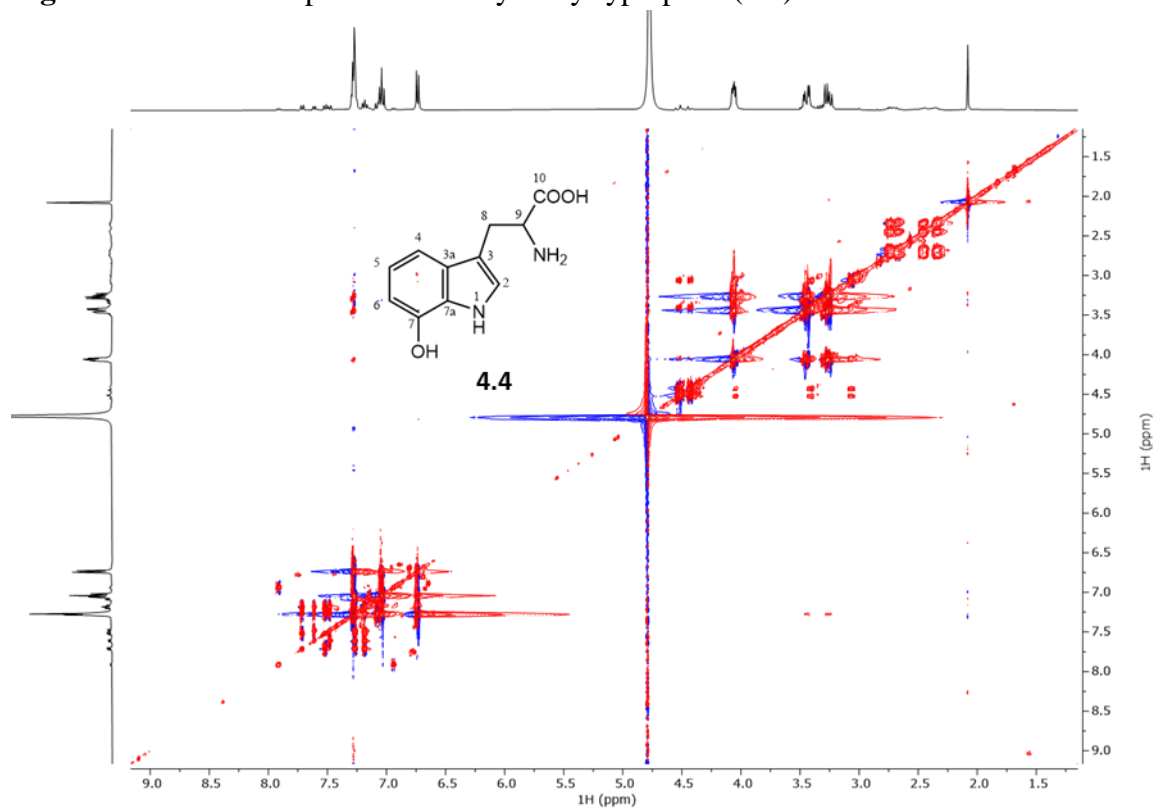


Figure B44. UV spectrum (H₂O) of 7-hydroxytryptophan (**4.4**).

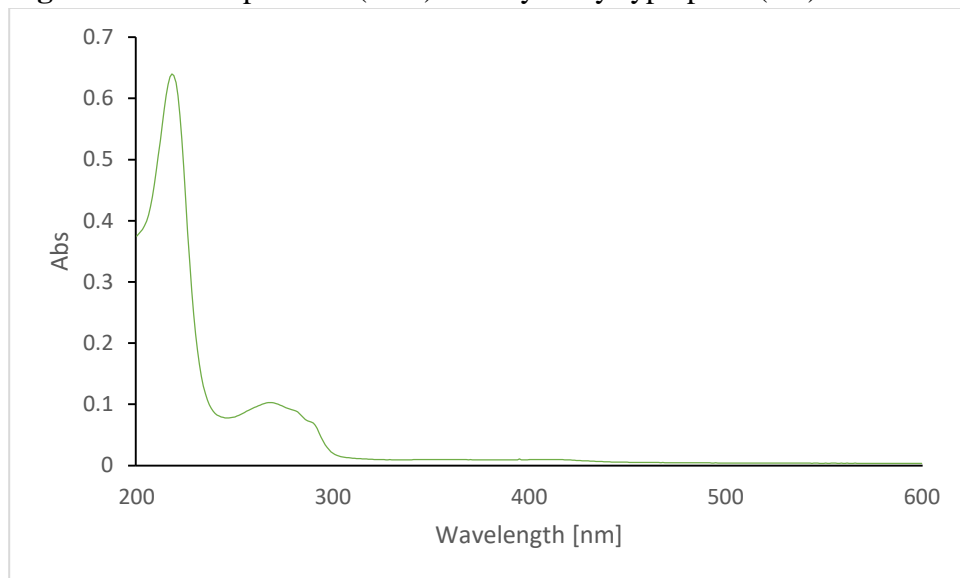


Figure B45. Calculated CD spectra of 1*R* (green) and 1*S* (red), compared with the experimental spectrum (black) of 7-hydroxytryptophan (**4.4**). The best similarity factor $S=0.9561$ was found for $\sigma=0.29$ eV and a shift of -3 nm for the *S*-isomer. The similarity factor for the enantiomer is only 0.0098.

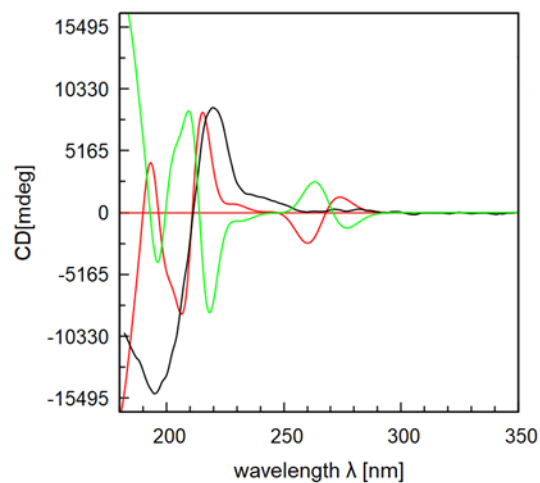


Figure B46. Positive ion HRESIMS spectrum of adenosine (4.5).

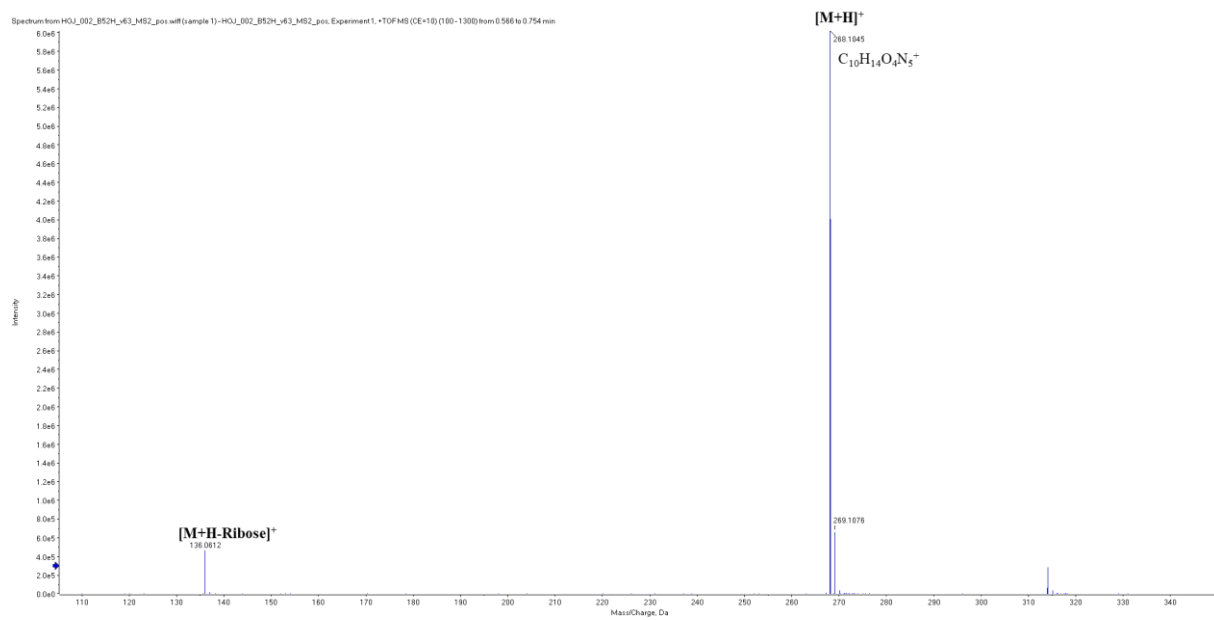


Figure B47. ^1H NMR spectrum (600 MHz, $\text{DMSO-}d_6$) of adenosine (**4.5**).

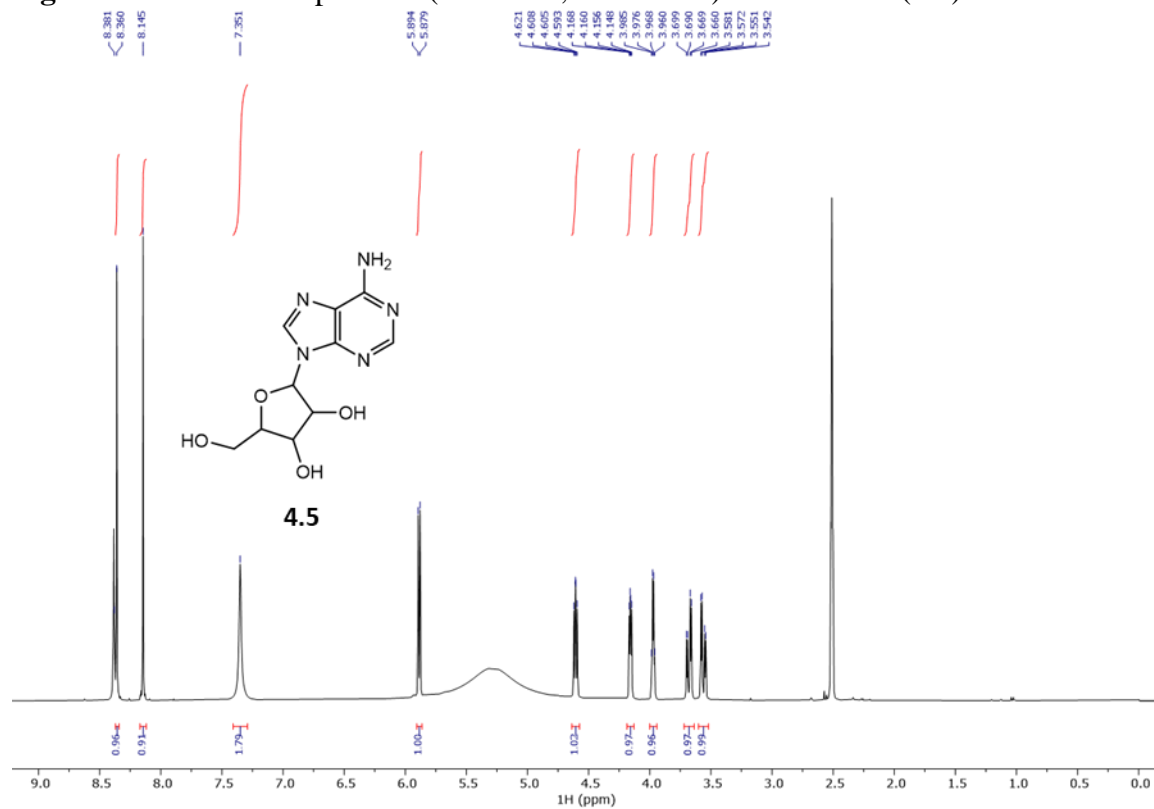


Figure B48. ^{13}C NMR spectrum (150 MHz, $\text{DMSO-}d_6$) of adenosine (**4.5**).

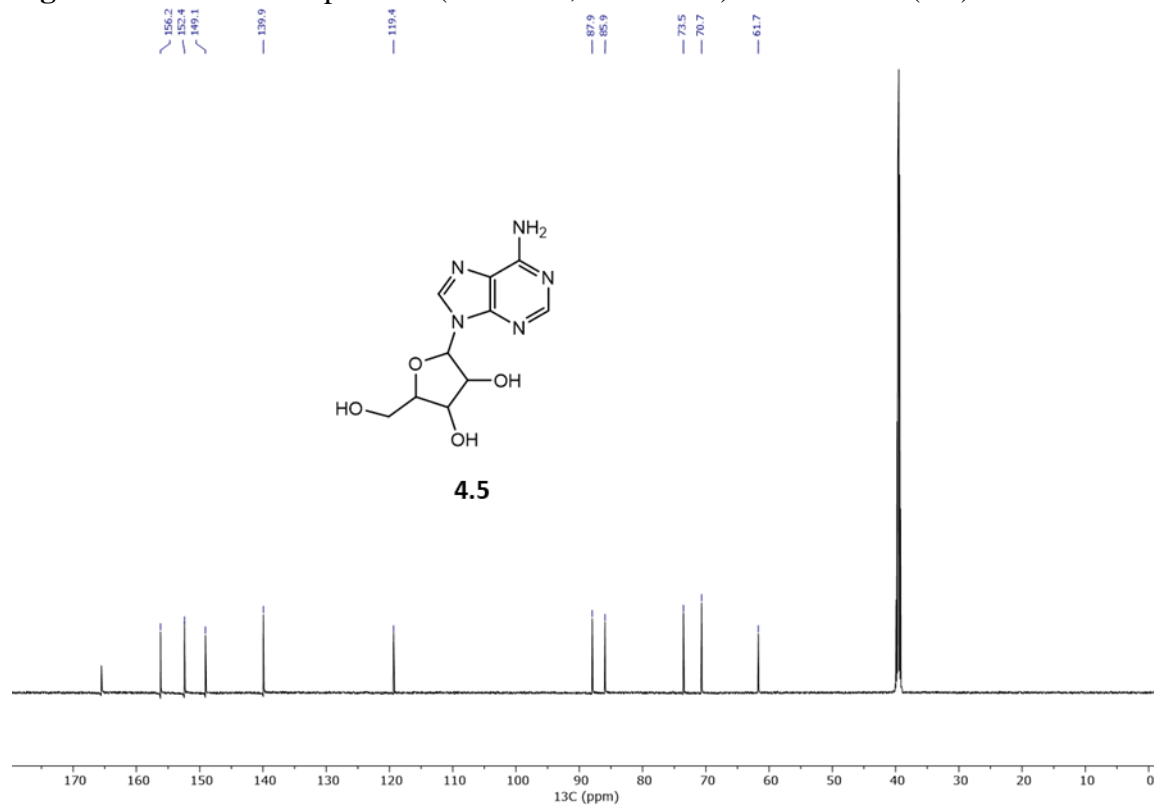


Figure B49. Positive ion HRESIMS spectrum of riboflavin (**4.6**).

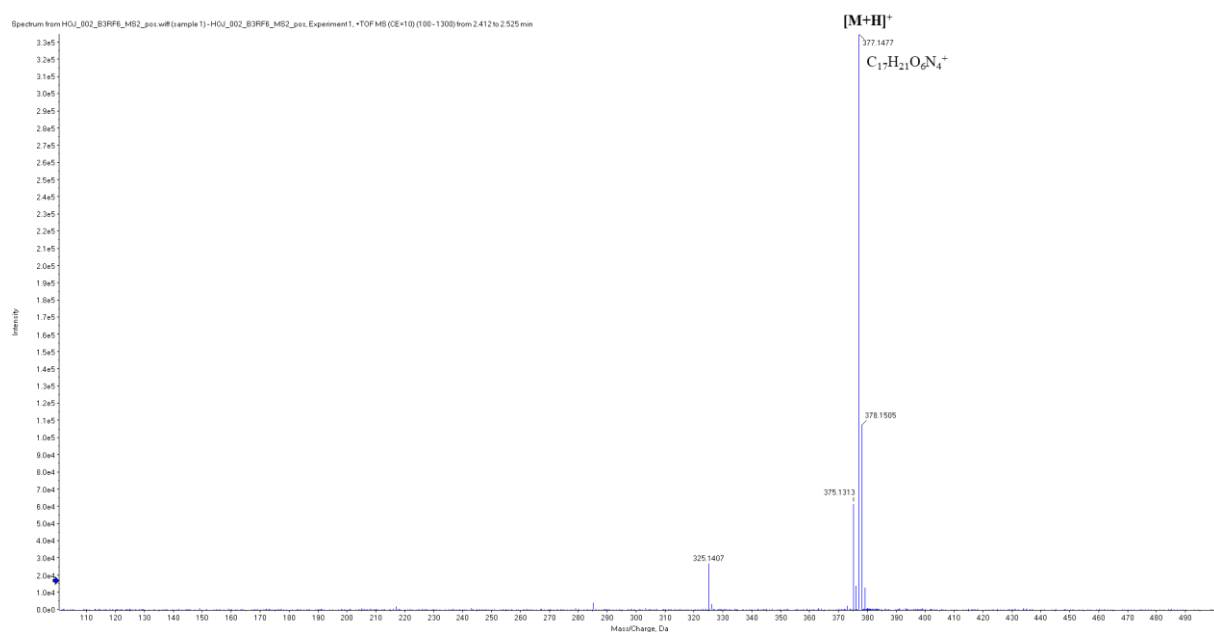


Figure B50. ^1H NMR spectrum (600 MHz, CD_3OD) of riboflavin (**4.6**).

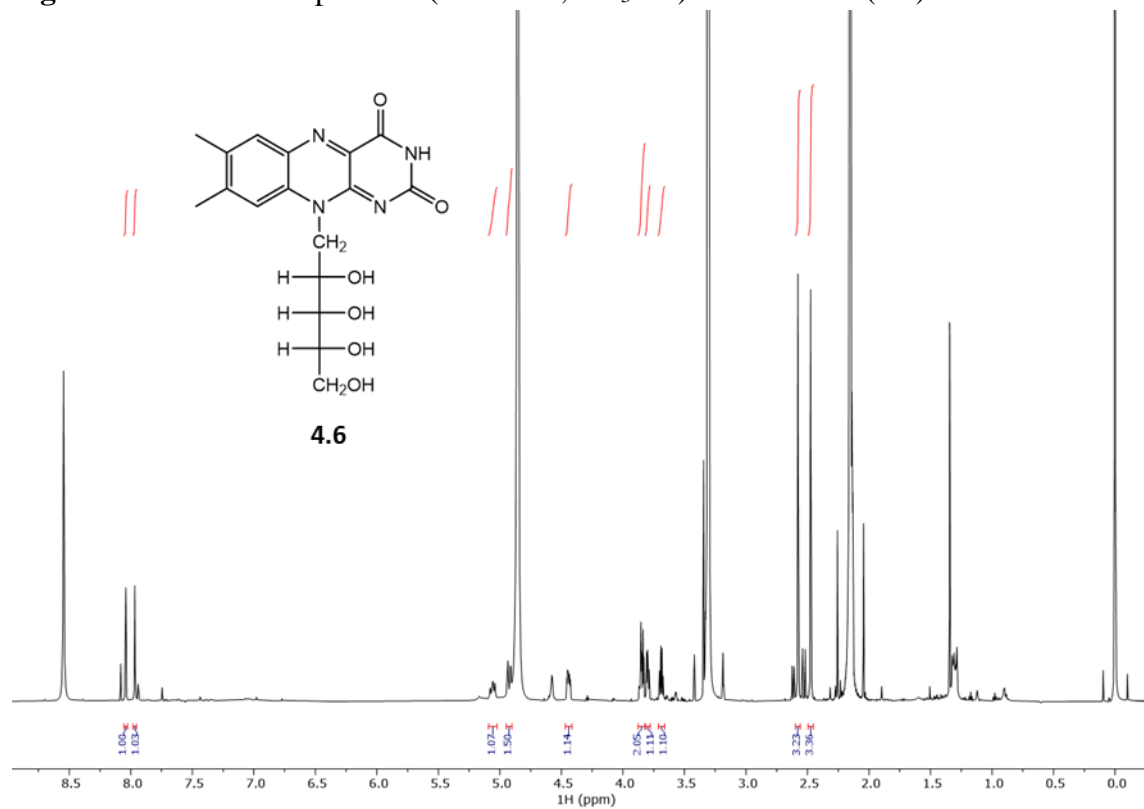


Figure B51. HSQC spectrum (CD_3OD) of riboflavin (**4.6**).

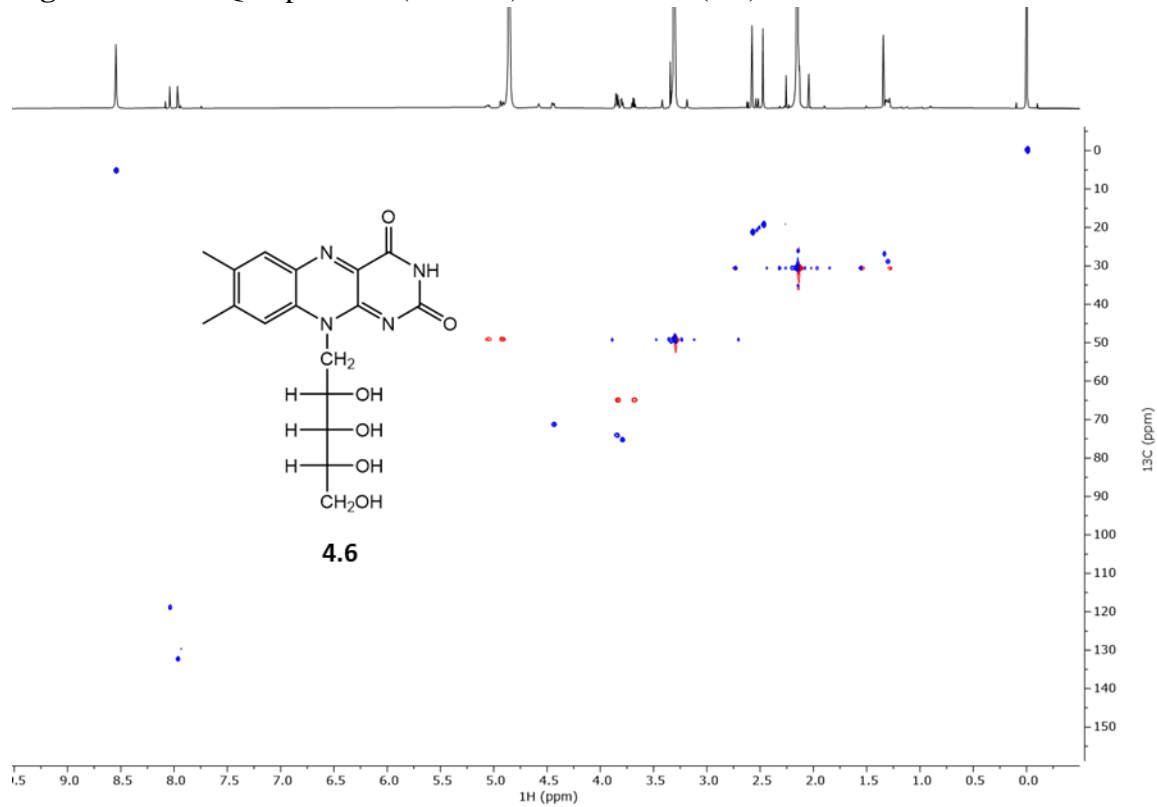
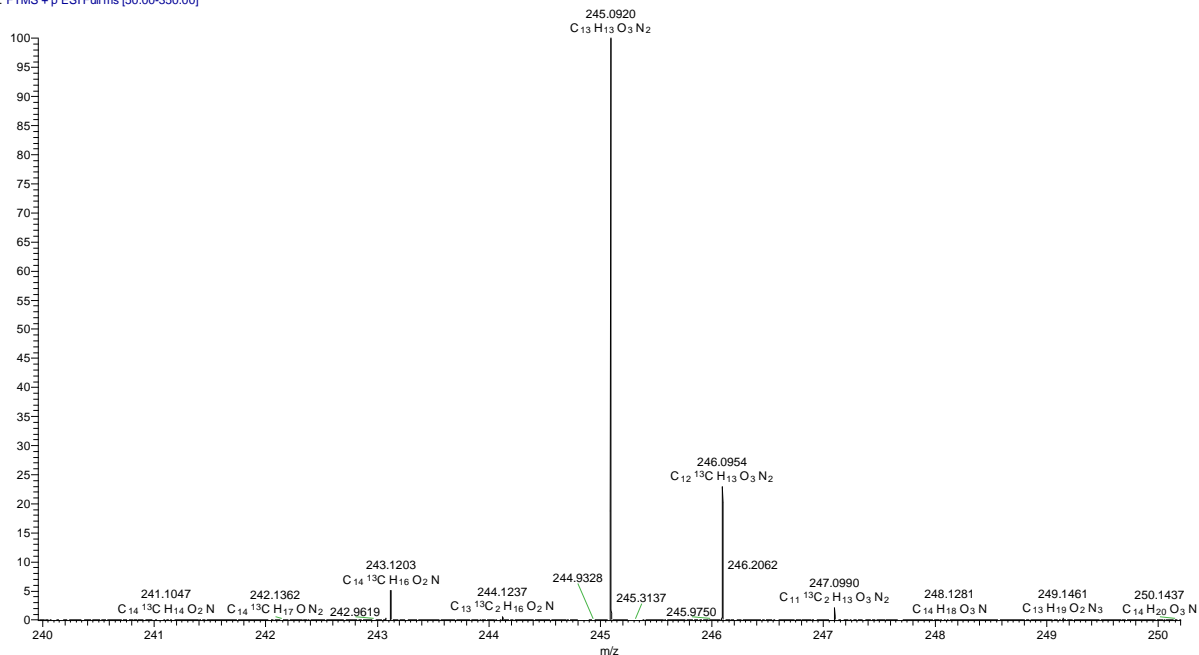


Figure B52. Positive ion HRESIMS spectrum of purpurascenine A (**4.1***) fed [3-¹³C]-pyruvate.

THL021_B1E_6P5_fullMS_1#1-124 RT: 0.00-0.51 AV: 124 NL: 1.65E6
T: FTMS + p ESI Full ms [50.00-350.00]



THL021_B1E_6P5_fullMS_1#1-124 RT: 0.00-0.51 AV: 124
T: FTMS + p ESI Full ms [50.00-350.00]
m/z = 239.9569-250.2036

m/z	Intensity	Relative	Composition
242.9619	1087.3	0.07	
243.0764	4717.7	0.29	C ₁₃ H ₁₁ O ₃ N ₂
243.1203	88498.6	5.37	C ₁₄ ¹³ C H ₁₆ O ₂ N
244.1237	9316.4	0.56	
244.9328	1371.0	0.08	
245.0830	688.8	0.04	C ₁₁ ¹³ C ₂ H ₁₁ O ₃ N ₂
245.0920	1649292.1	100.00	C ₁₃ H ₁₃ O ₃ N ₂
245.9750	1531.1	0.09	
246.0902	9093.6	0.55	
246.0954	379277.9	23.00	C ₁₂ ¹³ C ¹³ C H ₁₃ O ₃ N ₂
247.0579	2484.3	0.15	C ₁₅ ¹³ C H ₈ O ₂ N
247.0990	35876.1	2.18	C ₁₁ ¹³ C ₂ H ₁₃ O ₃ N ₂
247.1150	2735.2	0.17	
248.1281	2574.3	0.16	C ₁₄ H ₁₈ O ₃ N
249.1461	4757.6	0.29	
250.1437	1005.8	0.06	C ₁₄ H ₂₀ O ₃ N

Figure B53. ^1H NMR spectrum (600 MHz, CD_3OD) of purpurascenine A (**4.1***) fed $[3-^{13}\text{C}]$ -pyruvate.

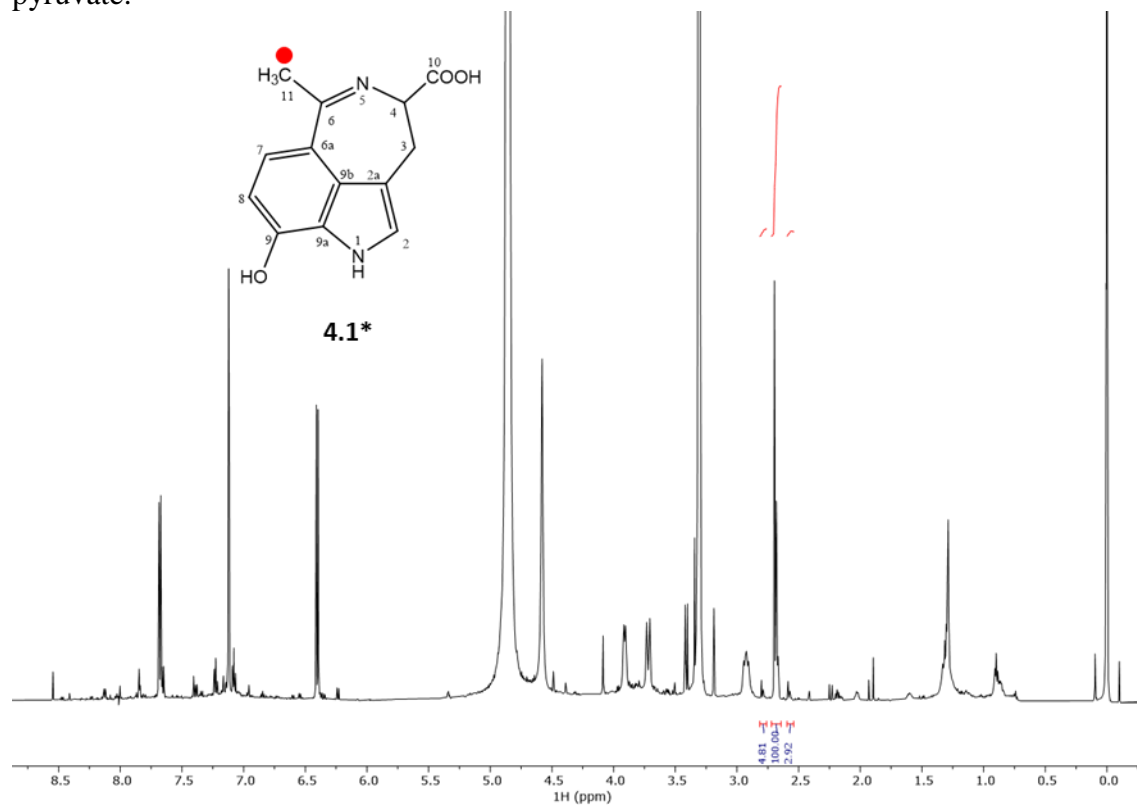


Figure B54. ^1H NMR spectrum (methyl signal) of purpurascenine A (**4.1**) fed $[3-^{13}\text{C}]$ -pyruvate.

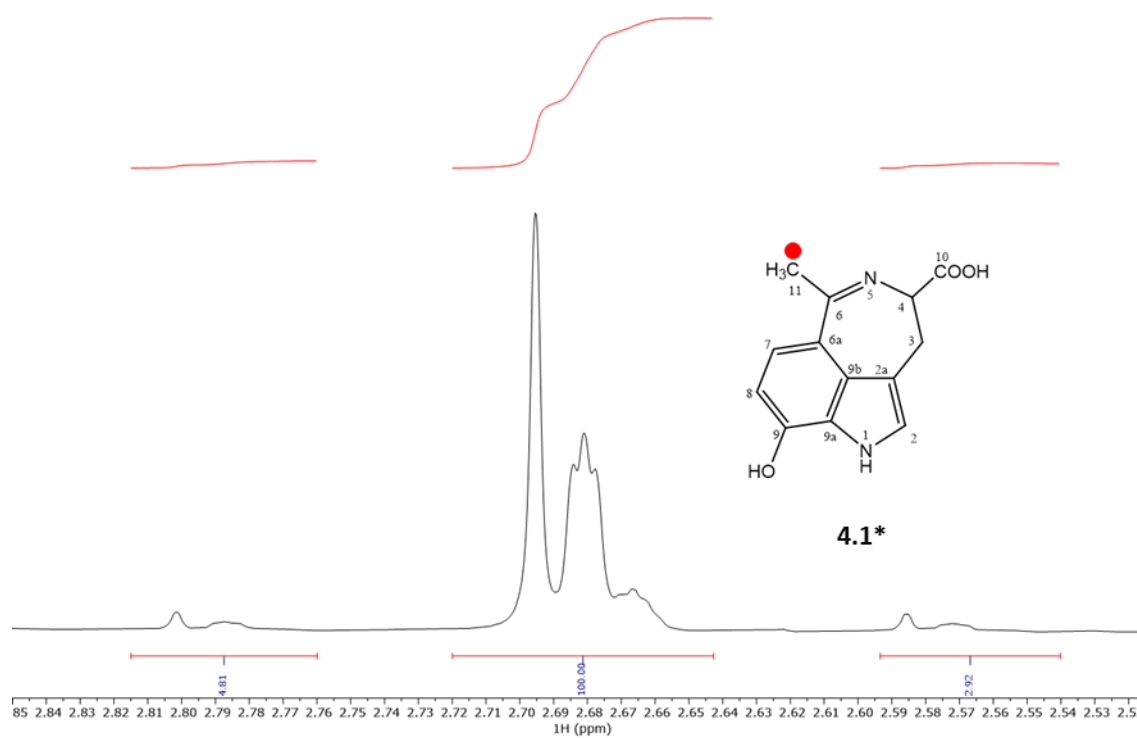


Figure B55. HSQC spectrum (CD₃OD) of purpurascenine A (**4.1***) fed [3-¹³C*]-pyruvate.

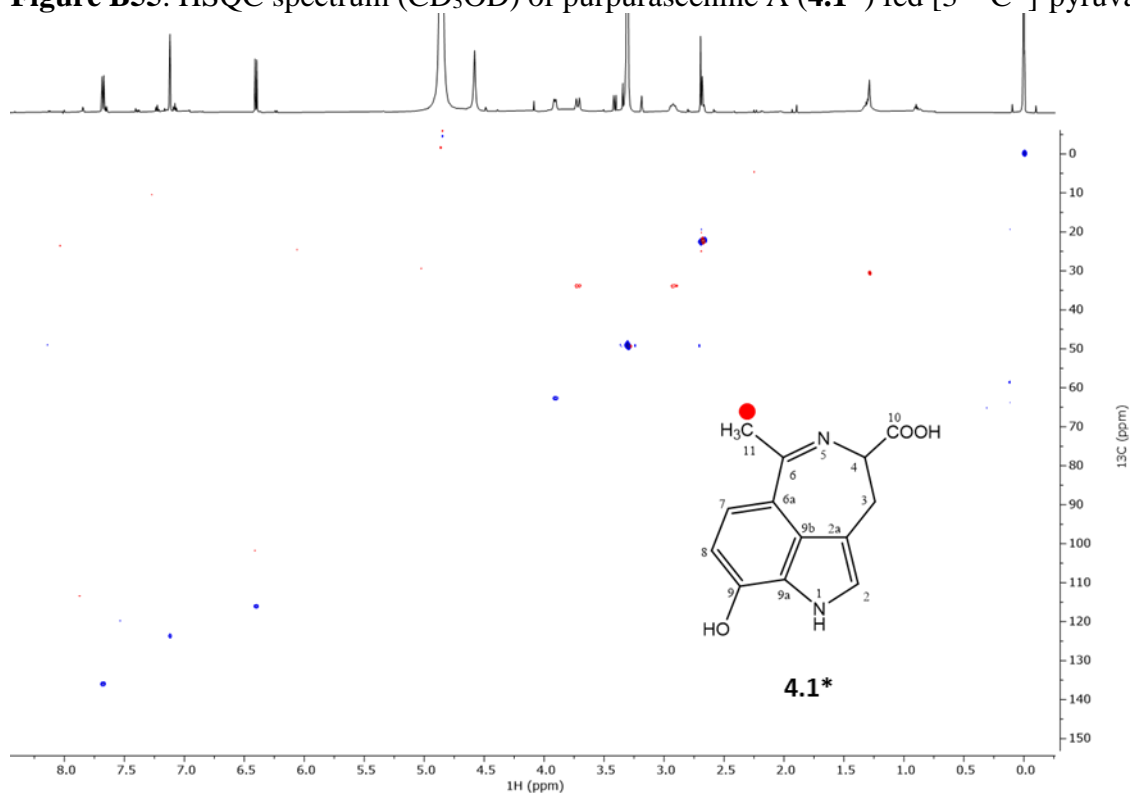


Figure B56. HSQC spectrum without ¹³C decoupling (CD₃OD) of purpurascenine A (**4.1***) fed [3-¹³C]-pyruvate.

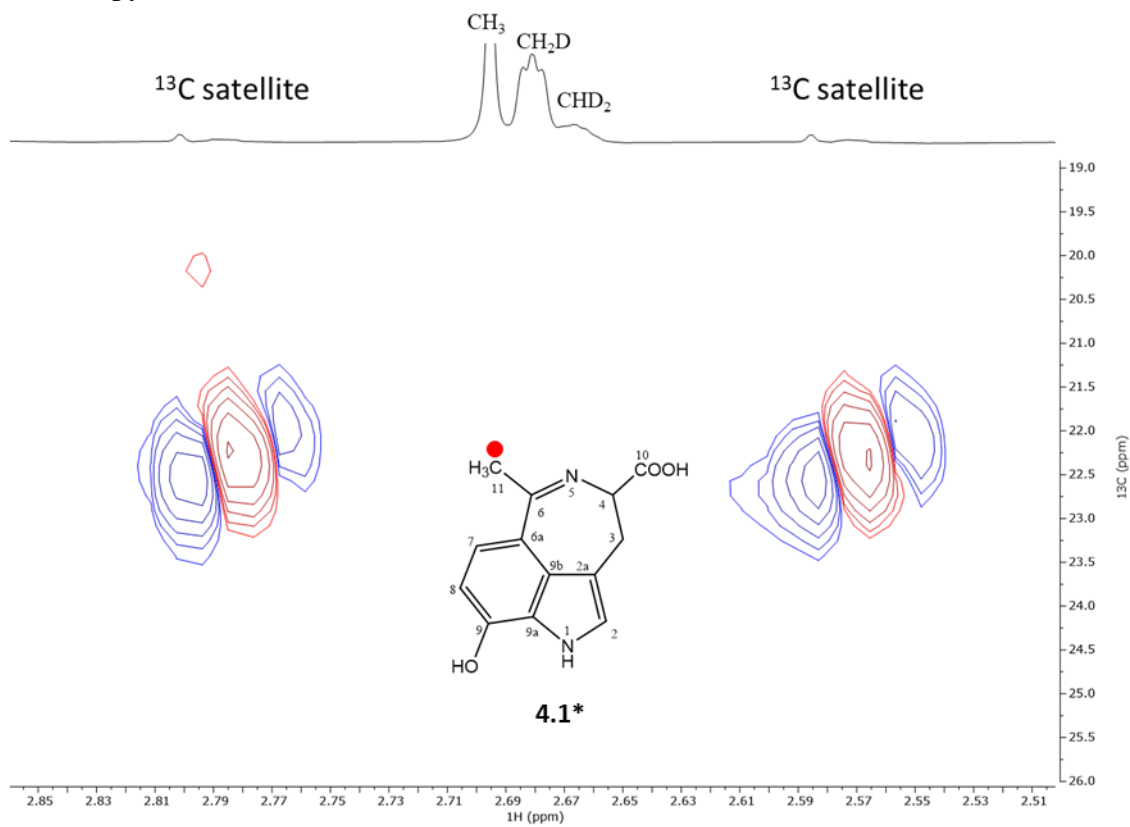


Figure B57. HMBC spectrum (CD₃OD) of purpurascenine A (**4.1***) fed [3-¹³C]-pyruvate.

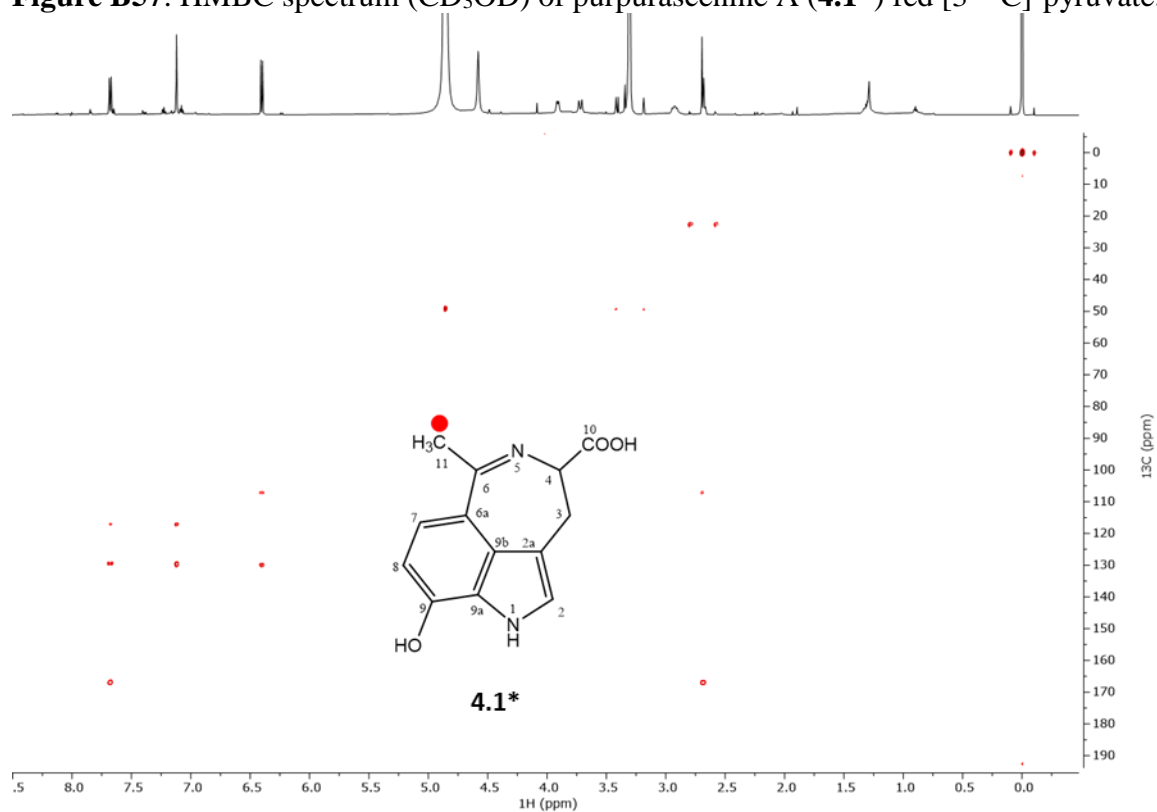


Figure B58. ¹H NMR spectrum of purpurascenine A (**4.1***) fed [3-¹³C]-pyruvate 5 months after the deuterium exchange was observed.

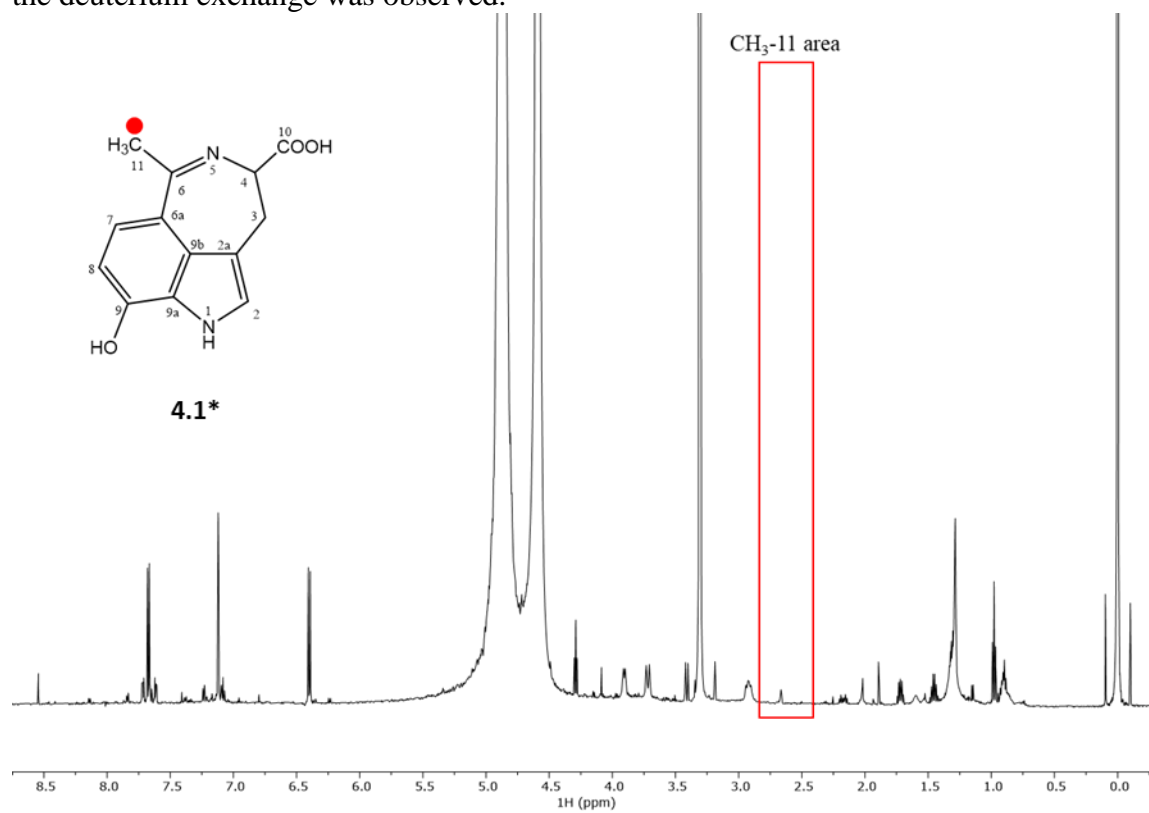
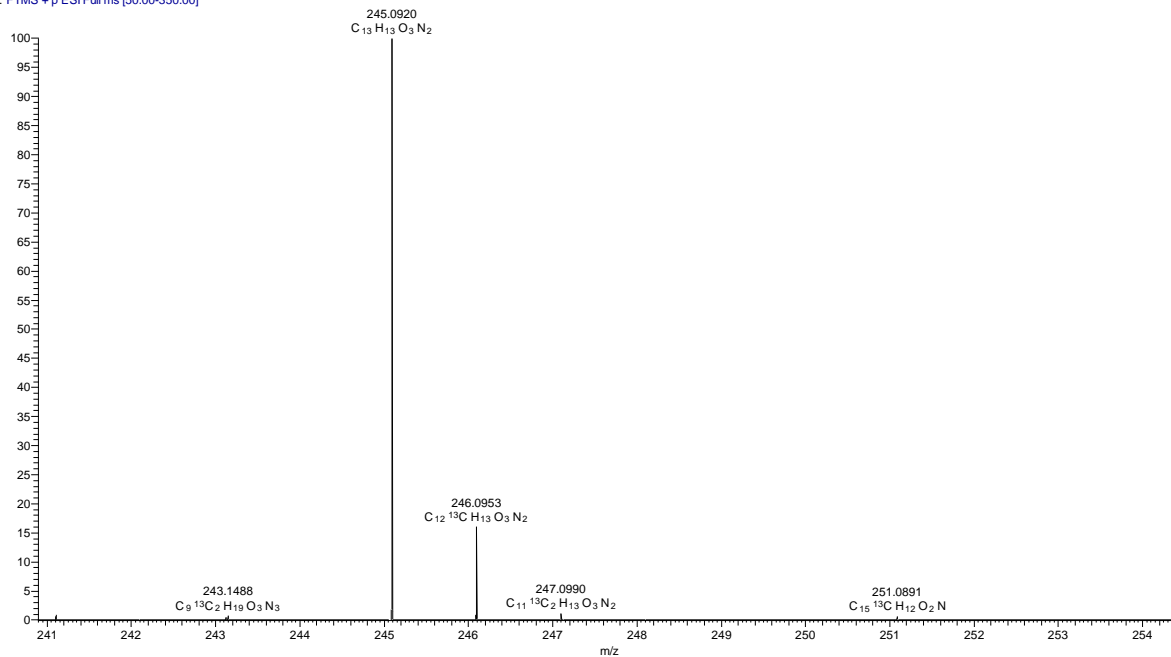


Figure B59. Positive ion HRESIMS spectrum of purpurascenine A (**4.1***) fed [3-¹³C]-alanine.

THL020_C3M_8P2_fullms_2#1 RT: 0.00 AV: 1 NL: 1.00E6
T: FTMS + p ESI Full ms [50.00-350.00]



THL020_C3M_8P2_fullms_2#1 RT: 0.00
T: FTMS + p ESI Full ms [50.00-350.00]
m/z = 240.8912-254.4561

m/z	Intensity	Relative	Composition
241.1043	8968.6	0.88	
242.0996	2586.1	0.25	
243.1207	4124.4	0.40	C ₁₄ ¹³ C H ₁₆ O ₂ N
243.1488	7235.9	0.71	C ₉ ¹³ C ₂ H ₁₉ O ₃ N ₃
245.0920	1020636.1	100.00	C ₁₃ H ₁₃ O ₃ N ₂
246.0892	9118.1	0.89	
246.0953	161458.0	15.82	C ₁₂ ¹³ C H ₁₃ O ₃ N ₂
247.0990	10428.5	1.02	C ₁₁ ¹³ C ₂ H ₁₃ O ₃ N ₂
247.1291	2434.9	0.24	
248.1006	2242.9	0.22	
251.0891	5607.4	0.55	C ₁₅ ¹³ C H ₁₂ O ₂ N
251.1006	2356.1	0.23	C ₁₄ ¹³ C H ₁₂ O ₂ N ₃

Figure S60. ^1H NMR spectrum (600 MHz, $\text{CD}_3\text{OD}/\text{D}_2\text{O} = 7/3$, v/v) of purpurascenine A (**1***) fed $[3\text{-}^{13}\text{C}]$ -alanine.

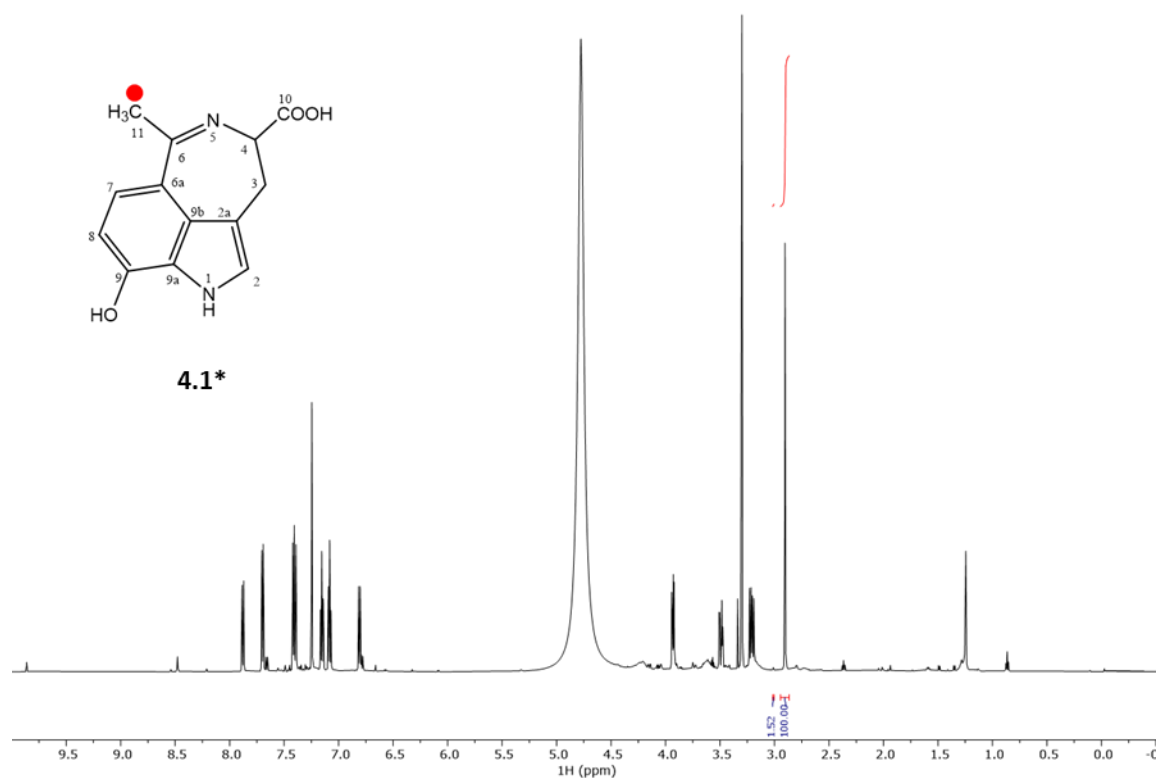


Figure B61. ^1H NMR spectrum (methyl signal) of purpurascenine A (**4.1***) fed $[3\text{-}^{13}\text{C}]$ -alanine.

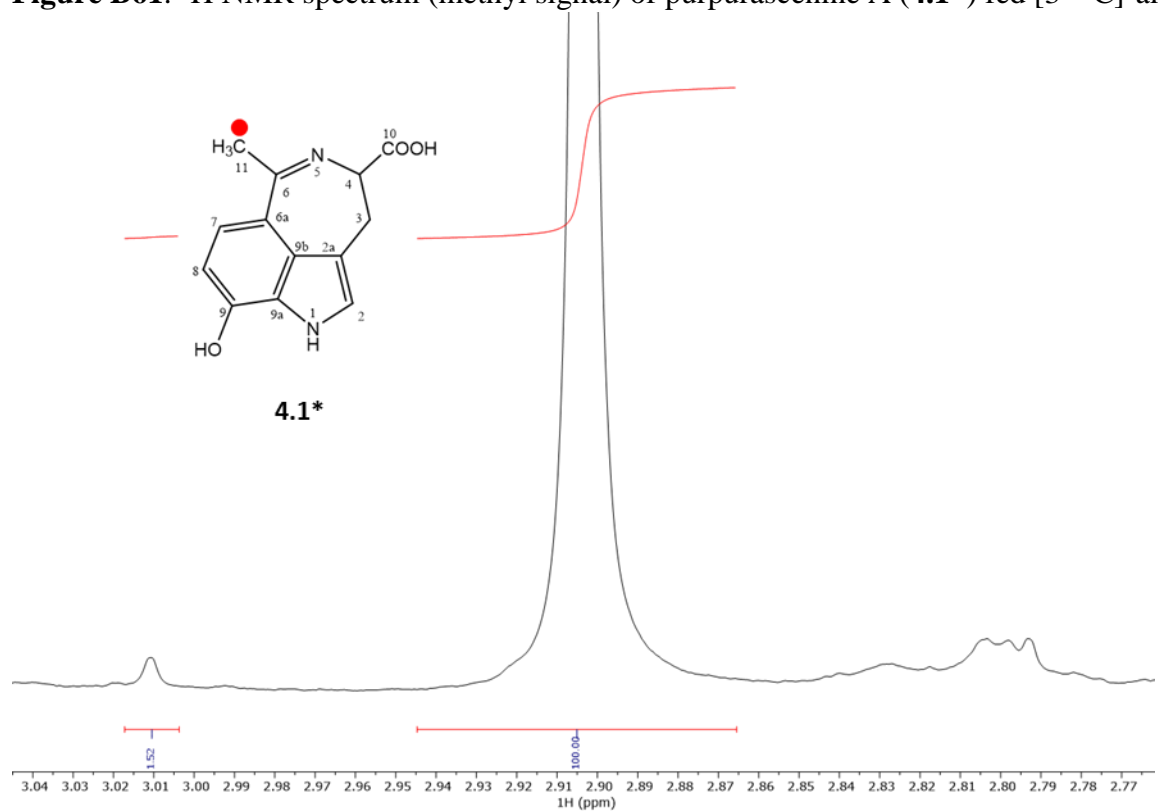
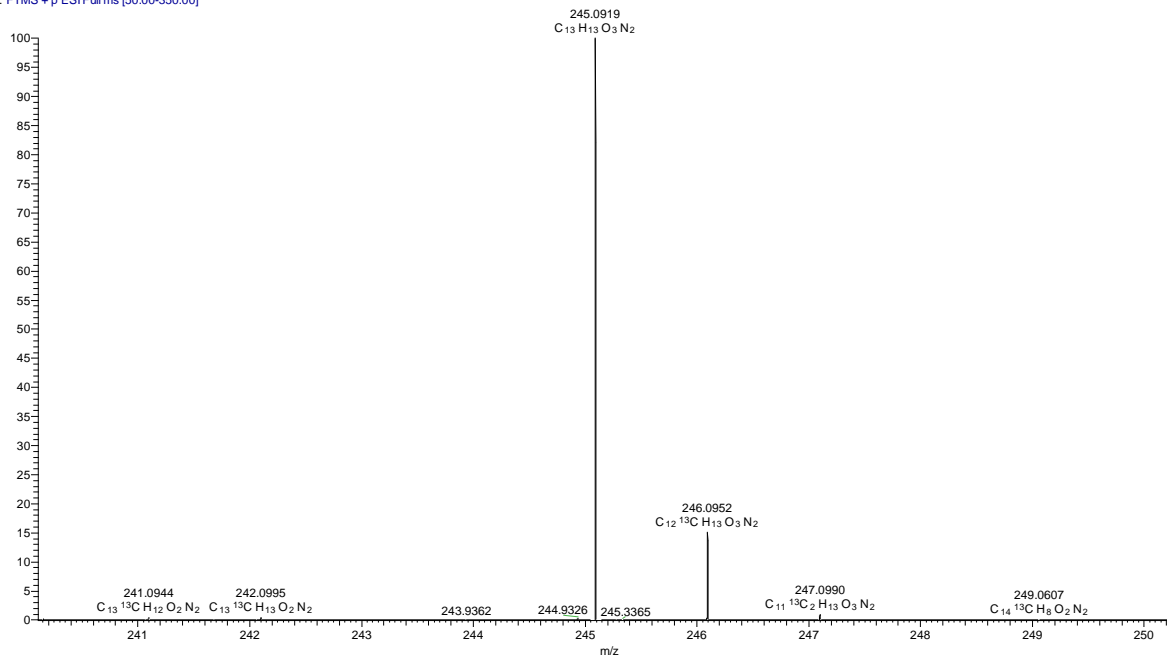


Figure B62. Positive ion HRESIMS spectrum of purpurascenine A (**4.1***) fed [2-¹³C]-acetate.

THL018_A1C4_10_fullMS_1#1 RT: 0.00 AV: 1 NL: 2.41E6
T: FTMS + p ESI Full ms [50.00-350.00]



THL018_A1C4_10_fullMS_1#1 RT: 0.00
T: FTMS + p ESI Full ms [50.00-350.00]
m/z = 240.1048-250.3277

m/z	Intensity	Relative	Composition
240.1569	7282.1	0.30	
241.0684	4599.8	0.19	C ₁₃ ¹³ C H ₁₀ O ₃ N
241.0944	9369.6	0.39	
241.1051	2334.6	0.10	C ₁₄ ¹³ C H ₁₄ O ₂ N
241.6842	2408.3	0.10	
242.0621	2445.0	0.10	C ₁₄ ¹³ C ₂ H ₆ N ₃
242.0995	11194.1	0.46	
243.9362	4733.3	0.20	
244.9326	8635.3	0.36	
245.0919	2410615.3	100.00	C ₁₃ H ₁₃ O ₃ N ₂
245.3365	2873.4	0.12	
246.0895	13945.7	0.58	
246.0952	369396.1	15.32	C ₁₂ ¹³ C H ₁₃ O ₃ N ₂
247.0990	24796.8	1.03	C ₁₁ ¹³ C ₂ H ₁₃ O ₃ N ₂
247.1078	2851.9	0.12	C ₁₃ H ₁₅ O ₃ N ₂
249.0607	2443.2	0.10	

Figure B63. ^1H NMR spectrum (600 MHz, $\text{CD}_3\text{OD}/\text{D}_2\text{O} = 5/1$, v/v) of purpurascenine A (**4.1***) fed $[2-^{13}\text{C}]$ -acetate.

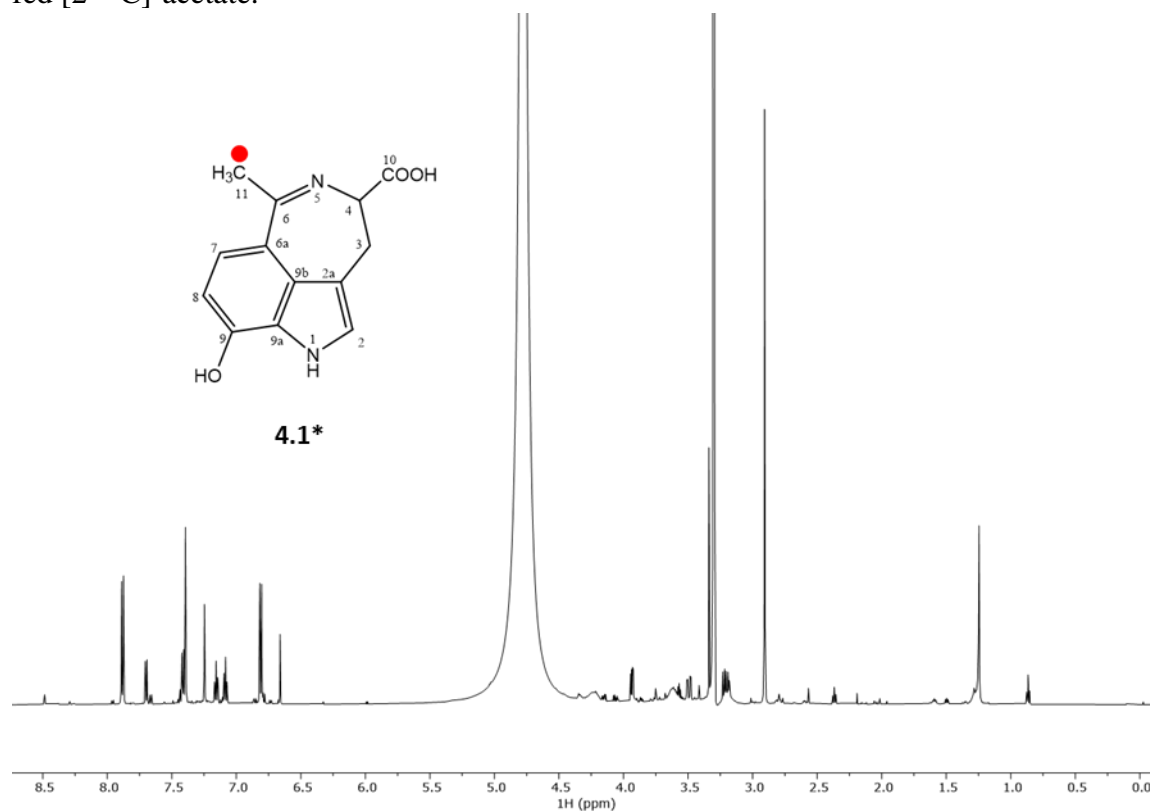


Figure B64. ^1H NMR spectrum (methyl signal) of purpurascenine A (**4.1***) fed $[2-^{13}\text{C}]$ -acetate.

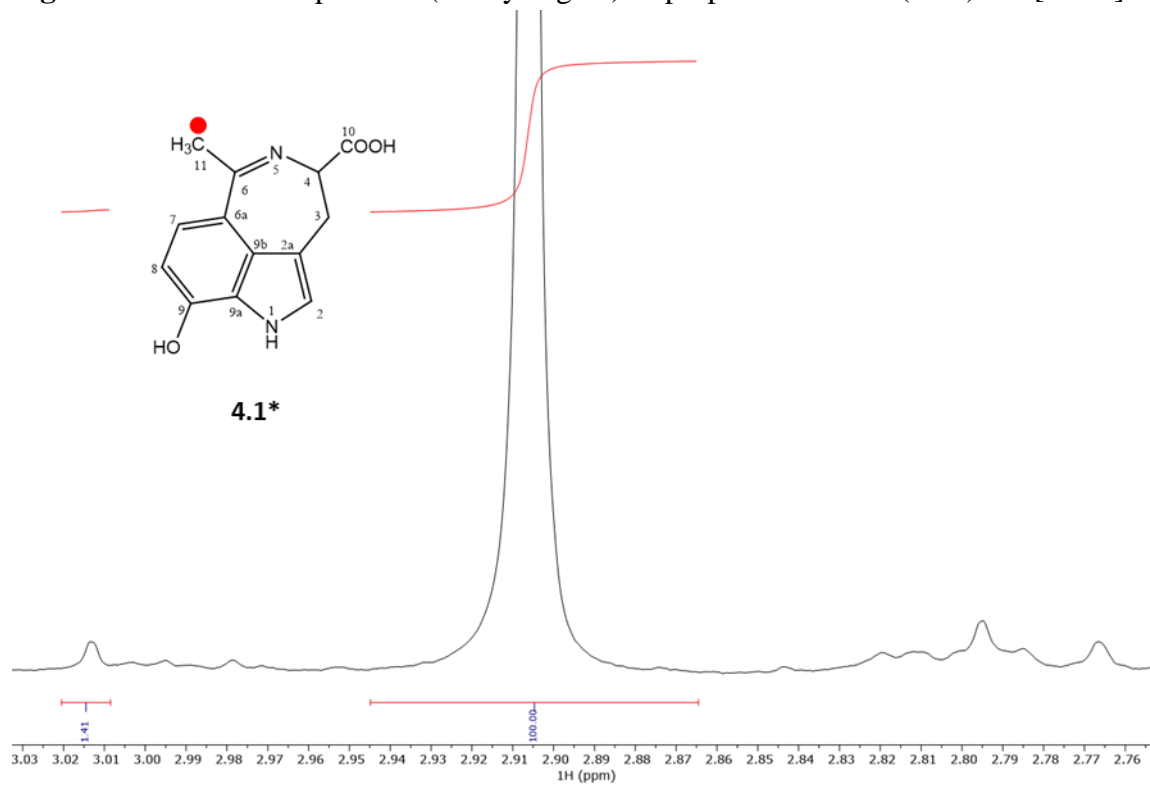


Figure B65. Cell viability of the human cancer cell lines PC-3 (prostate adenocarcinoma), HCT-116 (colorectal adenocarcinoma), and MCF-7 (breast ductal carcinoma) treated for 48 h with purpurascenine A (**4.1**) and the natural 5-HT_{2A} agonist serotonin (5-HT), respectively, as determined by a fluorometric resazurin-based cell viability assay. Data have been normalized to cell viabilities between 0% (represented by digitonin-treated cells; cytotoxic positive control) and 100% (represented by untreated cells; negative control).

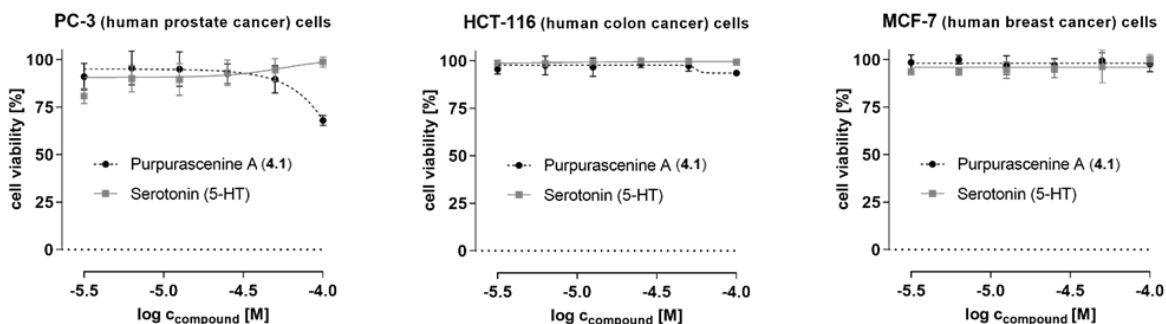


Figure B66. Monomer of the tertiary structure of the 5-HT_{2A} receptor. The binding site of the cocrystallized risperidone (in grey) and the best docking position of purpurascenine A (**4.1**) (in green) is shown left in the middle.

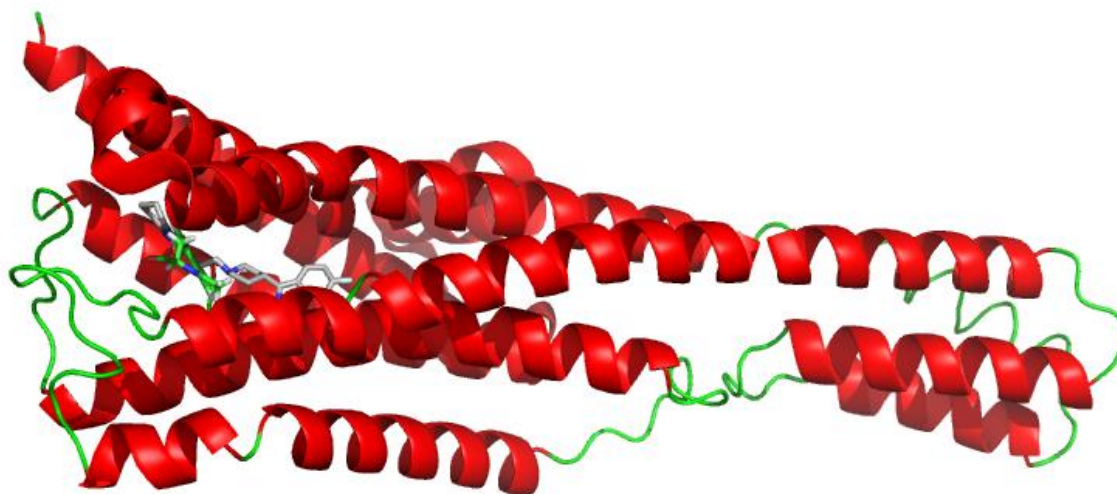


Table B1. Positive ion HRESIMSⁿ data of purpurascenines A-C (**4.1-4.3** and **4.1a**).

cpd	scan mode [<i>m/z</i> (NCE in%)]	<i>m/z</i> (fragment ion, relative intensity in %, error in ppm)
4.1	(+) full MS	245.0912 ([M+H] ⁺ , 74, 3.7)
	(+) MS ² [245.09 (30)]	199.0860 ([M+H-HCOOH] ⁺ = a , 100, 3.0), 131.0488 ([M-HCOOH-2HCN-C₄H₈] ⁺ , <1, 2.7)
	(+) MS ³ [245.09 (30)→ 199.09 (32)]	184.0626 ([a-CH₃] ⁺ , 100, 2.9), 181.0755 ([a-H₂O] ⁺ , 43, 2.8), 172.0752 ([a-HCN] ⁺ , 15, 2.9), 171.0912 ([a-CO] ⁺ , 12, 3.0), 131.0487 ([a-HCN-CH₃CN] ⁺ , <1, 3.0)
4.1a	(+) full MS	245.0919 ([M+H] ⁺ , 100, 0.5), 267.0740 ([M+Na] ⁺ , 3, 0.0)
	(+) MS ² [245.09 (30)]	199.0865 ([M+H-HCOOH] ⁺ = a , 100, 0.6), 131.0493 ([M-HCOOH-HCN-CH₃CN] ⁺ , <1, 1.6)
	(+) MS ³ [245.09 (30)→ 199.09 (30)]	184.0631 ([a-CH₃] ⁺ , 100, 0.1), 181.0760 ([a-H₂O] ⁺ , 43, 0.3), 172.0756 ([a-HCN] ⁺ , 16, 0.3), 171.0917 ([a-CO] ⁺ , 13, 0.0), 131.0491 ([a-HCN-CH₃CN] ⁺ , <1, 0.3)
4.2	(+) full MS	231.0757 ([M+H] ⁺ , 4, 2.9)
	(+) MS ² [231.08 (30)]	185.0704 ([M+H-HCOOH] ⁺ = b , 100, 3.0)
	(+) MS ³ [231.08 (30)→ 185.07 (33)]	167.0599 ([b-H₂O] ⁺ , 100, 2.6), 158.0596 ([b-HCN] ⁺ , 11, 2.7), 157.0917 ([b-CO] ⁺ , 30, 2.6), 131.0491 ([a-HCN-CH₃CN] ⁺ , <1, 3.0)
4.3	(+) full MS	287.1381 ([M+H] ⁺ , 10, 2.9)
	(+) MS ² [287.14 (30)]	241.1327 ([M+H-HCOOH] ⁺ , 100, 3.4), 131.0488 ([M-HCOOH-2HCN-C₄H₈] ⁺ , <1, 2.7)
	(+) MS ³ [287.14 (30)→ 241.13 (31)]	224.1063 ([M+H-HCOOH-NH₃] ⁺ , 21, 3.1), 199.0860 ([M+H-HCOOH-C₃H₆] ⁺ = a , 100, 2.9), 185.0704 ([M+H-HCOOH-C₄H₈] ⁺ = b , 32, 2.9)
	(+) MS ⁴ [287.14 (30)→241.13 (31)→ 199.09 (34)]	184.0627 ([a-CH₃] ⁺ , 49, 2.5), 181.0755 ([a-H₂O] ⁺ , 49, 2.7), 172.0752 ([a-HCN] ⁺ , 56, 2.7), 171.0912 ([a-CO] ⁺ , 28, 2.6),
	(+) MS ⁴ [287.14 (30)→241.13 (30)→ 185.07 (30)]	167.0599 ([b-H₂O] ⁺ , 100, 3.1), 158.0596 ([b-HCN] ⁺ , 20, 2.9), 157.0756 ([b-CO] ⁺ , 27, 3.0)

Table B2. NMR spectroscopic data (600/150 MHz, DMSO-d6) for purpurascenine A in enol (**4.1**) and keto form (**4.1a**)

Position	4.1			4.1a		
	δ_C , type	δ_H (<i>J</i> in Hz)	HMBC	δ_C , type	δ_H (<i>J</i> in Hz)	HMBC
1-NH		11.28, br s			11.16, br s	
2	121.7, CH	7.06, s	2a, 9a, 9b	120.5, CH	6.93 s	2a, 3, 9a, 9b
2a	115.4, qC			116.1, qC		
3	31.7, CH ₂	3.52 ^a	<i>n.d.</i>	32.5, CH ₂	3.59 ^a 2.58 dd (15.1, 9.8)	2, 2a, 4, 9b, 10
4	60.6, CH	4.81 ^a	<i>n.d.</i>	60.4, CH	3.43	2a, 3, 6, 10
6	162.4, qC			159.6, qC		
6a	105.1, qC			102.9, qC		
7	133.4, CH	7.53 d (9.0)	9b	134.5, CH	7.44 d (9.2)	2a, 6, 6a, 9, 9a, 9b
8	109.2, CH	6.23 d (9.0)	<i>n.d.</i>	115.9, CH	6.04 d (9.2)	6a, 9, 9a
9	149.8, qC			169.7, qC		
9a	126.8, qC			128.7, qC		
9b	127.5, qC			126.4, qC		
9-OH		9.5 br s				
10-CO ₂ H	169.5, qC	<i>n.d.</i>		170.6, qC	8.70 br s	
11-CH ₃	22.1, CH ₃	2.67 s	6, 6a, 7	21.7, CH ₃	2.52 s	6, 6a, 7

^a overlapping signal, chemical shift determined from ¹H, ¹³C HSQC; *n.d.* = not detected.

C Compound code assignment

Thesis compound number	Compound name	Experimental code (3LC)
3.1	pyromyxone A	THL001_2
3.2	pyromyxone B	THL001_3
3.3	pyromyxone C	THL003_8_2
3.4	pyromyxone D	THL004_14
4.1	purpurascenine A	THL010_32, HOJ005_B7_15
4.1*	purpurascenine A, labelled with [3- ¹³ C]-pyruvate	THL021_B1E_6P5
4.1*	purpurascenine A, labelled with [3- ¹³ C]-alanine	THL013_39, THL020_C3M_8P2
4.1*	purpurascenine A, labelled with [2- ¹³ C]-acetate	THL012_34, THL018_C1A4_10
4.1a	purpurascenine A (keto form)	DQD162_B2C
4.2	purpurascenine B	HOJ010_2B6B5, THL020_C6Acb
4.3	purpurascenine C	HOJ010_2B5_1GHT5, THL024_A2B3cb
4.4	7-hydroxytryptophan	THL020_C4E
4.5	adenosine	HOJ010_B52H_v63
4.6	riboflavin	HOJ002_B3RF_HPLC
5.1 (nat.)	ampullosporin F	THL014_A1C2_5
5.1 (syn.)	ampullosporin F	THL014_43
5.2 (nat.)	ampullosporin G	THL014_A1C2_6
5.2 (syn.)	ampullosporin G	THL014_44
5.3	ampullosporin A	THL014_A1C2_4, THL014_A1C2G
5.4	peptaibolin	THL014_41
5.5	chrysosporide	THL014_A1D2E
5.6	<i>cyclo</i> (Trp-Ser)	THL014_A1F4
5.7	<i>cyclo</i> (Trp-Ala)	THL014_A1F5

Declaration on the author contributions

Chapter 3: “Nor-guanacastepene pigments from the Chilean mushroom *Cortinarius pyromyxa*”

Y. T. H. Lam, G. Palfner, C. Lima, A. Porzel, W. Brandt, A. Frolov, H. Sultani, K. Franke, C. Wagner, K. Merzweiler, L. A. Wessjohann, and N. Arnold. *Phytochemistry* **2019**, 165, 112048, DOI: 10.1016/j.phytochem.2019.05.021.

In this work, Yen T. H. Lam carried out the isolation and structural elucidation of all compounds. Götz Palfner and Celia Lima performed the phylogenetic analyses. Andrea Porzel carried out the NMR experiments and provided help for the structural elucidation, while Andrej Frolov performed the MS experiments. The computational studies was done by Wolfgang Brandt. Haider Sultani carried out the antifungal assay, whereas Katrin Franke performed the antibacterial assay. The X-ray crystallography was accomplished by Christoph Wagner and Kurt Merzweiler. Yen T. H. Lam wrote the manuscript draft. The project was designed and supervised by Ludger A. Wessjohann and Norbert Arnold. All authors contributed to the writing and editing of the manuscript.

Chapter 4: “Purpurascenines A-C, azepinoindole alkaloids from *Cortinarius purpurascens* Fr.: isolation, biosynthesis, and activity studies on 5HT_{2A} receptor”

Yen T. H. Lam, Jana Hoppe, Dang N. Quang, Andrea Porzel, Alena Soboleva, Wolfgang Brandt, Robert Rennert, Hidayat Hussain, Mehdi D. Davari, Ludger Wessjohann and Norbert Arnold. *Manuscript in submission*.

In this project, Yen T. H. Lam carried out the isolation and structural elucidation of most of all compounds, as well as the feeding experiments. Dang N. Quang performed the initial isolation leading to the detection of the ketone isomer, while Jana Hoppe followed the isolation procedure optimized by Yen T. H. Lam to enhance the amount of isolated compounds. Andrea Porzel and Hidayat Hussain performed the NMR experiments, while Alena Soboleva carried out the MS experiments. The computational studies was done by Wolfgang Brandt and Mehdi D. Davari. Robert Rennert performed anticancer and receptor functional activation assays. Yen T. H. Lam wrote the main part of the manuscript draft, while Robert Rennert contributed to the bioassay analysis. The project was designed and supervised by Ludger A. Wessjohann and Norbert Arnold. All authors contributed to the writing and editing of the manuscript.

Chapter 5: “Rare glutamic acid methyl ester peptaibols from *Sepedonium ampullosporum* Damon KSH 534 exhibit promising antifungal and anticancer activity”

Yen T. H. Lam, Manuel G. Ricardo, Robert Rennert, Andrej Frolov, Andrea Porzel, Wolfgang Brandt, Pauline Stark, Bernhard Westermann and Norbert Arnold. *Int J Mol Sci* **2021**, 22 (23), 12718, DOI: 10.3390/ijms222312718.

In this study, Yen T. H. Lam carried out the isolation and structural elucidation of all compounds. Manuel G. Ricardo synthesized the novel compounds, which were purified and analyzed by Yen Thi Hai Lam. Robert Rennert performed anticancer assay. Andrea Porzel and Pauline Stark performed the NMR experiments, while Andrej Frolov carried out the MS experiments. The molecular docking studies was done by Wolfgang Brandt. Yen T. H. Lam wrote the main part of the manuscript draft, while Robert Rennert contributed to the bioassay and docking analysis. The project was designed and supervised by Bernhard Westermann and Norbert Arnold. All authors contributed to the writing and editing of the manuscript.

Curriculum Vitae

Name: Yen Thi Hai Lam

Date of birth: December 28th, 1990

Place of birth: Hung Yen, Vietnam

Nationality: Vietnamese

Email: haiyen.hnue@gmail.com

Languages: Vietnamese, English

Educational qualifications

- PhD in Organic Chemistry, Leibniz Institute of Plant Biochemistry/ Martin Luther University Halle-Wittenberg, Germany
- 2016-2022** *Supported by the MOET Vietnam (911 scholarship) for doctoral students*
- 2012-2014** Master's degree in Organic Chemistry, Hanoi National University of Education, Vietnam. (Thesis mark 10/10)
Topic: Study on chemical constituents of *Stemona pierrei* Gagn collected in Laos. (Supervisor: Prof. Quang Ngoc Dang)
- 2008-2012** Bachelor's degree in Chemistry and Education, Hanoi National University of Education, Vietnam. (Thesis mark 10/10)
Topic: Study on chemical constituents of *Dillenia indica* Linn. stem bark collected in Tuyen Quang. (Supervisor: Prof. Dien Huu Pham)

Fellowships/Awards/Honor

- 2022** Best Poster presentation award at the PSE-YSM conference in Crete, Greece.
- 2016-2020** Vietnam Ministry of Education and Training (MOET) Doctoral Fellowship
- 2012** Valedictorian of Faculty of Chemistry, Hanoi National University of Education, Vietnam.
- 2011** Best Prize at Scientific Research Contest for Students, Faculty of Chemistry, Hanoi National University of Education, Vietnam.
Fourth Prize at Scientific Research Contest for Students, Hanoi National University of Education, Vietnam.
- 2008-2012** Awards for outstanding students (in 6/8 semesters) of Hanoi National University of Education, Vietnam.

Work/Research Experience

- 2016-2022** Researcher at Department of Bioorganic Chemistry, Leibniz Institute of Plant Biochemistry, Germany
- 2013-2016** Lecturer and Researcher. Department of Organic Chemistry, Faculty of Chemistry, Hanoi National University of Education, Vietnam
- 2012-2013** Junior Lecturer. Department of Organic Chemistry, Faculty of Chemistry, Hanoi National University of Education, Vietnam

Oral and Poster Presentations (PhD research work)

- Aug. 2022** New peptaibols from *Sepedonium ampullosporum* Damon KSH534 exhibit promising antifungal and anticancer activities. **Yen T. H. Lam**, Ludger Wessjohann, Norbert Arnold, 6th International Symposium on Phytochemicals in Medicine and Food (6-ISPMPF), Hangzhou, China. (Oral presentation)
- May 2022** Purpurascenines A-C, azepino-indole alkaloids from *Cortinarius purpurascens* Fr.: isolation, identification, biosynthesis, and antagonistic activity with 5-HT_{2A} receptor. **Y. T. H. Lam**, Jana Hoppe, Dang Ngoc Quang, Andrea Porzel, Alena Soboleva, Wolfgang Brandt, Robert Rennert, Hidayat Hussain, Mehdi D. Davari, Ludger Wessjohann, Norbert Arnold. Trends in Natural Products Research: A PSE Young Scientists' Meeting (PSE-YSM), Crete Greece. (Poster presentation)
- Oct. 2018** The first pigment study on a Chilean Myxaciium species - *Cortinarius pyromyxa* reveals new guanacastepene-type terpenoids. **Yen T. H. Lam**, Ludger Wessjohann, Norbert Arnold, 56th Docktorandenworkshop, Naturstoffe: Chemie, Biologie und Ökologie, Leipzig, Germany. (Oral presentation)
- Sept. 2018** The first pigment study on a Chilean Myxaciium species - *Cortinarius pyromyxa* reveals new *nor*-guanacastepenes. **Y.T.H. Lam**; G. Plafner; A. Przel; W. Brandt, A. Frolov, C. Wagner, K. Merzweiler, L. Wessjohann, N. Arnold. 3rd European Conference on Natural Products, DECHEMA, Frankfurt am Main, Germany. (Poster presentation)
- June 2018** The first pigment study on a Chilean Myxaciium species - *Cortinarius pyromyxa* reveals new *nor*-guanacastepenes. **Y.T.H. Lam**; G. Plafner; A. Przel; W. Brandt; A. Frolov; C. Wagner; K. Merzweiler; L. Wessjohann; N. Arnold. Plant Science Student Conference, Gatersleben, Germany. (Poster presentation)
- June 2017** Secondary metabolites from toadstools of *Cortinarius purpurascens* Fr. and their biosynthesis. **Y.T.H. Lam**, D.N. Quang, L. Wessjohann, N. Arnold. Plant Science Student Conference, Halle (Saale), Germany. (Poster presentation)

List of Publications

1. **Yen T. H. Lam**, Manuel G. Ricardo, Robert Rennert, Andrej Frolov, Andrea Porzel, Wolfgang Brandt, Pauline Stark, Bernhard Westermann and Norbert Arnold. Rare glutamic acid methyl ester peptaibols from *Sepedonium ampullosporum* Damon KSH 534 exhibit promising antifungal and anticancer activity. *Int J Mol Sci* **2021**, 22, 12718.
2. **Yen T. H. Lam**, Götz Palfner, Lelia Lima, Andrea Porzel, Wolfgang Brandt, Andrej Frolov, Haider Sultani, Katrin Franke, Christoph Wagner, Kurt Merzweiler, Ludger Wessjohann and Norbert Arnold. Nor-guanacastepene pigments from the Chilean mushroom *Cortinarius pyromyxa*. *Phytochemistry* **2019**, 165, 112048.
3. **Yen T. H. Lam**, Phan Thi Anh, Souknaly Thoumma, Dang Ngoc Quang, Pham Huu Dien. Phytochemical study on *Stemona collinsae* Craig. roots collected in Laos. *Viet J Sci Techn*, **2016**, 54 (2B), 14-19.
4. Pham Cong Vu, Tran The Tung, **Yen T. H. Lam**, Nguyen Quyet Tien, Dang Ngoc Quang, Pham Huu Dien. The cytotoxic activity and volatile constituents of fruits and leaves of *Pandanus tectorius* Parkin ex. J.P. du Roi. *J Sci*, HNUE, **2015**, 60 (9), 9-13.
5. Pham Huu Dien, Souknaly Thoumma, Nguyen Thi Thanh Hoa, **Yen T. H. Lam**. Cytotoxic pyranocoumarins from *Paramignya trimera*. *Viet J Chem*, **2015**, 53 (4E2), 174-178.
6. Dang Ngoc Quang, Vong Anatha Khamko, Nguyen Thi Trang, **Yen T. H. Lam** and Pham Huu Dien. Stemofurans X-Y from the Roots of *Stemona* Species from Laos. *Nat Prod Commun*, **2014**, 9 (12), 1741 – 1742.
7. Pham Thi Huyen, Pham Van Cong, Bui Thi Lua, **Yen T. H. Lam**, Dang Ngoc Quang and Pham Huu Dien. Chemical constituents of *Stemona tuberosa* plant. *J Sci*, HNUE, **2014**, 59 (9), 37-42.
8. Nguyen Thi Thanh Hoa, Souknaly Thoumma, **Yen T. H. Lam** and Pham Huu Dien. Cytotoxic activity of *Paramignya trimera* (Oliv.) Guillaum plant extracts and their volatile chemical constituents. *J Sci*, HNUE, **2014**, 59 (9), 11-16.
9. Luong Thi Cuc Hoa, **Yen T. H. Lam**, Dang Ngoc Quang, Pham Huu Dien. Phytochemistry and cytotoxic activity of *Pandanus tectorius* Parkin. Ex J.P. du Roi leaves (collected in Thua Thien – Hue province). *J Sci*, HNUE, **2014**, 59 (1A), 174-181.
10. Ma Thi Cam Van, **Yen T. H. Lam**, Pham Huu Dien. Study on chemical constituents of *Morinda citrifolia* Linn. *J Sci*, HNUE, **2013**, 58 (9), 9-14.
11. Tran Thi Huyen, **Yen T. H. Lam**, Dang Ngoc Quang, Pham Huu Dien. A cytotoxicity of *Pandanus tectorius* Parkin Ex. J.P. du Roi plants extracts and isolated metabolites. Proceeding of the Eight Indochina Conference on Pharmaceutical Sciences: "ASEAN Pharmacy – Integration for Development", December 4th-5th, **2013**, Hochiminh City, Vietnam, 235-239.
12. **Yen T. H. Lam** and Pham Huu Dien. Study on chemical constituents of *Dillenia indica* Linn. stem bark collected in Tuyen Quang. *J Sci*, HNUE, **2013**, 58 (3), 50-54.
13. Phong Thi Thu Ha, Nguyen Thi Huyen, **Yen T. H. Lam**, Pham Huu Dien. Study on chemical constituents of *Celastrus Hindsii* Benth. Collected in Tuyen Quang province. *J Sci*, HNUE, **2013**, 51 (2C), 658-661.

14. Nguyen Thi Nhung, **Yen T. H. Lam**, Pham Huu Dien (2013). Study on chemical constituents of *Azadirachta indica* A. Juss. leaves collected in Ninh Thuan province. *J Sci*, HNUE, **2013**, 51 (2C), 809-813.
15. Truong Thu Huong, **Yen T. H. Lam**, Pham Huu Dien. Isolation, structural elucidation of the main compounds from Vietnamese anti-diabetic *Dillenia indica* Linn. and *Mirabilis jalapa* plants. Proceeding of Scientific Research Contest for Students, Hanoi National University of Education, **2011**, Hanoi, Vietnam, 117-124.
16. **Yen T. H. Lam**, Jana Hoppe, Dang Ngoc Quang, Andrea Porzel, Alena Soboleva, Wolfgang Brandt, Robert Rennert, Hidayat Hussain, Mehdi D. Davari, Ludger Wessjohann and Norbert Arnold. Purpurascenines A-C, azepino-indole alkaloids from *Cortinarius purpurascens* Fr.: isolation, identification, biosynthesis, and antagonistic activity with 5-HT_{2A} receptor. *In submission*.
17. Annegret Laub, **Yen T. H. Lam**, Yanira Mendez, Aldrin V. Vidal, Andrea Porzel, Jürgen Schmidt, Ludger A. Wessjohann, Bernhard Westermann, and Norbert Arnold. Isolation, identification and synthesis of two new cyclic pentapeptides from *Sepedonium microspermum* Besl. *In submission*.
18. **Yen T. H. Lam**, Erik Henze, Götz Palfner, Ursula Peintner, Felipe Galleguillos, and Norbert Arnold. A mycochemical and phylogenetic study on *Cortinarius pseudo-ignotus*. *In preparation*.
19. Mthandazo Dube, **Yen T. H. Lam**, Peter Imming and Norbert Arnold. Thiophenes from *Echinops kebericho* Menfis exhibit promising anthelmintic activity. *In preparation*.

Eidesstattliche Erklärung

Ich erkläre an Eides statt, dass ich die vorliegende Arbeit selbstständig und nur unter Verwendung der angegebenen Hilfsmittel und Quellen angefertigt habe.

Alle Stellen, die wörtlich oder sinngemäß aus Veröffentlichungen entnommen sind, habe ich als solche kenntlich gemacht. Des Weiteren versichere ich, dass ich diese Arbeit an keiner anderen Institution eingereicht habe.

Mir ist bekannt, dass bei Angabe falscher Aussagen die Prüfung als nicht bestanden gilt. Mit meiner Unterschrift versichere ich die Richtigkeit dieser Angaben und erkenne die rechtlichen Grundlagen an.

Datum

(Yen Thi Hai Lam)